VOLUME 80 NOVEMBER 18, 1976 NUMBER 24

JPCHAx

THE JOURNAL OF PHYSICAL CHEMISTRY

PUBLISHED BIWEEKLY BY THE AMERICAN CHEMICAL SOCIETY

THE JOURNAL OF

PHYSICAL CHEMISTRY

Published by the
AMERICAN CHEMICAL SOCIETY
BOOKS AND JOURNALS DIVISION
D. H. Michael Bowen, Director

Editorial Department: Charles R. Bertsch, Head; Marianne C. Brogan, Associate Head; Celia B. McFarland, Joseph E. Yurvati, Assistant Editors
Graphics and Production Department: Bacil Guiley, Head
Research and Development Department: Seldon W. Terrant, Head

Advertising Office: Centcom, Ltd., 50 W. State St., Westport, Conn. 06880.

Published biweekly by the American Chemical Society at 20th and Northampton Sts., Easton, Pennsylvania 18042. Second class postage paid at Washington, D.C. and at additional mailing offices.

Editorial Information

Instructions for authors are printed in the first issue of each volume. Please conform to these instructions when submitting manuscripts.

Manuscripts for publication should be submitted to *The Journal of Physical Chemistry*, Department of Chemistry, University of Minnesota, Minneapolis, Minn. 55455. Correspondence regarding **accepted papers and proofs** should be directed to the Editorial Department at the ACS Easton address.

Page charges of $60.00 per page are assessed for papers published in this journal. Ability to pay does not affect acceptance or scheduling of papers.

Bulk reprints or photocopies of individual articles are available. For information write to Business Operations, Books and Journals Division at the ACS Washington address.

Requests for **permission to reprint** should be directed to Permissions, Books and Journals Division at the ACS Washington address. The American Chemical Society and its Editors assume no responsibility for the statements and opinions advanced by contributors.

Subscription and Business Information

1976 Subscription rates—including surface postage

	U.S.	PUAS	Canada, Foreign
Member	$24.00	$29.75	$30.25
Nonmember	96.00	101.75	102.25
Supplementary material	15.00	19.00	20.00

Air mail and air freight rates are available from Membership & Subscription Services, at the ACS Columbus address.

New and renewal subscriptions should be sent with payment to the Office of the Controller at the ACS Washington address. **Changes of address** must include both old and new addresses with ZIP code and a recent mailing label. Send all address changes to the ACS Columbus address. Please allow six weeks for change to become effective. **Claims** for missing numbers will not be allowed if loss was due to failure of notice of change of address to be received in the time specified; if claim is dated (a) North America—more than 90 days beyond issue date, (b) all other foreign—more than 1 year beyond issue date; or if the reason given is "missing from files". Hard copy claims are handled at the ACS Columbus address.

Microfiche subscriptions are available at the same rates but are mailed first class to U.S. subscribers, air mail to the rest of the world. Direct all inquiries to Business Operations, Books and Journals Division, at the ACS Washington address or call (202) 872-4444. **Single issues** in hard copy and/or microfiche are available from Special Issues Sales at the ACS Washington address. Current year $4.75. Back issue rates available from Special Issues Sales. **Back volumes** are available in hard copy and/or microform. Write to Special Issues Sales at the ACS Washington address for further information. **Microfilm** editions of ACS periodical publications are available from volume 1 to the present. For further information, contact Special Issues Sales at the ACS Washington address. **Supplementary material** must be ordered directly from Business Operations, Books and Journals Division, at the ACS Washington address.

Microfiche	U.S.	PUAS, Canada	Other Foreign
Photocopy	$2.50	$3.00	$3.50
1–7 pages	4.00	5.50	7.00
8–20 pages	5.00	6.50	8.00

Orders over 20 pages are available only on microfiche, 4 × 6 in., 24X, negative, silver halide. Orders must state photocopy or microfiche if both are available. Full bibliographic citation including names of all authors and prepayment are required. Prices are subject to change.

American Chemical Society
1155 16th Street, N.W.
Washington, D.C. 20036
(202) 872-4600

Member & Subscription Services
American Chemical Society
P.O. Box 3337
Columbus, Ohio 43210
(614) 421-7230

Editorial Department
American Chemical Society
20th and Northampton Sts.
Easton, Pennsylvania 18042
(215) 258-9111

Notice to Authors last printed in the issue of January 1, 1976

THE JOURNAL OF

PHYSICAL CHEMISTRY

Volume 80, Number 24 November 18, 1976

JPCHAx 80(24) 2623–2716 (1976)

ISSN 0022-3654

Reversibility of the Pressure-Induced Intersystem Crossing in Methylene . . . . **F. Lahmani** 2623

Photobromination of Liquid 3-Methylpentane . . . . . **R. Arce* and L. Bartolomé** 2629

Transients and Specific Rates of Some Reactions of the Solvated Electron with Inorganic Ions in Liquid Ammonia Investigated by Nanosecond Pulse Radiolysis at 23 °C . . . **Farhataziz* and Pierre Cordier** 2635

Correlation of Photocurrent–Voltage Curves with Flat-Band Potential for Stable Photoelectrolysis of Water . . . . . **Jeffrey M. Bolts and Mark S. Wrighton*** 2641

Interpretation of Activation Parameters for Simple Electrode Reactions . . **Michael J. Weaver** 2645

Chemical Relaxation and Equilibrium Studies of Association in Aqueous Solutions of Bolaform Detergents. 1. Dodecane-1,12-bis(trimethylammonium bromide) . . . **S. Yiv, K. M. Kale, J. Lang, and R. Zana*** 2651

A Numerical Solution for the Material and Momentum Balance Equations for Finite Concentration Chromatography . **Jon F. Parcher,* T. H. Ho, and Henry W. Haynes, Jr.** 2656

Conductometric Studies on Association of Cyclodextrin with Colloidal Electrolytes . . . **Tsuneo Okubo, Hiromi Kitano, and Norio Ise*** 2661

Nitric Oxide Reduction with Ammonia over Cu(II)Y Zeolites . . . **W. Burton Williamson and Jack H. Lunsford*** 2664

Substituent Effects on the Rate of Decay of *p*-Benzosemiquinone Anion Radicals . . . **Alfred B. Sullivan and G. Fredric Reynolds*** 2671

A Fractional Charge Model in the Molecular Orbital Theory and Its Application to Molecules in Solutions and Solids . . . . . **J. Oakey Noell and Keiji Morokuma*** 2675

Molecular Orbital Calculations on the Optical Activity of Chiral Benzene Derivatives . . . **Harry Dickerson and Frederick S. Richardson*** 2686

Protonation of the 1-(Phenylazo)-2-naphtholhydrazone Tautomer: A CNDO Study . . . **Richard W. Bigelow** 2694

Ultrasonic Relaxation of $Cu(ClO_4)_2$ and $Cu(NO_3)_2$ in Ethylene Glycol . . . **M. Vincenzini, B. Sesta, M. Battistini, and S. Petrucci*** 2700 ■

COMMUNICATIONS TO THE EDITOR

Alleged Solubility Product Variability at Constant Pressure and Temperature . . . **Kenneth S. Pitzer** 2707

On the Variable Solubility Product of Calcium Fluoride . . . **Gary L. Bertrand* and Thomas E. Burchfield** 2707

Solubility Product Variability at Constant Pressure and Temperature . . . . **Walter E. Brown** 2708

Reply to Comments on Solubility Product Variation . **Robert I. Stearns and Alan F. Berndt*** 2709

Isotope Separation Using the Effect of Resonant Microwaves on the Rate of Triplet State Photochemistry in Solids . . . . . **Talal Akasheh and M. A. El-Sayed*** 2710

Stratospheric Formation and Photolysis of Chlorine Nitrate . . . **F. S. Rowland,* John E. Spencer, and Mario J. Molina** 2711

Estimated Relative Abundance of Chlorine Nitrate among Stratospheric Chlorine Compounds . . . **F. S. Rowland,* John E. Spencer, and Mario J. Molina** 2713

Additions and Corrections 2716

■ Supplementary material for this paper is available separately (consult the masthead page for ordering information); it will also appear following the paper in the microfilm edition of this journal.

* In papers with more than one author, the asterisk indicates the name of the author to whom inquiries about the paper should be addressed.

AUTHOR INDEX

Akasheh, T., 2710
Arce, R., 2629

Bartolomé, L., 2629
Battistini, M., 2700
Berndt, A. F., 2709
Bertrand, G. L., 2707
Bigelow, R. W., 2694
Bolts, J. M., 2641
Brown, W. E., 2708
Burchfield, T. E., 2707

Cordier, P., 2635

Dickerson, H., 2686

El-Sayed, M. A., 2710

Farhataziz, 2635

Haynes, H. W., Jr., 2656
Ho, T. H., 2656

Ise, N., 2661

Kale, K. M., 2651
Kitano, H., 2661

Lahmani, F., 2623
Lang, J., 2651
Lunsford, J. H., 2664

Molina, M. J., 2711, 2713
Morokuma, K., 2675

Noell, J. O., 2675

Okubo, T., 2661

Parcher, J. F., 2656
Petrucci, S., 2700
Pitzer, K. S., 2707

Reynolds, G. F., 2671
Richardson, F. S., 2686
Rowland, F. S., 2711, 2713

Sesta, B., 2700
Spencer, J. E., 2711, 2713
Stearns, R. I., 2709
Sullivan, A. B., 2671

Vincenzini, M., 2700

Weaver, M. J., 2645
Williamson, W. B., 2664
Wrighton, M. S., 2641

Yiv, S., 2651

Zana, R., 2651

THE JOURNAL OF
PHYSICAL CHEMISTRY

VOLUME 80, NUMBER 24 NOVEMBER 18, 1976

Reversibility of the Pressure-Induced Intersystem Crossing in Methylene

F. Lahmani

Laboratoire de Photophysique Moléculaire du CNRS, Université Paris Sud, 91405, Orsay, France *(Received January 15, 1976)*

Reactions of methylene with propane have been studied by measurement of the quantum yields of reaction products and the isobutane/*n*-butane ratios. Methylene was obtained by decomposition of diazirine through direct photolysis and by the triplet energy transfer from benzene and pyrazine. The results indicate that the primary product in the first case is $^1CH_2$ and in the latter $^3CH_2$. In the presence of inert gases the $^1CH_2/^3CH_2$ concentration ratio reaches a constant value which is independent of the primary reaction path. This effect may be explained in terms of the reversibility of the pressure-induced intersystem crossing. From a simple kinetic treatment the S–T energy gap in methylene may be estimated to be about 7.5 kcal/mol.

Introduction

In a number of works concerning reactions of methylene with propane, the following points have been well established:

Singlet methylene ($^1A_1$) inserts into a carbon–hydrogen bond of propane. The ratio of isomeric butanes resulting from this reaction is

$$R_{iB} = \frac{\text{isobutane}}{n\text{-butane}} = 0.40^1$$

The reaction of triplet methylene ($^3B_1$) with propane consists of hydrogen abstraction (formation of propyl and methyl radicals) followed by the customary reactions of combination and disproportionation of these radicals. The abstraction of secondary hydrogens vs. primary hydrogen atoms occurs with a probability higher by a factor 11–14.[2,3] This leads to a much higher value in the isobutane/*n*-butane ratio: $R_{iB} = 4$.

Singlet methylene is collisionally deactivated to triplet methylene. This pressure-induced S–T transition has been studied in detail by Eder and Carr[1] in ketene–propane–inert gas mixtures in presence of a few percent oxygen which acts as a very efficient scavenger of triplet methylene. On the other hand, Braun, Bass, and Pilling[4] have measured absolute rate constants for $^1CH_2 \rightarrow {}^3CH_2$ pressure-induced transitions by flash photolysis for several inert additives. In this case, because of the high concentration of transient species, $^3CH_2$ was shown to disappear in the bimolecular reaction $^3CH_2 + {}^3CH_2 \rightarrow C_2H_2 + H_2$. These two works do not contain any indication of a reverse T → S crossing at high pressure. Since the rate of this process should be much lower compared with the direct S → T crossing ($E_S - E_T \gg kT$), the reverse crossing could be hardly observed in presence of efficient scavenging reactions of the triplet methylene. More favorable conditions would be found in systems where the reactivity of the triplet is low as it is the case of aliphatic hydrocarbons[5] (e.g., propane). Since singlet methylene reacts very rapidly with propane,[6] one can expect a competition between the two processes:

$$^3CH_2 + C_3H_8 \rightarrow CH_3\cdot + C_3H_7\cdot$$

$$^3CH_2 + M \rightarrow {}^1CH_2 + M$$

As a matter of fact, insertion products (characteristic for $^1CH_2$) have been detected in systems containing a large excess of inert gas[3] where the collision rate would be sufficient to assure a complete depopulation of the singlet state. This result could be explained, as pointed out by Frey,[7] in terms of the reversibility of intersystem crossing in methylene. In order to have more quantitative information on this point, we have studied methylene–propane reactions using as the precursor of CH_2, diazirine either in its first singlet state, S_1, or in its triplet state, T_1, produced by energy transfer from benzene and pyrazine. Since the dissociation of the excited diazirine is a rapid process, an efficient intersystem crossing is not expected during the lifetime of the excited molecule. We can thus suppose that to conform ith the spin conservation rule, singlet methylene would be the primary product in the first case and triplet methylene in the latter. Thus a parallel study of the reaction products obtained in both cases would provide additional data about the reactivities of $^1CH_2$ and $^3CH_2$ and their interconversion rates.

Experimental Section

Chemicals. Diazirine was synthetized in small amounts according to the method described by Schmitz and Ohme[8] from methylenebis(ammonium sulfate) treated with hypochlorite (Dr. P. Le Perchec (Laboratoire des Carbocycles Orsay) is greatfully acknowledged for his help in the synthesis of diazirine). The product was swept by N_2, dried over BaO, and trapped in liquid nitrogen. After pumping off the gaseous nitrogen, diazirine was distilled under vacuum at −120 °C.

Propane, SF_6, butane, isobutane, ethylene, and ethane were products from l'Air liquide.

Pyrazine (Fluka) and benzene (Merck) were dried with BaO and distilled under vacuum.

Irradiation. Most of the photolysis experiments were carried out in a 20-ml (5-cm optical path) cylindrical cell closed with a grease-free stopcock. In the case of the benzene photosensitization experiments, a parallelipiped cell of 1 cm optical path and a volume of 8 ml was used. The cell was filled on a conventional high vacuum system. Vapors were expanded into a known volume (140 cm^3). The pressure was read on a thermocouple gauge calibrated for each gas by means of a MacLeod gauge or Bourdon type gauge and then condensed in liquid N_2 in a side arm of the photolysis cell. Mixing of the gases was assured by several freezing–warming cycles. The pressure of diazirine was controlled by measuring its absorption spectrum on a Cary 14 spectrophotometer ($\epsilon_{315\ nm}$ 410 M^{-1} cm^{-1}). The irradiation set up consisted of a water cooled 1000-W high-pressure SP 1000 Phillips mercury lamp; its light emitted in the 280–330-nm spectral region was reflected by a dielectric mirror and focused on the entrance slit of a M 25 Jobin Yvon monochromator. The main part of the cell volume was illuminated with a parallel beam which was then focused on the window of a thermopile (Hilger and Watts FT 16) used to monitor the transmitted light intensity under different experimental conditions. Absolute light intensities were measured by ferrioxalate actinometry described by Parker.[9] In the case of the benzene sensitization work, a low pressure mercury lamp was used with a chlorine filter (40-mm thickness, p = 1 atm) to prevent direct photolysis of diazirine in the 313-nm region. Benzene sensitized cis–trans isomerization of 2-butene[10] was used for actinometry.

Analysis. The decrease of the diazirine concentration was determined by spectrophotometry with a Cary 14 apparatus. The quenching of the fluorescence of benzene and phosphorescence of pyrazine was measured on a Hitachi-Perkin-Elmer spectrofluorimeter. Product analysis was performed by means of a Hewlett-Packard 5700 A FID gas chromatograph, using Porapak Q or S columns (⅛-in. diameter, 2-m length) with the oven temperature programmed from 30 to 150 °C. Products were identified from the retention times of pure samples. The ratio of C_6 hydrocarbons which were not separated on Porapak columns were determined separately with a 4-m dibenzyl ether column at 0 °C. *cis*- and *trans*-butene were measured with a diethylene glycol–$AgNO_3$ column at room temperature.

The whole irradiated sample was transferred under vacuum into a 2-ml Pyrex loop at liquid nitrogen temperature. After warming, the products were injected in the gas chromatographic apparatus by means of a gas sampling valve. The response of the gas chromatograph was calibrated for all products under the same injection conditions with mixtures of known composition in the same range as the photolyzed sample. Diazirine, the concentration of which was determined by spectrophotometry for each experiment, was used as an internal standard.

Results

1. *Photolysis of Diazirine.* The major photochemical products are ethylene, ethane, and diazomethane as it has been shown previously by Amrich and Bell.[11]

The quantum yield of decomposition of diazirine (3 Torr $< p <$ 12 Torr), $\phi_{-d} = 2.3 \pm 0.3$, is independent of the wavelength of excitation for λ_{exc} 323, 320.5, 315, 312.3, 307, and 300 nm ($\Delta\lambda$ = 1 nm). As long as only a small part of diazirine (<5%) is decomposed, the quantum yield of ethylene and ethane are $\phi_{C_2H_4} = 0.15 \pm 0.015$, $\phi_{C_2H_6} = 0.16 \pm 0.016$ for p(diazirine) = 8 Torr. Addition of SF_6 with an increasing pressure to 1 Torr of diazirine causes a decrease in the ratio of ethane to ethylene at 315 nm: C_2H_4 was shown to increase as the pressure of inert gas was increased up to 20 Torr while C_2H_6 remains constant. On the other hand, ethane is completely quenched and the ethylene yield decreases by a factor of 2 when 0.5 Torr of oxygen is added to 3 Torr of diazirine. These observations suggest that ethylene is due partially to the reaction of $^3CH_2$ with diazirine but give no information on the mechanism for production of ethane. Diazomethane was identified by its absorption spectrum in the 210–240-nm region. Its yield does not show a linear dependence on the number of photons absorbed but reaches a plateau which depends on the initial pressure of diazirine. The initial quantum yield of diazomethane calculated from optical density measurements at 217 nm (ϵ 13 400 M^{-1} cm^{-1})[12] is $\phi_{diazo} = 0.7 \pm 0.1$ for p(diazirine) = 11 Torr. In order to prevent the secondary destruction of diazomethane, we added to diazirine (3 Torr $< p <$ 11 Torr) acetic acid (p = 0.3 Torr) which reacts very rapidly with diazomethane (resulting in the formation of methyl acetate) but which does not react with diazirine, and does not influence the yield of ethylene and ethane. The concentration of methyl actate, which is a measure of the primary product, grows linearly with the number of photons absorbed, and its yield does not depend on the excitation energy (λ_{exc} 323, 320.5, 315, 307, and 300 nm). The formation of diazomethane was totally quenched by addition of 15 Torr of propane to 3 Torr of diazirine but was only partially suppressed in the presence of oxygen ($p(O_2)$ = 1 Torr). This result indicates that diazomethane is not a primary product of the photolysis of diazirine, and that some singlet methylene is involved in its formation.

2. *Photolysis of Diazirine–Propane Mixtures at 315 nm.* The major products were ethylene, ethane, n-butane, and isobutane (higher hydrocarbons have not been analyzed). The quantum yield of diazirine decomposition is $\phi_{-d} = 1.1 \pm 0.2$ for a propane–diazirine concentration ratio >30 and a total pressure of 25 Torr. The quantum yield of products are reported in Table I. Ethylene, which probably results from methylene reacting with diazirine, decreases with addition of propane as expected. Ethane, which should be mainly produced from propane–triplet methylene reactions at higher pressures of propane, was also shown to be formed in the photolysis of pure diazirine (see above). This could explain the observed quantum yield of ethane at low propane pressures. The yield of butane can be systematically underestimated if the "hot" butane resulting from the $^1CH_2$ insertion in propane is not totally stabilized in the pressure range used. This effect would, however, induce an increase of ϕ_B at higher pressures. Since no such increase was observed (see Table I), this effect is of minor importance in our experiments. The ratio of isomeric butanes, R_{iB} = iB/nB = 0.52 ± 0.03, is in agreement with Frey and Stevens.[13] In presence of a small amount of oxygen (0.1–0.2 Torr) which acts as a $^3CH_2$ scav-

TABLE I: Quantum Yields and R_{iB} Values in the Photolysis of Diazirine–Propane Mixtures [a]

p(diazirine), Torr	$p(C_3H_8)$, Torr	$p(SF_6)$,[b] Torr	$p(O_2)$, Torr	$\phi_{C_2H_4}$	$\phi_{C_2H_6}$	ϕ_{iB+nB}	R_{iB}[c]
0.50	7			0.105	0.17	0.60	0.48
0.37	12			0.095	0.19	0.70	0.50
0.72	25			0.053	0.16	0.64	0.50
0.40	36			0.026	0.165	0.685	0.55
1.05	24		0.2		0	0.57	0.39
0.62	55		0.2		0	0.55	0.40
3				0.15	0.15		
3	15			0.080	0.13	0.335	0.52
3	16		0.1	0.050	0	0.315	0.41
0.45	14	200				0.40	0.7
0.45	15	400				0.27	0.95
0.45	14.5	600				0.23	1.07
0.70	10.4	800				0.21	1.1
0.70	13	800	0.4			0.05	0.39

[a] λ_{exc} 315 ± 1.2 nm; $3 < I < 10 \times 10^{-8}$ einstein. [b] $\phi_{C_2H_4}$ and $\phi_{C_2H_6}$ have not been measured in the presence of SF_6. [c] R_{iB} = iB/nB.

enger, ϕ(butane) is about 10% lower than in the absence of oxygen, ethane is totally suppressed, and $R_{iB} = 0.40 \pm 0.02$ corresponding to the well-known ratio for isomeric butanes formed by insertion of $^1CH_2$ into the C–H bonds of propane. On the other hand, R_{iB} increases when an inert gas (SF_6) is added to diazirine (0.45 Torr) and propane (14 Torr) (see Figure 1a, Table I).

3. *Triplet Sensitized Photochemistry of Diazirine.* Two gas phase triplet sensitizers have been used to study the photochemistry of triplet diazirine in presence of propane: pyrazine, E_T = 72 kcal/mol, ϕ_T = 1,[14] and benzene, E_T = 85 kcal/mol, ϕ_T = 0.7.[9,12] The energy of the lowest triplet state of diazirine is not known experimentally since no phosphorescence has been reported, but it has been estimated theoretically at 3.2 eV (73.5 kcal/mol).[15] The triplet state of dimethyldiazirine has been directly observed by absorption at 421 nm (E_T = 68 kcal/mol).[16]

(a) *Pyrazine–Diazirine–Propane Systems.* Pyrazine was excited in a hot ban at 326 nm ($\Delta\lambda$ = 1 nm). At this wavelength, no direct decomposition of diazirine (0–0 absorption band at 323 nm) was found. The quantum yields of C_2H_4, C_2H_6, C_4H_{10}, and C_6H_{14} at increasing propane pressure are reported in Table II. The propane was added to a mixture of 0.35 Torr diazirine and 3.5 Torr of pyrazine. Under these conditions the phosphorescence of pyrazine was totally quenched. Plots of $1/\phi$ for C_2H_6, C_4H_{10}, and C_6H_{14} against $1/p$ may be approximated by straight lines as shown in Figure 2. The quantum yields extrapolated to infinite pressure of propane are $\phi_{C_2H_6}$ = 0.32, $\phi_{C_4H_{10}}$ = 0.28, and ϕ_{C_6} = 0.055. The ratio of isomeric butanes, R_{iB} = 2.4 ± 0.2, is independent of the propane pressure. When SF_6 is added to a mixture of pyrazine (3.5 Torr), diazirine (0.35 Torr), and propane (14 Torr) R_{iB} decreases (Figure 1b).

(b) *Benzene–Diazirine–Propane Systems.* Quantum yields of C_2, C_4, and C_6 hydrocarbons in benzene photosensitized decomposition of diazirine in the presence of propane are shown in Table III and Figure 3. Under our experimental conditions (p(benzene) = 1.6 Torr, p(diazirine) = 0.6 Torr) the role of singlet–singlet energy transfer should be of minor importance since benzene fluorescence was not quenched (<10%) by diazirine. The quantum yield of benzene sensitized decomposition of diazirine in the presence of propane (25 Torr) is $\phi_{-d} = 0.7 \pm 0.07$ and is not changed by the addition of 320 Torr of SF_6. This value is in good agreement with the triplet yield of benzene and indicates that the energy transfer from triplet benzene to diazirine is total for 0.6 Torr of diazirine and that every triplet diazirine resulting from the transfer dissociates. Besides ethylene and ethane, acetylene was found in the C_2 products. The formation of acetylene is probably due to the bimolecular recombination of triplet methylene followed by H_2 elimination:

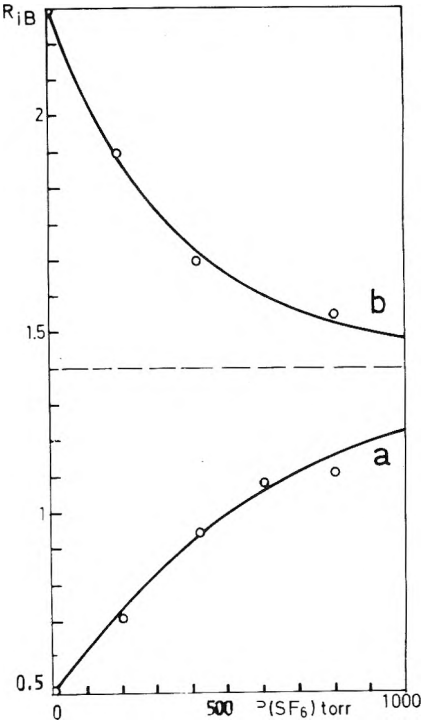

Figure 1. Ratio of isomeric butanes R_{iB} as a function of the pressure of SF_6: (a) λ_{exc} 315 ± 0.1 nm, p(diazirine) = 0.45 Torr, p(propane) = 15 Torr; (b) λ_{exc} 326 ± 0.1 nm, p(pyrazine) = 3.5 Torr, p(diazirine) = 0.35 Torr, p(propane) = 14 Torr.

$$^3CH_2 + {}^3CH_2 \rightarrow C_2H_4^* \rightarrow C_2H_2 + H_2$$

as has been previously shown by Braun, Bass, and Pilling[4] in flash photolysis experiments. The light intensity in these experiments was about a factor of 20 higher than in the case of pyrazine photosensitization ($I = 2.8 \times 10^{13}$ photons cm^{-3} s^{-1}). This difference may explain why C_2H_2 is not formed in the latter case.

The three isomeric C_6 hydrocarbons resulting from C_3H_7· radical combination are formed in the ratio n-hexane/2-methylpentane/2,3-dimethylbutane: 1/8/16. From this ex-

TABLE II: Quantum Yields and R_{iB} Values for Pyrazine Photosensitization of Diazirine in the Presence of Propane [a]

p(propane), Torr	p(SF_6), Torr	$\phi_{C_2H_4}$	$\phi_{C_2H_6}$	ϕ_{iB+nB}	ϕ_{C_6}	R_{iB}
12.5		0.054	0.144	0.159	0.023	2.4
14		0.057	0.153	0.163	0.026	2.3
21.5		0.043	0.18	0.177	0.031	2.44
32		0.045	0.24	0.213	0.037	2.38
47		0.041	0.23	0.224	0.041	2.6
54		0.035	0.256	0.236	0.041	2.38
158		0.015	0.28	0.22	0.048	2.40
17	400			0.20		1.7
15	800			0.22		1.58

[a] p(pyrazine) = 3.5 Torr; p(diazirine) = 0.35 Torr; λ_{exc} 326 ± 1 nm.

TABLE III: Quantum Yields and R_{iB} Values for Benzene Sensitization of Diazirine in the Presence of Propane [a]

p(propane), Torr	p(SF_6), Torr	$\phi_{C_2H_4}$	$\phi_{C_2H_6}$	$\phi_{C_2H_2}$	$\phi_{C_4H_{10}}$	ϕ_{C_6}	R_{iB}
0		0.081	0.027	0.107			
7		0.12	0.065	0.055	0.083		1.25
8.3		0.122	0.070	0.052	0.086	0.009	1.35
12		0.107	0.085	0.046	0.115		1.7
13.5		0.096	0.077	0.035	0.120	0.0135	1.6
25		0.125	0.12	0.029	0.19	0.033	1.7
26		0.125	0.125	0.0275	0.18		1.85
27	300				0.21		1.45
53		0.095	0.173	0.012	0.224	0.041	2.06
85		0.080		0.008	0.27	0.050	2.2

[a] λ_{exc} 253.7 nm. p(benzene) = 1.6 Torr; p(diazirine) = 0.6 Torr. ϕ's are expressed relative to the quantum yield of triplet benzene.

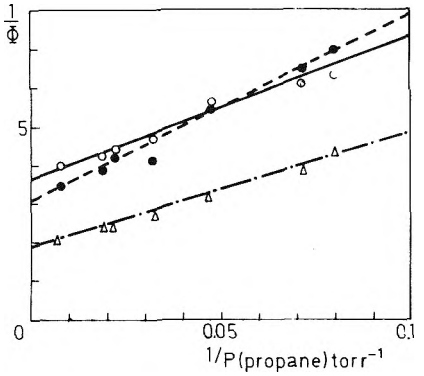

Figure 2. Pyrazine photosensitized decomposition of diazirine in the presence of propane. Plot of $1/\phi$ against the reciprocal of propane pressure: p(pyrazine) = 3.5 Torr, p(diazirine) = 0.35 Torr, λ 326 ± 1 nm; (—) butane, (- - - -) ethane, (- · - · -) C_6H_{14}.

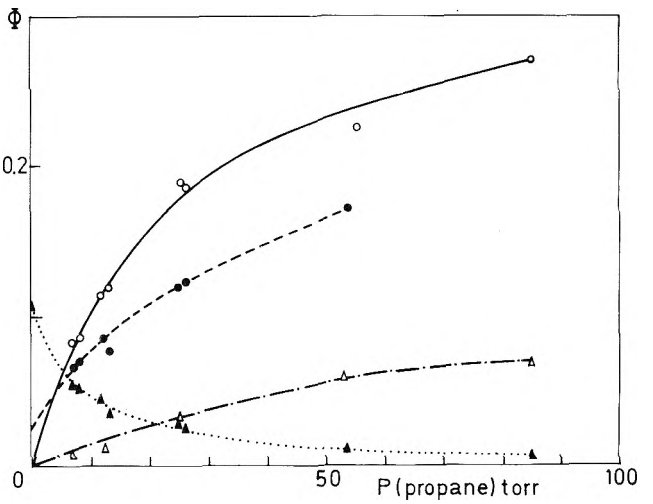

Figure 3. Quantum yield of products in benzene photosensitized decomposition of diazirine: p(benzene) = 1.6 Torr, p(diazirine) = 0.6 Torr, λ_{exc} 253.7 nm; (—) butane, (- - - -) ethane, (- · - · -) C_6H_{14}, (· · · ·) C_2H_2.

perimental ratio and the knowledge of the relative rate constants of disproportionation and combination of C_3H_7· radicals,[3] one can deduce the ratio of the stationary concentration of isopropyl radicals relative to that of *n*-propyl radicals as $[isopropyl]_{st}/[n\text{-}propyl]_{st}$ = 4.6. This ratio corrected for the disproportionation between CH_3· and C_3H_7· radicals gives R_{iB} = 4 for isomeric butanes resulting from triplet methylene. This result is in good agreement with the value found by Ho and Noyes[2] for ketene–propane mixtures and that of Ring and Rabinovitch[3] for diazomethane–propane–inert gas systems.

Table III shows that R_{iB} increases with the pressure of propane up to an extrapolated value of 2.3. This effect shows that a greater participation of $^1CH_2$ insertion products for low pressures of propane could be indicative of some energy transfer from singlet benzene to singlet diazirine. Under these conditions the propane pressure is not high enough to scavenge all triplet methylene and other reactions (e.g., $^3CH_2$ + CH_2N_2) may take place, while the singlet methylene is efficiently scavenged. Thus, even a low participation of singlet–singlet energy transfer (5%) would influence greatly the experimental ratio of isomeric butanes.

Addition of a foreign gas (400 Torr of SF_6) produces a decrease of R_{iB} as observed in pyrazine triplet energy transfer experiments.

Discussion

As has been shown before (with diazomethane and ketene as the sources of methylene) and confirmed in this work for the case of diazirine, the ratio of isomeric butanes resulting

from methylene reactions with propane is $R_{iB_1} = 0.4$ for $^1CH_2$ insertion reaction and $R_{iB_3} = 4$ for $^3CH_2$ hydrogen abstraction and subsequent combination of radicals.

From the experimental value of $R_{iB} = (iB_1 + iB_3)/(nB_1 + nB_3)$ and the known ratios R_{iB_1}, $iB_1/nB_1 = 0.4$ and $R_{iB_3} = iB_3/nB_3 = 4$ we can calculate the ratio of butane resulting from singlet methylene–B_1 and from triplet methylene–B_3 reactions (the subscripts 1 and 3 refer respectively to $^1CH_2$ and $^3CH_2$ reactions products):

$$\frac{B_1}{B_3} = \frac{nB_1 + iB_1}{nB_3 + iB_3} = \frac{1 + R_{iB_1}}{1 + R_{iB_3}}\left(\frac{R_{iB_3} - R_{iB}}{R_{iB} - R_{iB_1}}\right)$$

In the case of direct photolysis of diazirine

$$R_{iB} = 0.52 \pm 0.03 \qquad B_1/B_3 = 8.1 \pm 2.7$$

In the case of triplet photosensitization

$$R_{iB} = 2.4 \pm 0.2 \qquad B_1/B_3 = 0.22 \pm 0.09$$

At high pressures of added inert gas, the ratio of isomeric butane tends to the same limiting value $R_{iB} = 1.4 \pm 0.1$ independent of the primary excitation path corresponding to a ratio $B_1/B_3 = 0.73 \pm 0.11$.

The simplest explanation of this behavior may be given if it is assumed that the collision induced intersystem crossing is reversible in methylene and that the $^1CH_2 \rightleftarrows {}^3CH_2$ equilibrium is established at sufficiently high gas pressure. The process may be tentatively described by the following kinetic schemes.

(A) *Singlet Diazirine Dissociation*

$$CH_2N_2 \xrightarrow{h\nu} {}^1CH_2N_2$$

$$^1CH_2N_2 \xrightarrow{k_S} {}^1CH_2 + N_2 \qquad (1)$$

$$^1CH_2 + p \underset{k_{TS}}{\overset{k_{ST}}{\rightleftarrows}} {}^3CH_2 + p \qquad (2) \quad (2')$$

$$^1CH_2 + C_3H_8 \xrightarrow{k_{1p}} C_4H_{10} \qquad (3)$$

$$^1CH_2 + \text{diazirine} \xrightarrow{k_{1d}} C_2H_4, \text{ other products} \qquad (4)$$

$$^3CH_2 + C_3H_8 \xrightarrow{k_{3p}} CH_3\cdot + C_3H_7\cdot \qquad (5)$$

$$^3CH_2 + \text{diazirine} \xrightarrow{k_{3d}} C_2H_4, \text{ other products} \qquad (6)$$

(B) *Triplet Diazirine Dissociation*

$$^3S + \text{diazirine} \xrightarrow{k_{ET}} {}^3CH_2N_2 \qquad (7)$$

$$^3CH_2N_2 \xrightarrow{k_T} {}^3CH_2 + N_2 \qquad (8)$$

$$^3CH_2 + p \underset{k_{ST}}{\overset{k_{TS}}{\rightleftarrows}} {}^1CH_2 + p \qquad (2') \quad (2)$$

$$^3CH_2 + {}^3CH_2 \xrightarrow{k_\varepsilon} C_2H_2 + H_2 \qquad (9)$$

$$^3CH_2 + \text{propane} \xrightarrow{k_{3p}} CH_3\cdot + C_3H_7\cdot \qquad (5)$$

$$^3CH_2 + \text{diazirine or donor} \xrightarrow{k_{3x}} X \qquad (10)$$

$$^1CH_2 + \text{propane} \xrightarrow{k_{1p}} C_4H_{10} \qquad (3)$$

$$^1CH_2 + \text{diazirine or donor} \xrightarrow{k_{1x}} X \qquad (11)$$

^3S is a triplet sensitizer.

In these two schemes we assume that the only primary process is a very rapid dissociation from singlet diazirine to singlet methylene and from triplet diazirine to triplet methylene. We have therefore neglected radiationless paths from $^1CH_2N_2$ to $^3CH_2N_2$ followed by photochemical decomposition to $^3CH_2$ in the first case and from $^3CH_2N_2$ to the hot ground state of diazirine followed by thermal decomposition to $^1CH_2$ in the second one. Such an assumption can be justified in the first case by considering the quantum yield of butane in the presence of oxygen. $\phi_{BO_2} = 0.60 \pm 0.06$ should be equal to the ratio $k_{1p}/k_{1p} + k_{ST}$ and can be compared with the value of this ratio determined by Bell[6] provided it does not depend on the precursor of $^1CH_2$.[4] According to the result of Bell, $k_{1p}/k_{1p} + k_{ST} = 0.73 \pm 0.20$. Both values fall in the same limit of error. It seems, therefore, that S_1 to T_1 intersystem crossing in diazirine can be neglected. On the other hand, in the triplet sensitized experiments, assuming an eventual intersystem crossing from $^3CH_2N_2$ to hot ground state $CH_2N_2^*$, the addition of high pressures of SF_6 would have the effect of inducing vibrational relaxation of $CH_2N_2^*$, thus reducing the quantum yield of diazirine decomposition. It has been found that on benzene sensitization, the quantum yield of decomposition of diazirine was not influenced by the presence of 320 Torr of SF_6. Moreover, if $^1CH_2$ can be produced by a process different from reaction 2, an increase of R_{iB} would be expected with increasing pressures of propane: in the low propane pressure range, $k_{1p}[p] > k_{1d}[d]$ is still assured whereas $k_{3p}[p] > k_{3x}[d + S]$ is not satisfied and a larger participation of $^1CH_2$ in the butane yield should be obtained as the pressure of propane is lowered. It has been shown that R_{iB} is constant in the pyrazine sensitization experiments but increases with propane pressure in benzene sensitization experiments. This differing behavior can be explained by a small participation of singlet energy transfer from singlet benzene.

Under steady state conditions at pressures of propane high enough to assure $k_{3p}(p) > k_{3d}(d)$ or $k_{3x}(d + S)$ and $k_{1p}(p) > k_{1d}(d)$ or $k_{1x}[d + S]$, one can estimate the relative yields of butane resulting from $^1CH_2$ or $^3CH_2$ reactions with propane. In the case of singlet diazirine dissociation:

$$\frac{\phi_{B_1}}{\phi_{B_3}} = \frac{1}{f}\frac{k_{1p}}{k_{3p}}\frac{k_{3p} + k_{TS}^p}{k_{ST}^p} \qquad (I)$$

In the case of triplet diazirine dissociation:

$$\frac{\phi_{B_1}}{\phi_{B_3}} = \frac{1}{f}\frac{k_{1p}}{k_{3p}}\frac{k_{TS}^p}{k_{ST}^p + k_{1p}} \qquad (II)$$

In presence of inert gas where the equilibrium between triplet and singlet methylene is rapidly established:

$$\frac{\phi_{B_1}}{\phi_{B_3}} = \frac{1}{f}\frac{k_{1p}}{k_{3p}}\frac{k_{TS}^M}{k_{ST}^M} \qquad (III)$$

where f represents the fraction of radicals produced in reaction 5 which combine to form the isomeric butanes B_3. k_{ST}^p, k_{TS}^p, k_{ST}^M, and k_{TS}^M are the rate constants for direct and reverse intersystem crossing for propane and for SF_6, respectively. Although the rate constants k_{ST} have been shown to be approximately proportional[1] to the polarizability of the gas, the ratio k_{TS}/k_{ST} should not depend on the nature of the CH_2 collision partner. In order to determine the equilibrium con-

stant between $^1CH_2$ and $^3CH_2$ at room temperature using eq I, II, or III, a knowledge of f and k_{1p}/k_{3p} is required.

(a) *Determination of f.* Kinetic schemes A and B imply that $\phi_{B_1} + \phi_{B_3} = 1$ at high pressures of propane for the direct photolysis of diazirine as well as for the triplet photosensitization. In the first case: $\phi_{B_1} + \phi_{B_3} = 0.70 \pm 0.07$; $\phi_{B_1}/\phi_{B_3} = 8.1 \pm 1.6$; and $f = 0.20 \pm 0.06$. In the second case: $\phi_{B_1} + \phi_{B_3} = 0.27 \pm 0.03$; $\phi_{B_1}/\phi_{B_3} = 0.22 \pm 0.04$; and $f = 0.23 \pm 0.06$. The difference in f values is within the error limit.

(b) *Determination of* k_{1p}/k_{3p}. The rate constant k_{1p} for insertion of $^1CH_2$ in CH bonds of propane is known from the data of Bell:[6] $k_{1p} = 6.3 \pm 1.7 \times 10^{-12}$ cm^3 mol^{-1} s^{-1}. On the other hand, the measurement of acetylene quantum yields in benzene sensitization experiments in the absence and in the presence of propane allow the estimation of k_{3x} and k_{3p} relative to the rate constant k_a of reaction 9. k_a has been determined from flash photolysis experiments as $k_a = 5.3 \pm 1.5 \times 10^{-11}$ cm^3 mol^{-1} s^{-1}.[4] Kinetic scheme B yields the stationary concentration of $^3CH_2$:

$$[^3CH_2]_{ss} = \sqrt{\frac{I\phi_T\phi_{C_2H_2}}{k_a}}$$

where $I\phi_T$ is the rate of photon absorption multiplied by the quantum yield of triplet benzene and is equal to $2 \pm 0.2 \times 10^{13}$ mol s^{-1} cm^{-3} under our experimental conditions. In the absence of propane:

$$\phi^0_{C_2H_2} = \frac{k[^3CH_2]_{ss}^0}{k[^3CH_2]_{ss}^0 + k_{3x}(d + S)} = 0.106$$

$[^3CH_2]_{ss}^0 = 2 \times 10^{11}$ mol cm^{-3} and $k_{3x}(d + S) = 90$ s^{-1}. Assuming that benzene ($p = 1.6$ Torr) reacts more slowly than diazirine ($p = 0.6$ Torr) with $^3CH_2$, an upper limit for k_{3x} can be determined: $k_{3x} = 4 \pm 2 \times 10^{-15}$ cm^3 mol^{-1} s^{-1}. In the presence of 26 Torr of propane and under the same excitation conditions, $\phi_{C_2H_2}$ is reduced by a factor of 4

$$\phi_{C_2H_2} = \frac{k[^3CH_2]_{ss}}{k[^3CH_2]_{ss} + k_{3x}(d + S) + \left(k_{3p} + k_{TS}{}^p \frac{k_{ST}}{k_{ST} + k_{1p}}\right) \times (p)} = 0.026$$

thus the stationary concentration of $^3CH_2$ in this case is $(^3CH_2)_{ss}{}^p = 10$ mol cm^{-3} and

$$k_{3p} + k_{TS}\frac{k_{ST}}{k_{ST} + k_{1p}} = 1.3 \pm 0.4 \times 10^{-16} \text{ cm}^3 \text{ mol}^{-1} \text{ s}^{-1}$$

The experimental value of B_3/B_1 in eq II shows that $k_{TS}[k_{ST}/(k_{ST} + k_{1p})]$ can be neglected relative to k_{3p}. This estimation leads to a value for the ratio $k_{1p}/k_{3p} = 5 \pm 2 \times 10^4$. At high pressures of SF_6, where the equilibrium between singlet and triplet methylene is established, eq III yields the equilibrium constant:

$$K_M = \frac{[^1CH_2]}{[^3CH_2]} = \frac{k_{TS}{}^M}{k_{ST}{}^M} = 3.4 \pm 1.7 \times 10^{-6}$$

This value can be compared with the equilibrium constant for propane, K_p, calculated using either eq I or II, taking the value $k_{1p}/k_{1p} + k_{ST} = 0.60 + 0.06$ from our quantum yield measurements and taking $f = 0.21$. Equation I yields $K_p = k_{TS}{}^p/k_{ST}{}^p = 4 \pm 2 \times 10^{-6}$. Equation II yields $K_p = 2.33 \pm 1.2 \times 10^{-6}$. These results are in fairly good agreement.

From the constant K, one can calculate the energy difference between $^3CH_2$ and $^1CH_2$: ΔE_{TS}

$$K = \frac{Q_{R(^1CH_2)}}{Q_{R(^3CH_2)}} \frac{Q_{S(^1CH_2)}}{Q_{S(^3CH_2)}} e^{-\Delta E_{T\text{-}S}/RT}$$

where Q_R and Q_S are respectively the rotational and spin partition function for $^1CH_2$ and $^3CH_2$ (the vibrational partition function is not expected to introduce an important factor at room temperature since all vibrational frequencies are probably higher than 1000 cm^{-1}).[16] The ratio of rotational partition functions have been estimated using the rotational constants given by Herzberg.[17] One obtains $\Delta E_{T\text{-}S} = 7.5 \pm 0.7$ kcal/mol. This value is in fairly good agreement with the value deduced by Frey[7,22] from kinetic considerations similar to those described in this work, but much higher than those deduced from other experimental data which indicate very small energy separations of about 1–2 kcal/mol[18] and 2.5 kcal/mol.[19] As the rate constant for $^1CH_2$ insertion is several orders of magnitude higher than that of hydrogen abstraction by $^3CH_2$, no products of triplet methylene reactions with propane would be detected under our conditions for a small ΔE_{TS}. On the other hand, recent theoretical work[20,21] shows $\Delta E_{TS} = 11.5 \pm 2$ kcal/mol, which corresponds to an equilibrium constant $K \simeq 10^{-8}$. This value is certainly too high. In this case we would not be able to detect the products of singlet insertion. It is, however, to be pointed out that $\Delta E_{T\text{-}S}$ determined in this way is very sensitive to the k_{1p}/k_{3p} ratio. From our results we found $k_{1p}/k_{3p} \simeq 5 \times 10^4$, but estimates given by other authors vary between $\sim 10^2$ [4] and 10^7.[5] A more precise determination of k_{1p} and k_{3p} rate constants would be necessary in order to increase the accuracy of the $\Delta E_{T\text{-}S}$ evaluation.

References and Notes

(1) T. W. Eder and R. W. Carr, *J. Chem. Phys.*, **53**, 2258 (1970).
(2) S. H. Ho and W. A. Noyes, Jr., *J. Am. Chem. Soc.*, **39**, 5091 (1967).
(3) D. F. Ring and B. S. Rabinovitch, *Can. J. Chem.*, **46**, 2435 (1968).
(4) W. Braun, A. M. Bass, and M. Pilling, *J. Chem. Phys.*, **52**, 5232 (1970).
(5) F. S. Rowland, P. S. T. Lee, D. C. Montague, and R. L. Russell, *Discuss. Faraday Soc.*, **53**, 111 (1972).
(6) J. A. Bell, *J. Phys. Chem.*, **75**, 1537 (1971).
(7) H. M. Frey, *J. Chem. Soc., Chem. Commun.*, 1024 (1972).
(8) E. Schmitz and R. Ohme, *Tetrahedron Lett.*, 612 (1961).
(9) C. A. Parker, "Photoluminescence of Solutions", Elsevier, Amsterdam, 1968, p 208.
(10) H. O. Denschlag and E. K. C. Lee, *J. Am. Chem. Soc.*, **90**, 3628 (1968).
(11) M. J. Amrich and J. A. Bell, *J. Am. Chem. Soc.*, **86**, 292 (1964).
(12) J. F. Ogilvie, *Photochem. Photobiol.*, **19**, 65–89 (1969).
(13) H. M. Frey and I. D. R. Stevens, *Proc. Chem. Soc.*, **72**, (1962).
(14) N. Ivanoff, F. Lahmani, J. F. Delouis, and J. L. LeGouil, *J. Photochem.*, **2**, 199 (1973).
(15) M. B. Robin, H. Basch, W. A. Kuebler, K. W. Wilberg, and G. R. Ellison, *J. Chem. Phys.*, **51**, 45 (1969).
(16) L. C. Robertson and J. A. Merritt, *J. Chem. Phys.*, **56**, 2919 (1972).
(17) G. Herzberg, "Electronic Spectra of Polyatomic Molecules", Van Nostrand, Princeton, N.J., 1966, pp 583–584.
(18) R. W. Carr, T. W. Eder, and M. G. Topor, *J. Chem. Phys.*, **53**, 4716 (1970).
(19) M. L. Halberstadt and J. R. Nesby, *J. Am. Chem. Soc.*, **89**, 3417 (1967).
(20) C. F. Bender, H. F. Schaefer, III, D. R. Franceschetti, and L. C. Allen, *J. Am. Chem. Soc.*, **94**, 6888 (1972).
(21) P. J. Hay, W. J. Hunt, and W. A. Goddard, *Chem. Phys. Lett.*, **13**, 30 (1972).
(22) H. M. Frey and G. J. Kennedy, *J. Chem. Soc., Chem. Commun.*, 233 (1975).

Photobromination of Liquid 3-Methylpentane

R. Arce* and L. Bartolomé

Department of Chemistry, University of Puerto Rico, Rio Piedras, Puerto Rico 00931 *(Received December 29, 1975; Revised Manuscript Received August 9, 1976)*

Publication costs assisted by the University of Puerto Rico

The photochemical bromination of liquid 3-methylpentane was studied in the temperature range between 210 and 298 K to compare the liquid phase reactions with those in the gas phase. The quantum yield of Br_2 consumption varies from 0.06 at 210 K at an absorbed light intensity of 5.82×10^{15} photons cm^{-3} s^{-1} and an initial bromine concentration of 1.8×10^{-3} M to 524 at 298 K at an absorbed light intensity of 2.50×10^{14} photons cm^{-3} s^{-1} and initial bromine concentration of 1.7×10^{-3} M. The activation energy for the overall reaction is found to be 11 kcal/mol. Quantum yields have been determined for the formation of HBr and 3-methylpentyl bromides and are of the same order of magnitude as the yield for bromine consumption at 298 K. Kinetic studies show that the initial rate of bromine disappearance depends on the 0.6 power of the absorbed light intensity and on the 0.6 power of the initial bromine concentration. These results and the high quantum yields indicate that the bromination goes through an atom–radical chain mechanism. Hydrogen bromide and oxygen inhibit the reaction. The relative rate of substitition for tertiary relative to secondary hydrogen atoms is 42, and that for tertiary relative to primary is larger than 10^4. A comparison is made with previous photochlorination studies in 3-methylpentane.

Introduction

Gas phase photobromination of simple alkanes have been extensively studied by Van Artsdalen and co-workers.[1–4] Recently free radical bromination reactions have been reviewed by Thaler[5] and by Poutsma.[6] Irradiation of gaseous molecular bromine with 420-nm light produces dissociation of the molecule into two ground state atoms, each formed with 11 kcal/mol of kinetic energy. Although no conclusive kinetic studies of liquid phase photobromination of hydrocarbons are available, vapor phase investigations confirm that in the presence of a hydrocarbon the bromine atoms can initiate long, two-center chain reactions as follows:

$$Br_2 + h\nu\,(420\text{ nm}) \rightleftarrows 2Br + M \quad (1)$$

$$Br + RH \rightleftarrows R + HBr \quad (2)$$

$$R + Br_2 \rightarrow RBr + Br \quad (3)$$

$$Br + R \rightarrow RBr \quad (4)$$

$$R + R \rightarrow R_2 \quad (5)$$

From studies of the gas phase bromination of hydrocarbons it has been possible to determine values for the C–H bond dissociation energies and enthalpies of formation of the corresponding radicals.[1–4] Studies of relative reactivities in gas phase photobrominations have provided rate constants and activation energies for hydrogen abstraction by bromine atoms.[7,8]

The work reported here has been carried out to obtain quantitative data on the quantum yields of bromine consumption, hydrogen bromide and alkyl bromide formation in the photobromination of a branched alkane in the liquid phase, and to study the dependence on temperature and solvent rigidity. We have also obtained relative reactivities for the primary, secondary, and tertiary hydrogens and obtained evidence on the mechanism of termination of the photobromination. This study was designed to provide a comparison to previous studies of photobromination reactions in the gas phase.

The liquid solvent, 3-methylpentane (3MP), was used because it has been previously used as a rigid matrix for the study of trapped free radicals produced at 77 K by several techniques, and because its photobromination reactions could then be compared with previous photochlorination studies in 3MP.[9] In specific we were interested in comparing: (1) chain lengths, (2) the selectivity of chlorine and bromine with respect to the primary, secondary, and tertiary C–H bonds in 3MP, (3) the temperature at which the chain stops, and (4) the effect of temperature, matrix rigidity, and cage effects in both atom–radical chain reactions.

Experimental Section

Materials and Sample Preparation. Chemical Samples Co. 99% pure 3-methylpentane was purified by passage through 50-cm column of silica gel activated for 10 h at 425 °C and 100 cm of a mixture of aluminum oxide and silver nitrate to remove unsaturated compounds.[10] The effluent was degassed by the freeze–pump–thaw technique and by pumping on the liquid on a vacuum line, and finally stored over a sodium mirror. The only detectable impurity by gas chromatographic analysis was 2-methylpentane present at 0.5 mol %. The same procedure was used for the purification of cyclohexane (Fisher, spectroquality). Bromine (99.8%, Baker Analyzed) was bulb-to-bulb distilled under vacuum keeping the middle fraction. It was degassed by the freeze–pump–thaw technique, passed through a 15 cm column of P_2O_5 and finally stored on the vacuum line in a flask closed with a Delmar greaseless stopcock. To meter aliquots, the bromine-containing flask was surrounded by an ice–water bath and the bromine vapor was allowed to fill a flask of known volume at its vapor pressure.

Hydrogen bromide was generated from Baker Analyzed reagent aqueous HBr (47–49%) by reaction of the frozen solution with excess P_2O_5 on the vacuum line. The concentration of HBr was determined by a standard acid–base back titration discussed in the next section.

The cells used for irradiation were 1 × 1 cm i.d. square

quartz cells, Pyrex lollipop type cells of 2-cm pathlength, and 0.3 × 0.3 cm i.d. square quartz cells. Samples for irradiation were prepared as before.[9]

Irradiation Conditions. Illumination was provided by either an Osram HBO-200 W "super pressure" or an Osram HBO-500 W mercury arc and a Bausch and Lomb high intensity monochromator with a uv–visible grating using a band width at half-height of 15 nm centered at 420 nm. This arrangement gave an incident intensity of the order of 10^{13}–10^{16} photons cm^{-2} s^{-1}. The cells were kept in a reproducible position by a cell holder placed at the focus of the collimating lens of the monochromator. Light intensity variations were achieved by changing the distance between the collimating lens and the cell holder or by changing lamps (200 or 500 W).

Photolyses between 210 and 278 K in 1 × 1 cm i.d. quartz cells were done in a Model 20 Cryodine cryocooler (Cryogenic Tech. Inc.) with a liquid cell mount attached to the main cold head for cooling sealed samples. The liquid cell mount consisted of a drilled copper cylinder into which the quartz cell was fitted and with irradiation slots of an area of 1.1 cm^2. The mount was surrounded by a cylindrical aluminum vacuum chamber with quartz irradiation windows. The cell mount and cylindrical vacuum chamber were designed and constructed for us by Professor R. Arce-Blanco of the Physics Department, U.P.R. The temperature of the cell was monitored with a copper–constantan thermocouple positioned in direct contact with the cell and could be controlled to 2 K.

Actinometry and Quantum Yields Determination. For the purpose of determining quantum yields, the incident light intensity on the sample was measured by a ferrioxolate actinometer[11] both before and after each photolysis. The average of the two light intensities was used for the yield calculation. Fluctuations in light intensity during the experiments were of the order of 10%. For photolysis in the cryocooler, actinometry was done at room temperature before and after the photolysis at low temperatures.

The concentration of consumed bromine and the presence of 3-methylpentyl bromides formed by the photolysis were determined from the change in optical density of the sample at 420 and 220 nm, respectively, as measured with a Cary 14 spectrophotometer.

The initial quantum yield of Br_2 consumption was determined by two different calculation procedures similar to that of Johns.[12] By the first procedure, the quantum yield was determined from the slope of graph of $-d(Br_2)/dt$ vs. I_a where the change in concentration per unit time of irradiation at different intervals was obtained from the tangent to a graph of Br_2 concentration vs. irradiation time and I_a is the average absorbed light intensity in a given interval in units of photons cm^{-3} s^{-1}.

Quantum yields were also determined using the expression

$$\log (OD/OD_0) = (-\epsilon\Phi I_0/2.3) \int_0^t \left(\frac{1 - 10^{-OD}}{OD}\right) dt \quad (I)$$

by plotting $\log (OD/OD_0)$ vs. the integral and from the slope the quantum yield could be obtained. The integral was evaluated graphically from a graph of $(1 - 10^{-OD})/OD$ vs. irradiation time. Values of Φ agreed within the 15% experimental error of the measurement.

For the determination of the quantum yield of hydrogen bromide production, its concentration was determined by a standard acid–base back titration method. The equivalent point was determined either potentiometrically or using bromthymol blue as an indicator. After photolysis the sample was plunged into liquid nitrogen before the tip of the cell was broken, immediately after and on warming, the broken tip was submerged in 10 ml of NaOH of known concentration allowing the gaseous HBr to bubble through the basic solution. Finally the cell was washed with the same NaOH solution and then this NaOH solution was titrated with standard HCl. From the volume difference of a titration of 10 ml of NaOH blank and 10 ml of NaOH in which a photolyzed sample was poured into, the amount of HBr produced was calculated. In the calculation of the average absorbed light intensity for the HBr quantum yield determinations, the average optical density was calculated from changes in optical density of the order of 0.30 to 0.40 while in the bromine consumption yields the changes were from 0.05 to 0.10 OD units.

Alkyl bromides, dibromides, and hydrocarbon products were analyzed by gas chromatography with a Varian Aerograph Model 1400 gas chromatograph with flame ionization detector and nitrogen as the carrier gas in a 1.52 m × 0.32 cm i.d. stainless steel column packed with Varaport coated with 3% SE-30 at a column temperature of 45 °C and nitrogen flow rate of 30 ml min^{-1} or in a 2.56 m × 0.32 cm i.d. stainless steel column packed with 4% diisodecylphthalate on 60–80 mesh Chromosorb P at a column temperature of 80 °C and nitrogen flow rate of 40 ml min^{-1}. These columns gave adequate analytical separation of the products and the bromides were eluted in the order of their boiling points. The Varaport column was used mainly in the quantitative analysis to avoid decomposition of alkyl bromides because of shorter retention times and lower column temperatures. This column and conditions were also used in identification of the dibromides.

Identification of the alkyl bromides was based on a comparison of the retention time of the unknown compound with that obtained from a known 3-methylpentyl bromide either synthesized in our laboratory by treating the corresponding alcohol with aqueous HBr (47–49%) or from commercially available 3-(bromomethyl)pentane (Chemical Samples Corp.) and 3-bromo-3-methylpentane (Chemical Samples Corp.) at constant operating conditions. One of the dibromides was identified by comparing its retention time with that of 2,3-dibromo-3-methylpentane synthesized from the corresponding alkene. From plots of log (retention time) vs. boiling point of known compounds the boiling points of the unknowns were estimated.

The number of alkyl bromides molecules in photolyzed samples were determined from the area under each product peak assuming that they are proportional to the number of molecules injected. The integrated areas were compared to the areas under the peak of a standard solution of 3-(bromomethyl)pentane. The same detector sensitivity was assumed for this bromide as for the other 3MP bromides. The 3-(bromomethyl)pentane was added to photolyzed samples and used as an internal standard.

Results and Discussion

Absorption Spectrum and Extinction Coefficient of Br_2 in 3MP. The absorption spectrum of Br_2 dissolved in liquid 3MP has a maximum in the visible region at 420 nm similar to Br_2 gas[13] (Figure 1) but with slightly higher extinction coefficients. Analogously to chlorine dissolved in 3MP,[9] solutions of Br_2 in 3MP show an additional absorption in the 250–180-nm region which is absent in the gas. This absorption has been seen previously in Br_2–cyclohexane[14] and Br_2–*n*-

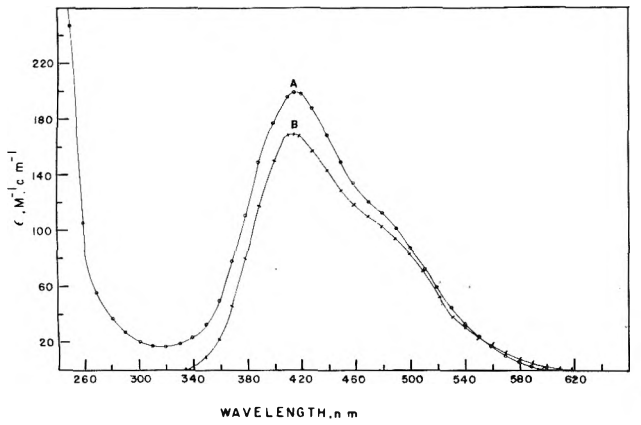

Figure 1. Absorption spectra of Br_2 (A) in the liquid 3MP at 298 K and (B) in the gas at 298 K.

heptane solutions[14] and assigned to a charge-transfer absorption.

The extinction coefficient of Br_2 in liquid 3MP was determined by the method previously described[9] for Cl_2. An initial Br_2 gas optical density of 0.294 in a volume of 12.2 ml was measured; after thorough mixing of the gaseous Br_2 with liquid 3MP (3.4 ml), about 95% of the Br_2 dissolved. The value of 200 ± 11 M^{-1} cm^{-1} at 420 nm obtained for the extinction coefficient of Br_2 in liquid 3MP compares to values reported for Br_2 in CCl_4 of 208[15] M^{-1} cm^{-1} and in cyclohexane of 200 M^{-1} cm^{-1}.[16] For gaseous Br_2, the absolute values of the extinction coefficients of Figure 1 are based on the literature value of 169 M^{-1} cm^{-1} [13] at 420 nm.

Bromine Quantum Yields, $\Phi(-Br_2)$. The initial quantum yield for Br_2 disappearance at 298 K varies from 524 at an absorbed light intensity of 2.50×10^{14} photons cm^{-3} s^{-1} to 2150 at 5.32×10^{12} photons cm^{-3} s^{-1} (Table I), while the yield of Cl_2 consumption in 3MP at room temperature is 1.9×10^4 [9] at 6.7×10^{12} photons cm^{-3} s^{-1}. These high yields clearly indicate a long chain reaction initiated by the bromine atoms conceivably the one represented by the mechanism presented in the Introduction. The difference in yields between Br_2 and Cl_2 can be accounted for by the differences in reactivity of the halogen atoms. Bromine reactions chains are shorter because propagation step 2 has a larger activation energy than the same step for chlorine reactions.[17] Similar long chains occur in other photobrominations of various gaseous hydrocarbons.[18] A quantum yield of 30–40 was reported by Jost[19] in 1931 for the gas phase photobromination of cyclohexane. Except for this last example, chain lengths larger than 10^3 Br_2 consumed per photon absorbed are evidence of low activation energies for the chain carrying steps.

Effect of Temperature on $\Phi(-Br_2)$. The effect of temperature on the initial quantum yield of Br_2 disappearance over the temperature range from 210 to 298 K is shown by the data of Table II. The concentrations in the second column of this table were obtained from Beer's law using the bromine extinction coefficient at room temperature and the observed optical density at each temperature. An increase in optical density of the solutions at low temperatures as compared to the room temperature value could be explained in terms of an increase in concentration due to the expected volume contraction. The extrapolated yield at 77 K, obtained from a graph of ln $\Phi(-Br_2)$ vs. $1/T$ was approximately 10^{-4}, which is in agreement with a value determined by Mazurak.[20] These results indicate that the reaction chain length decrease with decreasing temperature, as a result of either an increase in the probability of one or more of chain termination steps −1, 4, 5 relative to chain propagation step 2, or to a decrease in the quantum yield of initiating step 1. An Arrhenius plot of ln $\Phi(-Br_2)$ vs. $1/T$ (Figure 2) gives a temperature dependence of the overall rate which is clearly due to the bromine atom abstraction reaction 2, with an activation energy of approximately 11 ± 1 kcal/mol. Gas phase activation energies for hydrogen abstraction by bromine atoms of 13.2, 10.0, and 7.5 kcal/mol have been reported[18] for primary, secondary, and tertiary hydrogen bonds, respectively. A similar reduction in yield was observed with Cl_2 in 3MP,[9] but in this case the yield was greater than unity at temperatures over 80 K while for Br_2 the quantum yield fell below one at temperatures of 215–220 K. In the case of chlorine the activation energy of the propagation steps is of the order of 1 kcal/mol.[18]

TABLE I: Initial Rates and Quantum Yields of Bromine Consumption at 298 K

OD_0	$-d(Br_2)_0/dt$, molecules cm^{-3} s^{-1} $\times 10^{-16}$	I_a, photons cm^{-3} s^{-1} $\times 10^{-13}$	$\Phi(-Br_2)$
0.345	13.1	25.0	524
0.316	4.76	6.53	729
0.280	4.67	5.36	872
0.315	4.00	3.56	1124
0.323	4.19	3.55	1180
0.305	3.40	3.24	1048
0.320	3.76	2.82	1333
0.270	1.14	0.53	2150

A decrease in the quantum yield of chain initiation step 1 in addition to a decrease in the rate of propagation step 2 could possibly account for a decrease in $\Phi(-Br_2)$ below one at 210 K. Barring evidence to support the existence of another primary process which would be nondissociative or allow for concerted Br_2–RH reactions, one must conclude that bromine atoms recombine efficiently in the parent cage under conditions where the reaction Br + RH is prevented.

Effect of HBr and O_2 on the $\Phi(-Br_2)$. Quantum yields for Br_2 consumption at 298 K in the presence of HBr or O_2 are given in Table III. Both additives decreased the yields by a factor of 10^2 at concentrations of 10^{-2} and 10^{-3} M, respectively.

Inhibition of photobrominations by hydrogen bromide has been observed in gas phase brominations of several hydrocarbons.[1-4] The yield is decreased because of the reaction of 3-methylpentyl radicals with HBr, thus competing with the second chain-propagating step in which the radical reacts with Br_2 to produce the alkyl bromide. Inhibition of chlorination chain reactions by the HCl produced is not expected because of the endothermicity of the reaction of secondary or tertiary alkyl radicals with HCl.[6]

Oxygen inhibits the chain reaction by the reaction of oxygen with the 3-methylpentyl radicals forming less reactive peroxy radicals.[5] No catalytic effect of oxygen was observed under our oxygen concentration, as previously observed by Kharasch[21] and co-workers. The low quantum yields (30–40) obtained by Jost[19] for the system Br_2–cyclohexane could be explained in terms of the presence of an impurity such as oxygen, since we have repeated the photobromination of cyclohexane and obtained a yield of Br_2 consumption of 321 at an absorbed light intensity of 3.99×10^{13} photons cm^{-3} s^{-1}.

Product Quantum Yield and Identification. (a) *Alkyl Bromides. Gas Chromatography.* Aliquots of the photolyzed samples kept in the dark until the injection gave three gas

TABLE II: Quantum Yields of Br_2 Consumption as a Function of Temperature

T, K	$(Br_2)_0$, M × 10^3	$-d(Br_2)_0/dt$, molecules cm^{-3} s^{-1} × 10^{-15}	I_a, photons cm^{-3} s^{-1} × 10^{-14}	$\Phi(-Br_2)$
298	1.72	13.1	2.50	524
278	1.80	4.49	0.89	50
266	2.40	2.21	1.13	19.6
251	2.85	1.39	1.4	9.9
232	1.90	12.4	27.0	4.6
210	1.80	0.362	58.2	0.06

TABLE III: Effect of Added HBr and O_2 on $\Phi(-Br_2)$

Additive, concn, M	$(Br_2)_0$, M × 10^3	$-d(Br_2)_0/dt$, molecules cm^{-3} s^{-1} × 10^{-15}	I_a, photons cm^{-3} s^{-1} × 10^{-13}	$\Phi(-Br_2)$
HBr, 3.81 × 10^{-3}	1.80	2.51	2.31	109
HBr, 1.18 × 10^{-2}	1.55	0.41	3.37	12
O_2, 10^{-3}	2.73	6.14	43.0	14

TABLE IV: Quantum Yields for Alkyl Bromides Production at 298 K

	$(Br_2)_0$, M × 10^3	$d(t\text{-RBr})/dt$, molecules cm^{-3} s^{-1} × 10^{-17}	$d(s\text{-RBr})/dt$, molecules cm^{-3} s^{-1} × 10^{-17}	I_a, photons cm^{-3} s^{-1} × 10^{-13}	$\Phi(t\text{-RBr})$	$\Phi(s\text{-RBr})$	$\Phi(-Br_2)$	RBr/Br_2
1	5.6	2.33	0.20	6.77	3447	297	2767	1.4
2	4.0	1.15	0.13	5.64	2039	229	2344	0.95
3	9.2	1.5	0.1	6.86	2196	204	2536	0.95

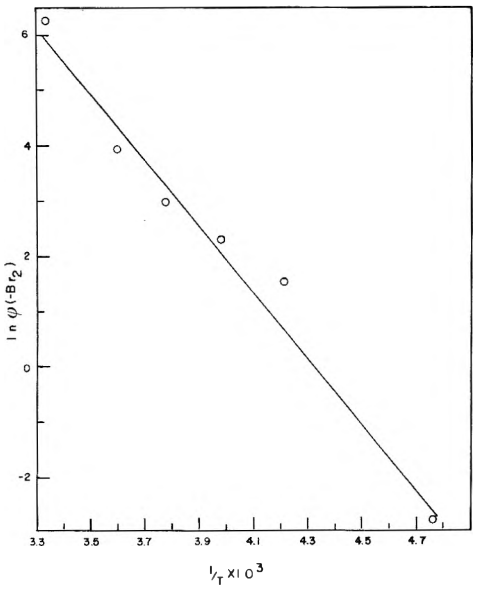

Figure 2. Temperature dependence of the quantum yield of Br_2 disappearance in 3MP.

chromatographic peaks, which were assigned to 3-methylpentane (bp 64 °C), 3-bromo-3-methylpentane (bp 139 °C), and 2-bromo-3-methylpentane (bp 140 °C). The primary bromides, 1-bromo-3-methylpentane (bp 148 °C) and 3-(bromomethyl)pentane (bp 144 °C) which would have been eluted after the tertiary and secondary bromides and easily resolved under our column conditions were not observed. The absolute yields for the tertiary (t-RBr) and secondary (s-RBr) 3-methylpentyl bromides at room temperature are given in Table IV. The tertiary bromide yield being on the average 10.5 times higher than the secondary bromide yield. The limits of detectability indicate that if primary bromides are produced, they must be present in amounts less than 10^{-4} times the amount of tertiary bromide present. In the last column of Table IV the ratio of the total number of 3-methylpentyl bromide molecules, as determined by gas chromatographic analysis, to the total number of bromine molecules consumed during the photolysis is given as a criterion of the material balance obtained in our experiments. Deviations from unity could be explained in terms of experimental errors in the injection technique, bromide concentration determination through measurement of peak areas by triangulation, and possible decomposition of the bromides.

The distribution of isomeric alkyl bromides in photobrominations constitutes a direct measure of the relative reactivities of the primary, secondary, and tertiary paraffinic hydrogens toward Br atoms. Relative reactivities per hydrogen atom for tertiary and secondary positions, k^t/k^s, of 42 were obtained for 3MP. In this calculation it was assumed that the extent of bromination was less than 0.1%, so that further bromination of the alkyl bromides was neglected, and that back reaction −2 did not alter the relative reactivities as previously found by Fettis et al.[8] Competitive brominations of n-butane and isobutane have been done at elevated temperatures in the gas phase by Anson et al.[7] and Fettis et al.[8] and values of 20[7] and 12.7[6] for k^t/k^s have been reported. In liquid 2-methylpentane the relative reactivity of a tertiary to a secondary hydrogen atom toward attack by a bromine atom was found to be 36.[22] An increased relative reactivity in the liquid as compared to gas phase could be accounted for in terms of cage effects which keep the Br atom at a particular C–H bond long enough although there may be other more reactive bonds in other parts of the molecule. Under our experimental conditions no primary bromides were observed,

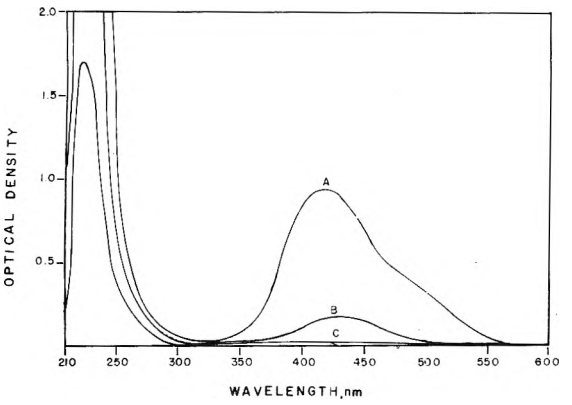

Figure 3. Uv-visible absorption spectra of a sample at different photolysis intervals: (A) unphotolyzed; (B) 15-s photolysis; (C) 45-s photolysis.

setting a minimum limit of $k^t/k^p \simeq 10^4$. In the photochlorination of liquid 3MP at 300 K the absolute yields of alkyl chlorides are[9] secondary, primary, tertiary while the relative reactivities[23] per hydrogen atom are 1.3, 0.36, and 3.6 for k^t/k^s, k^p/k^s, and k^t/k^p, respectively. The large difference in selectivity between bromine and chlorine is explained by the higher activation energies and relatively large difference in activation energies for the bromine abstraction of the different hydrogen atoms as compared to the analogous chlorine reactions.[5]

Two additional gas chromatographic peaks appeared on photolyzed samples still containing bromine (concentration less than 5×10^{-3} M) kept in the dark for several days. These peaks were not observed in samples analyzed immediately after photolysis. The two peaks eluted after the alkyl bromides. One of the peaks was assigned to the 2,3-dibromo-3-methylpentane (bp 188 °C) by comparing its retention time with the known compound, the other peak has been tentatively assigned to the 3-bromo-3-bromomethylpentane (bp 197 °C). The areas under these peaks increased with time while the area under the peak assigned to the tertiary monobromide decreased. After 5 days the yield of dibromides was still 10^{-2} smaller than the yields for the monobromides. In photolyzed samples to which a drop of mercury was added to remove the remaining unphotolyzed bromine, the formation of dibromides was inhibited.

Hydrocarbons having a secondary hydrogen adjacent to a tertiary position give high yields of tertiary bromides but in addition form dibromides.[22] In the case of photobromination of solutions of 25 mol % of Br_2 in 2-methylpentane the dibromide yield was 17.5%, this yield decreasing with decreasing Br_2 concentration.[22] Russell and Brown[22] have interpreted this dark reaction which leads to the formation of the dibromides, in terms of a mechanism in which Br produces the ionization of the tertiary bromide, followed by reaction of a second Br_2 with the high energy π-complex form of the carbonium ion.

Uv Optical Absorption of the Products. In one of the photolyses the changes in the uv–visible absorption spectrum of the sample were followed as a function of irradiation time (Figure 3). The spectrum of the unphotolyzed sample shows the usual bromine visible absorption with maximum at 420 nm, and uv band with onset around 250 nm assigned to the bromine–3MP charge transfer. At an intermediate time of photolysis the absorption of both bands have decreased but still the optical density in the uv is larger than 2.0 at wavelengths smaller than 250 nm. Finally, after depleting all the bromine from the sample a band in the uv region with maximum at 224 nm was observed. This band has been assigned to the uv absorption of the alkyl bromides by comparing it with the uv absorption of a 4.4×10^{-3} M solution of 3-(bromomethyl)pentane in 3MP which also shows a maximum at 223.7 nm. This absorption maximum compares well with the maxima of solutions of *sec*-butyl bromide (λ_{max} 207.5 nm) and *tert*-butyl bromide (λ_{max} 215 nm) in *n*-heptane reported by Kimura and Nagakura.[24] Hydrogen bromide could be possibly contributing to this uv absorption band since it has an extinction coefficient of 30 M^{-1} cm^{-1} [25] at 225 nm in the gas phase. No experimental test to confirm the contribution of HBr to the absorption was done.

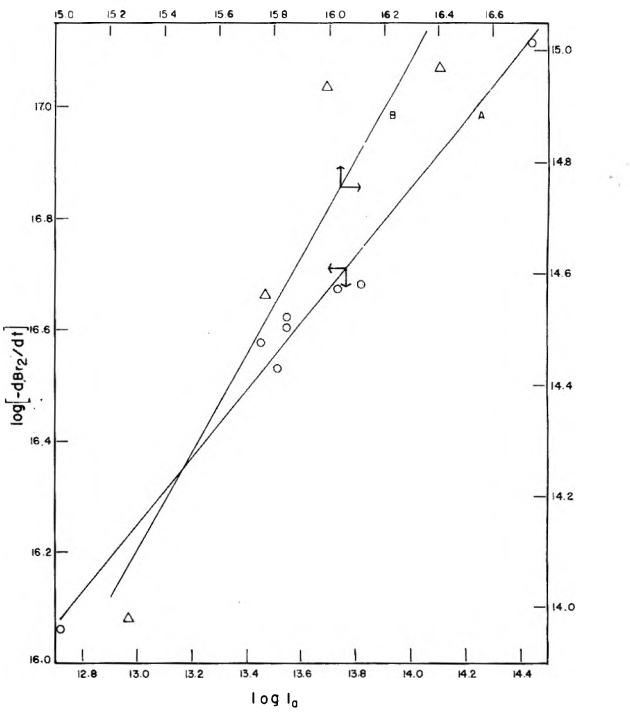

Figure 4. Dependence of rate of Br_2 disappearance on light intensity: (A) at 298 K, the values of I_a range from 25.0×10^{13} to 0.53×10^{13} photons cm^{-3} s^{-1} in a 1-cm cell; (B) at 210 K, the values of I_a range from 1.84×10^{15} to 2.15×10^{16} photons cm^{-3} s^{-1} in a 1-cm cell.

(b) *Hydrogen Bromide.* Using a standard acid–base back titration technique, quantum yields of HBr production of 520 and 1048 at absorbed light intensities of 7.25×10^{13} and 2.29×10^{13} photons cm^{-3} s^{-1} and initial Br_2 concentration of 1.7×10^{-3} M were obtained. In general lower values of Φ(HBr) were obtained as compared to values of $\Phi(-Br_2)$ at approximately the same absorbed light intensity and initial bromine concentration. This is due to inherent experimental errors and irreproducibility.

(c) *Hydrocarbon Products.* It was presumed that the chain lengths are long enough so that radical coupling reactions to produce $C_{12}H_{26}$ are insignificant. This was experimentally verified by gas chromatographic analysis, since no $C_{12}H_{26}$ peak was observed.

Dependence of the Initial Rate of Br_2 Disappearance at 298 and 210 K on Absorbed Light Intensity. The effect of absorbed light intensity on the initial rate of photobromination was investigated at 298 and 210 K by changing the distance between the sample holder and the collimating lens of the monochromator and maintaining the initial concentration of Br_2 approximately constant at 1.5×10^{-3} M (Table I). Figure 4 shows that at 298 K the initial experimental rate of bromine disappearance greatly depends on the absorbed light

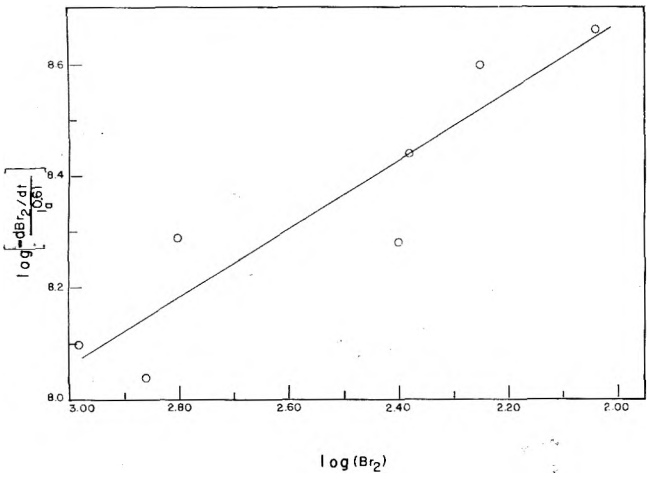

Figure 5. Dependence of rate of Br_2, disappearance on initial Br_2 concentration. The values of Br_2 concentration range from 1.1×10^{-3} to 9.15×10^{-3} M.

intensity at constant bromine concentration and is proportional to the 0.61 ± 0.03 power at constant initial Br_2 concentration. At 210 K the rate is proportional to the 0.9 ± 0.2 power at constant initial Br_2 concentration of 1.9×10^{-3} M. An experimental order in absorbed light intensity of 0.61 is evidence of a chain reaction, which according to the mechanistic rate expressions derived by Benson and Buss[18] for the rate of bromine disappearance for the postulated termination reactions, the chain can terminate by any of the possible termination steps −1, 4, 5. At 210 K the first-order dependence of the initial rate on the absorbed light intensity indicates that bromine atoms are not removed by reaction with nongeminate alkyl radicals or atoms.

Dependence of the Initial Rate of Br_2 Disappearance at 298 K on Br_2 Concentration. From the results shown in Figure 4, the experimental rate law for the initial rate of Br_2 disappearance could be expressed as

$$-\mathrm{d(Br_2)}/\mathrm{d}t = k_e I_a^{0.6}(\mathrm{Br_2})^n \qquad \text{(II)}$$

Since it is difficult to maintain the absorbed light intensity constant while the initial bromine concentration is changed, the order with respect to Br_2 was obtained from the slope of a graph of $\log [(-\mathrm{d(Br_2)_0}/\mathrm{d}t)/I_a^{0.61}]$ vs. $\log (\mathrm{Br_2})$ (Figure 5). A value of n equal to 0.6 ± 0.1 was obtained, suggesting that the chain reaction is terminated mainly through the radical–bromine atom recombination in accordance with the mechanistic rate expression derived by Benson and Buss[18] assuming step 4 as the main termination step. In the gas phase bromination studies[18] it has been difficult to distinguish between two terminating steps −1 and 4. Benson and Buss[18] have suggested that the bromination of alkanes with weaker C–H bonds than the primary (i.e., lower activation energy for reaction 2) results in larger kinetic chain lengths and termination via recombination of Br atoms become less significant. The photobromination of liquid 3MP could possibly be one of these examples since only tertiary and secondary hydrogens bonds are broken and the chain reactions are rather long.

Rate Equations and Rate Constants. The results obtained in this work could be summarized within the experimental errors in the following initial rate expression:

$$-\mathrm{d(Br_2)}/\mathrm{d}t = k_e I_a^{0.5}(\mathrm{Br_2})^{0.5} \qquad \text{(III)}$$

Using the data on the initial rates of reaction given in Table I, k_e was obtained giving an average value of 6.7 $s^{-1/2}$. Comparing this experimental initial rate expression with the mechanistic rate expression derived assuming termination mainly through radical–bromine atom recombination, k_e could be equated to $(k_3k_2/k_4)^{1/2}(\mathrm{RH})^{1/2}$, giving an experimental value for k_3k_2/k_4 of 9.7×10^{-21} cm^3 molecules^{-1} s^{-1}.

From the data of Table III, the initial bromine concentrations, the calculated k_e, and using mechanistic rate expression II, the inhibition constant, k_{-2}/k_3, was calculated to be 80. Values of the order of 1.5[3] and 1.74[4] have been reported for the inhibition constant in the gas phase photobromination of neopentane and isobutane.

Acknowledgment. The authors express their appreciation to Drs. George Simpson and A. Grimison who critically reviewed the manuscript. Support for this work was made available by the Dean of Studies of the University of Puerto Rico and is gratefully acknowledged.

References and Notes

(1) G. B. Kistiakowsky and E. R. Van Artsdalen, *J. Chem. Phys.*, **12**, 469 (1944).
(2) H. C. Anderson and E. R. Van Artsdalen, *J. Chem. Phys.*, **12**, 479 (1944).
(3) E. Hormats and E. R. Van Artsdalen, *J. Chem. Phys.*, **19**, 778 (1951).
(4) B. H. Eckstein, H. A. Scheraga, and E. R. Van Artsdalen, *J. Chem. Phys.*, **22**, 28 (1954).
(5) W. A. Thaler, *Methods Free Radical Chem.*, **2**, 121 (1969).
(6) M. L. Poutsma, *Free Radicals*, **2**, 159 (1973).
(7) P. C. Anson, P. S. Fredricks, and J. M. Tedder, *J. Chem. Soc.*, 918 (1959).
(8) G. C. Fettis, J. H. Knox, and A. F. Trotman-Dickenson, *J. Chem. Soc.*, 4177 (1960).
(9) J. E. Willard and R. Arce, *J. Phys. Chem.*, **76**, 1800 (1972).
(10) E. C. Murray and R. N. Keller, *J. Org. Chem.*, **34**, 7 (1969).
(11) (a) C. A. Parker, *Proc. R. Soc. London, Ser. A*, **220**, 104 (1953); (b) C. G. Hatchard and C. A. Parker, *ibid.*, **235**, 518 (1956).
(12) H. E. Johns, "Creation and Detection of the Excited State", Vol. 1, 1971, p 123.
(13) A. A. Passchier, J. D. Christian, and N. W. Gregory, *J. Phys. Chem.*, **71**, 937 (1967).
(14) D. F. Evans, *J. Chem. Phys.*, **23**, 1426 (1954).
(15) A. Popov and J. J. Mannion, *J. Am. Chem. Soc.*, **74**, 222 (1952).
(16) M. Posteiner and E. Treibr, *Chem. Ber.*, **74**, 964 (1961).
(17) A. F. Trotman-Dickenson, *Adv. Free Radical Chem.*, **1**, 1 (1965).
(18) S. W. Benson and J. Buss, *J. Chem. Phys.*, **28**, 301 (1958).
(19) W. Jost, *Z. Phys. Chem.*, Bodenstein Festband, 291 (1931).
(20) P. Mazurak, M.S. Thesis, University of Wisconsin, Madison, Wisc., 1966.
(21) (a) M. S. Kharasch, W. Hered, and F. R. Mayo, *J. Org. Chem.*, **6**, 818 (1941); (b) M. S. Kharasch and M. Z. Fineman, *J. Am. Chem. Soc.*, **63**, 2776 (1941).
(22) G. A. Russell and H. C. Brown, *J. Am. Chem. Soc.*, **77**, 4025 (1955).
(23) R. Arce-Quintero, Ph.D. Thesis, University of Wisconsin, 1970.
(24) K. Kimura and S. Nagakura, *Spectrochim. Acta*, **17**, 166 (1961).
(25) B. J. Huebert and R. M. Martin, *J. Phys. Chem.*, **72**, 3046 (1968).

Transients and Specific Rates of Some Reactions of the Solvated Electron with Inorganic Ions in Liquid Ammonia Investigated by Nanosecond Pulse Radiolysis at 23 °C

Farhatazlz* and Pierre Cordier[1]

Radiation Laboratory,[2] University of Notre Dame, Notre Dame, Indiana 46556 *(Received June 22, 1976)*

Publication costs assisted by the U.S. Energy Research and Development Administration

For ammoniacal solutions at 23 °C, the absorption spectrum of CuCl and the transient absorption spectra of Ni^+, Zn^+, Cd^+, Hg. Tl, and Pb^+ are given. For the solvent liquid ammonia at 23 °C and in units of $M^{-1}\ s^{-1}$, the measured specific rates of reactions of e_{am}^- with inorganic solutes follow in parentheses after each solute: Cu^+ (2.5×10^8), Hg^+ (2.3×10^{11}), Tl^+ (1.2×10^{12}), Fe^{2+} (1.2×10^9 at zero ionic strength), Co^{2+} (5.7×10^{11}), Ni^{2+} (1.1×10^{11}), Cu^{2+} (8.3×10^{11}), Zn^{2+} (1.3×10^{10}), Cd^{2+} (4.6×10^{11}), Hg^{2+} (3.2×10^{11}), Pb^{2+} (5.6×10^{11}), Al^{3+} ($<6 \times 10^6$), Cr^{3+} (5.8×10^{10}), Fe^{3+} (4.9×10^{11} at zero ionic strength), Co^{3+} (7.7×10^{11}), Ce^{3+} (3.1×10^{11}), Ce^{4+} (1.5×10^{11}), NO_3^- (1.2×10^8 at zero ionic strength), ClO_4^- (no reaction), I^- (no reaction). Only the reaction of e_{am}^- with Tl^+ appears to be a diffusion-controlled reaction. For the solvent liquid ammonia at 25 °C, the standard free energy changes for the reactions of e_{am}^- with metal cations mentioned above have been computed. The activation-controlled specific rate increases and attains a plateau value with the increasing negative free energy of the reaction. This relationship is consistent with a quantum mechanical description of an exothermic electron transfer reaction, in which the theory is formulated by treating the reaction as the nonradiative decay of a "supermolecule" consisting of the electron donor, the electron acceptor, and the polar solvent.

Introduction

The specific rates measured by nanosecond pulse radiolysis of many reactions of the solvated electron, e_{am}^-, in liquid ammonia, and identification of some transient products of these reactions have been reported previously.[3-6] In this paper, further applications of the above technique to investigations of transients and specific rates of the reactions of e_{am}^- with some inorganic ions are reported. Recently, in a theoretical study of exothermic electron transfer reactions (ETR), a quantum mechanical description of ETR was formulated by treating the reaction as the nonradiative decay of a "supermolecule" consisting of the electron donor, the electron acceptor, and the polar solvent.[7] The study indicates that with an increasing negative free energy of the reaction, the activation-controlled specific rate, k_a, of ETR will increase and attain a plateau value for some conditions. However, in the theory given by Marcus[8] a parabolic dependence of k_a of ETR with an increasing negative free energy of the reaction is predicted. For reactions of e_{am}^- with metal cations investigated in the present studies, an effort will be made to explore the relationship between k_a and free energy of the reaction.

Experimental Section

Baker analyzed reagents: $HgCl_2$, $HgNO_3 \cdot H_2O$, $KClO_4$, $NaNO_3$, and $Ni(NO_3)_2 \cdot 6H_2O$; Fisher certified reagents: $Cr(NO_3)_3 \cdot 9H_2O$, $Cu(NO_3)_2 \cdot 3H_2O$, $Hg(NO_3)_2 \cdot H_2O$, and $Zn(NO_3)_2 \cdot 6H_2O$; Matheson Coleman and Bell reagents: $Al(NO_3)_3 \cdot 9H_2O$, $Cd(NO_3)_2 \cdot 4H_2O$, $Co(NO_3)_2 \cdot 6H_2O$, and $Pb(NO_3)_2$: AlI_3(99.99+%), $Fe(ClO_4)_2 \cdot 6H_2O$, and $Fe(ClO_4)_3$ from Ventron Corporation; $TlClO_4$, $Ce(NO_3)_3 \cdot 2NH_4NO_3 \cdot 4H_2O$, and $Ce(NO_3)_4 \cdot 2NH_4NO_3$ from K and K Laboratories; analytical reagent KI from Mallinkrodt and $[Co(NH_3)_6]Cl_3$ from Eastman Kodak were used as received. By heating at 190–200 °C in a drying oven for ~300 h, $Cd(NO_3)_2 \cdot 4H_2O$ was dehydrated.[9] Cuprous chloride was prepared by the method described by Keller and Wycoff.[10] Tetramminezinc(II) nitrate was prepared by the method described by McElroy and Laitinen.[11]

The purification of ammonia,[12] the irradiation cell,[3] and the vacuum line[3] have been described elsewhere. All samples were degassed and contained 1.56 g of liquid ammonia. For solutions which could not be prepared by direct weighing of solutes, a known volume (maximum 50 μl at room temperature) of an aqueous or methanolic solution of the required solute concentration was injected into the irradiation cell from a microsyringe, and the solvent was removed by evacuation prior to filling the cell with ammonia. For hydrated solutes, no special procedures were adopted to remove water of hydration. However, samples were evacuated until a constant pressure of $\sim 10^{-6}$ mm Hg was attained. To avoid the decomposition of $Fe(ClO_4)_2 \cdot 6H_2O$, the evacuation of the sample was performed at 77 K.

The pulse radiolysis system and the split-beam technique are described elsewhere.[12] The split-beam technique permits the splitting of analyzing light beam into two light beams and then allows a simultaneous monitoring of the transient absorption signal at two different wavelengths. Its application to the measurement of transient absorption spectrum was described previously.[5] The infrared detector (Judson J10U) used in present studies had a 0–100% risetime of ~50 ns at 77 K. The photovoltaic indium antimonide detector (Judson J10U) is manufactured by Judson Research and Manufacturing Co., Conshohocken, Pa. For the measurement of risetime, the detector was exposed to a 500-ns rectangular pulse of 900-nm light from a Monsanto ME-5 infrared light emitting diode (risetime 8 ns and falltime 11 ns), and time required to reach a maximum flat signal on a Tektronix 7000 series oscilloscope (risetime less than 1 ns) was measured. The samples

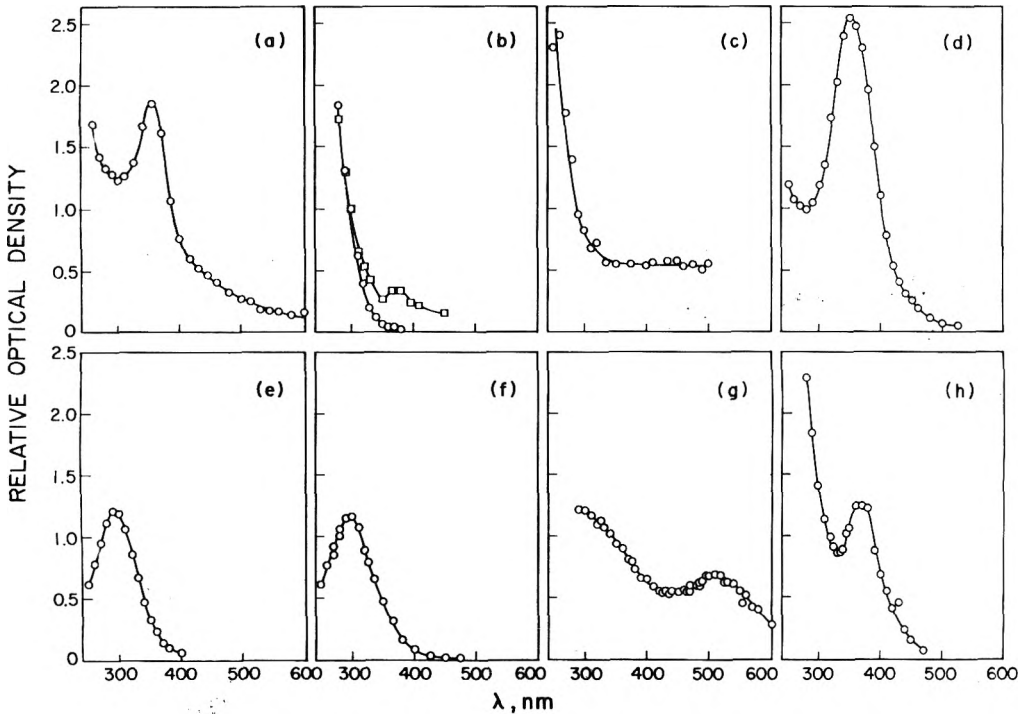

Figure 1. Transient absorption spectra induced by a 5- to 30-ns pulse of electrons in ammoniacal solutions of metal salts at 23 °C. (a) 2.6 mM nickel nitrate, 150 ns after the pulse, spectrum ascribed to Ni^+; (b) O, CuCl no irradiation; □, 2.5 mM cupric nitrate, immediately after the pulse; (c) 2.9 mM tetramminezinc(II) nitrate, 20 ns after the pulse, spectrum ascribed to Zn^+; (d) 6.4 mM cadmium nitrate, 100 ns after the pulse, spectrum ascribed to Cd^+; (e) 5 mM mercurous nitrate, immediately after the pulse, spectrum ascribed to Hg; (f) saturated solution of mercuric chloride, immediately after the pulse, spectrum ascribed to Hg; (g) 2.4 mM thallous perchlorate, immediately after the pulse, spectrum ascribed to Tl; (h) 2.4 mM lead nitrate, immediately after the pulse, spectrum ascribed to Pb^+.

were irradiated at ~23 °C with 5- to 30-ns pulses of ~10-MeV electrons from the Notre Dame Linac.

At room temperature, absorption spectra of various solutes in liquid ammonia were measured with a Cary 14R spectrophotometer.

Results

Spectral Characteristics of the Solutes. The absorption spectrum of CuCl in liquid ammonia at room temperature is shown in Figure 1b. In the format of "solute, absorbing species, extinction coefficient in units of M^{-1} cm^{-1}, and wavelength in units of nm", some extinction coefficients of ammoniacal solutions at room temperature are: CuCl, Cu^+, 43, 340; $NaNO_3$, NO_3^-, 6.1, 310 (maximum absorption); ferrous perchlorate, iron species, 77, 260, ceric ammonium nitrate, cerium species, 532, 262; KI, I^-, 40, 295.

Transient Absorption Spectra. The transient absorption spectra were induced in various ammoniacal solutions by a pulse of electrons. The spectra were measured by the split-beam technique.[5] The transient absorption spectra are shown in Figure 1. The smallest wavelength in the ultraviolet for a transient spectrum is the wavelength below which the solute absorbs significantly.

For ammoniacal solutions of nickel nitrate, mercuric chloride, cadmium nitrate, and lead nitrate, the transient spectra 7 μs after the electron pulse were the same as spectra shown in Figure 1 for earlier times.

For ammoniacal solutions of $TlClO_4$, the peaks at 290 and 510 nm in the transient spectrum observed immediately after the electron pulse (cf. Figure 1g) disappeared in 7 μs, and a new broad peak appeared at ~430 nm.

For ammoniacal solutions of mercurous nitrate, the peak at 295 nm in the transient spectrum observed immediately after the pulse (cf. Figure 1e) decayed considerably in 7 μs, and, below 270 nm, the absorption simultaneously rose sharply with the decreasing wavelength.

For ammoniacal solutions of tetramminezinc(II) nitrate, the transient absorption spectrum shown in Figure 1c transformed, in 7 μs, to a spectrum which had no significant absorption below 300 nm, and had a peak absorption at 460 nm.

For ammoniacal solutions of cupric nitrate, the changes in the transient absorption spectrum with the increasing time after the electron pulse were complex.

In ~3 mM solutions of NH_4I or NH_4Cl, transient absorptions were similar to those in neat ammonia.[3]

Specific Rates. For determination of specific rates of the reactions of e_{am}^- with various solutes (except ferrous perchlorate), irradiation conditions were fixed such that the transient signal of e_{am}^- in neat liquid ammonia showed negligible decay 1.5 μs after the pulse.[3] The concentrations of the solutes were fixed to give pseudo-first-order kinetics. Decay of e_{am}^- absorption at 1.73 μ was studied. For a particular solute, at least four determinations of the pseudo-first-order specific rate were made for each concentration of the solute, and at least four different concentrations were used. Specific rates were calculated by dividing the pseudo-first-order specific rates with the respective concentrations of the solute. In allocating a specific rate to a particular ion, a complete ionization of the respective solute is implicit. An average of at least three values of the specific rate for a particular concentration of the ion was calculated. Such average values of specific rates for at least three different concentrations of an ion were further averaged to give the final value of the specific rate. The results are summarized in Table I. The reaction of e_{am}^- with Fe^{3+} was not investigated directly, because solution

TABLE I: Specific Rates (M^{-1} s^{-1}) for Some Reactions of Solvated Electrons in Liquid Ammonia at 23 °C and in Water at Room Temperature

Solute	Concn range in NH_3	Reacting ion[a]	$k(e_{am}^-)$[b]		$k(e_{aq}^-)$[c]
			k_{obsd}	k_a	
CuCl	3–15 mM	Cu^+	2.5×10^8	2.5×10^8	
$HgNO_3 \cdot H_2O$	12–50 μM	Hg^+	2.3×10^{11}	2.8×10^{11}	
$TlClO_4$	10–22 μM	Tl^+	1.2×10^{12}		$(2.8–5.4) \times 10^{10}$
$Fe(ClO_4)_2 \cdot 6H_2O$	1.9–5.58 mM	Fe^{2+}	1.2×10^9 [d]	1.2×10^9	1.2×10^8
$Co(NO_3)_2 \cdot 6H_2O$	10–20 μM	Co^{2+}	5.7×10^{11}	7.1×10^{11}	$(0.95–1.35) \times 10^{10}$
$Ni(NO_3)_2 \cdot 6H_2O$	18–40 μM	Ni^{2+}	1.1×10^{11}	1.2×10^{11}	$(1.2–2.3) \times 10^{10}$
$Cu(NO_3)_2 \cdot 3H_2O$	9–20 μM	Cu^{2+}	8.3×10^{11}	1.2×10^{12}	$(2.9–4.5) \times 10^{10}$
$Zn(NO_3)_2 \cdot 6H_2O$	50–100 μM	Zn^{2+}	1.3×10^{10}	1.3×10^{10}	$(0.56–2) \times 10^9$
$Cd(NO_3)_2$	9–19 μM	Cd^{2+}	4.6×10^{11}	5.5×10^{11}	$(1.7–6.4) \times 10^{10}$
$Hg(NO_3)_2 \cdot H_2O$	20–60 μM	Hg^{2+}	3.2×10^{11}	3.6×10^{11}	
$Pb(NO_3)_2$	13–27 μM	Pb^{2+}	5.6×10^{11}	7.0×10^{11}	$(1.3–3.9) \times 10^{10}$
AlI_3	11 mM	Al^{3+}	$<6 \times 10^6$ [e]		2×10^9
$Cr(NO_3)_3 \cdot 9H_2O$	50–110 μM	Cr^{3+}	5.8×10^{10}	5.9×10^{10}	
		Fe^{3+}	4.9×10^{11} [d]	5.5×10^{11}	$\sim 5 \times 10^{10}$
$[Co(NH_3)_6]Cl_3$	9–18 μM	Co^{3+}	7.7×10^{11}	9.4×10^{11}	$(7.6–9) \times 10^{10}$
$Ce(NO_3)_3 \cdot 2NH_4NO_3 \cdot 4H_2O$	80–140 μM	Ce^{3+}	3.1×10^{11}	3.3×10^{11}	$<10^9$
$Ce(NO_3)_4 \cdot 2NH_4NO_3$	30–50 μM	Ce^{4+}	1.5×10^{11}	1.5×10^{11}	
$Al(NO_3)_3 \cdot 9H_2O$	1.8→4.5 mM	NO_3^-	$(1.5 \rightarrow 1.9) \times 10^8$ [f]		
$NaNO_3$	4.8–22 mM	NO_3^-	1.2×10^8 [d]		$(0.75–2.5) \times 10^{10}$
$KClO_4$	38 mM	ClO_4^-	No reaction		$<10^5$
KI	27 mM	I^-	No reaction		$<2.4 \times 10^5$

[a] No distinction is implied between fully ionized and ion pair species. Also, no distinction is implied between ammoniated and ammonolyzed ions. [b] Present work; k_{obsd} is measured specific rate and k_a is calculated activation-controlled specific rate (cf. text). [c] From ref 25 and 26. [d] Value for zero ionic strength. It was obtained by extrapolation of a plot of log k_{obsd} vs. (ionic strength)$^{1/2}$. [e] Calculated for a 10% decay of e_{am}^- in 1.6 μs which is assumed to be not observable. [f] Because of ionic strength effects, values are higher than $k = 1.2 \times 10^8$ M^{-1} s^{-1} for the reaction of e_{am}^- with NO_3^- at zero ionic strength.

of Fe^{3+} in liquid ammonia could not be prepared from $Fe(ClO_4)_3$ or $Fe(NO_3)_3 \cdot 9H_2O$.

For 4.8, 11, 18, and 22 mM solutions of $NaNO_3$, the specific rates in units of 10^8 M^{-1} s^{-1} for the reaction of e_{am}^- with NO_3^- are 1.7, 1.9, 2.2, and 2.4, respectively.

A significant lowering of decay rate of e_{am}^- in ammoniacal solutions of Hg^+ or Hg^{2+} occurs between successive pulses. Apparently, in these experiments, Hg^+ and Hg^{2+} are converted by a chain mechanism to species which do not react with e_{am}^-.

Reaction of Fe^{2+} with e_{am}^-. The decay of e_{am}^- in ammoniacal solutions of ferrous perchlorate (1.9–5.6 mM) was investigated. The solutions of concentrations >5.6 mM ferrous perchlorate would give a brown precipitate at room temperature. The salient features of the decay were as follows. (1) It was not pseudo first order. The initial decay of a particular kinetic run would fit to a pseudo-first-order plot. However, pseudo-first-order specific rates obtained for a particular concentration of ferrous perchlorate were not independent of dose per pulse, i.e., initial concentration of e_{am}^-. Also, for the same dose per pulse, pseudo-first-order specific rates obtained for different initial concentrations of ferrous perchlorate would not give the same specific rate for each initial concentration of ferrous perchlorate. (2) For initial decay, a plot of the reciprocal of the optical density at 1.73 μ of e_{am}^- vs. time was linear. Such linear plots were obtained for a dose of 0.3–40 μM of e_{am}^- per pulse.[13] However, for the same concentration of ferrous perchlorate, the slope of this plot would increase with decreasing dose per pulse. (3) For the highest dose per pulse, the slopes of above-mentioned plots were the same for all concentrations of ferrous perchlorate studied. These observations suggest the following mechanism for the decay of e_{am}^- in ammoniacal solutions of ferrous perchlorate:

$$Fe^{2+} + e_{am}^- \xrightarrow{k_1} Fe^+ \quad (1)$$

$$X + e_{am}^- \xrightarrow{k_2} \text{products} \quad (2)$$

In reactions 1 and 2, X is a transient and its initial concentration is similar to the initial concentration of e_{am}^-, and k_1 and k_2 are the specific rates for reactions 1 and 2, respectively. For experimental conditions in which reaction 1 is pseudo first order (as in the present situation), a standard kinetic treatment of reactions 1 and 2 gives[14]

$$\frac{[e_{am}^-]_0 (k' + k_2[e_{am}^-]_t)}{[e_{am}^-]_t (k' + k_2[e_{am}^-]_0)} = e^{k't} \quad (3)$$

in which t is time, $[e_{am}^-]_0$ and $[e_{am}^-]_t$ are concentrations of e_{am}^- at time 0 and t and k' is the product of k_1 and $[Fe^{2+}]_0$ which is initial concentration of Fe^{2+}. If $k't$ is considerably smaller than 1, then eq 3 can be approximated by

$$\frac{1}{[e_{am}^-]_t} = \left[\frac{k'}{[e_{am}^-]_0} + k_2\right] t + \frac{1}{[e_{am}^-]_0} \quad (4)$$

For experimental conditions in this study, k' is $\sim 10^6$ s^{-1} (cf. Table II). Thus, for $t = 0.5$ μs, $k't$ is ~0.5, and for such a situation the reduction of eq 3 to eq 4 would involve ~10% error. For 1.9 mM ferrous perchlorate and $[e_{am}^-]_0 = 0.3$ μM (the conditions for the slowest decay of e_{am}^-), about 30% decay of e_{am}^- would occur in 0.5 μs. Therefore, for such times, the analysis of data by eq 4 would be reasonably accurate. For an initial concentration of ferrous perchlorate and a particular dose per pulse, it is obvious from eq 4 that a plot of $1/[e_{am}^-]_t$ vs. t would be linear with a slope of $[k'/[e_{am}^-]_0 + k_2]$ and an intercept of $1/[e_{am}^-]_0$. Further, for an initial concentration of ferrous perchlorate and various doses per pulse, a plot of $[k'/[e_{am}^-]_0 + k_2]$ vs. $1/[e_{am}^-]_0$ would be also linear with a slope

TABLE II: Specific Rates for the Reactions of e_{am}^- with Fe^{2+} (k_1) and Fe^{3+} (k_2) in Ammoniacal Solutions of Ferrous Perchlorate at 23 °C

Initial concn of $Fe(ClO_4)_2$, mM	k_1[a]	k_2[b]
0	12[c]	4.9[c]
1.90	4.2	3.3
1.92	3.9	3.0
2.69	3.2	2.6
2.82	3.0	2.6
4.36	2.2	2.2
5.58	1.9	2.3

[a] Units 10^8 M^{-1} s^{-1}. [b] Units 10^{11} M^{-1} s^{-1}. [c] Values obtained by extrapolation of a plot of log k vs. (ionic strength)$^{1/2}$.

of k' and an intercept of k_2. For 1.9 mM solution of ferrous perchlorate, a plot of $1/[e_{am}^-]_t$ vs. t and also the plot of $[k'/[e_{am}^-]_0 + k_2]$ vs. $1/[e_{am}^-]_0$ are shown in Figures 2 and 3. The optical density of e_{am}^- at 1.73 μ was normalized to 1 cm path length, and it was converted to the concentration of e_{am}^- by using a measured value of 4.4×10^4 M^{-1} cm^{-1} for the extinction coefficient (which was obtained by the use of interference filter) of e_{am}^- at 1.73 μ. The true extinction coefficient[15] of e_{am}^- at 1.73 μ is 4.6×10^4 M^{-1} cm^{-1}. Similarly, the data for other concentrations of ferrous perchlorate were also analyzed. To calculate values of k_1, the values of k' were divided by the respective values of initial concentrations of ferrous perchlorate. The results are summarized in Table II.

Discussion

Transient Absorption Spectra. In pulse radiolysis of ammoniacal solutions of KNO_3,[6] $KClO_4$,[6] or NH_4Cl, no transient absorptions except for those in neat NH_3[3] are observed. Thus transient absorptions (cf. Figure 1) induced by an electron pulse in various ammoniacal solutions of metal salts (nitrates, perchlorates, and chloride) are ascribed to transients of the respective metals. All transient spectra have been measured at earliest times which were greater than the times required for completion of the reactions of e_{am}^- with the respective metal ions (cf. Table I for specific rates). Therefore, spectra in Figure 1 are initial spectra. For ammoniacal solutions of nickel nitrate, tetramminezinc(II) nitrate, cadmium nitrate, mercurous nitrate, thallous perchlorate, and lead nitrate, the respective transient spectra in Figure 1 are ascribed to Ni^+, Zn^+, Cd^+, Hg, Tl, and Pb^+, respectively. A comparison of the initial transient spectrum induced in ammoniacal solutions of cupric nitrate with the absorption spectrum of CuCl in liquid ammonia indicates that even initially the transient spectrum is not purely of Cu^+. The transient spectrum induced in ammoniacal solutions of $HgCl_2$ is ascribed to Hg which can be produced by a dissociative electron capture of e_{am}^- by $HgCl_2$. The spectrum is very similar to the spectrum of Hg shown in Figure 1e. For metal ions (except for cupric ion) investigated in present studies, the transient spectra induced in aqueous solutions by pulse radiolysis have been studied by many investigators.[16-23] However, these are not directly comparable with the spectra in present studies.

Specific Rates. In pulse radiolysis of ammoniacal solutions of ferrous perchlorate, the decay of e_{am}^- can be understood in terms of concomitant reactions 1 and 2. We postulate that in reaction 2 e_{am}^- reacts with Fe^{3+} which is produced by the reaction of NH_2 and Fe^{2+}. The values of specific rates for the reactions of e_{am}^- with Fe^{2+} and Fe^{3+} (cf. Table II) decrease with the increasing ionic strength of the solution. The reverse is true for the reaction of e_{am}^- with NO_3^-. The results can be

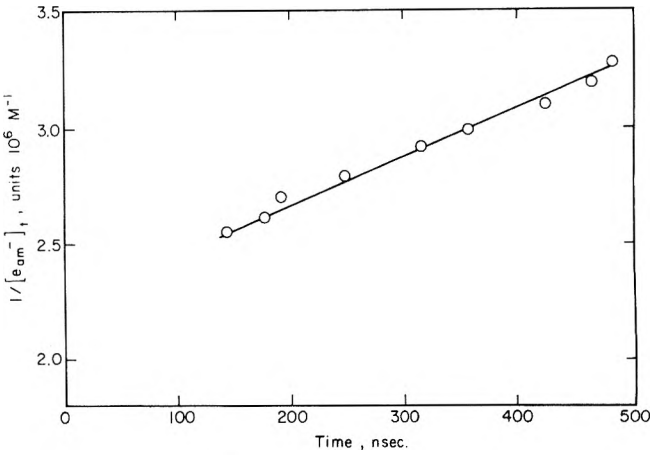

Figure 2. Plot of $1/[e_{am}^-]_t$ vs. t for a 5-ns pulse of electrons to a 1.9 mM ferrous perchlorate solution in liquid ammonia at 23 °C.

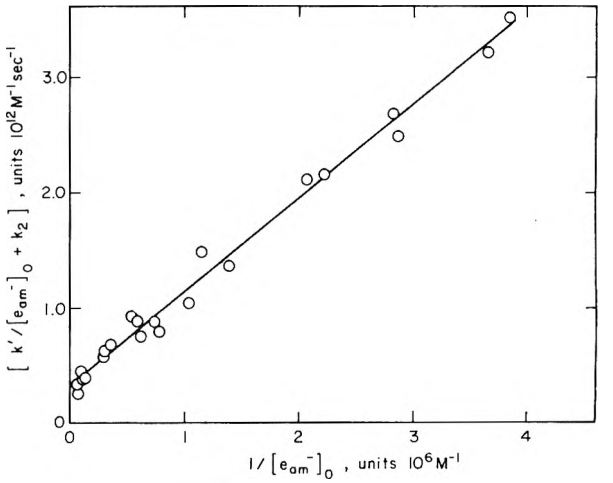

Figure 3. Plot of $[k'/[e_{am}^-]_0 + k_2]$ vs. $1/[e_{am}^-]_0$ for 1.9 mM ferrous perchlorate solution in liquid ammonia at 23 °C. For explanation of k' and k_2 consult text.

interpreted, at least qualitatively, in terms of salt effect on kinetics of ionic reactions. The plots of log of specific rates vs. square root of ionic strength were linear. However, the slopes were not in agreement with the theory. One complicating factor may be that at concentrations used in these experiments, ferrous perchlorate and $NaNO_3$ are not completely ionized in ammoniacal solutions.

For 0.9 mM $NaNO_3$, a previously determined value[3] of $<7.9 \times 10^7$ M^{-1} s^{-1} for the specific rate of e_{am}^- with NO_3^- agrees poorly with the value of 1.4×10^8 M^{-1} s^{-1} for the same concentration of NO_3^- obtained by extrapolation from the present results. For the reaction of Cu^{2+} with e_{am}^-, a combination of a value[24] of 1.5×10^{11} M^{-1} s^{-1} for the specific rate at −45 °C with the present results at 23 °C gives 3.4 kcal mol^{-1} for the activation energy.

An application of the Smoluchowski–Debye equation for diffusion-controlled reactions to reaction of e_{am}^- with NH_4^+ gives[3] 1.4×10^{12} M^{-1} s^{-1} for the specific rate at 25 °C. For the assumption that reaction radii and diffusion coefficients of divalent, trivalent, and tetravalent positive ions are the same as those of NH_4^+, the application of the Smoluchowski–Debye equation for diffusion-controlled reactions to reactions of e_{am}^- with divalent, trivalent, and tetravalent positive ions gives 2.8×10^{12}, 4.3×10^{12}, and 5.7×10^{12} M^{-1} s^{-1}, respectively, for specific rates, k_d, at 25 °C. A comparison of calculated values

TABLE III: Thermodynamics of Solvation of Metal Cations in Liquid Ammonia at 25 °C

Species	γ, Å[a]	γ_{eff}, Å	ϵ_{eff}	$\Delta F°(M_g)$ or $\Delta F°(M_g^{z+})$, kcal mol^{-1}	$\Delta F_{el}°$, kcal mol^{-1} For γ_{eff}	$\Delta F_{el}°$, kcal mol^{-1} For ϵ_{eff}	$\Delta F°(M_{sol}^{z+})$,[b] kcal mol^{-1} For γ_{eff}	$\Delta F°(M_{sol}^{z+})$,[b] kcal mol^{-1} For ϵ_{eff}
Hg				7.6				
Hg^+	1.27	1.97[c]	3.65[d]	249.4	−79.3	−94.9	171.4	155.8
Hg^{2+}	1.10	1.51	3.35	683.8	−413.7	−423.3	271.4	261.8
Cu				71.4				
Cu^+	0.96	1.2	4.32	251.4	−130.2	−132.9	122.6	119.9
Cu^{2+}	0.72	1.42[c]	4.02[d]	719.8	−440.0	−693.0	281.1	28.1
Tl				35.2				
Tl^+	1.47	2.00	3.09	178.0	−78.1	−76.4	101.2	102.9
Fe^+	(0.94)	1.64[c]	2.3[d]	272.2	−95.2	−99.8	178.3	173.7
Fe^{2+}	0.74	1.45	2.0	646.9	−430.8	−448.7	217.4	199.6
Fe^{3+}	0.64	1.43	1.74	1355	−983.0	−995.8	373.6	360.9
Co^+	(0.92)	1.62[c]	2.38[d]	273.8	−96.4	−104.5	178.7	170.7
Co^{2+}	0.72	1.36	2.08	668.6	−459.4	−478.9	210.5	191.9
Co^{3+}	0.63	1.33[c]	1.78[d]	1443	−1057	−1036	387.1	408.0
Ni^+	(0.89)	1.59[c]	2.37[d]	269.8	−98.2	−107.8	172.9	163.4
Ni^{2+}	0.69	1.33	2.07	689.7	−469.7	−497.2	221.3	193.8
Zn^+	0.88	1.58[c]	2.28[d]	240.4	−98.9	−105.9	142.9	135.9
Zn^{2+}	0.74	1.36	1.98	656.6	−459.4	−444.2	198.5	213.8
Cd^+	1.14	1.84[c]	2.85[d]	227.0	−84.9	−94.5	143.4	145.7
Cd^{2+}	0.97	1.53	2.55	618.8	−408.3	−416.1	211.8	204.0
Pb^+	(1.40)	2.10[c]	2.97[d]	210.8	−74.4	−78.7	137.8	133.5
Pb^{2+}	1.20	1.84	2.67	559.4	−339.5	−346.2	221.2	214.5
Al^{2+}	(0.61)	1.31[c]	1.85[d]	643.9	−476.9	−499.6	168.4	145.7
Al^{3+}	0.51	1.34	1.55	1302	−1049	−1037	254.2	266.2
Cr^{2+}	0.89	1.47	2.20	623.5	−425.0	−405.9	199.7	218.9
Cr^{3+}	0.63	1.42	1.86	1339	−989.9	−1097	350.8	244.1
Ce^{2+}	(1.13)	1.83[c]		471.1	−340.6		131.8	
Ce^{3+}	1.03	1.73[c]		938.8	−810.6		129.5	
Ce^{4+}	0.92	1.62[c]		1787	−1543		245.8	

[a] From ref 36c. The values in parentheses were calculated by assuming that crystal radius of a monovalent ion is 0.2 Å greater than the crystal radius for the same divalent ion, and the crystal radius of a trivalent ion is 0.1 Å smaller than the crystal radius of the same divalent ion. [b] For the neutral species M_{sol}, $\Delta F°(M_{sol}) = \Delta F°(M_g) + 1.325$ kcal mol^{-1}. [c] Values calculated by assuming that $\gamma_{eff} = \gamma + 0.7$ Å. [d] Values calculated by assuming that ϵ_{eff} increases by 0.3 units per unit charge decrease on an ion.

of k_d with observed specific rates, k_{obsd}, given in Table I indicates that only the reaction of e_{am}^- with Tl^+ can be a diffusion-controlled reaction. However, in aqueous solutions, reactions of e_{aq}^- with many ions given in Table I are diffusion-controlled reactions (cf. specific rates for e_{aq}^- reactions[25,26] in Table I).

Dependence of k_a on the Free Energy of the Reaction. For any reaction of e_{am}^-, k_{obsd}, k_d, and k_a are related by[8]

$$\frac{1}{k_{obsd}} = \frac{1}{k_d} + \frac{1}{k_a} \tag{5}$$

For values of k_d given earlier in the discussion and values of k_{obsd} given in Table I, values of k_a were calculated for various reactions of e_{am}^- with metal ions, and are given in Table I.

For a metal ion (charge $z+$) dissolved in liquid ammonia, M_{sol}^{z+}, the reaction of e_{am}^- is

$$M_{sol}^{z+} + e_{am}^- \rightarrow M_{sol}^{(z-1)+} \tag{6}$$

The standard free energy change, $\Delta F_r°$, of reaction 6, $\Delta F°(M_{sol}^{(z-1)+})$, $\Delta F°(M_{sol}^{z+})$, and $\Delta F°(e_{am}^-)$ [the standard free energies of formation of $M_{sol}^{(z-1)+}$, M_{sol}^{z+}, and e_{am}^-, respectively], are related by

$$\Delta F_r° + \Delta F°(e_{am}^-) = \Delta F°(M_{sol}^{(z-1)+}) - \Delta F°(M_{sol}^{z+}) \tag{7}$$

Thus a relationship between $\Delta F_r°$ and k_a can directly be explored in terms of $\Delta F_r° + \Delta F°(e_{am}^-)$, and k_a. At 25 °C, from values of free energies of formation of various ions and neutral atoms dissolved in liquid ammonia (cf. Table III), values of $\Delta F_r° + \Delta F°(e_{am}^-)$ were calculated for various reactions of e_{am}^- with metal ions. A plot of log k_a vs. $\Delta F_r° + \Delta F°(e_{am}^-)$ is shown in Figure 4. An important feature of the plot is that k_a increases and attains an apparent plateau value with the increasing negative value of $\Delta F_r° + \Delta F°(e_{am}^-)$, i.e., $\Delta F_r°$. Such a behavior contradicts the theory of Marcus, in which a parabolic dependence between log k_a and $\Delta F_r°$ is predicted.[8] However, a quantum mechanical description of ETR,[7] in which the reaction is treated as the nonradiative decay of a "supermolecule" consisting of the electron donor, the electron acceptor, and the polar solvent, predicts the observed relationship (Figure 4) between log k_a and $\Delta F_r°$. The quantum mechanical theory also predicts that the activation energy of an ETR will be temperature dependent.[7,27] Therefore, for the reactions of e_{am}^- with metal ions discussed in present communication, a study of temperature effects on specific rates will be interesting.

Appendix

For the discussion of the free energies of formation, the standard state of a gaseous species is 1 atm fugacity and the 1 M standard state refers to a solvated species. Following the treatment given by Noyes for hydration of ions,[28] the solvation of gaseous cations, M_g^{z+}, in polar solvents can be elucidated by the use of reactions

$$M_g^{z+} \rightarrow M_{sol}^{z+} \qquad (\Delta F_{sol}°) \tag{A1}$$

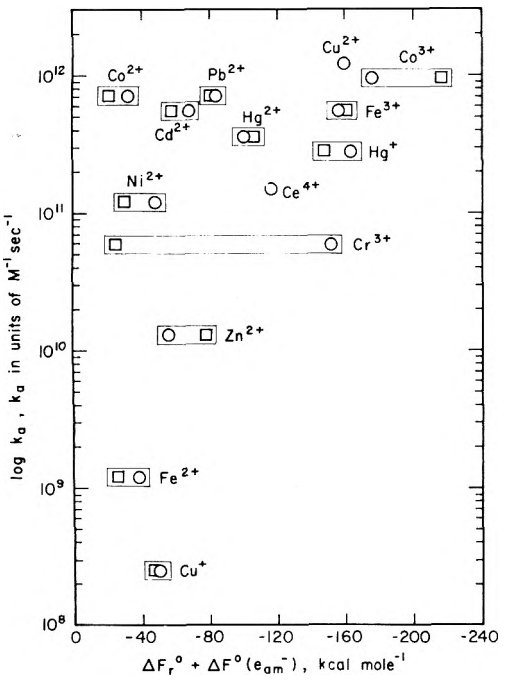

Figure 4. Plot of log k_a vs. $[\Delta F_r^\circ + \Delta F^\circ(e_{am}^-)]$: □, values based on effective dielectric constant; ○, values based on effective radii. Consult Appendix for definitions of effective radius and effective dielectric constant.

and

$$N_g \rightarrow N_{sol} \quad (\Delta F_{neut}^\circ) \tag{A2}$$

The standard free energy changes for reactions A1 and A2 are ΔF_{sol}° and ΔF_{neut}°, respectively. In reaction A2, N_g is a gaseous monoatomic neutral species of the same radius as M_g^{z+} and N_{sol} is the same neutral species in the solvated state. The solvation of M_g^{z+} can be conceived to proceed by discharging M_g^{z+}, solvating the neutral species, and then recharging it. Then one can write

$$\Delta F_{sol}^\circ = \Delta F_{neut}^\circ + \Delta F_{el}^\circ \tag{A3}$$

in which ΔF_{el}° is the electrostatic free energy change for a reversible transfer of charge $z+$ for a conducting sphere (of a size equal to the size of N) in vacuo to a same size sphere in the solvent. For $\Delta F_{sol}^\circ = \Delta F^\circ(M_{sol}^{z+}) - \Delta F^\circ(M_g^{z+})$, eq A3 gives

$$\Delta F^\circ(M_{sol}^{z+}) = \Delta F^\circ(M_g^{z+}) + \Delta F_{neut}^\circ + \Delta F_{el}^\circ \tag{A4}$$

Thus, $\Delta F^\circ(M_{sol}^{z+})$ can be calculated if one can compute $\Delta F^\circ(M_g^{z+})$, ΔF_{neut}°, and ΔF_{el}°.

Computation of $\Delta F^\circ(M_g^{z+})$. At 25 °C, from tabulated values[29] of standard free energies of formation of gaseous metals, $\Delta F^\circ(M_g)$, standard enthalpies of formation of gaseous metals, $\Delta H^\circ(M_g)$, and standard enthalpies of formation of gaseous ions, $\Delta H^\circ(M_g^{z+})$, the values of $\Delta F^\circ(M_g^{z+})$ were computed by the application of

$$\Delta F^\circ(M_g^{z+}) = \Delta F^\circ(M_g) + \Delta H^\circ(M_g^{z+}) - \Delta H^\circ(M_g) - RT \ln \frac{Q(M_g^{z+})}{Q(M_g)} \tag{A5}$$

In eq A5, R is the gas constant, T is absolute temperature, and $Q(M_g)$ and $Q(M_g^{z+})$ are electronic partition functions of M_g and M_g^{z+}, respectively. For all species (except cerium and its ions) listed in Table III, the tabulated data[30] of atomic energy levels were used to compute electronic partition functions. For Ce, Ce^{2+}, and Ce^{3+}, the data of atomic energy levels were taken from others sources.[31-33] In case of Ce^{4+}, no data of atomic energy levels were available. Thus, for computation of $\Delta F^\circ(Ce_g^{4+})$, the partition function term (which is small) in eq A5 was ignored. The results of computation are given in Table III.

Estimation of ΔF_{neut}°. The quantity ΔF_{neut}° was calculated by applying zero energy assumption. This assumption states that, for a monoatomic neutral species, the free energy of formation in 1 M standard state in gas and in solution is the same.[28] At 25 °C, ΔF_{neut}° for all species[28] is 1.325 kcal mol^{-1}. The values of $\Delta F^\circ(M_{sol})$ listed in Table III were calculated by adding 1.325 kcal mol^{-1} to values of $\Delta F^\circ(M_g)$.

Estimation of ΔF_{el}°. In principle, ΔF_{el}° can be calculated by the Born equation for charging:

$$\Delta F_{el}^\circ(\text{Born}) = -\frac{z^2}{2\gamma}\left(1 - \frac{1}{\epsilon}\right) \tag{A6}$$

in which γ is the radius of an ion and ϵ is the dielectric constant of the solvent. However, Noyes[28] has shown that for hydration of ions, the use of crystallographic radii of ions and dielectric constant of water in eq A6 does not give values of ΔF_{el}°(Born) equal to evaluated values of ΔF_{el}° for ions. However, an equality between ΔF_{el}° and ΔF_{el}°(Born) can be established either replacing γ by an effective radius, γ_{eff}, or ϵ by an effective dielectric constant. Noyes has given either parameter for hydration of ions. By two approaches, the treatment given by Noyes can be extended to estimate ΔF_e° for ions in other polar solvents. In one approach, the effective radii of ions estimated for water can be assumed to be solvent independent. Using this approach and 16.9 for dielectric constant for ammonia[34] at 25 °C, the values of ΔF_{el}° were calculated for various ions. The results are summarized in Table III. In the second approach, the values of effective dielectric constant for ammonia, $\epsilon_{eff}(NH_3)$, were estimated from the values given by Noyes of effective dielectric constant for water, $\epsilon_{eff}(H_2O)$, by applying the Lorentz–Lorenz equation[35]

$$\frac{\epsilon_{eff}(H_2O) - 1}{\epsilon_{eff}(H_2O) + 2} = \frac{V_m(NH_3)}{V_m(H_2O)} \frac{\alpha_{H_2O}}{\alpha_{NH_3}} \frac{\epsilon_{eff}(NH_3) - 1}{\epsilon_{eff}(NH_3) + 2} \tag{A7}$$

in which $V_m(NH_3)$ and $V_m(H_2O)$ are molar volumes of NH_3 and H_2O, respectively, and α_{NH_3} and α_{H_2O} are molar polarizabilities of NH_3 and H_2O, respectively. At 25 °C, $V_m(NH_3)$ = 28.3 ml mol^{-1},[36a] $V_m(H_2O)$ = 18.1 ml mol^{-1},[36b] $\alpha_{NH_3} = 2.145 \times 10^{-24}$ cm^3 mol^{-1},[37] and $\alpha_{H_2O} = 1.444 \times 10^{-24}$ cm^3 mol^{-1}.[37] The calculated values of $\epsilon_{eff}(NH_3)$ are given in Table III. Substituting these values of $\epsilon_{eff}(NH_3)$ and values of γ of respective ions (given in Table III) in eq A6, the values of ΔF_{el}° were calculated. The results are given in Table III.

References and Notes

(1) Permanent address: Laboratoire de Physico-Chimie des Rayonnements, Universite de Paris-Sud Centre d'Orsay, 9145 Orsay, France.
(2) The Radiation Laboratory of the University of Notre Dame is operated under contract with the U.S. Energy Research and Development Administration. This is ERDA Document No. COO-38-1052.
(3) L. M. Perkey and Farhataziz, *Int. J. Radiat. Phys. Chem.*, **7**, 719 (1975).
(4) Farhataziz and L. M. Perkey, *J. Phys. Chem.*, **79**, 1651 (1975).
(5) Farhataziz and L. M. Perkey, *J. Phys. Chem.*, **80**, 122 (1976).
(6) Farhataziz, P. Cordier, and L. M. Perkey, *Radiat. Res.*, in press.
(7) J. Ulstrup and J. Jortner, *J. Chem. Phys.*, **63**, 4358 (1975).
(8) R. A. Marcus in "Solvated Electron", R. F. Gould, Ed., American Chemical Society, Washington, D.C., 1965, p 138.
(9) L. G. Berg, E. E. Sidorova, V. V. Vlasov, Yu I. Sozin, and K. N. Avvakumova, *Russ. J. Inorg. Chem.*, **9**, 299 (1964).
(10) R. N. Keller and H. D. Wycoff in "Inorganic Syntheses", Vol. II, W. C. Fernelius, Ed., McGraw-Hill, New York, N.Y., 1946, p 1.
(11) A. D. McElroy and H. A. Laitinen, *J. Phys. Chem.*, **57**, 564 (1953).
(12) Farhataziz, L. M. Perkey, and R. R. Hentz, *J. Chem. Phys.*, **60**, 4383 (1974).

(13) The dose per pulse was varied by adjusting beam current and duration of pulse
(14) Z. G. Szabo in "Comprehensive Chemical Kinetics", Vol. 2, C. H. Bamford and C. F. H. Tipper, Ed., Elsevier, New York, N.Y. 1969, p 46.
(15) Farhataziz, L. M. Perkey, and R. R. Hentz, *J. Chem. Phys.*, **60**, 717 (1974).
(16) J. H. Baxendale, E. M. Fielden, and J. P. Keene, *Proc. R. Soc., London, Ser. A*, **286**, 320 (1965).
(17) M. Kelm, J. Lilie, A. Henglein, and E. Janata, *J. Phys. Chem.*, **78**, 882 (1974).
(18) G. V. Buxton and R. M. Sellers, *J. Chem. Soc., Faraday Trans. 1*, **71**, 558 (1975).
(19) M. Kelm, J. Lilie, and A. Henglein, *J. Chem. Soc., Faraday Trans. 1*, **5**, 1132 (1975).
(20) M. Farraggi and A. Amozig, *Int. J. Radiat. Phys. Chem.*, **4**, 353 (1972).
(21) N. B. Nazhat and K.-D. Asmus, *J. Phys. Chem.*, **77**, 614 (1973).
(22) B. Cercek, M. Ebert, and A. J. Swallow, *J. Chem. Soc. A*, 612 (1966).
(23) H. Jungbluth, J. Beyrich, and K.-D. Asmus, *J. Phys. Chem.*, **80**, 1049 (1976).
(24) J. Belloni, P. Cordier, and J. Delaire, *Chem. Phys. Lett.*, **27**, 241 (1974).
(25) M. Anbar, M. Bambenek, and A. B. Ross, *Natl. Stand. Ref. Data Ser., Natl. Bur. Stand.*, **No. 43** (1973).
(26) A. B. Ross, *Natl. Stand. Ref. Data Ser., Natl. Bur. Stand.*, **No. 43**, Suppl. (1975).
(27) N. R. Kestner, J. Logan, and J. Jortner, *J. Phys. Chem.*, **78**, 2148 (1974).
(28) R. M. Noyes, *J. Am. Chem. Soc.*, **84**, 513 (1962).
(29) "Selected Values of Chemical Thermodynamic Properties", *Natl. Bur. Stand. Techn. Notes*, **No. 270-3, 270-4, 270-7.**
(30) "Atomic Energy Levels", *Natl. Bur. Stand. Circ.*, **No. 467.**
(31) W. C. Martin, *Phys. Rev. A*, **3**, 3 (1971).
(32) J. Sugar, *J. Opt. Soc. Am.*, **55**, 33 (1965).
(33) R. J. Lang, *Can. J. Res. A*, **14**, 127 (1936).
(34) W. L. Jolly and C. J. Hallada, in "Non-Aqueous Solvent Systems", T. C. Waddington, Ed., Academic Press, New York, N.Y., 1965, p 5.
(35) The Lorentz–Lorenz equation is used for high frequency dielectric constant. The values[27] of $\epsilon_{eff}(H_2O)$ at 25 °C for various ions are very similar to values of high frequency dielectric constants of liquids.
(36) R. C. Weast, Ed., "Handbook of Chemistry and Physics", 52d ed, Chemical Rubber Publishing Company, Cleveland, Ohio, 1971–1972: (a) p E-22; (b) p F-11; (c) p F-171.
(37) E. A. Moelwyn-Hughes, "Physical Chemistry", 2d ed, Pergamon Press, New York, N.Y., 1964, p 383.

Correlation of Photocurrent–Voltage Curves with Flat-Band Potential for Stable Photoelectrodes for the Photoelectrolysis of Water

Jeffrey M. Bolts and Mark S. Wrighton*[1]

Department of Chemistry, Massachusetts Institute of Technology, Cambridge, Massachusetts 02139 *(Received June 16, 1976)*

Using the differential capacitance technique, the flat-band potential of n-type TiO_2, SnO_2, $SrTiO_3$, $KTaO_3$, and $KTa_{0.77}Nb_{0.23}O_3$ electrodes has been determined as a function of pH in aqueous electrolytes. Plots of flat-band potential vs. pH are linear in all cases and have a slope of ~0.059 V/pH unit. The flat-band potential correlates nicely with the onset for photoanodic currents corresponding to O_2 evolution at the n-type semiconductor and H_2 at the dark Pt cathode. The ordering of flat-band potentials at a given pH is $SrTiO_3 \sim KTaO_3 \sim KTa_{0.77}Nb_{0.23}O_3 > TiO_2 > SnO_2$ (SnO_2 most positive vs. SCE).

The photoassisted electrolysis of H_2O according to

$$H_2O \rightarrow H_2 + 0.5O_2 \quad (1)$$

has been achieved using electrochemical cells employing certain n-type semiconductors as photoanodes.[2-11] The key result is that reaction 1 can be sustained using photoelectrochemical cells where the electrical energy required is significantly lower than that thermodynamically demanded, since the photoeffect can contribute substantially to the energetic requirements. These results have sparked considerable interest in the possibility of converting light to chemical fuels using photoelectrolytic processes.

Studies in this laboratory have established that TiO_2,[2] SnO_2,[3] $SrTiO_3$,[4] $KaTaO_3$,[5] and $KTa_{0.77}Nb_{0.23}O_3$,[5] as n-type semiconductors, serve as stable photoanodes in alkaline aqueous electrolytes. All of these materials have large band gaps, E_{BG} ($\geq$3.0 eV), and, unfortunately, according to simple models for semiconductor photoelectrodes, do not respond to light of longer wavelength than that corresponding to E_{BG}. This fact alone makes these materials poor candidates for photoelectrochemical cells for the conversion of solar energy, since only a small fraction of the sun's emission is $\geq$3.0 eV.[12] Additionally, we note a poor match of E_{BG} of the stable photoelectrodes and the energy necessary to drive reaction 1 which is 1.23 eV.[13]

In considering light receptor electrodes for photoelectrochemical cells another criterion is the absolute position of the valence (VB) and conduction bands (CB). Fast electron transfer across the electrolyte–semiconductor interface occurs when the appropriate band overlaps the redox level of the electrolyte.[14] This is important since recombination of the photogenerated electron–hole pair competes with the electron transfer, and thus these relative rates influence quantum efficiency. Secondly, the absolute placement of the bands effectively controls the degree of band bending, E_B, since the surface Fermi level, E_F, for the heavily doped n-type metal oxide semiconductor essentially coincides with the CB level. The value of E_B is generally taken as the difference between E_F and the "Fermi level" of the electrolyte which is taken as the redox potential, E_{redox}, for the reaction occurring at the photoelectrode:[14]

$$E_B = E_F - E_{redox} \quad (2)$$

For reaction 1 and for n-type semiconductor photoelectrodes E_{redox} is the $O_2|OH^-$ potential. The maximum open-circuit photopotential is E_B,[14] and if E_B exceeds 1.23 V, then it is possible to run reaction 1 without any other energy source other than the light. To the extent that E_B falls short of 1.23 V (plus any required overvoltage) one requires an additional energy input assisting the effect; an applied potential, V_{appl}, must be supplied to provide the difference. Since $E_F \approx E_{CB}$ for the materials of interest here, we can conclude from this discussion that the CB position must be $\geq$1.23 V above the $O_2|OH^-$ potential, or in other words above the $H^+|H_2$ po-

tential. For rapid and energetically feasible electron transfer to the photogenerated hole of the n-type semiconductor the VB must be at least slightly below the $O_2|OH^-$ level. The ideal situation is as sketched in Scheme I.

Scheme I

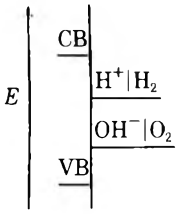

Often one may be unable to measure the position of the VB and CB from photopotential measurements. However, current–voltage properties can be used as a guide to the band positions. For example, the decomposition voltage is ~0.2 V for electrolysis of H_2O upon irradiation of a TiO_2-based (photoanode, Pt cathode) photoelectrochemical cell. This is slightly more than 1 V lower than thermodynamically required to electrolyze H_2O, and indicates that the TiO_2 CB is at least 1 V above the $O_2|OH^-$ potential. The position of the bands can be determined from the intercept of plots of (differential capacitance)$^{-2}$ against potential.[14] At the intercept potential the value of E_B is ~0 (no band bending). A comparison of this so-called flat-band potential, E_{FB}, for several electrodes allows a direct assessment of the relative decomposition voltage for a photoelectrochemical cell. Moreover, the E_{FB} values and the current–voltage properties together allow one to determine overvoltages on the photoelectrodes, i.e., how much larger than 1.23 V must ($E_B + V_{appl}$) be to obtain the flow of current corresponding to reaction 1.

In this paper we report a set of current–voltage curves under identical conditions for TiO_2, SnO_2, $SrTiO_3$, $KTaO_3$, and $KTa_{0.77}Nb_{0.23}O_3$ photoelectrodes and correlate these with E_{FB} determinations. The pH dependence of E_{FB} is also reported. Importantly, these measurements are for the same electrode materials we have used in our previous studies[2-5] allowing a good check of internal consistency and comparison with earlier[9,15,16] and contemporary E_{FB} determinations.[6a] Finally, these studies allow evaluation of the doping level in the semiconductors used in this laboratory, and completes our characterization of these single-crystal electrode materials.

Results and Discussion

1. *Current–Voltage Curves.* Current–voltage properties of SnO_2, TiO_2, $SrTiO_3$, $KTaO_3$, and $KTa_{0.77}Nb_{0.23}O_3$ have been reported previously, but in separate studies and often under quite variable conditions. Consequently, we measured the current–voltage behavior of these five electrodes under conditions as uniform as possible and the results are reproduced in Figure 1. Each data point on the curves is for an equilibrated current. The electrolyte used was 5.6 M NaOH and the irradiation source was the 254-nm output from a low-pressure Hg lamp. The electrolyte is representative of that used in our previous demonstrations of electrode durability and energy conversion efficiency.

In the present context, our major point to make here is that the potential onset for the flow of current corresponding to reaction 1 differs by about 0.7 V for the five electrodes studied. In each case, over the potential range shown in Figure 1, the Pt-cathode potential was essentially constant at ~−1.1 V vs. SCE or very nearly the value expected for the hydrogen electrode in strong base. Beginning with the most negative (vs. SCE) onset the ordering of onset potentials is as follows:

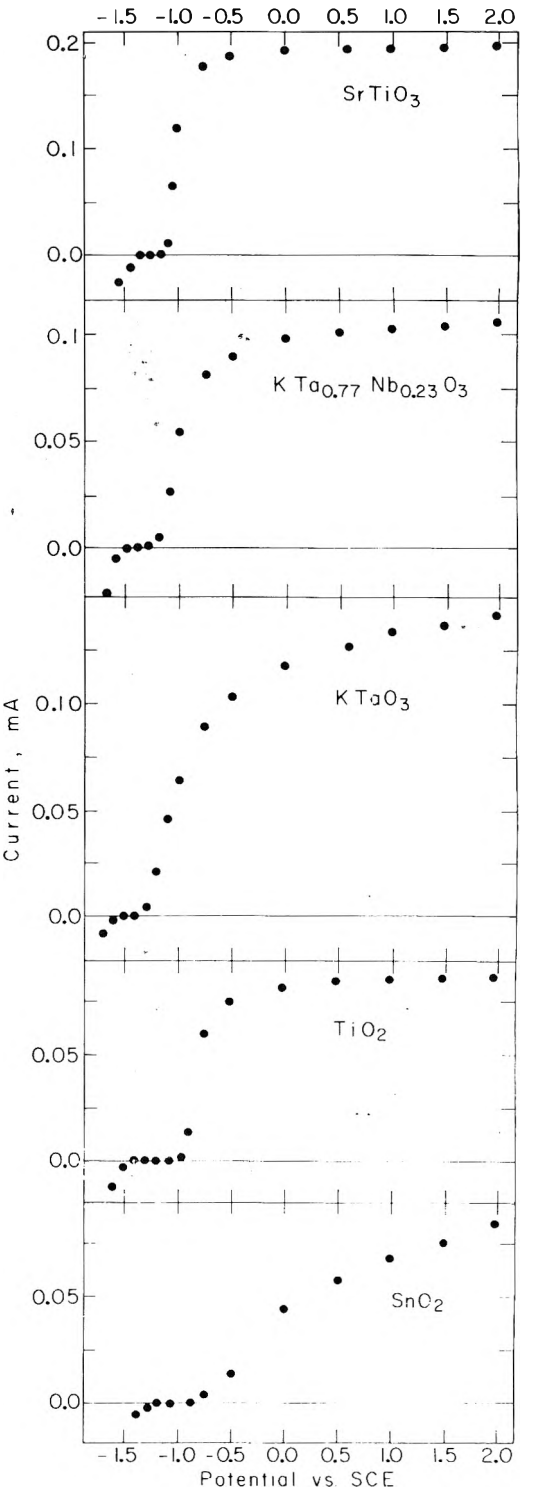

Figure 1. Photocurrent–potential curves for n-type semiconductor photoelectrodes. All data recorded in 5.6 M NaOH using 254-nm irradiation. No *dark* anodic current was observed in the potential range studied, and the *dark* cathodic (negative) current was unaffected by irradiation. In all cases the Pt cathode potential was measured to be −1.1 V vs. SCE when the photoelectrode was more positive than −1.3 V vs. SCE. Each point shown is an equilibrated (constant) current.

$SrTiO_3 \sim KTaO_3 \sim KTa_{0.77}Nb_{0.23}O_3 > TiO_2 > SnO_2$. That is, the materials $SrTiO_3$, $KTaO_3$, $KTa_{0.77}Nb_{0.23}O_3$ are superior to TiO_2 which in turn is better than SnO_2 in terms of the value of V_{appl} needed to achieve a given photocurrent.

2. *Flat-Band Potential Measurements.* Differential ca-

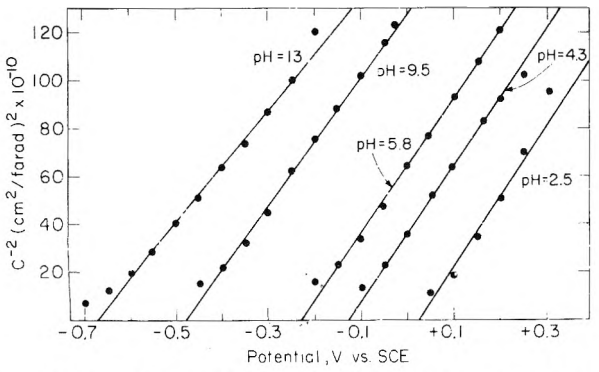

Figure 2. Mott–Schottky plots for SnO_2 as a function of pH at 298 K.

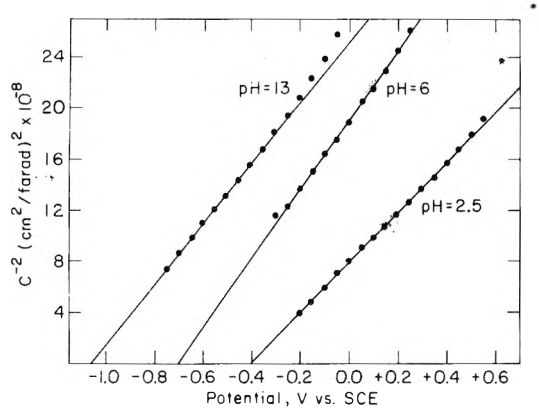

Figure 3. Mott–Schottky plots for TiO_2 as a function of pH at 298 K.

pacitance determinations were made at a constant set of conditions as a function of pH and of potential. The best data we obtained yielded plots of C^{-2} against potential (vs. SCE) at a given pH which are linear with a slope independent of pH, with intercepts moving more negative vs. SCE with increasing pH. The intercepts are taken as the value of E_{FB}, and the slope of these so-called Mott–Schottky plots[14] allows calculation of the donor density, N_D, according to

$$\text{slope} = 2/q\kappa\epsilon N_D \tag{3}$$

where κ is the dielectric constant of the semiconductor, ϵ is the permittivity of vacuum, and q is the electronic charge. Representative plots of C^{-2} vs. V (vs. SCE) are given in Figures 2, 3, and 4 for SnO_2, TiO_2, and $KTa_{0.77}Nb_{0.23}O_3$, respectively, at several pH's. Figure 5 shows plots of E_{FB} as a function of pH for the five electrodes. The solid straight lines shown in Figure 5 are drawn with a slope of 0.059 V/pH. The plots for the $SrTiO_3$, $KTaO_3$, and $KTa_{0.77}Nb_{0.23}O_3$ are very similar and fall at more negative potentials than for TiO_2 which in turn is at more negative potentials than SnO_2. Given the contrariness of measuring E_{FB} by the differential capacitance method, the dependence of E_{FB} on pH is reasonably uniform and the data points fall very close to the lines having a slope of 0.059 V/pH.

We note that the anodic current onset from the current–voltage curves falls close to the E_{FB} value established above and this lends credence to the statement that the current–voltage curves provide a good indication of E_B values. The linear pH dependence of E_{FB} with slope of 0.059 V/pH has been found by other workers[14] for metal oxide semiconductors and is associated with the protonation/deprotonation equilibrium of the electrode *surface*. Unfortunately, the tremendously large shifts in E_{FB} do not mean that E_B is changed,

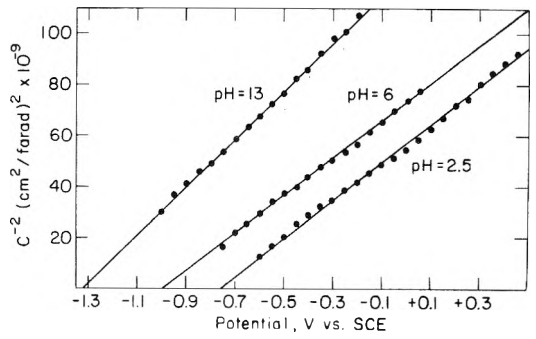

Figure 4. Mott–Schottky plots for $KTa_{0.77}Nb_{0.23}O_3$ as a function of pH at 298 K.

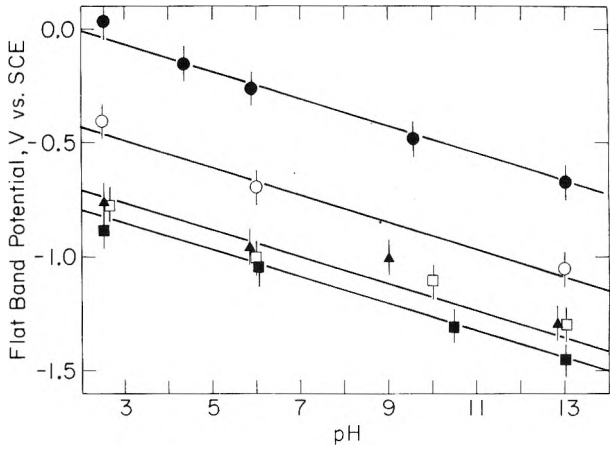

Figure 5. Dependence of flat-band potential (E_{FB}) on pH for SnO_2 (●); TiO_2 (○); $KTaO_3$ (▲); $KTa_{0.77}Nb_{0.23}O_3$ (□); and $SrTiO_3$ (■).

since E_{redox} also moves 0.059 V/pH. That is, $E_F - E_{redox}$ remains a constant since both have the same pH dependence. Indeed, a principle conclusion from the plots shown in Figure 5 is that the theoretical optical → chemical energy conversion efficiency is independent of pH, to the extent that E_{FB} vs. pH values fall on a straight line with a slope of 0.059 V/pH. Choice of pH, then, can confidently be made on the basis of other factors such as corrosiveness, cathode or anode stability, electron transfer rates, etc.

Now, assuming that $E_{FB} \approx E_{CB}$ we can determine the absolute band positions for the five electrodes studied here, since we know E_{BG}. The pertinent values are given in Table I, along with determinations of the donor densities from the slopes of the Mott–Schottky plots for each electrode. The large values of N_D justify the assumption that $E_{FB} \approx E_{CB}$. The placement of the bands (potential vs. SCE) is given in Figure 6 for a pH 13 electrolyte. From the information in Figure 6 we can point to three reasons why SnO_2 is the worst electrode for use in driving reaction 1: (i) E_{BG} is largest, (ii) E_{CB} is lowest yielding the smallest E_B, and (iii) E_{VB} is lowest, suggesting relatively low electron transfer rates unless there is a high density of surface states. For the other electrodes E_{VB} is at a comparable position (1.9 ± 0.2 V vs. SCE), and it is the ~0.25–0.38 V difference in E_{CB} which really distinguishes the TiO_2 from the perovskite materials. In all cases the E_{VB} position is significantly below the $O_2|OH^-$ couple which is at ~0.2 V vs. SCE at pH 13. Thus E_{VB} is more than 1.5 V below the redox level in each case and implicates an important role for surface states in the oxidation reaction at the photoelectrode, since otherwise we would expect slow interfacial electron transfer.

To improve the solar energy conversion efficiency for

TABLE I: Characteristics of Stable Photoelectrodes

Electrode	E_{BG}, eV[a]	Donor concn, cm^{-3}[b]	E_{VB}[c]	$E_{FB} \cong E_{CB}$[c]	E_B[d]
SnO_2	3.5	2×10^{18}	+2.8	−0.7	0.6
TiO_2	3.0	3×10^{20}	$+1.9_5$	-1.0_5	1.0
$KTaO_3$	3.4	1×10^{18}	+2.1	−1.3	1.2
$KTa_{0.77}Nb_{0.23}O_3$	~3.2	$0.2–7 \times 10^{18}$	+1.9	−1.3	1.2
$SrTiO_3$	3.2	5×10^{19}	+1.8	−1.4	1.3

[a] Assumed to be equal to wavelength onset of photocurrent from ref 2–5. [b] From slope of Mott–Schottky plots, cf. eq 3 in text and the Experimental Section. [c] All for pH 13 and vs. SCE. E_{FB} is from intercept of Mott-Schottky plot and E_{VB} is determined from the fact that E_{CB} is E_{BG} above E_{VB}. [d] E_B is independent of pH (2.5–13) and is determined from eq 2 of text.

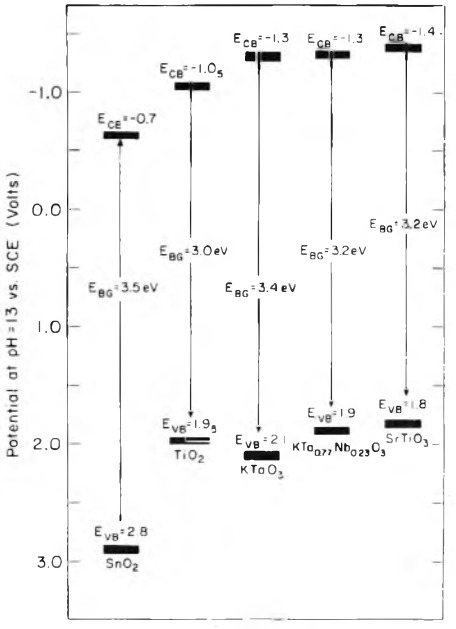

Figure 6. Position of conduction band (CB) and valence band (VB) vs. SCE at pH 13 for the five photoelectrodes studied. Cf. Scheme I and note that the $H_2|H^+$ couple is at ~−1.0 V vs. SCE and the $O_2|OH^-$ couple is at ~0.2 V vs. SCE at pH 13.

photoelectrolytic cells, one must lower the value of E_{BG} compared to those for the materials studied here. However to maintain the good current–voltage properties attained with the perovskites one must use a material having E_{CB} at or above the $H_2|H^+$ potential (~−1.1 V vs. SCE, pH ~13). The recent report[17] on n-type WO_3 (E_{BG} = 2.8 eV) as a *stable* photoanode is noteworthy. From the information given[17] concerning current–voltage behavior we can infer that E_{CB} for WO_3 is significantly lower than the $H_2|H^+$ level, and thus, while the wavelength response (onset at 2.8 eV) improved compared to the systems described here, the current–voltage properties suffer. This means that we must raise the level of the VB to lower E_{BG}. Unfortunately, raising the VB will likely contribute to the susceptibility of the electrode to photoanodic dissolution. This follows from the fact that the VB can be associated with the bonding electrons, and raising this level should contribute in a general way to instability. We note that ZnO having a value of E_{VB} just slightly higher[18] than TiO_2 undergoes photoanodic dissolution.[18,19]

In the main, the results reported herein are in good agreement with previous measurements of E_{FB} for TiO_2,[6a,9] $SrTiO_3$,[6a] SnO_2,[15] and $KTaO_3$.[16] No pH dependent data were previously reported for $KTaO_3$ but our results are not exceptional in this regard. We do see E_{FB} values which differ by up to ~0.3 V for the various determinations. However, this variation is not unexpected, since the method is not ideal and different materials preparations can alter the surface properties. The agreement with the current–voltage curves is very good, and it is this correlation that we wish to emphasize. Additionally, the value of ($E_B + V_{appl}$) does not exceed 1.23 V by a large amount. Indeed, with the exception of SnO_2 it appears that the value of ($E_B + V_{appl}$) necessary to observe 50% of the maximum photoeffect is within ~0.2 V of 1.23 V. Since H_2 evolution at Pt occurs with a small overvoltage at low current density, we can conclude that the discrepancy between ($E_B + V_{appl}$) and 1.23 V is the O_2 overvoltage. The overvoltage seems low except for SnO_2. Even at higher current densities we have noticed that the overvoltages for O_2 evolution are fairly low compared to the values[20] for metal electrodes. If the overvoltage at the photoelectrode is generally nil, then the photoelectrochemical cell for the electrolysis of H_2O will have a key advantage over an electrolytic cell in series with a solid state photovoltaic device to drive the electrolysis. However, a real test of whether there is an overvoltage must await a case where the VB level is comparable to the E_{redox} level for O_2 evolution.

Experimental Section

Electrochemical Cell. The electrochemical cells used in this study consisted of a Pt-wire cathode, approximately 20 mm in length and 1 mm in diameter, and n-type semiconductor anodes. A saturated calomel electrode (SCE) was used as a reference electrode for potential measurements.

Preparation of Anodes. Single-crystal n-type semiconducting metal oxides previously used[2–5] were employed in this work. Ohmic contact between a copper wire and the semiconductor was established by rubbing a Ga–In eutectic onto one face of the semiconductor. The copper wire was attached using conducting silver epoxy. The copper wire was threaded through 4-mm glass tubing for rigid support and all exposed metal was subsequently insulated with epoxy. Electrodes[2–5] of SnO_2, TiO_2, $SrTiO_3$, $KTaO_3$, and $KTa_{0.77}Nb_{0.23}O_3$ were prepared.

Photocurrent vs. Potential. Photocurrent vs. potential was measured for all five semiconductor electrodes using 5.6 M NaOH electrolyte and the irradiation from a low-pressure Hg lamp with principal output at 254 nm. A point by point curve was taken for each electrode allowing the photocurrent to equilibrate at each potential point. The three electrode configuration was employed and the potentiostat employed was a Heath EUA-19-2 polarography module. The Pt cathode potential was determined to be constant over the entire scan and was at about −1.1 V vs. SCE in each case.

Determination of Differential Capacitance. Capacitance measurements were made at 200 Hz using a Hewlett Packard 4260A universal bridge and an external Hewlett Packard 200AB oscillator. Although the bridge could be balanced using an internal null detector, greater accuracy was achieved by displaying the detector output on an oscilliscope, and visually minimizing the signal amplitude and phase difference.

The bias voltage was applied between the Pt and semiconductor electrodes (through the bridge leads) and the potential difference between the anode and SCE was recorded on a Data Precision 1450 digital multimeter. Capacitance measurements were made at 50-mV steps over the ranges indicated in the figures. The capacitance measurements were

made using a 0.5 M K_2SO_4 electrolyte with added H_2SO_4 or NaOH to adjust the pH between 2.5 and 13. The pH was measured with a Corning pH meter.

The values of N_D were determined from the slope of C^{-2} vs. potential. The N_D values are given in the table and were calculated using the following values for the dielectric constant κ: TiO_2 (173);[21] SnO_2 (23.4);[21] $SrTiO_3$ (310);[22] $KTaO_3$ (243).[23] The dielectric constant of $KTa_{0.77}Nb_{0.23}O_3$ has not been reported, but $KTa_{0.65}Nb_{0.35}O_3$ is ~6000[24] and we thus calculated N_D for the $KTa_{0.77}Nb_{0.23}O_3$ for $\kappa = 243$ and $\kappa = 6000$ assuming these to represent the limits. The two limits are given in Table I. In calculating N_D using eq 3 the value of ϵ used was 8.854×10^{-12} F/m, and the value of q used was 1.602×10^{-19} C.

Acknowledgment. We acknowledge the support of the National Aeronautics and Space Administration and the M.I.T. Cabot Solar Energy Fund.

References and Notes

(1) Fellow of the Alfred P. Sloan Foundation, 1974–1976, and recipient of a Dreyfus Teacher-Scholar Grant, 1975–1980.
(2) M. S. Wrighton, D. S. Ginley, P. T. Wolczanski, A. B. Ellis, D. L. Morse, and A. Linz, *Proc. Natl. Acad. Sci. U.S.A.*, **72**, 1518 (1975).
(3) M. S. Wrighton, D. L. Morse, A. B. Ellis, D. S. Ginley, and H. B. Abrahamson, *J. Am. Chem. Soc.*, **98**, 44 (1976).
(4) M. S. Wrighton, A. B. Ellis, P. T. Wolczanski, D. L. Morse, H. B. Abrahamson, and D. S. Ginley, *J. Am. Chem. Soc.*, **98**, 2774 (1976).
(5) A. B. Ellis, S. W. Kaiser, and M. S. Wrighton, *J. Phys. Chem.*, **80**, 1325 (1976).
(6) (a) T. Watanabe, A. Fujishima, and K. Honda, *Bull. Chem. Soc. Jpn.*, **49**, 355 (1976); (b) A. Fujishima, K. Kohayakawa, and K. Honda, *ibid.*, **48**, 1041 (1975); (c) A. Fujishima and K. Honda, *Nature (London)*, 238 (1972).
(7) J. Keeney, D. H. Weinstein, and G. M. Haas, *Nature (London)*, **253**, 719 (1975).
(8) W. Gissler, P. L. Lensi, and S. Pizzini, *J. Appl. Electrochem.*, **6**, 9 (1976).
(9) K. L. Hardee and A. J. Bard, *J. Electrochem. Soc.*, **122**, 739 (1975).
(10) A. J. Nozik, *Nature (London)*, **257**, 383 (1975).
(11) (a) J. G. Mavroides, J. A. Kafalas, and D. F. Kolesar, *Appl. Phys. Lett.*, **28**, 241 (1976); (b) J. G. Mavroices, D. I. Tchernev, J. A. Kafalas, and D. F. Kolesar, *Mater. Res. Bull.*, **10**, 1023 (1975).
(12) M. D. Archer, *J. Appl. Electrochem.*, **5**, 17 (1975).
(13) W. M. Latimer, "Oxidation Potentials", 2nd ed, Prentice Hall, Englewood Cliffs, N.J., 1952.
(14) H. Gerischer in "Physical Chemistry", Vol. IXA, H. Eyring, D. Henderson, and W. Jost, Ed., Academic Press, New York, N.Y., 1970, Chapter 5 and references therein.
(15) F. Möllers and R. Memming, *Ber. Bunsenges. Phys. Chem.*, **76**, 469 (1972).
(16) P. J. Boddy, D. Kahng, and Y. S. Chen, *Electrochim. Acta*, **13**, 1311 (1968).
(17) G. Hodes, D. Cahen, and J. Manassen, *Nature (London)*, **260**, 312 (1976).
(18) F. Lohmann, *Ber. Bunsenges. Phys. Chem.*, **70**, 428 (1966).
(19) R. Williams, *J. Chem. Phys.*, **32**, 1505 (1960).
(20) D. A. Skoog and D. M. West, "Fundamentals of Analytical Chemistry", Holt, Rinehart and Winston, New York, N.Y., 1963, p 523.
(21) N. Bogoriditskii, I. Mityureva, and I. Fridberg, *Sov. Phys. Solid State*, **4**, 1753 (1963).
(22) G. A. Samara and A. A. Giardini, *Phys. Rev.*, **140**, A955 (1965).
(23) S. H. Wemple, *Phys. Rev.*, **140**, A1575 (1965).
(24) F. S. Chen, J. E. Geusic, S. K. Kurtz, J. G. Skinner, and S. H. Wemple, *J. Appl. Phys.*, **37**, 388 (1966).

Interpretation of Activation Parameters for Simple Electrode Reactions

Michael J. Weaver

Department of Chemistry, Michigan State University, East Lansing, Michigan 48824 *(Received April 8, 1976)*

The physical significance of the alternative experimental definitions of electrochemical activation parameters are analyzed in relation to the actual barrier heights to electron transfer (the "true" activation parameters). Although Temkin's "ideal" enthalpy of activation as defined by the temperature dependence of the rate constant evaluated at a constant Galvani potential ϕ_m is most closely related to the corresponding true parameter at the same electrode potential, the ideal parameter evaluated at $\phi_m = 0$ has no particular theoretical significance for simple electron transfer reactions. However, the "real" enthalpy of activation obtained from the temperature dependence of the standard rate constant has, contrary to common belief, considerable theoretical significance as it is equal to the true enthalpy of activation for zero enthalpic driving force and is closely related to the "intrinsic reorganization factor" λ of the Marcus theory of electron transfer. Although the true entropies and volumes of activation for a single electrochemical step can only be extracted from ideal activation parameters evaluated at ϕ_m = constant, the real entropies and volumes of activation derived from the temperature and pressure coefficients of the standard rate constant always equal the mean of the ideal quantities for the forward and backward electrochemical reactions when the transfer coefficient $\alpha = 0.5$. The experimental evaluation of both real and ideal electrochemical activation parameters should provide important insights into the nature of outer-sphere electrode reactions and may provide diagnostic criteria for the distinction between inner- and outer-sphere electrode reactions.

Introduction

The evaluation of activation parameters for simple homogeneous electron transfer reactions, particularly of heats and entropies of activation, have frequently been made in addition to measurements of the rate constants themselves. Although the relative values of these activation parameters are not always diagnostic of reaction type (in particular, they do not appear to offer a clear-cut distinction between inner- and outer-sphere mechanisms involving metal complexes[1,2]), their

evaluation has important theoretical implications,[2-5] and provides a much fuller description of the kinetic processes involved.[6]

However, measurements and hence interpretation of activation parameters for the analogous electrochemical processes have remained extremely rare, even by comparison with the relative scarcity of good-quality rate data for simple redox processes at electrodes. One reason for this state of affairs can perhaps be traced to the widely expressed viewpoint (for example, see ref 7–15) that theoretically meaningful activation parameters for electrochemical reactions can only be obtained by varying the temperature or external pressure while holding the single electrode potential at zero[7-10,12,13] (or at least constant) at the interface in question. As the absolute values of the single metal–solution potential difference, or even its temperature and pressure derivatives are thermodynamically inaccessible quantities,[7,8,16] it is generally considered that activation parameters for electrochemical reactions are not "experimentally accessible" on the same basis as for ordinary chemical reactions, such as electron transfer processes between reactants present in homogeneous solution.

On the other hand, Marcus[17] has derived theoretical expressions for the electrochemical free energy of activation at the standard electrode potential for simple electrode processes, and shown that the standard free energies of activation of the corresponding electrochemical and homogeneous self-exchange reactions are closely related when the former quantity is determined at the standard electrode potential for the half-cell reaction under consideration. Some authors (e.g., ref 3 and 4) have interpreted enthalpies of activation obtained from the temperature dependence of the standard rate constant, but without a detailed discussion of their theoretical significance. Still other conditions for the measurement of electrochemical activation parameters have also been suggested, but primarily from the standpoint of experimental expedience.[12,13]

In view of this apparent confusion, it seems desirable to carefully examine the physical meaning of the alternative formulations of electrochemical activation parameters, and in particular their relation to the widely studied and theoretically unambiguous activation parameters that can be defined for homogeneous electron transfer processes. Such an examination forms the objective of the present communication.

Alternative Formulations of Electrochemical Activation Parameters

The rate constant for a simple electrochemical reaction can be written as[17]

$$k_e = Z_e \kappa \rho \exp\left(\frac{\Delta \overline{G}^{\circ}_{\ddagger}}{RT}\right) \tag{1}$$

where Z_e is the heterogeneous collision frequency, κ and ρ are constants expected to be close to unity,[17,18] $\Delta \overline{G}^{\circ}_{\ddagger}$ is the standard electrochemical free energy of activation, and the other terms have their usual significance. When discussing activation parameters, the overall electrochemical free energy of activation $\Delta \overline{G}^{\circ}_{\ddagger}$ has often been separated into its so-called "chemical" and "electrical" components,[8,20] resulting in expressions such as eq 2 for a one-electron reduction reaction:

$$k_e = Z_e \kappa \rho \exp\left(-\frac{\Delta G^{\circ}_{\ddagger}}{RT}\right) \exp(-\alpha f \phi_m) \tag{2}$$

where ϕ_m is the inner (Galvani) potential difference across the metal–solution interface, α is the (apparent) electrochemical transfer coefficient, $\Delta G^{\circ}_{\ddagger}$ is a "chemical" standard free energy of activation equal to $\Delta \overline{G}^{\circ}_{\ddagger}$ when $\phi_m = 0$, and $f = F/RT$. Further, $\Delta G^{\circ}_{\ddagger}$ has been separated into enthalpic and entropic components yielding

$$k_e = Z_e \kappa \rho \exp\left(\frac{\Delta S^{\circ}_{\ddagger}}{R}\right) \exp\left(-\frac{\Delta H^{\circ}_{\ddagger}}{RT}\right) \exp(-\alpha f \phi_m) \tag{3}$$

The enthalpy of activation extracted from an Arrhenius plot of $R \ln k_e$ vs. $1/T$ for the condition $\phi_m = 0$ (therefore making the assumption that both $\Delta H^{\circ}_{\ddagger}$ and $\Delta S^{\circ}_{\ddagger}$ are temperature independent) has been termed an "ideal" enthalpy of activation[7] $(\Delta H^{\circ}_{\ddagger})_{ideal}$. It was originally defined[7] for the more general condition ϕ_m = constant. In particular, eq 2 can be rewritten in the form

$$k_e = Z_e \kappa \rho \exp\left[-\frac{(\Delta \overline{G}^{\circ}_{\ddagger})^{\phi_m^{\circ}}}{RT}\right] \exp[-\alpha f(\phi_m - \phi_m^{\circ})] \tag{4}$$

$$k_e = Z_e \kappa \rho \exp\left(\frac{\Delta S^{\circ}_{\ddagger}}{R}\right)_{ideal} \times \exp\left[-\left(\frac{\Delta H^{\circ}_{\ddagger}}{RT}\right)^{\phi_m^{\circ}}_{ideal}\right] \exp[-\alpha f(\phi_m - \phi_m^{\circ})] \tag{5}$$

ϕ_m° is the Galvani potential which corresponds to the standard electrode potential E° of the reaction under consideration at a given temperature T. $(\Delta H^{\circ}_{\ddagger})^{\phi_m^{\circ}}_{ideal}$ is the ideal enthalpy of activation corresponding to this standard potential; it is obtained from the slope of an Arrhenius plot evaluated at ϕ_m°, and is therefore the appropriate single value of $\Delta H^{\circ}_{\ddagger}$ which is required to satisfy eq 5 at various temperatures for a given value of ϕ_m. Similarly, $(\Delta S^{\circ}_{\ddagger})_{ideal}$ is an ideal entropy of activation obtained by re-inserting $(\Delta H^{\circ}_{\ddagger})^{\phi_m^{\circ}}_{ideal}$ back into eq 5.

Alternatively, eq 4 can be rewritten in terms of cell potentials:

$$k_e = Z_e \kappa \rho \exp\left[-\frac{(\Delta \overline{G}^{\circ}_{\ddagger})^{E^{\circ}}}{RT}\right] \exp[-\alpha f(E - E^{\circ})] \tag{6}$$

where E is the electrode potential that corresponds to the Galvani potential ϕ_m. The two exponential terms in eq 6 will be numerically identical with those in eq 4. However, the individual enthalpy and entropy of activation determined from an Arrhenius plot evaluated at the constant *cell* potential E° will generally differ from the corresponding ideal parameters that are determined at constant ϕ_m° as generally $(\partial \phi_m/\partial T)_{E^{\circ}} \equiv (d\phi_m^{\circ}/dT) \neq 0$; these quantities have been termed "real" activation parameters, as expressed in

$$k_e = Z_e \kappa \rho \exp\left(\frac{\Delta S^{\circ}_{\ddagger}}{R}\right)_{real} \times \exp\left[-\left(\frac{\Delta H^{\circ}_{\ddagger}}{RT}\right)^{E^{\circ}}_{real}\right] \exp[-\alpha f(E - E^{\circ})] \tag{7}$$

Two relationships between ideal and real enthalpies of activation have been derived.[7,8] As at a given electrode potential where $\phi_m \equiv \eta^{\circ} (= E - E^{\circ})$

$$-R\left(\frac{\partial \ln k_e}{\partial(1/T)}\right)_{\eta^{\circ}} = (\Delta H^{\circ}_{\ddagger})_{real} = (\Delta H^{\circ}_{\ddagger})^{\phi_m}_{ideal} + \frac{\alpha F}{T}\left(\frac{\partial \phi_m}{(1/T)}\right)_{\eta^{\circ}} \tag{8}$$

and as

$$\left(\frac{\partial \phi_m}{\partial(1/T)}\right)_{\eta^{\circ}} = -T^2\left(\frac{\partial \phi_m}{\partial T}\right)_{\eta^{\circ}} = -T^2\frac{\Delta S^{\circ}}{F}$$

then

$$(\Delta H^{\circ}_{\ddagger})^{\phi_m}_{ideal} = (\Delta H^{\circ}_{\ddagger})^{\eta^{\circ}}_{real} + \alpha T \Delta S^{\circ} \tag{9}$$

Also, for the corresponding ideal and real parameters defined at $\phi_m = 0$ and $E°$ (i.e., $\eta° = 0$), respectively, it has been shown that[7,8]

$$(\Delta H^\circ_\pm)^{\phi_m=0}_{ideal} = (\Delta H^\circ_\pm)^{\eta^\circ=0}_{real} + \alpha(\Delta H°)^{\phi_m=0} \quad (10)$$

$\Delta S°$ and $(\Delta H°)^{\phi_m=0}$ are the changes in standard entropy and enthalpy, respectively, in passing from the reactant to the product states, the latter referring to a potential where $\phi_m = 0$. $\Delta S°$ is assumed to be independent of electrode potential.[24] α is either the apparent or intrinsic electrochemical transfer coefficient,[25] depending on whether or not the measured rate constants employed to evaluate the activation parameters have been corrected for double-layer effects.

By combining eq 4–8, the relationship between the real and ideal entropies of activation is found to be

$$(\Delta S^\circ_\pm)_{ideal} = (\Delta S^\circ_\pm)_{real} + \alpha\Delta S° \quad (11)$$

Also, both "ideal" and "real" volumes of activation $(\Delta V^\circ_\pm)_{ideal}$ and $(\Delta V^\circ_\pm)_{real}$ have been similarly defined[11,14,15] from the dependence of $\ln k_e$ upon the external pressure under conditions of constant ϕ_m and $\eta°$, respectively. At a given potential where $\phi_m \equiv \eta°$, $(\Delta V^\circ_\pm)_{ideal}$ and $(\Delta V^\circ_\pm)_{real}$ have been shown[14,15] to be related via

$$(\Delta V^\circ_\pm)_{ideal} = (\Delta V^\circ_\pm)_{real} + \alpha\Delta V° \quad (12)$$

where $\Delta V°$ is the difference in partial molar volume between the reactant and product.

As neither $\Delta S°$, $\Delta H°$, nor $\Delta V°$ are susceptible to direct experimental determination, ideal activation parameters can only be obtained from the measurable real parameters by recourse to extrathermodynamic estimates of these single ion quantities.[26]

We shall now consider the relative theoretical and interpretative merits, and experimental accessibility of real and ideal activation parameters.

Physical Interpretation

We shall consider, for convenience, the one-electron electrochemical reduction sequence

$$\underset{\text{I}}{Ox + M(e^-,\phi_m)} \rightleftarrows \underset{\text{II}}{Ox\cdots M(e^-,\phi_m)} \rightarrow \underset{\text{III}}{Red\cdots M(\phi_m)} \rightleftarrows \underset{\text{IV}}{Red + M(\phi_m)} \quad (13)$$

where $M(e^-,\phi_m)$ denotes that the reacting electron is held at a Galvani potential ϕ_m with respect to the bulk solution, and the intermediate states labeled II and III represent configurations immediately prior to, and following, the rate-determining activation process that yields electron transfer, respectively.[17,27] The energetic differences between states I and II, and III and IV give rise to the so-called "double-layer effects".[27]

For this electrode reaction under a given set of experimental conditions (i.e., electrolyte composition, temperature, electrode potential, etc.), the forward activation process will be associated with the unambiguously definable enthalpic and entropic barriers with respect to state I, $\Delta\overline{H}^\circ_{\pm-I}$ and $\Delta S^\circ_{\pm-I}$ respectively, in addition to the overall free energy of activation $\overline{G}^\circ_{\pm-I}$ that was defined in eq 1. These quantities, which are clearly the parameters of theoretical interest, will be labeled "true" activation parameters. Such quantities must be carefully distinguished from the "ideal" and "real" activation parameters which are experimental quantities obtained from the temperature coefficients of electrode reaction rates.

For ordinary chemical reactions, the apparent enthalpy and entropy of activation that are extracted from an Arrhenius plot are usually identified with the true activation parameters. An assumption implicit in this procedure is that the true enthalpy and entropy of activation are not significantly dependent upon temperature, which is questionable in some cases.[28] For the electrochemical reduction (13), the two "reactants" are the bulk reactant Ox and the electron residing within the electrode material. Although the latter reactant is not required to be thermally activated, the electrode potential will affect the true enthalpy of activation via variations in the electrochemical potential $\bar{\mu}^\circ_e$ of the reacting electron.[21,29] As $\bar{\mu}^\circ_e$ can only be held constant at varying temperatures by holding constant the thermodynamically inaccessible Galvani potential ϕ_m rather than the measurable cell potential E, then it follows that the true enthalpy, and hence entropy of activation for an electrochemical reaction at a given electrode potential can be more closely identified with the "ideal" rather than the "real" activation parameters. However, the true enthalpy of activation at a given potential ϕ_m, $(\Delta\overline{H}^\circ_{\pm-I})^{\phi_m}_{true}$, is still expected to generally differ from $(\Delta H^\circ_{\pm-I})^{\phi_m}_{ideal}$ determined from the Arrhenius slope of $R \ln k_e$ vs. $1/T$. This is because the activated state is located within, and state I outside the double-layer region, giving rise to a component of $(\Delta\overline{H}^\circ_{\pm-I})^{\phi_m}_{true}$, $(\Delta H^\circ_{\pm-I})_{dl}$ resulting from the effect of the double layer upon the enthalpy of the activated state. For outer-sphere reactions, $(\Delta H^\circ_{\pm-I})_{dl}$ will be determined by the potential difference across the diffuse layer, ϕ_2, which in turn is dependent on the excess electrode charge density q_m, rather than ϕ_m. Thus $(\Delta H^\circ_{\pm-I})^{q_m}_{dl}$ and therefore $(\Delta H^\circ_{\pm-I})^{\phi_m}_{true}$ will generally be dependent on temperature. This temperature dependence can be estimated from a knowledge of $(\partial q_m/\partial T)\phi_m$ using a diffuse layer model such as the Gouy–Chapman–Stern theory coupled with the Frumkin equation.[30] Thus[31]

$$-\left[\frac{R\,\partial(\ln k_e)^{\phi_m}}{\partial(1/T)}\right] = (\Delta H^\circ_{\pm-I})^{\phi_m}_{ideal} = (\Delta\overline{H}^\circ_{\pm-I})^{\phi_m}_{true} + \frac{1}{T}\left[\frac{\partial(\Delta\overline{H}^\circ_{\pm-I})^{\phi_m}_{true}}{\partial(1/T)}\right] \quad (14)$$

The thermodynamic inaccessibilty of ϕ_m, and hence ideal activation parameters, has led to the common and even conventional assertion that true electrochemical activation parameters cannot be experimentally determined, at least not with useful precision. Moreover, the assertion has been made[7-10,13] that only ideal enthalpies of activation evaluated at the (experimentally inaccessible) potential $\phi_m = 0$ are "theoretically meaningful" on the same basis as those for ordinary chemical reactions. This often-quoted conclusion was originally made,[7] and subsequently reaffirmed,[8-10,32] by workers primarily concerned with the proton discharge reaction. As the formation of the activated state for this particular electrode reaction has been considered (at least under some conditions) to involve proton transfer from H_3O^+ to the metal surface with only subsequent charge neutralization,[32] theoretical calculations of the barrier height using this model need to be compared with experimental ideal enthalpies of activation evaluated for the condition $\phi_m = 0$, where the presence of the electrode will not affect the energetics of the proton transfer act.[10,32]

However, for simple electrochemical reactions controlled by electron rather than atom transfer, quite a different situation is encountered. At the standard potential, $E°$, for the overall reaction 13, the standard electrochemical potential of the reacting electron, $\bar{\mu}^\circ_{M,e^-}$, will equal the difference in the standard electrochemical potentials for Ox and Red, $(\bar{\mu}^\circ_{Red} -$

$\bar{\mu}^{\circ}_{Ox}$).[33] Neither $\bar{\mu}^{\circ}_{M,e^-}$ nor $(\bar{\mu}^{\circ}_{Red} - \bar{\mu}^{\circ}_{Ox})$ are susceptible to thermodynamic determination.[34] In the corresponding chemical self-exchange reaction

$$\underset{\text{I}}{Ox + Red_{\bigstar}} \rightleftarrows \underset{\text{II}}{Ox \cdots Red_{\bigstar}} \rightarrow \underset{\text{III}}{Red \cdots Ox_{\bigstar}} \rightleftarrows \underset{\text{IV}}{Red + Ox_{\bigstar}} \quad (15)$$

the reacting electron is provided by the tagged reactant $Red_{\bigstar}$. There is a clear parallel between the heterogeneous and homogeneous "reductants" $M(e^-,E^\circ)$ and $Red_{\bigstar}$ in that both serve to maintain the standard free energy of the overall reactions 13 and 15 at zero at all temperatures.[17]

As Marcus has shown,[17] a close parallel therefore exists between the standard free energies of activation for corresponding electrochemical and chemical self-exchange reactions when the former are evaluated at E°. This relationship arises because the calculation of $\Delta G^{\circ}_{\ddagger}$ for all simple outer-sphere electron transfer reactions is facilitated when the standard free energies of the reactant and product states are equal.[17] In the heterogeneous case only one ionic particle is required to be activated as opposed to two particles in the homogeneous case. However, in *neither* case is the free energy required for a single ion to reach the activated state obtainable experimentally. Thus for homogeneous reactions, only a total free energy that is required for the activation of both reactants is measured; for heterogeneous reactions a similar summation over the ionic reactant and the reactant (or product) electron is involved, although only the former reactant is required to be thermally activated in this case. Therefore, for simple electrochemical redox reactions, the (unknown) modification of the free energy barrier caused by the presence of a nonzero ϕ_m at the standard potential E° actually facilitates theoretical estimation of the barrier height.[17]

Further, the (experimentally accessible) real enthalpy of activation evaluated at the standard potential E° also has considerable significance. Thus, the ideal and real enthalpies of activation measured at the standard potential $E^\circ \equiv \phi^{\circ}_m$ for the reaction sequence 13 are related by eq 16 (cf. eq 9):

$$(\Delta H^{\circ}_{\ddagger-I})^{\phi_m^\circ}_{ideal} = (\Delta H^{\circ}_{\ddagger-I})^{E^\circ}_{real} + \alpha T \Delta S^{\circ}_{IV-I} \quad (16)$$

where ΔS°_{IV-I} is the entropy of the final state IV with respect to the initial state I. However at E°, as noted above,[17] $\Delta G^{\circ}_{IV-I} = 0$, and therefore $(\Delta H^{\circ}_{IV-I})^{E^\circ} = T\Delta S^{\circ}_{IV-I}$ (note only the enthalpic term is considered to be potential dependent[28]). As $\delta(\Delta H^{\circ}_{\ddagger-I}) = \alpha\delta(\Delta H^{\circ}_{IV-I})$, then the ideal enthalpy of activation at a potential where $\Delta H^{\circ}_{IV-I} = 0$ will be

$$(\Delta H^{\circ}_{\ddagger-I})^{\Delta H=0}_{ideal} = (\Delta H^{\circ}_{\ddagger-I})^{\phi_m^\circ}_{ideal} - \alpha\Delta H^{\circ}_{IV-I} = (\Delta H^{\circ}_{\ddagger-I})^{\phi_m^\circ}_{ideal} - \alpha T\Delta S^{\circ}_{IV-I} \quad (17)$$

Combining eq 16 and 17 yields the simple result

$$(\Delta H^{\circ}_{\ddagger-I})^{E^\circ}_{real} = (\Delta H^{\circ}_{\ddagger-I})^{\Delta H=0}_{ideal} \quad (18)$$

Thus the real enthalpy of activation measured at E°, i.e., from the temperature dependence of the standard rate constant, can be directly identified with the ideal enthalpy of activation at the (thermodynamically immeasurable) potential where the electrode reaction exhibits zero enthalpic driving force, $\Delta H^{\circ}_{IV-I} = 0$. This fact was also noted by Randles.[35] The true enthalpy of activation at this potential may be obtained from $(\Delta H^{\circ}_{\ddagger-I})^{E^\circ}_{real}$ by taking into account the variation of $(\Delta H^{\circ}_{\ddagger-I})^{\Delta H=0}$ with temperature due to double layer effects by using eq 19 (cf. eq 14 above):

$$R\left[\frac{\partial(\ln k_e)}{\partial(1/T)}\right]_{E^\circ} = (\Delta H^{\circ}_{\ddagger-I})^{E^\circ}_{real} = (\Delta \overline{H}^{\circ}_{\ddagger-I})^{\Delta H=0}_{true} + \frac{1}{T}\left[\frac{\partial(\Delta \overline{H}^{\circ}_{\ddagger-I})^{\Delta H=0}_{true}}{\partial(1/T)}\right] \quad (19)$$

The theoretical significance of this parameter can be illustrated by considering the Marcus theory.[17] According to this treatment, the standard rate constant k_s can be written for reaction 13 as[17]

$$\ln k_s = \ln Z_e\kappa\rho - \frac{(\Delta G^{\circ}_{\ddagger-I})^{E^\circ}}{RT} = \ln Z_e\kappa\rho - \frac{1}{RT}\left[\frac{\Delta G^{\circ}_{II-I} + \Delta G^{\circ}_{III-IV}}{2} + \frac{\lambda_e}{4}\right] \quad (20)$$

where λ_e is the "intrinsic reorganization factor".[4,17] From the theoretical expression for λ_e, its temperature dependence can be shown to be small (cf. ref 36). Therefore, assuming for simplicity that the enthalpic and entropic components of ΔG°_{II-I} and $\Delta G^{\circ}_{III-IV}$ are not appreciably temperature dependent (any known temperature dependence of these quantities can be taken into account as outlined above, e.g., in eq 14), then we can write[31]

$$-R\left(\frac{d\ln k_s}{d(1/T)}\right) = (\Delta H^{\circ}_{\ddagger-I})^{E^\circ}_{real} = \frac{\Delta H^{\circ}_{II-I} + \Delta H^{\circ}_{III-IV}}{2} + \frac{\lambda_e}{4} \quad (21)$$

Therefore by comparing the real enthalpy of activation with the standard free energy of activation, both determined at E°, the magnitude of the entropic work terms $(\Delta S^{\circ}_{II-I} + \Delta S^{\circ}_{III-IV})$ may be estimated. Alternatively, if these terms can be assumed to be small, then the term $\ln Z_e\kappa\rho$ in eq 20 can be independently assessed and, for example, the possible presence of nonadiabaticity effects detected ($\kappa \ll 1$).

Of particular interest is the relationship between activation parameters for corresponding electrochemical and chemical self-exchange reactions (reactions 13 and 15).

For the chemical self-exchange reaction 15 one can write[17] (cf. eq 20 and 21)

$$\ln k_c = \ln Z_c\kappa\rho - \frac{\Delta G^{\circ}_{\ddagger-I}}{RT} = \ln Z_c\kappa\rho - \frac{1}{RT}\left[\frac{(\Delta G^{\circ}_{II-I} + \Delta G^{\circ}_{III-IV})}{2} + \frac{\lambda_c}{4}\right] \quad (22)$$

where the various terms containing the "c" subscripts have the same significance for the homogeneous reaction 15 as for the heterogeneous reaction 13. Further, if the enthalpic and entropic components of the terms in eq 22 exhibit no temperature dependence,[28] we can write

$$-R\left(\frac{d\ln k_c}{d(1/T)}\right) = \Delta H^{\circ}_{\ddagger-I} = \frac{\Delta H^{\circ}_{II-I} + \Delta H^{\circ}_{III-IV}}{2} + \frac{\lambda_c}{4} \quad (23)$$

Therefore comparisons of activation parameters via eq 21 and 23, in addition to the more conventional comparisons of absolute reaction rates via eq 20 and 22, should be useful in probing the similarities and differences between electrochemical and chemical electron transfer processes. In practice, the true enthalpy and entropy of activation should be easier to quantitatively obtain for electrochemical, rather than chemical electron transfer reactions as the conventional electrostatic theory employed to predict the behavior of the work terms ΔG°_{II-I} and $\Delta G^{\circ}_{III-IV}$ has met with somewhat more experimental success for the former, compared with the latter

reaction type. (These models, which are closely analogous, are the coupled Guoy–Chapman–Stern–Frumkin,[30] and the Debye–Hückel–Bronsted treatments,[37] respectively.)

However, in order to extract the true electrochemical entropy of activation $(\Delta S^\circ_{\pm-I})_{true}$ from experimental data, measurements of ideal rather than real activation enthalpies must be made and equations such as (5) and (14) employed. Thus the true activation entropy may either be extracted from the true activation enthalpy (together with a rate constant at a single temperature) or, equivalently, be obtained from the ideal activation entropy as (cf. eq 14)

$$(\Delta S_{\pm-I})_{true} = (\Delta S^\circ_{\pm-I})_{ideal} - \frac{1}{T^2}\left[\frac{\partial(\Delta \overline{H}^\circ_{\pm-I})^{\phi_m}_{true}}{\partial(1/T)}\right] \quad (24)$$

Estimates of $(\partial\phi_m/\partial T)_{E^\circ}$ required to construct Arrhenius plots at constant ϕ_m, rather than at the standard potential E°, can be made with reasonable precision from experimental estimates of half-cell entropies[26,38,39] since $F(\partial\phi_m/\partial T)_{E^\circ} = \Delta S^\circ$. By determining the coefficient $(\partial\phi_m/\partial T)_{E^\circ}$ with E° measured against a reference electrode for an electrode reaction for which good estimates of ΔS° are available, the coefficient $(\partial\phi_m/\partial T)_E$ can be determined and used to estimate ideal activation parameters for electrode reactions where ΔS° is unknown and therefore where eq 9 or 11 cannot be utilized. It should be noted that the magnitude of the ideal entropy of activation will be at least partly influenced by the reaction entropy ΔS° as the activated state is expected to be to some extent intermediate in structure between the reactant and product. Therefore interpretation of such quantities will not be in general as simple as the entropy of activation for a homogeneous self-exchange reaction, for example, where ΔS° is clearly always zero.

However, real entropies of activation also have theoretical significance. Thus from eq 11 if $\alpha = 0.5$, we can sum the real and ideal entropies of activation for the forward and backward electrochemical reactions to obtain

$$(\Delta S^\circ_{\pm-I})_{real} + (\Delta S^\circ_{\pm-IV})_{real} = (\Delta S^\circ_{\pm-I})_{ideal} + (\Delta S^\circ_{\pm-IV})_{ideal} \quad (25)$$

However, as at E°, $(\Delta H^\circ_{\pm-I})^{E^\circ}_{real} = (\Delta H^\circ_{\pm-IV})^{E^\circ}_{real}$, then it follows that generally[29] $(\Delta S^\circ_{\pm-I})_{real} = (\Delta S^\circ_{\pm-IV})_{real}$. Hence eq 25 can be rewritten as

$$(\Delta S^\circ_{\pm-I})_{real} = 0.5(\Delta S^\circ_{\pm-I} + \Delta S^\circ_{\pm-IV}) \quad (26)$$

Therefore, when $\alpha = 0.5$, the real entropy of activation is simply the mean of the ideal entropies of activation for the forward and backward reactions.

As absolute entropies for simple ions vary markedly with the ionic charge,[38] ΔS° for electrochemical reactions can be large and considerable differences will often be obtained between the corresponding real and ideal activation parameters. For example, for the reaction $Fe^{3+} + e^- \rightarrow Fe^{2+}$, $\Delta S^\circ \approx 40$ eu,[38] which for $\alpha = 0.5$ yields from eq 9 a difference between $(\Delta H^\circ_\pm)_{real}$ and $(\Delta H^\circ_\pm)_{ideal}$ measured at the same potential of ca. 7 kcal mol^{-1} at room temperature.

For reactions where the standard potential and its temperature dependence are unknown, real activation parameters cannot be evaluated. Ideal activation parameters may be obtained as before from a knowledge of $(\partial\phi_m/\partial T)_{E_{ref}}$, although simple theoretical interpretation will be precluded as the "driving force" term $E - E^\circ$ is unknown[17] (this will also be true of homogeneous redox processes where the equilibrium constant is unknown).[17] However, the ideal entropy of activation may still be determined at any potential from the ideal enthalpy of activation determined at that potential.

The assertion has been made[14,15] that only ideal, and not real volumes of activation (eq 12) have theoretical or mechanistic significance. However, if $\alpha = 0.5$, the real and ideal volumes of activation for the forward and backward electrochemical reactions can be summed eliminating the ΔV° term, and as at least at E°, $(\Delta V^\circ_{\pm-I})_{real} = (\Delta V^\circ_{\pm-IV})_{real}$, we obtain (cf. eq 26)

$$(\Delta V^\circ_{\pm-I})_{real} = 0.5(\Delta V^\circ_{\pm-I} + \Delta V^\circ_{\pm-IV}) \quad (27)$$

Again, therefore the real activation parameter is simply the mean of the ideal activation parameters for the forward and backward reactions. Although more information is obtained from the evaluation of ideal volumes (and entropies) of activation compared to the corresponding real activation parameters as the former quantities refer to the activation of a single ion, the latter quantities are nevertheless instructive as they yield direct information about the relative structure of the activated state as compared to the reactant and product states.

Applications to Experimental Data

We shall now examine some experimental results in the light of the above arguments. The early data of Randles and Somerton[40] represent some of the few determinations of real activation parameters for simple redox electrode reactions. Although their data were not corrected for double-layer effects, they found that the resulting frequency factors A obtained from the relation $k_s = A \exp[-(\Delta H^\circ_\pm)^{E^\circ}_{real}/RT]$ were in the majority of systems studied of the order of $Z_e(\approx 10^4$ cm s^{-1}). In view of eq 7 and 26 this suggests that the sum $(\Delta S^\circ_{\pm-I} + \Delta S^\circ_{\pm-IV})_{ideal}$ is small, and therefore the entropy of the activated state lies roughly midway between that for the reactant and product states providing the reactions are adiabatic (i.e., $\kappa\rho \sim 1$).

Unfortunately, the comparison of corresponding electrochemical and chemical enthalpies of activation is severely limited at present by the scarcity of experimental determination of the former quantity. Moreover, no systematic studies of double-layer effects as a function of temperature appear to have been made so that true activation parameters can only be approximately estimated from ideal or real parameters.[41] However for both $V^{3+}|V^{2+}$ and $Fe^{3+}|Fe^{2+}$ couples the electrochemical real heats of activation $(\Delta H^\circ_{\pm-I})^{E^\circ}_{real}$ (7.3 and 9 kcal mol^{-1} respectively[41,40]) are markedly larger than the value of one-half of the enthalpy of activation $(\Delta H^\circ_{\pm-I})^{ex}$ for the corresponding homogeneous self-exchange reactions (13.2 and 9.9 kcal mol^{-1}, respectively[42,43]) that would have been expected from eq 21 and 23 by assuming that $\lambda_e = 0.5\lambda_c$.[17] This result that $(\Delta H^\circ_{\pm-III})^{E^\circ}_{real} > 0.5(\Delta H^\circ_{\pm-I})^{ex}$ contrasts with the success of the "Marcus correlation" between rate constants for electrochemical and homogeneous self-exchange reactions which suggests that $(\Delta G^\circ_{\pm-I})^{E^\circ} \approx 0.5(\Delta G^\circ_{\pm-I})^{ex}$ and has been used to support the assertion that $\lambda_e = 0.5\lambda_c$ for outer-sphere reactions.[44] This disparity results from the markedly different apparent entropies of activation exhibited by these two reaction types. Thus, these[42,43] and other homogeneous electron transfer reactions[1,2] between multi-charged cationic reactants exhibit large and negative apparent entropies of activation (> -20 eu). In contrast, the real entropies of activation for the $V^{3+}|V^{2+}$ and $Fe^{3+}|Fe^{2+}$ reactions are small[37] (or even positive[38]). The former result could arise from negative values of ΔS°_{II-I} and ΔS°_{III-IV} due to solvent ordering in the highly charged collision complexes. It is also possible that this apparently negative $\Delta S^\circ_\pm$ found for these homogeneous reactions partly arises from an approximately linear increase in the true

activation enthalpy with increasing temperature due to the decrease in the dielectric constant and a consequent increase in the electrostatic work terms ΔH°_{II-I} and ΔH°_{IV-III} as the temperature is increased.[28] Consequently (cf. eq 14), the measured activation enthalpy $(\Delta H^\circ_{\pm-I})^{ex}$ can be more closely identified with $(\Delta H^\circ_{\pm-II})_{true}$ rather than $(\Delta H^\circ_{\pm-I})_{true}$. In contrast, it is expected that $(\Delta H^\circ_{\pm-I})^{E^\circ}_{real} < (\Delta H^\circ_{\pm-II})^{\Delta H=0}_{true}$ for these systems.[41] Hence it follows that also $(\Delta H^\circ_{\pm-II})^{\Delta H=0}_{true} > 0.5(\Delta H^\circ_{\pm-II})^{ex}_{true}$ which indicates that $\lambda_e > 0.5\lambda_c$. This result could arise from the inability of the electrochemical reactant to penetrate the inner layer of solvent molecules adjacent to the electrode surface, with consequently a reduced interaction of the reactant ion with its image charge in the electrode and a higher electrochemical activation energy.[17,44,45] However, more quantitative electrochemical data are required before this notion can be properly tested.

Extension to Inner-Sphere Processes

The kinetic treatments described above for outer-sphere reactions can also be formally applied to inner-sphere processes,[27,46,47] such as ligand-bridged reactions.[48] The preexponential term $Z_e\kappa\rho$ can conveniently be replaced by the term kT/h of absolute rate theory, describing the frequency of passage of the specifically adsorbed intermediate toward the activation barrier. However, the extraction of true activation parameters for this class of electrode reactions is hampered by uncertainties in the variations of $(\Delta H^\circ_{\pm-I})_{true}$ and $(\Delta S^\circ_{\pm-I})_{true}$ with temperature. For the outer-sphere reactions considered above, the transformation of the experimental ideal and real quantities to the true activation parameters using equations such as (14) can be achieved by estimating the variation of the true parameters with temperature using electrostatic diffuse layer theory. For inner-sphere reactions, such variations cannot be theoretically estimated with confidence, and the appropriate electrical conditions (constant electrode charge, Galvani potential?) under which terms such as ΔH°_{II-I} and ΔS°_{II-I} will be maintained constant with varying temperature are unclear.[49]

Nevertheless, it may be expected that the relative values of activation parameters, particularly entropies of activation for a series of related electrode reactions, could be sensitive to the structure of the transition state and therefore of potential value in mechanism diagnosis. Measurements of ideal activation parameters for a series of electrode reactions known to follow simple inner- and outer-sphere pathways are underway in this laboratory.

Conclusions

At least for simple electrochemical redox reactions, it is apparent that the enthalpy of activation evaluated at the (experimentally indeterminable) zero Galvani potential difference ($\phi_m = 0$) is of no particular theoretical significance. As Marcus has shown,[17] theoretical estimation of the electrochemical free electrochemical free energy of activation $\Delta\overline{G}^\circ_{\pm-I}$ is facilitated at the standard potential of the half-cell reaction under consideration as here the driving force term $\Delta\overline{G}^\circ_{IV-I}$ is zero. The enthalpy of activation $(\Delta\overline{H}^\circ_{\pm-I})^{\Delta H=0}$ measured at a potential where $\Delta\overline{H}^\circ_{IV-I} = 0$ is a closely related quantity; both $(\Delta\overline{G}^\circ_{\pm-I})^{\Delta G=0}$ and $(\Delta\overline{H}^\circ_{\pm-I})^{\Delta H=0}$ are directly related to $\Delta G^\circ_{\pm-I}$ and $\Delta H^\circ_{\pm-I}$, respectively, for the corresponding homogeneous self-exchange reaction. The true electrochemical enthalpy of activation corresponding to any known electrode potential can only be obtained directly by constructing Arrhenius plots at constant ϕ_m (where the free energy of the reactant or product electron remains constant) therefore obtaining ideal enthalpies of activation,[7] and then correcting for any residual variation of $\Delta H^\circ_{\pm-I}$ with temperature. However, the so-called real enthalpy of activation[7] $(\Delta H^\circ_{\pm-I})^{E^\circ}_{real}$ obtained from an Arrhenius plot evaluated at E° can be directly identified with $(\Delta\overline{H}^\circ_{\pm-I})^{\Delta H=0}$. Therefore for simple redox reactions for which E° can be determined for single electron transfer step, the real enthalpy of activation determined at E°, rather than the corresponding ideal parameter, has the most direct theoretical significance.

For reactions with a symmetrical barrier to electron transfer ($\alpha = 0.5$) the real entropies and volumes of activation are equal to the mean of the actual parameters for the forward and backward processes. However, in order to extract the individual parameters, measurements of ideal entropies and volumes of activation are required. Although the required values of, for example, $(\partial\phi_m/\partial T)_E$ are not thermodynamically accessible, a number of routes are available for which these quantities can be estimated with satisfactory precision.

Therefore, at least for outer-sphere electrode reactions, the experimental separation of the electrochemical free energy of activation into its true enthalpic and entropic components is a relatively straightforward procedure, yielding parameters of direct theoretical significance. It is unfortunate that so few quantitative electrochemical rate measurements have been made as a function of temperature. Such measurements have considerable utility in identifying the various factors contributing to the measured rate constant, and may also be sensitive to the differences in the structure of the activated state expected for inner-sphere compared to outer-sphere processes.

References and Notes

(1) H. Taube, "Electron Transfer Reactions of Complex Ions in Solution", Academic Press, New York, N.Y., 1970, pp 59–62.
(2) However, see R. C. Patel, R. E. Ball, J. F. Endicott, and R. G. Hughes, *Inorg. Chem.*, **9**, 23 (1970).
(3) R. A. Marcus, *Can. J. Chem.*, **37**, 155 (1959).
(4) R. A. Marcus, *Electrochim. Acta*, **13**, 995 (1968).
(5) R. A. Marcus and N. Sutin, *Inorg. Chem.*, **14**, 213 (1975).
(6) For example, see R. G. Wilkins, "The Study of Kinetics and Mechanism of Reactions of Transition Metal Complexes", Allyn and Bacon, Boston, Mass., 1974, Chapter 2.
(7) M. Temkin, *Zh. Fiz. Khim.*, **22**, 1081 (1948).
(8) B. E. Conway, "Theory and Principles of Electrode Processes", Ronald Press, New York, N.Y., 1965, Chapter 6.
(9) B. E. Conway and D. J. MacKinnon, *J. Electrochem. Soc.*, **116**, 1665 (1969).
(10) M. Salomon, *J. Electrochem. Soc.*, **113**, 940 (1966).
(11) G. J. Hills and S. Hsieh, *Chem. Ing. Tech.*, **44**, 216 (1972).
(12) A. A. Vlček, *Collect. Czech. Chem. Commun.*, **24**, 3538 (1959).
(13) R. Tamamushi, *Rev. Polarogr.*, **10**, 1 (1962); also see N. Maki and N. Tanaka in "An Encyclopedia of Electrochemistry", Vol. III, A. J. Bard, Ed., Marcel Dekker, New York, N.Y., 1975, Chapter 2.
(14) L. I. Krishtalik, *J. Electrochem. Soc.*, **113**, 1117 (1966).
(15) B. E. Conway in "Techniques of Electrochemistry", Vol. I, E. Yeager and A. J. Salkind, Ed., Wiley-Interscience, New York, N.Y., 1972, p 521.
(16) For example, see S. Trasatti, *J. Electroanal. Chem.*, **52**, 313 (1974); **66**, 155 (1975); A. N. Frumkin and B. Damaskin, *ibid.*, **66**, 150 (1975).
(17) R. A. Marcus, *J. Chem. Phys.*, **43**, 679 (1965), and previous references cited therein.
(18) Use of the preexponential factor $Z_e\kappa\rho$ results in a more generally valid, albeit similar expression than does the use of the conventional factor kT/h employed in absolute reaction rate theory.[19]
(19) W. L. Reynolds and R. L. Lumry, "Mechanisms of Electron Transfer", Ronald Press, New York, N.Y., 1966, p 119.
(20) Actually the condition $\phi_m = 0$ does *not* eliminate the electron term from the rate equation as written using the classical treatment of electrode kinetics[21,22] as the potential-independent part of the electron free energy arising from interactions of the electron with the bulk metal electrode phase[23] will still be present when $\phi_m = 0$.
(21) R. Parsons, *Trans. Faraday Soc.*, **47**, 1332 (1951).
(22) P. Delahay, "Double Layer and Electrode Kinetics", Interscience, New York, N.Y., 1965, Chapter 7.
(23) R. Parsons in "Modern Aspects of Electrochemistry", J. O'M. Bockris and B. E. Conway, Ed., Academic Press, New York, N.Y., 1954, Chapter 3.
(24) Note that the absolute entropy of free electrons in metals is probably negligibly small. For example, see N. F. Mott and H. Jones, "The Theory of the Properties of Metals and Alloys", Oxford University Press, London,

1936, Chapter 6.
(25) R. Parsons, *Croat, Chem. Acta*, **42**, 281 (1970).
(26) For example, see B. E. Conway and J. O'M. Bockris, ref 23, Chapter 2.
(27) D. M. Mohilner, *J. Phys. Chem.*, **73**, 2652 (1969).
(28) A temperature dependence of $(\Delta H^{\ddagger})_{true}$ would be expected, for example, when the reaction heat ΔH° is appreciably temperature dependent, i.e., when the heat capacity of the reactants and products significantly differ. Also for ionic reactions, the variation in the dielectric constant with temperature would be expected to lead to a variation in $(\Delta H^{\ddagger})_{true}$ with temperature. See, for example, ref 6; I. D. Clark and R. P. Wayne in "Comprehensive Chemical Kinetics", Vol. 2, C. H. Bamford and C. F. H. Tipper, Ed., Elsevier, Amsterdam, 1969, pp 328–31; N. R. Kestner, J. Logan, and J. Jortner, *J. Phys. Chem.*, **78**, 2148 (1974).
(29) The true entropy of activation can be considered to be essentially independent of potential as $\Delta S^{\circ}_{\ddagger}$ is probably potential independent.[24] However, this presupposes the absence of $\Delta S^{\circ}_{\ddagger}$ changes arising from subtle variations in the structure of the activated state as the electrode potential is altered.
(30) Reference 22, Chapter 9.
(31) Neglecting the temperature dependence of the collision frequency, Z_e.
(32) M. Salomon, C. G. Enke, and B. E. Conway, *J. Chem. Phys.*, **43**, 3989 (1965).
(33) If, as usual, the reaction medium contains a large excess of indifferent electrolyte, the standard state chosen should correspond to these conditions, i.e., the appropriate "formal potential" rather than E° should be employed.
(34) E. A. Guggenheim, *J. Phys. Chem.*, **33**, 842 (1929); **34**, 1540 (1930).
(35) J. E. B. Randles, *Trans. Faraday Soc.*, **48**, 828 (1952).
(36) Reference 19, pp 128–129.
(37) For example, see B. Perlmutter-Hayman, *Progr. React. Kinet.*, **6**, 239 (1971).
(38) R. E. Powell and W. M. Latimer, *J. Chem. Phys.*, **19**, 1139 (1951).
(39) J. E. B. Randles and K. S. Whiteley, *Trans. Faraday Soc.*, **52**, 1509 (1956); G. Milazzo in "Polarography 1964", Vol. I, G. J. Hills, Ed., Macmillan, London, 1966, p 79. Also see G. Milazzo, N. Bonciocat, and M. Borda, *Electrochim. Acta*, **21**, 349 (1976).
(40) J. E. B. Randles and K. W. Somerton, *Trans. Faraday Soc.*, **48**, 937 (1952).
(41) K. M. Joshi, W. Mehl, and R. Parsons, "Transactions of the Symposium on Electrode Processes", E. Yeager, Ed., Wiley, New York, N.Y. 1961, p 249, and following discussion.
(42) K. V. Krishnamurty and A. C. Wahl, *J. Am. Chem. Soc.*, **80**, 5921 (1958).
(43) J. Silverman and R. W. Dodson, *J. Phys. Chem.*, **56**, 846 (1952).
(44) R. A. Marcus, *J. Phys. Chem.*, **67**, 853 (1963).
(45) J. M. Hale, "Reactions of Molecules at Electrodes", N. S. Hush, Ed., Interscience, New York, N.Y., 1971, Chapter 4; N. S. Hush, *Electrochim. Acta*, **13**, 1005 (1968).
(46) D. M. Mohilner and P. Delahay, *J. Phys. Chem.*, **67**, 588 (1963).
(47) M. J. Weaver and F. C. Anson, *J. Electroanal. Chem.*, **58**, 81 (1975).
(48) M. J. Weaver and F. C. Anson, *J. Electroanal. Chem.*, **58**, 95 (1975).
(49) The complexities surrounding the definitions and interpretations of enthalpies and entropies of adsorption for electrochemical interfaces have been eruditely discussed by Parsons.[50] In ref 50, constancy of electrode charge was considered to be the appropriate electrical condition for the determination of these adsorption parameters. However, constancy of the Galvani potential may maintain these parameters more nearly constant with varying temperature as a constant solvent orientation in the inner layer may be maintained under these latter conditions.
(50) R. Parsons, *Can. J. Chem.*, **37**, 308 (1959).

Chemical Relaxation and Equilibrium Studies of Association in Aqueous Solutions of Bolaform Detergents. 1. Dodecane-1,12-bis(trimethylammonium bromide)

S. Yiv, K. M. Kale, J. Lang, and R. Zana*

CNRS, Centre de Recherches sur les Macromolécules, 6, rue Boussingault, 67083, Strasbourg, Cedex, France *(Received March 15, 1976)*

Publication costs assisted by the Centre National de la Recherche Scientifique

The self-association of dodecamethonium bromide in aqueous solution has been investigated by means of chemical relaxation (ultrasonic absorption, T-jump, p-jump, and shock tube), density, conductivity, and emf measurements. No relaxation process could be detected and no rapid changes of apparent molal volume, conductivity, and emf have been found in the concentration range where micellization was reported to occur by other workers. From the results it is concluded that at concentration below 0.1 M the aggregated dodecamethonium ions retain most of their hydration water. The aggregates of dodecamethonium ions appear to be very loose and to contain only a very small number of monomers.

I. Introduction

Chemical relaxation studies (p-jump, T-jump, shock tube, and ultrasonic absorption) have provided us with a variety of information, thus far not available, on micellar solutions of ionic detergents.[1–4] It must be remembered that these systems are characterized by two relaxation times differing by as much as two to three orders of magnitude. The short relaxation time (τ_1) has been associated to reaction 1 where a detergent ion A is exchanged between the micelle A_n (micellar number n) and the surrounding solution. The long relaxation time (τ_2) has been assigned to reaction 2 where micelles form or dissolve.

$$A + A_{n-1} \underset{k^-}{\overset{k^+}{\rightleftharpoons}} A_n \quad (1)$$

$$nA \rightleftharpoons A_n \quad (2)$$

The expressions of the rate constants k^+ and k^- have been derived for the first time by Aniansson and Wall.[5] The model adopted by these authors involves a diffusive motion of the hydrophobic tail of the detergent ion, out of the micelle, perpendicular to the micellar surface. It is restricted to linear detergent ions with one charged end. If there existed micelles constituted of linear detergent ions whose both ends are electrically charged (bis or bolaform detergents) the dissociation (or association) of such an ion from (or to) a micelle would proceed very differently from that of a singly charged detergent ion with an identical hydrophobic moiety. Indeed, the diffusive motion invoked above would be energetically very unlikely because one charged end of the bolaform detergent would have to cross the micelle hydrophobic core. The kinetic behavior of micelle forming bolaform detergents

should therefore considerably differ from that of singly charged detergents.

This reasoning prompted us to undertake the study of the bolaform detergent dodecane-1,12-bis(trimethylammonium bromide) or dodecamethonium bromide ($C_{12}Me_6$) by means of the chemical relaxation methods used in our previous studies of ionic detergent solutions. Indeed, from the results of surface tension and dye spectral change measurements[6] it appears that $C_{12}Me_6$ forms micelles at concentration between 0.02 and 0.05 M. In order to check this finding the densities, conductivities, and emf of $C_{12}Me_6$ solutions have also been measured. Indeed it is now well established that density measurements can be used to obtain informations on micelle formation in detergent solutions.[7,8] The apparent molal volume vs. concentration curve shows a large increase at the critical micelle concentration (cmc), which corresponds to the volume change upon micellization. On the other hand, conductivity measurements constitute one of the best methods to obtain the cmc of ionic detergents in aqueous solutions.[9] Finally emf measurements permit the determination of the cmc of ionic detergent, and of the degree of counterion association to micelles.[10] For the sake of comparison, the model detergent dodecane–trimethylammonium bromide ($C_{12}Me_3$), where the formation of micelle is well characterized,[11] was also investigated.

Another purpose of our work was to try to obtain some information on the conformation of the hydrophobic chain of $C_{12}Me_6$. Indeed Menger and Wrenn[6] have shown that long-chain bolaform ions, such as $C_{12}Me_6$ are folded at the air–water interface. However these authors could not infer whether the hydrophobic chain of $C_{12}Me_6$ takes a linear or folded conformation inside the micelles. More recently, Johnson and Fleming[12] have measured the apparent molal volumes ϕ_v of hexamethonium and decamethonium bromides (C_6Me_6 and $C_{10}Me_6$, respectively). From the shape of the ϕ_v vs. concentration curve they concluded that these compounds do not form micelles, and that the hydrophobic chain may be partly folded in solution.

II. Experimental Section

Materials. $C_{12}Me_6$ and $C_{12}Me_3$ were prepared as described by Menger and Wrenn.[6] The products were purified by three recrystallizations from ether–ethanol mixtures. The purity of $C_{12}Me_6$ was checked by elementary chemical analysis.

Anal. Calcd for $C_{12}Me_6$: C, 48.44; H, 9.48; N, 6.28; B, 35.8. Found: C, 48.51; H, 9.59; N, 6.33; B, 34.9.

Methods. The various chemical relaxation equipment used in this work has been described elsewhere.[1-3] The T-jump investigations were performed in the presence of eosine because $C_{12}Me_6$ and $C_{12}Me_3$ do not absorb light in the range of wavelength available on our equipment. We have shown in a previous study[13] that a dye can be used to follow the relaxation process associated with reaction 2 spectrophotometrically, provided that the (dye)/(detergent) concentration ratio is kept below 0.005–0.01.

The density measurement were performed at 25 ± 0.01 °C using an improved[14] automatic densimeter (Anton Parr DMA 02) with an estimated accuracy of $\pm 5 \times 10^{-6}$ g/cm^3. The solutions were prepared by weighing the amounts of detergent and water. The molar concentration C could then be determined with great accuracy after measuring the density d of the solution. The apparent molal volume ϕ_v was calculated by means of

$$\phi_v = \frac{M}{d_0} - 10^3 \frac{d - d_0}{d_0 C} \qquad (3)$$

where M is the molecular weight of $C_{12}Me_6$ and $d_0 = 0.997\,047$ g/cm^3,[15] the density of water at 25 °C.

The conductivities were measured, using a Wayne Kerr B641 conductivity bridge operated at 1592 Hz and 25 °C.

The emf (E) measurements were performed using the concentration cell:

Ag/AgBr electrode || detergent solution at concentration C_0 || NH_4NO_3 saturated agar-agar bridge || detergent solution at concentration C || Ag/AgBr electrode

The potential difference between the two electrodes was measured by means of a digital voltmeter Schlumberger Type VB 2029 to within 0.1 mV. Below the cmc, for fairly dilute solutions the plot E vs. $\log a/a_0$ (where a refers to the activity calculated from the concentration C by means of Davies equation) is a straight line with a slope close to 59 mV. The micellization brings about a rapid change of slope at the cmc, because part of the counterions are bound on the micelle. The degree of counterion association can be directly evaluated from the change of slope.[10]

III. Results

1. *Ultrasonic Absorption.* Figure 1 shows the plots of the absorption α/f^2 (where α is the absorption coefficient and f the ultrasonic frequency) against the concentration C, at 2.82 MHz for $C_{12}Me_6$ and $C_{12}Me_3$. A large excess absorption with respect to water is found for $C_{12}Me_3$ solutions at $C >$ cmc, as for other ionic detergents.[1,3] On the contrary, at concentrations around 0.05 M, and up to 0.2 M, i.e., well above the reported range of micellization,[6] the $C_{12}Me_6$ solutions show only a negligible excess absorption. Thus, ultrasonic absorption measurements provide no evidence of micelle formation (in the usual sense of the word) in $C_{12}Me_6$ solutions below 0.2 M. At higher concentrations the absorption increases and shows a change of slope at around 0.7 M. One may be tempted to associate this effect to some association or micellization. It should be kept in mind however that at a concentration of 0.7 M the average distance between two $C_{12}Me_6$ ions is comparable to or even smaller than the length of the bolaform ion (≈20 Å). Strong solute–solute interactions are therefore to be expected, even though no specific association may occur, and may give rise to the observed change of α/f^2. This conclusion is substantiated by the results of apparent molal volume measurements (see section III4).

2. *T-Jump.* Relaxation signals of extremely small amplitude were observed with $C_{12}Me_6$ in the presence of eosine above and *below* the reported cmc range for this detergent (0.02 to 0.05 M[6]). In addition, the relaxation time evaluated from this signal was found to be dependent on the dye concentration. These findings suggest that the observed relaxation process is associated with some eosine–$C_{12}Me_6$ interaction. Indeed, for classical detergents, the perturbation of equilibrium 2 by a T-jump usually gives rise to fairly large relaxation signals, with a relaxation time independent of the dye concentration.[3,13] For instance, with a 0.04 M $C_{12}Me_3$ solution at 25 °C, and a ratio (eosine)/($C_{12}Me_3$) = 0.005, a T-jump of 2.2 °C gave rise to a relaxation signal of about 1.1% of the total photometric signal. In this case the dye–detergent interaction was not detected because the associated relaxation amplitude is negligibly small relatively to that of the micelle formation–dissolution equilibrium, in the experimental conditions. (It is however possible to find conditions where the first process can be quantitatively investigated[16] by means of stopped-

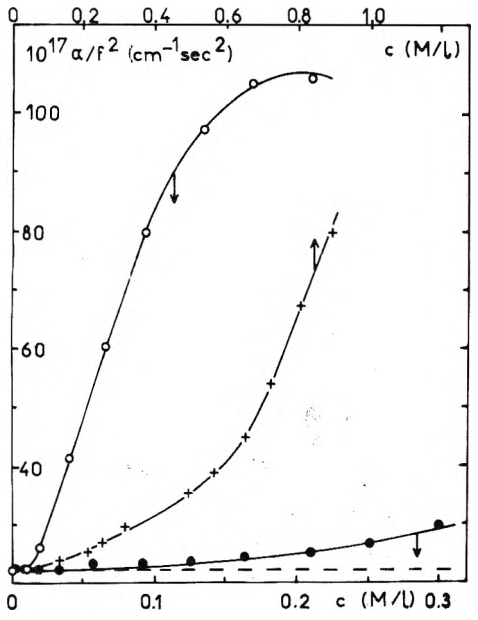

Figure 1. Plot of the ultrasonic absorption α/f^2 against the concentration at 25 °C and 2.82 MHz for $C_{12}Me_3$ (O) and $C_{12}Me_6$ in dilute (●) and concentrated (+) solutions. The horizontal broken line represents the absorption of water.

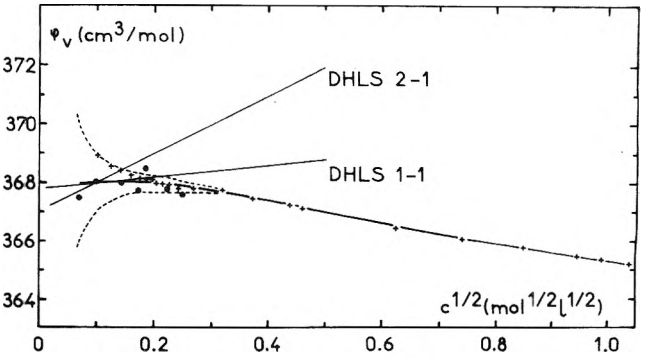

Figure 2. Plot of the apparent molal volume ϕ_v of $C_{12}Me_6$ against $C^{1/2}$ at 25 °C. The symbols + and ● refer to two independent runs of experiments performed on samples obtained in two different preparations. DHLS 2-1 and DHLS 1-1 refer to the Debye-Hückel limiting slopes for a 2-1 and a 1-1 electrolyte, respectively. The dashed curves 1 and 2 were drawn assuming an uncertainty of 5 ppm in the density measurements.

flow.) The results obtained with $C_{12}Me_6$ suggest that the relaxation time associated with reaction 2 is, for this detergent, outside the available time range of our T-jump equipment (3 μs to 1 s), and/or that the relaxation occurs with an extremely small amplitude. The second possibility appears more likely in view of the T-jump results obtained with other detergents (see ref 3 and references therein), and of the fact that some aggregation appears to occur in $C_{12}Me_6$ solutions.[6]

3. *Shock Tube and p-Jump.* No relaxation signals could be detected by means of these two methods with $C_{12}Me_6$. On the contrary, a relaxation process of fairly large amplitude was found with $C_{12}Me_3$. The associated relaxation time τ_2 was in good agreement with that determined by T-jump at the same temperature and concentration, in the presence of eosine. $1/\tau_2$ showed the usual decrease upon increasing C, found for several detergents.[2-4] A full account of these results will be given in a future report. As in the case of the T-jump experiments it is believed that the amplitude of the relaxation signal for $C_{12}Me_6$ is negligibly small. This conclusion is further substantiated by the results described in the three next paragraphs.

4. *Density Measurements.* The apparent molal volume ϕ_v vs. $C^{1/2}$ curve for $C_{12}Me_6$ is shown on Figure 2. This curve shows no special feature in the range 0.02–0.05 M where micellization was reported to occur.[6] The fact that there is no volume change ΔV upon association of $C_{12}Me_6$ explains that no relaxation could be detected by means of ultrasonic absorption, shock tube, and p-jump. Indeed the relaxation amplitude is proportional to ΔV^2 for the first method and to ΔV for the two others. Note that the micellization of $C_{12}Me_3$ has been found to bring about a volume increase of 8.5 cm^3/mol.[11b]

The extrapolation to zero concentration of the ϕ_v vs. $C^{1/2}$ curve yields $\phi_v^0 = 367.0 \pm 1$ cm^3/mol. The difference between this value and that for decamethonium bromide (332.4 cm^3/mol[12]) is of 34.6 cm^3/mol, instead of an expected value of 32 cm^3/mol, on the basis of a volume increment of 16 cm^3/mol of methylene group.[7,11b] Moreover the curve ϕ_v vs. $C^{1/2}$ obtained for $C_{12}Me_6$ does not show the sharp decrease reported at concentration below 0.04 M for $C_{10}Me_6$ and C_6Me_6.[12] These points are further discussed in section IV3.

5. *Conductivity Measurements.* The results are shown in Figure 3 where Λ is the equivalent conductivity and N the concentration in equivalent per liter. For $C_{12}Me_3$ the results fall on two straight lines whose intersection yields a cmc of 0.0153 M. his result is in agreement with those of other workers.[11a] In the case of $C_{12}Me_6$ the Λ vs. $N^{1/2}$ curve shows no rapid change in the concentration range between 0.02 and 0.05 M where other workers[6] concluded that micellization takes place. In the dilute range ($C \sim 10^{-3}$ M) the slope of the Λ vs. $N^{1/2}$ curve for $C_{12}Me_6$ is close to the Debye-Hückel limiting value for a 2–1 electrolyte. It must also be noted that this plot shows a curvature opposite to that expected if micellization had occurred in the range of concentration from 10^{-3} to about 10^{-1} M.

Our results for $C_{12}Me_6$ are very similar to those obtained by Brown et al.[17] in a conductivity study of two diammonium salts: 1-*N*-morpholino- and di-*N*-propyl-10-*N*-piperidinodecane dihydrochlorides. The Λ vs. $N^{1/2}$ plots for these two compounds do not show any rapid change but only a curvature similar to that of the curve for $C_{12}Me_6$ on Figure 3. Brown et al. concluded that "diammonium salts with ten carbon atoms between the ionic groups follows the course of normal electrolytes" up to 0.25 M and therefore do not form micelles. Our results extend this conclusion to a diammonium salt with 12 carbon atoms between the ionic groups.

6. *Emf Measurements.* The results are shown in Figure 4. For $C_{12}Me_3$ the plot E vs. log a/a_0 shows a break at a ratio a/a_0 corresponding to a concentration of about 0.015 M, i.e., very close to the cmc value obtained from ultrasonic and conductivity measurements. For $C_{12}Me_6$ the emf increases linearly with log a/a_0 up to a concentration of about 0.1 M. Above this concentration the plot E vs. log a/a_0 shows an increasing curvature. This result is to be compared with that of Figure 1: the ultrasonic absorption of $C_{12}Me_6$ shows a very small increase at $C > 0.1$–0.2 M.

IV. Discussion

1. *Association in Solutions of $C_{12}Me_6$.* The results obtained in this study by means of very different methods do not provide any evidence of micelle formation in solutions of dodecamethonium bromide at $C < 0.1$ M. Other workers,[6] however, have concluded that micellization takes place in $C_{12}Me_6$ solutions, and reported cmc values between 0.02 and 0.05 M. The

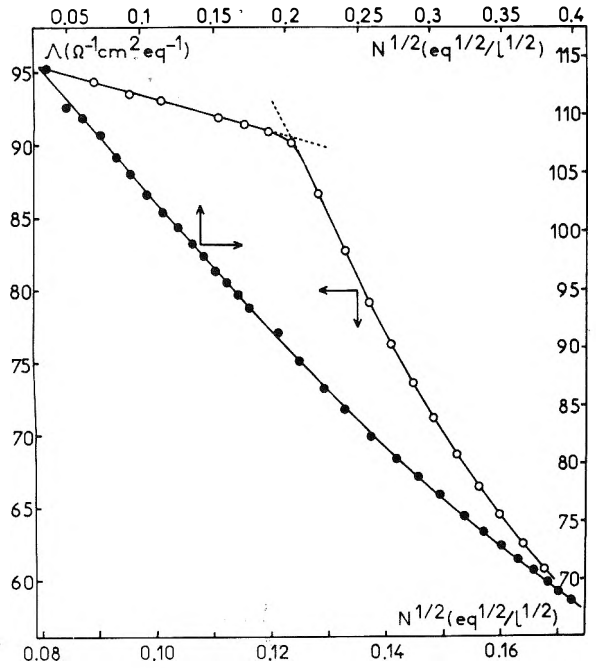

Figure 3. Plot of the equivalent conductivity Λ against (normality) $N^{1/2}$ at 25 °C for $C_{12}Me_6$ (●) and $C_{12}Me_3$ (O).

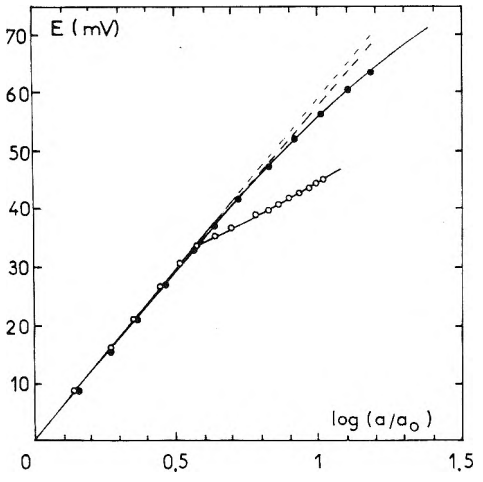

Figure 4. Plot of the emf E vs. log a/a_0 for (●) $C_{12}Me_6$ (initial concentration 1.2×10^{-2} M) and (O) $C_{12}Me_3$ (initial concentration 4×10^{-3} M).

only way to reconcile these results with those obtained in our work is to assume that the aggregates which are formed in $C_{12}Me_6$ solutions at concentrations below 0.1 M are extremely loose and contain a very small number of $C_{12}Me_6$ ions (these aggregates may in fact be only dimers or trimers). Indeed, the density measurements, in agreement with the results of ultrasonic absorption, p-jump, and shock tube, have shown that the volume change ΔV upon association must be very small. Moreover, the T-jump results indicate that the enthalpy change ΔH upon association must also be ver small. Indeed the amplitude of the relaxation transients in T-jump experiment is proportional to ΔH, and this amplitude appears to be very small for $C_{12}Me_6$. Since ΔV and ΔH are essentially due to changes of hydration upon association it may be concluded that the associated $C_{12}Me_6$ ions retain most of their hydration water and that their association is very loose.

On the other hand, the following results indicate that the number of $C_{12}Me_6$ ions per aggregate is very small: (1) the absence of a break on the Λ vs. (concentration)$^{1/2}$ and E vs. log a/a_0 curves for $C_{12}Me_6$; (2) the very progressive change of surface tension σ with concentration (Figure 2 of ref 6 shows that for $C_{12}(Bu)_6$ the decrease of σ continues even at concentration well above the reported cmc; an even more pronounced decrease of σ at C above the assumed cmc is likely for $C_{12}Me_6$); (3) the very different values found for the "cmc" of $C_{12}Me_6$ by means of surface tension (0.02–0.03 M) and dye absorption spectral change (0.04–0.05 M) measurements. These two methods thus yield "cmc" values in a ratio of about 2, while for classical detergents the difference is usually of only 10–20%.[18] The high value found for the "cmc" of $C_{12}Me_6$ by the dye spectral change method may in fact be associated with a dye induced aggregation of $C_{12}Me_6$ ions.[11a,19] This effect appears even more likely when it is pointed out that an anionic dye was used in the study of alkylmethonium bromides[6] which are cationic compounds. On the other hand, the decrease of surface tension of $C_{12}Me_6$ solutions upon increasing concentration[6] may simply reflect a very progressive association of the dodecamethonium ions in a wide range of concentration.

It must be pointed out that changes of surface tension with concentration similar to those reported for bolaform detergents have also been found for symmetrical tetraalkylammonium (TAA) halides[20] with the exception of tetramethylammonium halides. These changes have been attributed to the aggregation of TAA cations. This aggregation, however, appears to be much closer to micelle formation than the process by which very loose and small aggregates of $C_{12}Me_6$ are formed. Indeed, it gives rise to large excess ultrasonic absorptions[21] and to significant volumes changes.[22] It is also noteworthy that measurements of dye spectral change[23] and of differential spectroscopy in the presence of benzene[24] have yielded for tetrabutylammonium halides apparent cmc values of 0.015–0.04 M, i.e., much smaller than the concentration of about 1 M where benzene solubilization,[25] apparent molal volumes,[26] and ultrasonic absorption[21] convincingly reveal the formation of multiple charged aggregates. The association pattern in bolaform detergent solutions may be very similar to that in solutions of TAA halides. At $C < 0.1$ M some very loose aggregates (possibly dimers or trimers) may be formed, which induce a sigmoidal decrease of surface tension. However changes of volume, enthalpy, conductivity, etc. brought about by the association of $C_{12}Me_6$ may be too small to be detected by the methods used in our investigation (note that the solutions of tetramethylammonium halides also show a normal behavior in contrast to larger TAA halides). On this assumption, an increased hydrophobicity of the head groups of the bolaform detergent, as for instance in going from $C_{12}Me_6$ to $C_{12}(Bu)_6$, may result in a stronger self-association and in detectable relaxation signals. Our results, however, make it difficult to talk of cmc and of micelles of $C_{12}Me_6$ at concentrations below 0.1 M. Indeed the word micelle, in its usual sense, refers to aggregates containing a fairly large number of detergent ions and with a hydrophobic core impenetrable to water. Such is clearly not the case for $C_{12}Me_6$ aggregates at $C < 0.1$ M.

As a last argument, if needed, in favor of this conclusion it must be added that concentrated solutions of $C_{12}Me_6$ have been investigated by x-ray scattering in our laboratory.[27] No evidence could be found for the existence of mesomorphic phases. Since true micellar solutions give rise to mesomorphic phases upon increasing the detergent concentration, it appears that true micelles do not occur in $C_{12}Me_3$ solutions.

The difference of behavior between $C_{12}Me_6$ and $C_{12}Me_3$ is clearly related to the presence of an additional trimethylammonium group in the former. This group is quite hydrophilic and may bring about such a shift of the hydrophilic–lyophilic balance that while $C_{12}Me_3$ is on the hydrophobic side, $C_{12}Me_6$ may be on the hydrophilic side. On this assumption $C_{12}Me_6$ would not form micelles in the usual sense of the word.

2. *Conformation of the Paraffinic Chain of $C_{12}Me_6$.* Our results appear to rule out the possibility of an equilibrium between a completely folded and a stretched conformation of the hydrophobic chain of $C_{12}Me_6$ in aqueous solution. Indeed, such a process should be accompanied by a sizable volume change owing to the variation of hydrophobic surface exposed to water. On the other hand, the unfolding of the paraffinic chain involves hindered rotations, with relaxation times well in the submicrosecond range,[28] i.e., in the time range covered by the ultrasonic absorption method (from 0.3 to 0.001 μs). Thus the two conditions are fulfilled for the folding–unfolding equilibrium to give rise to a relaxational ultrasonic absorption. Since no relaxation was observed one of the two conformers must strongly predominate. The possibility of an equilibrium between partly folded conformations differing only slightly in volume cannot be discarded because it would also give rise to a very small ultrasonic absorption.

There is at the present time no clear-cut evidence of chain folding for bolaform ions in aqueous solutions. Johnson and Fleming[12] observed a larger decrease of ϕ_v at $C > 0.16$ M for $C_{10}Me_6$ than for C_6Me_6 and related it with a possible curving of the hydrocarbon chain. However, it must be recalled that a decrease of ϕ_v at increasing C is a general feature of symmetrical and unsymmetrical tetraalkylammonium ions.[29,30] Various explanations have been proposed to this effect (see ref 29a and references therein) which also hold for C_nMe_6 compounds. For this reason we do not believe that the shape of the ϕ_v vs. $C^{1/2}$ curves for C_nMe_6 provides convincing evidence for chain curving.

3. *Limiting Apparent Molal Volumes of Bolaform Detergents.* Some comments must be made about the ϕ_v^0 values reported for C_6Me_6 and $C_{10}Me_6$[12] and that for $C_{12}Me_6$, obtained in this work. The curve ϕ_v vs. $C^{1/2}$ of Figure 2 shows in the lower concentration range a plateau, or a very small decrease of ϕ_v. The experimental errors, however, do not permit one to determine whether the limiting Debye–Hückel behavior is reached (we have shown on Figure 3 the limiting slopes for a 1–1 and a 2–1 electrolyte). These findings are in agreement with those of other workers in studies of tetraalkylammonium salts.[29] In most instances the limiting behavior is reached below 0.01 M. Since bolaform detergents are 2–1 electrolytes,[17,30,31] this limit is expected to be even further lowered. Nevertheless, Johnson and Fleming[12] assumed that the limiting 2–1 electrolyte behavior is reached at a concentration of about 0.04 M on the basis of the ϕ_v value obtained for the most dilute solution investigated ca. 0.012 M, for both C_6Me_6 and $C_{10}Me_6$. If this point is discarded because it is anyhow the least accurate, the ϕ_v vs. $C^{1/2}$ curves in ref 12 become very similar to the one of Figure 2, and yield ϕ_v^0 values of 270 and 334.4 cm^3/mol for C_6Me_6 and $C_{10}Me_6$, respectively. Our extrapolated value for $\phi_v^0(C_{12}Me_6)$ would then correspond to an increment of 16.3 ± 0.5 cm^3/mol of CH_2 group, in agreement with the values usually found for this quantity in the case of classical detergents[7,11b] and other compounds.[32] This result may be taken as additional evidence against chain folding in bolaform solutions because such an effect would cause a change in $\phi_v^0(CH_2)$.

Conclusions

Density, conductivity, and emf measurements show no evidence of micelle formation in solution of dodecamethonium bromide at concentrations below 0.1 M, thereby confirming the results of ultasonic absorption, T-jump, p-jump, and shock tube investigations. Our results indicate that this detergent does not form true micelles but rather some extremely loose aggregates of very small aggregation number where the bolaform ions retain most of their hydration water.

Acknowledgments. The authors are pleased to thank Professor H. Hoffmann for making available the p-jump and shock-tube equipment and Dr. J. Francois for the densimeter.

References and Notes

(1) E. Graber, J. Lang, and R. Zana, *Kolloid. Z. Z. Polym.*, **238**, 470, 479 (1970).
(2) R. Folger, H. Hoffmann, and W. Ulbricht, *Ber. Bunsenges. Phys. Chem.*, **78**, 986 (1974).
(3) J. Lang, C. Tondre, R. Zana, R. Bauer, H. Hoffmann, and W. Ulbricht, *J. Phys. Chem.*, **79**, 276 (1975).
(4) A. G. Aniansson, S. Wall, M. Almgren, H. Hoffmann, J. Kiellmann, W. Ulbricht, R. Zana, J. Lang, and C. Tondre, *J. Phys. Chem.*, **80**, 905 (1976).
(5) A. G. Aniansson and S. Wall, *J. Phys. Chem.*, **78**, 1024 (1974); **79**, 857 (1975).
(6) F. M. Menger and S. Wrenn, *J. Phys. Chem.*, **78**, 1387 (1974).
(7) J. E. Desnoyers and M. Arel, *Can. J. Chem.*, **45**, 359 (1967); P. Leduc and J. Desnoyers, *Can. J. Chem.*, **51**, 2993 (1973); P. Leduc, J. L. Fortier, and J. Desnoyers, *J. Phys. Chem.*, **78**, 1217 (1974); K. Shinoda and T. Soda, *ibid.*, **67**, 2072 (1963); F. Franks, M. Quickenden, J. Ravenhill, and H. T. Smith, *ibid.*, **72**, 2668 (1968).
(8) K. Kale and R. Zana, submitted for publication.
(9) P. Mukerjee, *Adv. Colloid Interface Sci.*, **1**, 241 (1967).
(10) E. Keh, C. Gavach, and J. Guastella, *C. R. Acad. Sci. (Paris), Ser. C*, **263**, 1488 (1966); K. Shirahama, *Bull. Chem. Soc. Jpn.*, **47**, 3165 (1974), and references therein.
(11) (a) P. Mukerjee and K. Mysels, *Natl. Stand. Ref. Data Ser., Natl. Bur. Stand.*, **No. 36** (1970); E. Anacker, R. Rush, and S. Johnson, *J. Phys. Chem.*, **68**, 81 (1964); (b) J. M. Corkill, J. Goodman, and T. Walker, *Trans. Faraday Soc.*, **63**, 768 (1967).
(12) J. R. Johnson and R. Fleming, *J. Phys. Chem.*, **79**, 2327 (1975).
(13) C. Tondre, J. Lang, and R. Zana, *J. Colloid Interface Sci.*, **52**, 372 (1975).
(14) J. Francois, R. Clement, and E. Franta, *C. R. Acad. Sci. (Paris), Ser. C*, **273**, 1577 (1973).
(15) G. S. Kell, *J. Chem. Eng. Data*, **12**, 66 (1967).
(16) N. Tatsumoto, K. Takeda, S. Isshiki, and T. Yasunaga, *Bull. Chem. Soc. Jpn.*, **47**, 289 (1974); K. Takeda, N. Tatsumoto, and T. Yasunaga, *J. Colloid Interface Sci.*, **47**, 128 (1974); B. Robinson, N. White, and C. Mateo, *Adv. Mol. Relaxation Processes*, **7**, 321 (1975).
(17) G. L. Brown, P. Grieger, and P. A. Kraus, *J. Am. Chem. Soc.*, **71**, 95 (1949).
(18) P. T. Jacobs, R. D. Geer, and E. Anacker, *J. Colloid Interface Sci.*, **39**, 611 (1972).
(19) R. L. Reeves, *J. Am. Chem. Soc.*, **97**, 6019 (1975).
(20) K. Tamaki, *Bull. Chem. Soc. Jpn.*, **40**, 38 (1967); **47**, 2764 (1974).
(21) M. J. Blandamer, M. J. Foster, N. J. Hidden, and M. C. Symons, *Trans. Faraday Soc.*, **64**, 3247 (1968); G. Atkinson, R. Garnsey, and M. J. Tait, "Hydrogen Bonded Solvent Systems", A. K. Covington and P. Jones, Ed., Taylor and Francis, London, 1968, p 161.
(22) W. Y. Wen and K. Nara, *J. Phys. Chem.*, **71**, 3907 (1967); W. Y. Wen, K. Nara, and R. H. Wood, *ibid.*, **72**, 3048 (1968).
(23) S. Lindenbaum and G. E. Boyd, *J. Phys. Chem.*, **68**, 911 (1964); H. C. Gregor, M. Rothenberg, and N. Finc., *ibid.*, **67**, 1110 (1963).
(24) S. Rehfeld, *J. Am. Chem. Soc.*, **95**, 4489 (1973).
(25) H. E. Wirth and A. LoSurdo, *J. Phys. Chem.*, **72**, 751 (1968).
(26) W. Y. Wen and S. Saito, *J. Phys. Chem.*, **68**, 2639 (1964).
(27) D. Guillon and A. Skoulios, private communication.
(28) J. E. Piercy and M. G. Rao, *J. Chem. Phys.*, **46**, 3951 (1967); E. Wyn-Jones and W. Orville-Thomas, *Adv. Mol. Relaxation Processes*, **2**, 201 (1972); M. Cochran, P. Jones, A. North, and R. Pethrick, *J. Chem. Soc., Faraday Trans. 2*, **68**, 1719 (1972).
(29) (a) L. H. Laliberté and B. Conway, *J. Phys. Chem.*, **74**, 4116 (1970); (b) L. A. Dunn, *Trans. Faraday Soc.*, **64**, 1898 (1968); F. Franks and T. Smith, *ibid.*, **63**, 2586 (1967).
(30) (a) T. L. Broadwater and F. D. Evans, *J. Phys. Chem.*, **73**, 164 (1969); (b) *ibid.*, **73**, 3985 (1969).
(31) R. Fuoss and V. F. Chu, *J. Am. Chem. Soc.*, **73**, 949 (1951); M. Yokoi and G. Atkinson, *ibid.*, **83**, 4367 (1961); J. Nicholson and R. Fuoss, *ibid.*, **77**, 198 (1955); O. Brody and R. Fuoss, *J. Phys. Chem.*, **60**, 156 (1956).
(32) C. Jolicoeur and G. Lacroix, *Can. J. Chem.*, **54**, 624 (1976); S. Cabani, G. Conti, and L. Lepori, *J. Phys. Chem.*, **78**, 1030 (1974).

A Numerical Solution for the Material and Momentum Balance Equations for Finite Concentration Chromatography

Jon F. Parcher,* T. H. Ho, and Henry W. Haynes, Jr.

Department of Chemistry and Department of Chemical Engineering, The University of Mississippi, University, Mississippi 38677
(Received August 20, 1975; Revised Manuscript Received May 3, 1976)

Publication costs assisted by the National Science Foundation

The material and momentum balance equations are solved for a chromatographic system with a single solute at finite concentrations, composition dependent gas phase viscosity, and a finite pressure drop across the column. The equations are solved numerically and shown to be reasonably accurate for a set of seven chromatographic systems which had been studied previously by static methods or which could be accurately described by a theoretical model.

Introduction

There are several different forms of chromatographic retention theories. Each theory utilizes some form of material or momentum balance equations written for a concentration gradient in the column, ad the theories differ only in the simplifying assumptions used to reduce the mathematical complexity of the system. The complete description of a chromatographic system with finite solute concentrations is too complex for any analytical solution and it is common practice to utilize several simplifying assumptions regarding the partition or adsorption kinetics, the predominant dispersion mechanism(s), and the pressure gradient across the length of the column.

It is usually assumed that the kinetics of the adsorption or partition processes are very rapid compared to the velocity of the concentration gradient. This is generally a valid assumption and can be verified by studying the effect of carrier gas flow rate on the measured experimental parameters.

In the special case of finite concentration chromatography, it is commonly assumed that the shape of the solute peak or "break through" curve is determined solely by the shape of the equilibrium isotherm and the pressure variations caused by the condensation of the solute in the liquid phase. The validity of this assumption depends upon the isotherm and the concentration of solute in the system. Valentin and Guiochon[1] have recently presented a convincing argument for the second-order nature of diffusion and mass-transfer contributions to the shape of large concentration boundaries in a chromatographic column. The secondary effects can be minimized but never completely removed. One method used to minimize diffusion and nonequilibrium effects is to operate at a velocity corresponding to a minimum plate height (HETP) and this is possible only if the column is operated at a significant pressure drop.

The primary distinguishing feature of the various extant retention theories is the treatment of the pressure gradient across a column and the composition dependence of the gas phase viscosity. Usually, the viscosity of the gas phase is assumed to be constant, even though it may actually vary drastically with composition. The assumptions regarding the pressure gradient are usually (i) the total pressure is uniform throughout the column, (ii) the total pressure is a linear function of the distance from the inlet, or (iii) the square of the total pressure is a linear function of the distance from the inlet.

In many cases, none of these assumptions concerning the gas phase viscosity and the pressure gradient are realistic. It is the purpose of this paper to show that the momentum and material balance equations can be solved under these conditions by numerical techniques. Today's widespread usage of high-speed computers means that it is not necessary to resort to physically unrealistic assumptions for the sole purpose of obtaining a solution to a complex system of equations.

Material and Momentum Balance Equations

The situation which we wish to describe mathematically is one in which finite concentrations of a single solute are introduced into the column at large carrier gas flow rates, which necessitates a finite pressure drop across the length of the column. In addition, the viscosity of the solute and carrier gas may differ appreciably causing the viscosity of the gas phase to be composition dependent. It will be assumed that any heat effects are small so that the column operates isothermally. In general, the concentrations, velocity, and quantities dependent upon concentration are all functions of time, t, and position, z, in the column. Under these conditions the mass balance equations for the solute concentration and total (solute + carrier) concentration are

$$\frac{\partial}{\partial z}(C_A V) + \theta_g \frac{\partial C_A}{\partial t} + \theta_l \frac{\partial Q_A}{\partial t} = 0 \tag{1}$$

$$\frac{\partial}{\partial z}(C_t V) + \theta_g \frac{\partial C_t}{\partial t} + \theta_l \frac{\partial Q_A}{\partial t} = 0 \tag{2}$$

where C_A and C_t are the concentrations (M) of the solute and the solute plus carrier gas in the mobile phase, respectively; V is the superficial velocity (cm/s); θ_g and θ_l are the ratios of the areas of the gas and liquid phases to the area of the empty column; and of pure liquid phase. The superficial velocity, V, is defined as the volume flow rate divided by the area of the *empty* column and is related to the interstitial velocity, v, by the relation $V = v\theta_g$. We have expressed the mass balance equations in terms of θ and V; however, the equations can be expressed equally well using the interstitial velocity and the volumes of the gas and liquid phases.

* Author to whom correspondence should be addressed at the Department of Chemistry.

The momentum balance equation for flow in packed beds is usually written in the form of Darcy's law:

$$V = \frac{-8.314 \times 10^6 K_p T}{(1 + BC_t)2\eta}\left(\frac{\partial C_t}{\partial z}\right) \tag{3}$$

where K_p is the permeability of the column (cm^2); T is the absolute temperature (K); η is the gas phase viscosity (cP); and B is the second virial coefficient of the gas. If the usual carrier gases and pressures encountered in gas chromatography are assumed, the term $BC_T \ll 1$ and can be neglected.

$$V = -\frac{\mathcal{H}}{\eta}\frac{\partial C_T}{\partial z} \tag{4}$$

where $\mathcal{H} = 8.314 \times 10^6 K_p T$. Two additional equations are required to complete the problem formulation. These are the equation relating viscosity to concentration:

$$\eta = \eta(C_A, C_T) \tag{5}$$

and the equilibrium isotherm:

$$Q_A = Q_A(C_A) \tag{6}$$

Probably the most accurate and convenient method for calculating the viscosity of a gas mixture at low pressure is that proposed by Wilke.[2,3]

$$\eta = \frac{\eta_1}{1 + Y_2\phi_{12}/Y_1} + \frac{\eta_2}{1 + Y_1\phi_{21}/Y_2} \tag{7}$$

$$\phi_{ij} = [1 + [\eta_i/\eta_j]^{1/2}[M_j/M_i]^{1/4}]^2/[\sqrt{8}[1 + M_i/M_j]^{1/2}]$$

where η_1 and η_2 are the viscosities of the pure component 1 and pure component 2, respectively, Y_i is the gas phase mole fraction of component i, and M_i is the molecular weight of component i. The parameters ϕ_{12} and ϕ_{21} are constants for a given system and temperature, and thus it is possible to obtain a tractable expression for the derivative $(\partial\eta/\partial Y)$ required for the solution of the differential equations.

The exact mathematical model for the equilibrium isotherm will depend upon the system used. In the case of partition isotherms, the two best models are those based on the Wilson equation[4,5] or the Flory–Huggins equation,[6,7] and numerous isotherm equations are available for adsorption isotherms. The mathematical model for the equilibrium isotherm is critically important because the methods for measuring isotherms by frontal chromatography do not yield isotherm data directly but rather the best parameters for an isotherm equation.

Numerical Solution for the Partial Differential Equations

The set of equations given below completely and rigorously describes the system with the assumptions regarding kinetic and mass transfer contributions to the boundary shape.

(i)	Solute material balance	(eq 1)
(ii)	Total material balance	(eq 2)
(iii)	Momentum balance	(eq 4)
(iv)	Gas phase viscosity	(eq 7)
(v)	Equilibrium isotherm	

Application of the appropriate boundary conditions to this set of equations (i–v) gives a mathematical description of the chromatographic situation described previously.

Elimination of V between eq 1, 2, and 4 and writing the total mass balance in terms of C_t^2 the following (unrestricted) mass balance equations are obtained: solute:

$$\alpha\frac{\partial C_A}{\partial z} + \beta C_A = \frac{\partial C_A}{\partial t} \tag{8}$$

total:

$$\gamma\frac{\partial^2 C_t^2}{\partial z^2} + \delta\frac{\partial C_t^2}{\partial z} + \epsilon = \frac{\partial C_t^2}{\partial t} \tag{9}$$

where:

$$\alpha = \left\{\frac{\psi}{2\eta C_t\left[\theta_g + \theta_l\dfrac{\partial Q_A}{\partial C_A}\right]}\right\}\frac{\partial C_t^2}{\partial z}$$

$$\beta = \frac{\psi}{2\eta C_t\theta_L\dfrac{\partial Q_A}{\partial C_A}}\left\{\frac{\partial^2 C_t^2}{\partial z^2} - \frac{1}{2C_t^2}\left[\frac{\partial C_t^2}{\partial z}\right]^2 - \frac{1}{\eta}\left[\frac{\partial C_t^2}{\partial z}\right]\frac{\partial \eta}{\partial z}\right\}$$

$$\gamma = \frac{\psi C_t}{\eta\theta_g}$$

$$\delta = \frac{-\gamma}{\eta}\left[\frac{\partial \eta}{\partial z}\right]$$

$$\epsilon = \frac{-2\theta_l C_t}{\theta_g}\left[\frac{\partial Q_A}{\partial C_A}\right]\left[\frac{\partial C_A}{\partial t}\right]$$

These equations, eq 8 and 9, were solved simultaneously without introducing any simplifying assumptions regarding the gas phase viscosity or pressure. One of the nonlinear partial differential equations is an initial value problem and the other is a boundary value problem. The equations were solved by using finite difference approximations on a two dimensional grid in time, t, and distance, z. The boundary value problem solution employed the Crank–Nicolson method, and the initial value problem was solved using the centered difference method.[8] The computations were aided by off setting the two grids by one-half increment in the z direction. For realistic isotherm parameters, the scheme converges rapidly to a stable solution. Occasionally, oscillations were observed in the solution, however, these could be removed by optimization of the $\Delta t/\Delta z$ ratio.

Measurement of Partition Isotherms

The basic approach for obtaining a partition isotherm from an experimental frontal chromatogram involves (i) an initial estimate of the isotherm in the form of an isotherm equation, (ii) solution of the differential equations for the system to produce a calculated output of solute concentration at the detector as a function of time, and (iii) adjustment of the parameters in the isotherm equation to produce concurrence of the observed and calculated chromatograms.

The validity of this approach was tested by comparison with chromatographic systems which had been studied previously by static methods or could be accurately described by a theoretical model.

Mathematical Model for the Partition Isotherms

The momentum and material balance equations describing the system are best written in terms of concentration, rather than the more common units of mole fraction or partial pressure. For this reason, we express the partition isotherms as the molar concentration of the solute in the liquid phase or solvent, Q_A, as a function of the molar concentration of the solute in the gas phase, C_A, i.e., $Q_A = Q_A(C_A)$. This is an unusual, but acceptable, method for expressing the isotherm and can be readily converted to the more common form of mole fraction of solute in the liquid phase as a function of the relative partial pressure.

Raoult's law provides a model for nonelectrolyte systems

and an isotherm equation can be obtained from any accurate empirical or theoretical equation relating the activity coefficient of the solute, γ_A, to liquid phase composition. Everett[9] has shown that the activity coefficient corrected to zero total pressure is related to the gas and liquid phase compositions by the equation

$$\ln \gamma_A = \ln \frac{C_A RT}{P_A^0 X_A} + \frac{P}{RT}[2Y_A B_{AA} + 2(1 - Y_A)B_{AC} - \bar{V}_A] - \frac{P_A^0}{RT}[B_{AA} - V_A^0] \quad (10)$$

where γ_A is the Raoult's law activity coefficient of the solute in the liquid phase; X_A is the mole fraction of the solute in the liquid phase; P is the total pressure (Torr); B_{ij} is the second virial coefficient; and $\bar{V}_A$ and V_A^0 are the partial molar and molar volumes of the solute, respectively.

In practice, the value of B_{ij} is usually very small because of the relatively inert carrier gas used in gas chromatography and the molar volume of the solute is relatively small so the molar volume is usually substituted for the partial molar volume. The relation between the concentration of solute, Q_A, and the mole fraction of solute, X_A, given by

$$X_A = \frac{Q_A V_1^0}{1 + Q_A V_1^0} \quad (11)$$

where V_1^0 is the molar volume of the solvent (liquid phase). To a first approximation the concentration of the solute in the gas phase is related to the mole fraction by the relation

$$Y_1 \approx C_A RT/P \quad (12)$$

Equation 1 reduces to

$$\ln \gamma_A = \ln \frac{C_A RT(1 + Q_A V_1^0)}{P_A^0 Q_A V_1^0} + 2B_{AA}C_A - \frac{PV_A^0}{RT} - \frac{P_A^0}{RT}(B_{AA} - V_A^0) \quad (13)$$

Numerous authors[10,11] have shown that nonelectrolyte systems, especially alkanes, can be described by the equation

$$\ln \gamma_A = \ln \frac{\phi_A}{X_A} + \left(1 - \frac{r_A}{r_1}\right)\phi_1 + \chi\phi_1^2 \quad (14)$$

where ϕ_i is the volume fraction of the ith component, γ_A is the Raoult's law activity coefficient of the solute, χ is the Flory interaction parameter; and r_i is the hard core volume of component i. Substitution of eq 14 into eq 13 leads to one form of an isotherm equation

$$Q_A = \frac{\frac{r_1}{r_A V_1^0}\left[\frac{C_A}{C_A^0}\right]}{\psi e^{-2B_{AA}C_A} - C_A/C_A^0} \quad (15)$$

where $C_A^0 = P_A^0/RT$ is the saturation concentration of pure solute (M) and

$$\ln \psi = C_A^0(B_{AA} - V_A^0) + \frac{PV_A^0}{RT} + \frac{r_1 - r_A}{r_1 + r_A Q_A V_3^0} + \frac{\chi r_1^2}{(r_1 + r_A Q_A V_1^0)^2}$$

Common chromatographic systems have the properties that $r_1 \gg r_A$ and $0.1 \leq \chi \leq 1.0$ and ψ may be small and relatively independent of Q. If this is the case, eq 6 may be cast in the form of an empirical isotherm equation

$$Q = \frac{K_1 C_A}{e^{-2B_{AA}C_A} - K_2 C_A} \quad (16)$$

where $K_1 \simeq r_1/(r_A V_1^0 C_A^0 \psi)$ and $K_2 \simeq 1/(\psi C_A^0)$.

A similar form of equation can be derived from Wilson's equation. The form of these equations is very similar to the classical Langmuir isotherm equation and the K_1 and K_2 parameters can be evaluated by linearization of the equation.

Evaluation of Literature Data

Three basic sets of literature data were used as reference sets for this investigation. McGlashan and Williamson[12] measured the solubility of n-hexane in n-hexadecane at 30 °C. Ashworth and Everett[10] measured n-hexane in squalane at 40 °C, cyclohexane in squalane at 40 °C, benzene in squalane at 40 °C, and n-pentane in squalane at 40 °C. Two sets of data were obtained from theoretical calculations by Martire.[11] The systems were n-pentane in n-dotriacontane and n-heptane in n-tetratriacontane at 80 °C.

The isotherm parameters calculated from eq 16 for these systems are given in Table I. The limiting factor in the isotherm measurement technique is the accuracy of the isotherm equation. Equation 16 fit some of the reference systems well but the fit was only marginal for other systems. The system which deviated the most from the equation was cyclohexane in squalane with an average relative deviation of 5% in the observed and calculated Q_A values, however, the remaining systems all had much lower deviations. Table I also includes the values of $1/C_A^0$, which is the limiting value of $K_2(\psi = 1)$ and it is obvious that for the particular systems studied the expected values of K_2 are very close to the observed, indicating that ψ is close to unity.

Experimental Section

The chromatographs used in this investigation were modified Beckman instruments and have been fully described previously.[13] The solutes were all chromatoquality or GC-Spectrophotometric quality solvents. The liquid phases were recrystallized, if necessary, until only one peak was observed in the chromatogram of the liquid phase on SE-30.

The permeability of the column was measured from the flow rate and pressure drop across the column when pure carrier gas was passing through the column. It was assumed that this permeability was independent of the flow rate and gas phase composition. Thus, during the experiment, the inlet pressures were maintained constant and the flow rate varied significantly because of the sorption effect and the variation of the gas phase viscosity. No attempt was made to measure or control the flow rate during the experiment; only the inlet pressures were monitered and controlled.

Experimental Results

1. *n-Hexane in n-Hexadecane at 30 °C.* This system at 30 °C produced a diffuse sorption profile and a sharp desorption profile. The desorption front was not utilized although it is possible to obtain one point on the isotherm from this type of an experiment. One experiment at a high relative concentration $C_A/C_A^0 = 0.88$ was performed at a flow rate of 40 ml/min and a moderate pressure drop $\Delta P/P_0 \simeq 0.25$. The isotherm parameters producing the closest fit of the experimental and calculated chromatograms were $K_1 = 414$, and $K_2 = 93.1$, with a standard deviation between the observed and calculated data of 4.6×10^{-5}. This is moderately close to the literature values given in Table I. However, it is obvious that one ex-

TABLE I: Regression Values for the K_1 and K_2 Values of the Reference Systems

System	K_1	K_2	$1/C_A^0$
1. n-C_6/n-C_{16}/30 °C	387.7	99.9	101.1
2. n-C_5/n-C_{32}/80 °C	23.4	8.39	7.97
3. n-C_6/squalane/40 °C	205.0	68.2	69.93
4. Cyclohexane/Sq/40 °C	381.9	100.6	105.7
5. Benzene/Sq/40 °C	286.4	102.0	106.8
6. n-C_5/Sq/40 °C	68.7	24.7	22.50
7. n-C_7/n-C_{34}/80 °C	124.8	50.7	51.49

TABLE II: Experimental Results for the n-Pentane in n-Dotriacontane System at 80 °C

Flow rate, ml/min	Expt			K_1 = 23.99	
	K_1	K_2	$10^4\sigma$	K_2	$10^4\sigma$
51	27.9	7.90	1.1	12.2	8.3
26	25.5	6.90	1.3	8.73	3.5
18	26.4	6.87	1.0	9.71	5.6

TABLE III: Experimental Results for the System n-Hexane in Squalane at 40 °C

Flow rate, ml/min	Expt			K_1 = 207.1	
	K_1	K_2	$10^4\sigma$	K_2	$10^4\sigma$
26	205.	69.9	0.8	69.6	0.8
12	214.	70.0	1.6	70.8	1.8

TABLE IV: Experimental Results for the System Cyclohexane in Squalane at 40 °C

Flow rate, ml/min	Expt			K_1 = 388.9	
	K_1	K_2	$10^4\sigma$	K_2	$10^4\sigma$
170	401	101	0.13	103	0.5
68	407	103	0.6	105	0.8
16	422	103	0.5	106	1.3

TABLE V: Experimental Results for Benzene in Squalane at 40 °C

Flow rate, ml/min	Expt			K_1 = 299.8	
	K_1	K_2	$10^4\sigma$	K_2	$10^4\sigma$
165	306	99.9	0.5	101	0.5
79	313	98.4	1.2	100	1.3
38	321	88.9	0.2	93.2	1.3
18	310	104	0.3	105	0.5

TABLE VI: Experimental Results for 3-Pentanone in n-Dotriacontane at 80 °C

Maximum C_A/C_A^0	Expt			K_1 = 69.4	
	K_1	K_2	$10^4\sigma$	K_2	$10^4\sigma$
0.07	67.1	95.1	0.1		
0.14	69.0	76.9	0.3	75.2	0.4
0.15	69.9	70.5	0.3	72.6	0.3
0.34	74.6	56.8	0.8	64.7	1.8
0.55	84.2	52.0	0.9	61.8	6.6
0.56	74.5	54.0	1.8	58.0	2.7
0.56	81.4	54.0	1.9	62.5	4.6

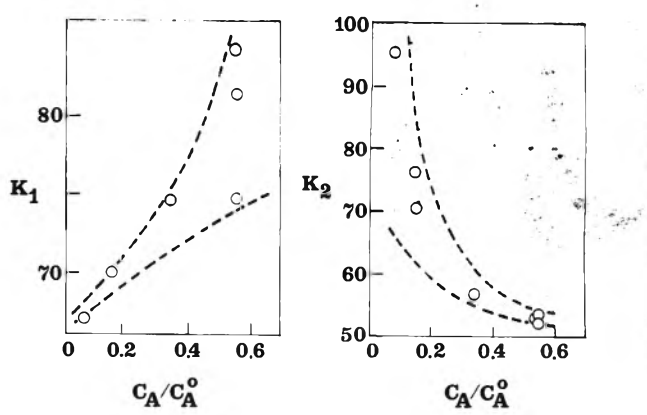

Figure 1. Variation of the calculated isotherm parameters, K_1 and K_2, with the maximum gas phase concentration of solute for 3-pentanone in n-dotriacontane at 80 °C. The dotted lines have no physical significance and are included only to give a general indication of the uncertainity in the data.

periment at high concentrations is not adequate to accurately determine both the limiting slope and the curvature of the isotherm. In principle, one could run two experiments. The first at low concentrations to accurately measure K_1 and the second at high concentration to determine K_2. However a frontalgram at low concentrations gives the same type of information as an elution experiment and is far more difficult to perform. Thus, we have chosen to measure K_1 by an elution experiment at infinite dilution and then use this K_1 and measure only K_2 from the high concentration frontal experiment. K_1 can be obtained from the specific retention volume of the solute, V_g^0, by the simple relation

$$K_1 = V_g^0 \rho \left(\frac{T_c}{273.2}\right) \tag{17}$$

where ρ = the density of the liquid phase at T_c (g/ml). The specific retention volume of n-hexane in n-hexadecane at 30 °C is 454.4 ml/g. This corresponds to a K_1 value of 386.4, in excellent agreement with the literature value of 387.7. Using this value of K_1, the K_2 producing the best fit for the chromatogram was 95.7 also in good agreement with the value in Table I. The standard deviation of the chromatograms increased to 1.3×10^{-4}.

2. *n-Pentane in n-Dotriacontane at 80 °C.* The maximum concentration for this system was limited by the liquid saturator to a maximum relative concentration of less than 0.25, so the value of K_2 is less accurate. The value of K_1 obtained by elution was 23.99 and the results of this experiment at three different flow rates are given in Table II. These data are in good agreement with the reference data of Table I, however, the precision is limited by the low concentration, $C_A/C_A^0 \leq 0.25$. There is no systematic variation of K_2 with flow rate although the K_2 value at the highest flow rate is questionable.

3. *n-Hexane in Squalane at 40 °C.* Two experiments were carried out at $C_A/C_A^0 \leq 0.80$ at two different flow rates. The K_1 value calculated from the specific retention volume was 207.1. The experimental results are given in Table III and are in excellent agreement with the literature values.

4. *Cyclohexane in Squalane at 40 °C.* This system was investigated at a higher concentration ($C/C_0 \leq 0.85$) and a wider flow rate range. The results for this system are presented in Table IV. It is obvious that the flow rate or pressure drop across the column has little effect in the calculated parameters

TABLE VII: Experimental Results for *n*-Heptane in *n*-Tetratriacontane at 80 °C

Maximum C_A/C_A^0	Expt K_1	Expt K_2	Expt $10^4\sigma$
0.02	122	48.3	0.005
0.10	118	52.1	0.08
0.21	108	56.2	0.7
0.61	103	51.8	0.9

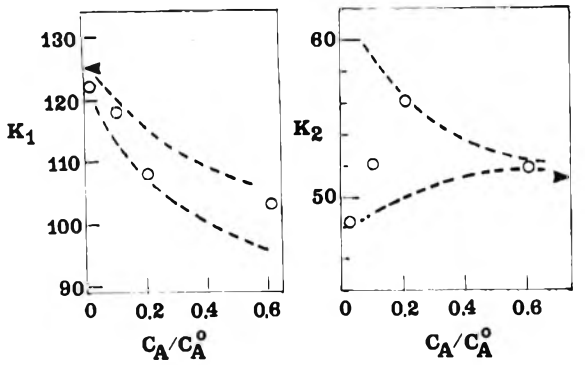

Figure 2. Concentration dependence of the isotherm parameters for *n*-heptane in *n*-tetratriacontane at 80 °C. ◀ indicates observed K_1 and K_2 values.

even though the pressure crop was varied significantly ($0.1 \leq \Delta P/P_0 \leq 1.1$).

5. *Benzene in Squalane at 40 °C.* At $C_A/C_A^0 \leq 0.82$, this system was also investigated over a wide range of flow rates and the results are presented in Table V. Again, there is no systematic variation of K_1 or K_2 with flow rate or pressure drop and the agreement with the literature values is reasonable, except for the data at 38 ml/min.

6. *3-Pentanone in n-Dotriacontane at 80 °C.* In this case, there is no literature data available for the isotherm. However, the system was investigated over a range of concentrations to determine the effect of this parameter on the calculated isotherm. The results are given in Table VI. This study shows that there is a systematic variation of K_1 and K_2 with the maximum concentration of solute. This variation is shown in Figure 1 and illustrates the large uncertainties in K_1 at higher C/C_A^0 and K_2 at low concentrations. This again points out the fact that it is difficult to determine both K_1 and K_2 from a single experiment and that the combination of an elution experiment at infinite dilution and a frontal experiment at high C/C_A^0 is the optimum combination.

7. *n-Heptane in n-Tetratriacontane at 80 °C.* Experiments for this system were run at four concentrations to check the extrapolated values of K_1 and K_2 at low and high concentrations against the observed values. The K_1 calculated from the specific retention volume was 125.8 in excellent agreement with the observed value of 124.8. The results of this study are given in Table VII and Figure 2. The extrapolated values of K_1 at low concentration and K_2 at high concentrations are 124 and 52. These are in good agreement with the observed values. It should be pointed out that in this particular case, there was a very low error between the observed and calculated chromatogram as indicated by the σ values in the table. This experiment also illustrates the approach which could be used for a system in which the specific retention volume was unobtainable, due to peak asymmetry or very strong adsorption.

TABLE VIII: Comparison of Two Chromatographic Methods for the Partition Isotherms of *n*-heptane in *n*-Tetratriacontane at 80 °C

C/C_A^0	Theor[a]	Diffuse boundary	Elution on a plateau
0.014	0.032	0.035	0.036
0.077	0.192	0.203	0.215
0.161	0.450	0.469	0.481
0.460	1.83	2.15	2.09

[a] Reference 11.

Summary

It has been shown that a numerical solution to the mass and momentum balance equations can be used to accurately measure equilibrium isotherms by gas chromatography. This method is accurate for columns with a large pressure drop, high solute concentration, and composition dependent gas phase viscosity. The method does not require a measurement of the solute + carrier gas flow rate or a calibrated detector. The technique is fast compared to static measurements and complementary to these in the concentration ranges covered and far superior in terms of the temperature range of the instrumentation.

The main disadvantages are the requirements for extensive computer time and an accurate mathematical model for the isotherm. In addition the detector must be linear over a wide concentration range and relatively flow insensitive. Obviously, the method is limited to systems with a diffuse boundary for either the sorption or desorption mode.

This approach also complements the other two forms of frontal chromatography, e.g., elution on a plateau and frontal analysis with a sharp boundary. The proper combination of these three methods can be used to measure the isotherm of any suitable chromatographic system.

For example, the technique of elution on a plateau was used to measure the isotherm for the *n*-heptane in *n*-tetratriacontane system. The results of this study are shown in Table VIII for the four separate experiments. The results for the diffuse front are also shown for comparison and the agreement is good in the limited range of the experiment. The two chromatographic measurements agree within ca. 3%. However, the chromatographic data are systematically higher (~15%) than the theoretically calculated data. Unfortunately, there are no static data available for this system for an absolute determination of the accuracy of the experiment and theoretical data.

Acknowledgments. This work was supported by Grant No. GP-36885X from the National Science Foundation. The authors wish to express their appreciation to Mr. T. N. Westlake, Jr., for his assistance in the experimental portion of this investigation.

References and Notes

(1) P. Valentin and G. Guiochon, *Sep. Sci.*, **10**, 245 (1975).
(2) C. R. Wilke, *J. Chem. Phys.*, **18**, 517 (1950).
(3) R. C. Reid and T. K. Sherwood, "The Properties of Gas and Liquids", 2d ed, McGraw-Hill, New York, N.Y., 1966, p 420.
(4) G. M. Wilson, *J. Am. Chem. Soc.*, **86**, 127 (1964).
(5) R. V. Orye and J. M. Prausnitz, *Ind. Eng. Chem.*, **57**, 18 (1965).
(6) P. J. Flory, *J. Chem. Phys.*, **10**, 51 (1942).
(7) M. L. Huggins, *Ann. N.Y. Acad. Sci.*, **43**, 1 (1942).
(8) D. U. von Rosenberg, "Methods for the Numerical Solution of Partial Dif-

ferential Equations", American Elsevier, New York, N.Y., 1969.
(9) D. H. Everett, *Trans. Faraday Soc.*, **61**, 1637 (1965).
(10) A. J. Ashworth and D. H. Everett, *Trans. Faraday Soc.*, **56**, 1609 (1960).
(11) G. M. Janini and D. E. Martire, *J. Chem. Soc., Faraday Trans. 2*, **70**, 837 (1974).
(12) M. L. McGlashan and A. G. Williamson, *Trans. Faraday Soc.*, **57**, 588 (1961).
(13) C. L. Hussey and J. F. Parcher, *J. Chromatogr.*, **92**, 47 (1974).

Conductometric Studies on Association of Cyclodextrin with Colloidal Electrolytes

Tsuneo Okubo, Hiromi Kitano, and Norio Ise*

Department of Polymer Chemistry, Kyoto University, Kyoto, Japan *(Received April 13, 1976)*

Conductance and surface tension measurements are carried out for the system, H_2O + colloidal electrolyte + cyclodextrin. The apparent critical micelle concentrations (cmc) of the electrolytes, i.e., sodium lauryl sulfate (NaLS) and cetyltrimethylammonium bromide (CTABr), are found to increase upon the addition of α- and β-cyclodextrins (αCD and βCD) in aqueous, ethanol–aqueous, and *N*-methylacetamide–aqueous media. It is concluded that the cyclodextrins form 1:1 complexes with the colloidal electrolytes. The association constant, K, increases in the order NaLS–αCD < NaLS–βCD < CTABr–αCD < CTABr–βCD. The free energy, enthalpy, and entropy of association for the CTABr–βCD system are −4.6 kcal mol^{-1}, −3.4 kcal mol^{-1}, and 4 eu at 35 °C, respectively. The equivalent conductances of monomeric (Λ_m), micelle (Λ_{mic}), and associated (with cyclodextrins) state electrolytes (Λ_{assoc}) are evaluated. For both of NaLS and CTABr, Λ_m is slightly larger than Λ_{assoc}, and strikingly larger than Λ_{mic} in aqueous media. By addition of ethanol, Λ_m and Λ_{assoc} decrease and Λ_{mic} increases, whereas Λ_m, Λ_{assoc}, and Λ_{mic} decrease with increasing content of *N*-methylacetamide. The surface tension of a CTABr solution increased with addition of β-CD.

Introduction

It has been well known that cyclodextrin forms complexes with a variety of molecular species.[1,2] Schlenk and Sano[3] demonstrated by solubility measurements that α- and β-cyclodextrins interact with long-chain aliphatic carboxylic acids. Therefore, ionic surfactants such as sodium lauryl sulfate and cetyltrimethylammonium bromide are expected to interact with cyclodextrin. The association constants of cyclodextrin with various molecular species were determined mainly by using changes of the absorbance of species in the uv region. Therefore, it has been difficult to determine the association constants for species having no chromophoric groups. We tried to overcome the difficulty by conductometric measurements. In the present report, we discuss complex formation of cyclodextrin with colloidal electrolytes by the conductometric method. Conductometric studies on surfactants have been carried out by various researchers.[4] However, the equivalent conductances of monomeric- and micelle-state electrolytes have not often been discussed. Such quantities are also studied in this paper.

Experimental Section

Materials. α- and β-cyclodextrins were obtained from Nakarai Chemical Co., Kyoto, and used without further purification. Cetyltrimethylammonium bromide (CTABr) and sodium lauryl sulfate (NaLS) were purchased from Nakarai Chemical Co. These two surfactants were further purified by recrystallization from water. Deionized water obtained with cation- and anion-exchange resins was used for the preparation of solutions. Spectroscopic grade ethanol was used. *N*-Methylacetamide obtained from Tokyo Kasei Organic Chemicals Co., Tokyo, was further purified by distillation (10.5 mmHg at 83 °C).

Conductance Measurements. The conductivity was measured by a Wayne-Kerr autobalance precision bridge (B-331) at a frequency of 1592 Hz and a recorder (Type SP-H, Riken Denshi Co., Tokyo). The capacitance correction was automatically effected and the precision of the conductivity is believed to be ±0.01%. Two types of conductivity cells having platinum plates were used: a Jones-Ballinger type cell[5] (cell constant = 4.97 cm^{-1}) and a conductivity cell (cell constant = 4.80 cm^{-1}) equipped with water-circulating jacket.

Surface Tension Measurements. The surface tensions of aqueous mixtures of cyclodextrin and surfactant were measured by using a Wilhelmy type surface tensiometer (Shimadzu Type ST-1). A ground glass measuring plate was suspended from an electrobalance by a glass fiber wire into solution in a glass container, the inner diameter of which was 4 cm. The measurements were carried out at room temperature around 25 °C.

Results and Discussion

The specific conductances, κ, of the H_2O + NaLS + αCD system as a function of NaLS concentration are given in Figure 1. The κ values of NaLS solution in the absence of CD were in agreement with those reported by Goddard and Benson[6] within experimental error. The characteristic feature of the κ–[surfactant] profile is that there can be drawn two straight lines having different slopes, as is clearly shown in the figure. The point of intersection corresponds to the apparent critical micelle concentration, m^*. The m^* of NaLS was clearly observed to become larger upon the addition of αCD. A similar feature was also obtained for other systems, i.e., H_2O + NaLS

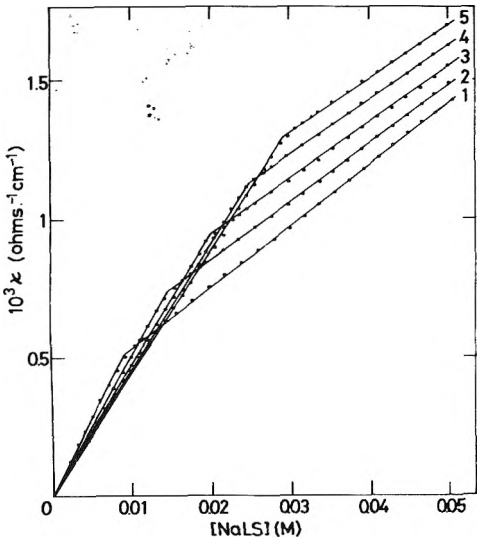

Figure 1. Conductances of the H_2O + NaLS + αCD system as a function of surfactant concentration at 25 °C: curve 1, initial concentration of αCD = 0 M; curve 2, 0.0114 M; curve 3, 0.0229 M; curve 4, 0.0343 M; curve 5, 0.0457 M.

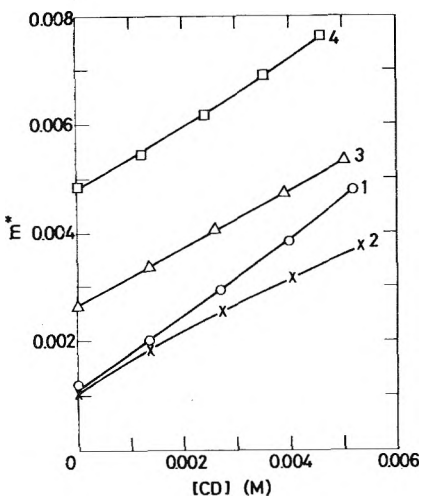

Figure 2. Apparent cmc, m^*, as a function of CD concentration in the H_2O + CTABr + βCD (curve 1), H_2O + CTABr + αCD (2), H_2O + 4 M EtOH + CTABr + βCD (3), and H_2O + 3 M NMA + CTABr + βCD (4) systems at 25 °C.

TABLE I: Equivalent Conductances of Surfactant Ions in Monomeric (Λ_m), Associated (Λ_{assoc}), and Micelle States (Λ_{mic}) and Association Constants of Micelle Electrolyte and α- and β-Cyclodextrin[a]

	Temp, °C	Ω^{-1} cm^2 Λ_m	Λ_{assoc}	Λ_{mic}	K, M^{-1}
CTABr–βCD	25	84	78	22	2240
	35	101	90	29	1850
	45	118	108	37	1560
CTABr–αCD	25	79	78	21	1110
NaLS–βCD	25	57	48	22	356
NaLS–αCD	25	58	44	22	111

[a] In H_2O.

TABLE II: Equivalent Conductances of Surfactant Ions in Monomeric (Λ_m), Associated (Λ_{assoc}), and Micelle States (Λ_{mic}) and Association Constants of Surfactant Electrolyte and α- or β-Cyclodextrin at 25 °C

	Solvent	Ω^{-1} cm^2 Λ_m	Λ_{assoc}	Λ_{mic}	K, M^{-1}
CTABr–βCD	1 M EtOH	74	65	23	2000
	2 M	65	58	24	1670
	3 M	57	44	26	690
	4 M	49	39	30	450
CTABr–βCD	0.5 M NMA	73	65	21	1190
	1 M	67	59	20	1140
	2 M	57	48	19	620
	3 M	45	34	18	270

+ βCD, H_2O + cetyltrimethylammonium bromide (CTABr) + αCD, H_2O + CTABr + βCD, H_2O + ethanol + CTABr + βCD. The cmc, m^*, was increased in all systems by the addition of CD. Figure 2 demonstrates the change of m^* in the various systems containing CTABr and CD.

We assume here a 1:1 type association as given by

$$S + CD \rightleftharpoons S \cdot CD \tag{1}$$

where S and CD indicate surfactant and cyclodextrin, respectively. When the concentrations of the monomeric-, associated-, and micelle-state electrolytes are denoted by m_m, m_{assoc}, and m_{mic}, respectively, the total concentration of the electrolyte, m, is given by $m_m + m_{assoc} + m_{mic}$. We assume here that m^* is given by $m_m + m_{assoc}$. Then, the association constant of monomeric electrolyte with cyclodextrin, K, is calculated by

$$K = \frac{m_{assoc}}{m_m\,CD_f} = \frac{m^* - m_m}{m_m(CD - m^* + m_m)} \tag{2}$$

where CD and CD_f denote the total concentration and the concentration of free-state cyclodextrin, respectively. The values of K obtained using eq 2 are compiled in Tables I and II. The accuracy was within ±5% under our experimental condition.

It should be noted here that the values of K can be determined without knowledge of m^* from conductometric measurements; when the association equilibrium given by eq 1 is valid, the following holds between κ and K when CD $\gg m$ and $m \leq m^*$:

$$\frac{1000(\kappa_0 - \kappa)}{CD} = K \cdot 1000\kappa - \Lambda_{assoc} mK \tag{3}$$

where κ_0, CD, and m are the conductance of the solution containing only S, the total concentrations of CD and S, respectively (in this case $m_{mic} = 0$, or $m = m_m + m_{assoc}$). Λ_{assoc} is the equivalent conductance of the electrolyte associated with cyclodextrin. From the $1000(\kappa_0 - \kappa)/CD$ vs. 1000κ plots at constant value of m, the values of K and Λ_{assoc} can be obtained. Figure 3 gives plots for the system, H_2O + NaLS + βCD, at 25 °C. The values of K and Λ_{assoc} were obtained to be 360 M^{-1} and 50 Ω^{-1} cm^2 from the straight line. As is clear from the figure, the accuracy is not good (about ±20%), even if the experimental accuracy of κ is high (±0.1% under the present experimental condition). This is due to the small difference between the equivalent conductance of monomeric electrolyte, Λ_m, and that of associated one, Λ_{assoc}. Thus, we must stress here that the more accurate values of K are obtained by using m^* (eq 2) rather than using eq 3.

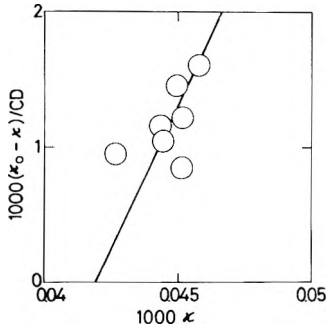

Figure 3. $1000(\kappa_0 - \kappa)/CD$ vs. 1000κ plots for the H_2O + NaLS + βCD system at 25 °C.

Next, the equivalent conductances of monomeric-, associated-, and micelle-state electrolytes (Λ_m, Λ_{assoc}, and Λ_{mic}, respectively) are evaluated. When $m \leq m^*$, the conductance of solution, κ, is given by the sum of the ionic conductances of monomeric (κ_m) and associated state electrolyte (κ_{assoc}). Therefore, Λ_{assoc} is determined from the slope of the line in the concentration region between 0 and m^* by using

$$\kappa = \kappa_m + \kappa_{assoc} = \frac{\Lambda_m m}{1000(1 + KCD_0)} + \frac{\Lambda_{assoc} KCD_0 m}{1000(1 + KCD_0)} = \frac{\Lambda_m + \Lambda_{assoc} KCD_0}{1000(1 + KCD_0)} m \qquad m \leq m^* \tag{4}$$

where CD_0 denotes the concentration of CD when the concentration of surfactant is m. The value of Λ_m is determined from the slope when cyclodextrin is absent, i.e., $CD_0 = 0$. It should be noted here that eq 3 is easily derived from eq 4, when Λ_m is equal to $1000\kappa_0/m$. When $m \geq m^*$, the conductance of solution is given by

$$\kappa = \kappa_m + \kappa_{assoc} + \kappa_{mic} = \frac{\Lambda_m m^*}{1000(1 + KCD_0)} + \frac{\Lambda_{assoc} KCD_0 m^*}{1000(1 + KCD_0)} + \frac{\Lambda_{mic}(m - m^*)}{1000} = \frac{\Lambda_m + \Lambda_{assoc} KCD_0 - \Lambda_{mic}}{1000(1 + KCD_0)} m^* + \frac{\Lambda_{mic}}{1000} m \qquad m \geq m^* \tag{5}$$

Λ_{mic} is, therefore, calculated from the slope of the κ vs. m plots in the concentration region above m^*. Λ_{mic} means, of course, the equivalent conductance of micelle-state electrolyte with reference to monomer unit. The real ionic equivalent conductance of the aggregated micelle as a whole can be obtained if the aggregation number of the micelle is known. It should be noted that we assumed the changes of Λ_m, Λ_{assoc}, and Λ_{mic} with surfactant concentration being negligibly small in eq 4 and 5. The concentration of monomer is not strictly constant above the cmc by mass action theory of the micellization equilibrium. We furthermore assumed a constancy of monomer concentration above m^*, which could be permissible for the micelles of large aggregation numbers. The changes of Λ_m, Λ_{assoc}, and Λ_{mic} with various concentrations of cyclodextrin were within ±5% in our experiments. This constancy implies the validity of eq 1 of the assumption of a 1:1 type reversible complex formation. In Tables I and II, Λ_m, Λ_{assoc}, and Λ_{mic} are compiled.

The Λ_{mic} values of CTABr and NaLS are close to each other (21 ~22 Ω^{-1} cm^2 at 25 °C). Equivalent conductivities of various colloidal electrolytes have been reported to be between

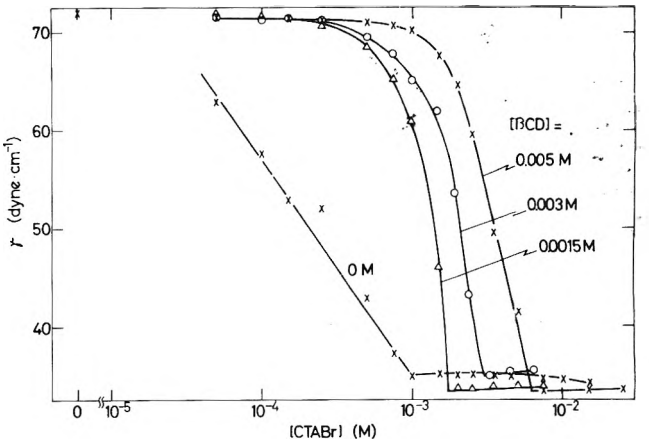

Figure 4. Surface tension of aqueous solutions of CTABr in the presence of βCD at 25 °C. The values by the curves are the concentration of βCD.

20 and 35 Ω^{-1} cm^2 at 0.1 M and at 25 °C.[4,7-10] Thus, the Λ_{mic} obtained by us may be reasonable. As is clear in the tables, Λ_m of CTABr is larger than that of NaLS. Λ_{mic} was strikingly smaller than Λ_m, which is easily understood from the bulkiness of micelle state electrolyte. Λ_{assoc} is comparatively smaller than Λ_m (about 5 to 30%) and strikingly larger than Λ_{mic}. Λ_m, Λ_{assoc}, and Λ_{mic} of the system H_2O + CTABr + βCD increased with increasing temperature. Furthermore, the increase of K was in the order NaLS–αCD < NaLS–βCD < CTABr–αCD < CTABr–βCD. This order may be attributed to the difference of the hydrophobicities of the surfactant and cyclodextrin, i.e., NaLS < CTABr, αCD < βCD in the strength order. K increased with temperature. The free energy, enthalpy, and entropy of the association process of β-cyclodextrin with CTABr were −4.6 kcal mol^{-1}, −3.4 kcal mol^{-1}, and 4 eu, respectively, at 35 °C. The exothermic enthalpy observed in the present system was also obtained for the association with dye studied by Cramer et al.[11] Both Λ_m and Λ_{assoc} decreased upon the addition of ethanol or N-methylacetamide. It should be noted here that Λ_{mic} increased with ethanol, whereas it decreased with N-methylacetamide. This may imply that the aggregation number of the micelle-state electrolyte decreases on account of weakening of hydrophobic attractive forces between hydrocarbon parts of CTABr by ethanol. In the case of N-methylacetamide, the mobility of the micelle-state electrolyte may be small because the micelle is solvated on account of high dipole moment of the organic solvent. Finally, the K values sharply decreased with increasing fraction of organic solvent. This may be partly due to the fact that the hydrophobic attractive interactions between cyclodextrin and colloidal electrolyte are weakened by the organic solvent.

It should be mentioned here that the apparent increase of cmc upon the addition of CD implies a portion of the available monomers in the micellization process is removed by complexation of monomers with CD. The surface tension, γ, of the system H_2O + CTABr + βCD as a function of [CTABr] is demonstrated in Figure 4. The aqueous solution of cyclodextrin did not show any surface activity. Upon the addition of small amounts of CTABr to the aqueous CD solution, γ did not decrease. However, γ was observed to decrease at higher CTABr concentration and then remained constant. The apparent cmc values, m^*, obtained from the surface tension measurements were also increased upon the addition of CD and agreed with those from the conductance measurements within experimental error. If the associated state electrolyte has no surface activity, the observed surface activity of the

H_2O + CTABr + βCD system is attributed to the monomeric state electrolyte. The association constant, therefore, can be determined by using the γ–[CTABr] profile in the presence of CD and that in its absence. The determination was, however, not carried out because of the comparatively large experimental error of γ particularly in the concentration regions of CTABr where γ sharply decreases.

References and Notes

(1) F. Cramer and H. Hettler, *Naturwissenschaften*, **54**, 625 (1967).
(2) J. A. Thoma and L. Steward, "Starch: Chemistry and Technology", Vol. 1, R. L. Whistler and E. F. Paschall, Ed., Academic Press, New York, N.Y., 1965 p 209.
(3) H. Schlenk and D. M. Sano, *J. Am. Chem. Soc.*, **83**, 2312 (1961).
(4) See, for example, A. Lottermoser and F. Püschel, *Kolloid Z.*, **63**, 175 (1933); E. L. McBain, W. B. Dye, and S. A. Johnston, *J. Am. Chem. Soc.*, **61**, 3210 (1939); A. B. Scott and H. V. Tartar, *ibid.*, **65**, 692 (1943); E. C. Evers and C. A. Kraus, *ibid.*, **70**, 3049 (1948); D. C. Robins and I. L. Thomas, *J. Colloid Interface Sci.*, **26**, 407 (1968); J. E. Adderson and H. Taylor, *J. Pharm. Pharmacol.*, **23**, 311 (1971).
(5) J. Jones and M. Ballinger, *J. Am. Chem. Soc.*, **53**, 411 (1931).
(6) E. D. Goddard and G. C. Benson, *Can. J. Chem.*, **35**, 986 (1957).
(7) A. W. Ralston and d. N. Eggenberger, *J. Am. Chem. Soc.*, **70**, 436 (1948).
(8) G. D. Parfitt and A. L. Smith, *Trans. Faraday Soc.*, **61**, 2736 (1965).
(9) A. W. Ralston, D. N. Eggenberger, H. J. Harwood, and P. L. DuBrow, *J. Am. Chem. Soc.*, **69**, 2095 (1947).
(10) A. W. Ralston, C. W. Hoerr, and E. J. Hoffman, *J. Am. Chem. Soc.*, **64**, 97 (1942).
(11) F. Cramer, W. Saenger, and H.-Ch. Spatz, *J. Am. Chem. Soc.*, **89**, 14 (1967).

Nitric Oxide Reduction with Ammonia over Cu(II)Y Zeolites

W. Burton Williamson and Jack H. Lunsford*

Department of Chemistry, Texas A&M University, College Station, Texas 77843

(Received June 16, 1976)

Publication costs assisted by The Robert A. Welch Foundation

Nitric oxide reduction with ammonia to nitrogen, nitrous oxide, and water over CuY zeolites has been studied in the temperature range from 80 to 150 °C. An unusual catalytic activity–temperature profile was observed with a maximum rate observed at 110 °C, similar to that recently reported by Seiyama et al. The reaction rate was first order in NO and zero order in NH_3. The rate was proportional to the degree of Cu^{2+} ion exchange. For a 6.5% CuY sample a turnover number of 0.13 NO molecules per minute per Cu^{2+} ion was observed at 108 °C and a NO pressure of 50 Torr. The reduction of NO with $^{15}NH_3$ indicated that the product $^{14}N^{15}N$ derived one nitrogen atom from each of the reactants; whereas, the product $^{14}N_2O$ was derived from NO. A kinetic isotope effect of $k_{NH_3}/k_{ND_3} \simeq 1.5$ was observed at 112 °C when substituting ND_3 for NH_3, but was not observed at 130 °C. The slow step in the reaction mechanism at temperatures less than 110 °C involves the reaction of coordinated ammonia with nitric oxide. Above 110 °C the reduction of the blue Cu(II) complex to a white Cu(I) complex becomes significant as confirmed by electron paramagnetic resonance. At the higher temperatures the reaction mechanism includes an oxidation–reduction step in which the oxidation of the Cu(I) complex is much slower than the reduction of Cu(II). Infrared and EPR evidence is interpreted in terms of a reactive $[Cu(NH_3)_4]^{2+}$ complex which is bound to the zeolite through a bridging nitro group.

Introduction

The catalytic reduction of nitric oxide has been extensively studied over the past 15 years due to its significance in air pollution. The ideal method of NO removal from industrial and automotive effluents would be its direct dissociation to nitrogen and oxygen; however, in the absence of a catalyst that will promote a significant rate of NO decomposition, the catalytic reduction of NO with various reducing agents is a primary means of its removal. The catalytic reduction of NO with ammonia is an effective method for the removal of NO_x from the exhaust systems of industrial boilers, furnaces, and nitric acid plants. The high selectivity of NH_3 for NO, combined with the enhanced reaction rate in the presence of O_2[1] makes NH_3 the preferred reducing agent over CO, H_2, or hydrocarbons, which are less selective for reaction with NO. The selectivity of ammonia for NO reduction was first reported by Andersen et al.[2] over Pt, Pd, Ru, Co, and Ni catalysts. Numerous other catalysts have since been employed for NO reduction, including various metals, transition metal oxides, and mixed metal oxide catalysts. These catalysts, as well as the thermodynamics, kinetics, and mechanisms for surface reactions of NO are referenced in two recent reviews.[3,4]

Isotopic studies using NO and NH_3 molecules labeled with ^{15}N have been used to study the mechanism of the N–N pair formation in the products of nitrogen and nitrous oxide over Pt,[5] Cu,[6] and Ru.[7] A deuterium kinetic isotope effect (KIE) was observed when deuterated ammonia was substituted for NH_3 in the reaction with NO over a Pt catalyst.[8] This KIE indicated that the rate-determining step may involve the splitting of a N–H bond in the adsorbed layer.

Chemisorption studies of NO on copper catalysts indicated that cupric ions adsorb NO whereas little chemisorption is found on cuprous ions.[9,10] An electron paramagnetic resonance (EPR) signal due to a Cu^+–NO complex in a Cu(I)Y zeolite was observed only at temperatures below 150 K.[11] Naccache and co-workers[12] have suggested that the NO ligand is doubly

coordinated to a Cu^+ ion and a lattice oxygen of the zeolite. Adsorption of NO on dehydrated Cu(II)Y zeolites at room temperature decreased the Cu^{2+} EPR signal intensity, while infrared studies revealed an intense, sharp band at 1918 cm^{-1} attributed to NO^+.[12]

The catalytic reduction of NO with NH_3 over CuY zeolites has been recently reported by Seiyama et al.[10,13] Their results indicate an unusual catalytic activity–temperature profile with a maximum activity at 120 °C. They interpret their kinetic data by a Langmuir–Hinshelwood type of reaction between NO and NH_3 coordinated to Cu(II) ions.

In a study related to the NO reduction (oxidation of NH_3 by NO), ammonia oxidation by molecular oxygen over Cu(II)Y zeolites has been previously reported from this laboratory.[14] The adsorption of NH_3 in Cu(II)Y zeolites results in a square-planar $[Cu(NH_3)_4]^{2+}$ complex as indicated by EPR[15-17] and infrared[17] studies. The rate of reaction of this complex with molecular oxygen from 160 to 185 °C was found to be first order in NH_3 or complex concentration and independent of oxygen pressures.

The purpose of the present research was to extend the previous work to include the parallel reaction of NO reduction with NH_3 in Cu(II)Y zeolites. A further investigation of the catalytic activity was centered around the rate maximum. Electron paramagnetic resonance spectroscopy, infrared spectroscopy, and mass spectrometry were utilized in an attempt to identify the reactive intermediates and to clarify the mechanism for NO reduction.

Experimental Section

Catalyst Preparation and Pretreatment. The copper(II) zeolites were prepared and analyzed for copper content as described in a previous investigation.[14] Three exchange levels of 1.9, 4.1, and 12.8 Cu^{2+} ions/unit cell (6.5, 14, and 44% CuY, respectively) were studied. The zeolite samples were activated by outgassing at room temperature for 1 h, and then heating in vacuo at 110 °C for 1 h. The copper zeolites were light green in color.

The $^{14}NH_3$ (Matheson), $^{15}NH_3$ enriched to 95% ^{15}N (Bio-Rad Labs), ND_3 enriched to 99%D (Stohler Isotope Chemicals), and Ar were used without further purification. Nitric oxide was purified by flowing the gas slowly (50 cm^3/min) through a cold trap at the melting point of pentane (−131.5 °C) to remove nitrous oxide and nitrogen dioxide before collection in a storage bulb. Mass spectrometric analysis of the purified NO indicated impurities of ≤1.2% N_2 and <1% N_2O.

Kinetic Experiments. A closed circulating system having a volume of 0.50 l was utilized in this study. The gases were circulated over the catalyst bed at a pumping rate of 0.5 l/min as measured against atmospheric pressure. By increasing the pumping speed and decreasing the weight and particle size of the catalyst, the reaction rate was shown not to be limited by diffusion within the reactor. A thermocouple located in a well beneath the catalyst bed was used to measure the catalyst temperature.

For the kinetic experiments a known amount of catalyst (0.07–0.5 g) was placed on a porous Vycor catalyst bed in the reactor and pretreated. Following the catalyst activation the reactor was filled first with ammonia and then with argon and nitric oxide. The experimental order of the reaction was determined by varying the initial pressures of ammonia and nitric oxide for reaction. Initial NH_3 pressures were varied from 27 to 105 Torr, while NO pressures ranged from 30 to 105 Torr. Following these preliminary studies the reaction mixture usually consisted of 50 Torr of NH_3 and 50 Torr of NO. Argon (10 Torr) was then added to this reaction mixture for a total pressure of 110 Torr at 27 °C. The argon was monitored as an internal standard to minimize errors caused by fluctuations in the sensitivity of the mass spectrometer and to account for a decrease in the total number of moles in the gas phase during the reaction.

The reactant gases were thoroughly mixed at room temperature before increasing the temperature for reaction. The reaction temperature was regulated by placing a cylindrical furnace around the catalyst bed which was maintained within ±1 °C of a given temperature by a temperature controller. The kinetic studies included temperatures from 80 to 150 °C. The reaction times ranged from 5 to 26 h, depending upon the reaction temperature, the amount of catalyst used, and the copper content of the catalyst. A uniform pumping speed was maintained throughout an experiment.

Small quantities of gas were removed periodically during the reaction and analyzed with a CEC 21-614 mass spectrometer. The gas samples were scanned from *m/e* 14 to 46 to monitor the concentrations of nitric oxide, argon, and the formation of the products N_2 and N_2O. One sample was analyzed for H_2, and only a trace amount was detected. Ammonia and water could not be measured quantitatively due to their partial adsorption on the catalyst and walls of the system.

Electron Paramagnetic Resonance Experiments. The EPR experiments were conducted in a reactor having a volume of 60 ml. Weighed amounts of catalysts (0.06–0.07 g) were given a similar pretreatment as described previously. The EPR measurements were made using a Varian E6S spectrometer which was operated in the X-band region. The g values were determined by using a 2,2-diphenyl-1-picrylhydrazyl (DPPH) standard (g = 2.0036). A sample of pitch in KCl was used as a reference standard for intensity. The EPR spectra were recorded at room temperature to minimize the disproportionation reaction of nitric oxide to N_2O and NO_2 which becomes more favorable on a NaY zeolite at lower temperatures.[18]

In following the copper(II) reduction to copper(I) the catalyst was maintained at the desired reaction temperature by an oil bath. After heating the catalyst in a mixture of reactant gases for 15 min to allow a steady state to be reached, the sample was evacuated briefly (5 s) to remove excess gases, thus preventing reoxidation of the catalyst by nitric oxide as it was cooled to room temperature.

Infrared Experiments. Infrared measurements were recorded at room temperature with a cell similar to one described previously.[18] Additional spectra were recorded at reaction temperatures in a stainless steel cell fitted with silver bromide windows. A T-shaped cell contained a sample holder which consisted of a short Vycor glass tubing. A slot midway along the length of the tubing allowed for the insertion of a 1 × 2 cm wafer sample into a U-shaped holder. A heating filament was coiled around the Vycor cylinder and regulated by a temperature controller. A thermocouple placed in a thermowell near the sample was used to measure the temperature. The spectra were recorded with a Beckman IR-9 spectrophotometer, which was operated in the transmittance mode. The programming of the slit widths was such that the resolution in the bending region was better than 3 cm^{-1}.

The zeolite samples were pressed into wafers between stainless steel dies using a pressure of 2×10^3 kg/cm^2. These self-supporting wafers had a resulting density varying from 3 to 6 mg of dry zeolite/cm^2. The maximum single beam transmission for each sample was approximately 50%.

TABLE I: Rate Data for the Reduction of Nitric Oxide with Ammonia over Cu(II)Y Zeolite in a Closed System

% exchange of Cu^{2+}	Cu^{2+}/unit cell	T, °C	Rate constant,[a] $h^{-1}\ g^{-1}$	d(NO)/dt,[b] molecules $min^{-1}\ Cu^{-1}$	Av selectivity[c] N_2/N_2O
6.5	1.9	79	0.135	0.021	0.5 ± 0.2
		93	0.179	0.028	1.3
		103	0.560	0.091	1.9
		105	0.650	0.101	2.0
		106	0.722	0.112	2.1
		108	0.813	0.126	2.3
		116	0.526	0.082	2.7
		126	0.356	0.055	2.7
		134	0.107	0.017	2.9
		149	0.067	0.010	3.7
		392	0.880	0.137	
14	4.1	97	0.432	0.031	1.7
		110	1.285	0.093	2.3
		127	0.655	0.047	2.8
44	12.8	98	0.865	0.020	1.9
		109	3.214	0.074	2.2
		124	2.163	0.050	2.5
6.5[d]	1.9	95	0.168	0.026	1.8
		104	0.377	0.059	2:1
		110	0.622	0.097	2.1
		127	0.209	0.032	2.7

[a] The average calculated error is 1.7% of the rate constant; extent of reaction up to 75% conversion of NO. [b] Initial rate under conditions of 50 Torr of NO. [c] Average ratio of N-containing products over a period of 75% conversion of NO. The average error during the reaction period was ±0.2 with no definite trends with time. [d] The catalyst was pretreated to 500 °C.

Results

Reaction Kinetics. The experimental order of the reaction was established by determining the rate dependence on the partial pressures of ammonia and nitric oxide. At initial nitric oxide pressure of 30, 60, and 105 Torr at 103 °C with a constant initial ammonia pressure of 52 Torr, the nitric oxide pressure followed a first-order decay. Varying initial ammonia pressures from 27 to 105 Torr with a constant NO pressure of 60 Torr had no effect upon the reaction rate for NO removal. Products observed from the reaction were nitrogen, nitrous oxide, and water. The two overall paths for NO reduction are

$$4NH_3 + 6NO \rightarrow 5N_2 + 6H_2O \quad (1)$$

and

$$2NH_3 + 8NO \rightarrow 5N_2O + 3H_2O \quad (2)$$

For the pressures used in these experiments the rate law can be expressed as

$$d[NO]/dt = -k[NO]^1[NH_3]^0 \quad (3)$$

The rate of change of nitric oxide concentration is d[NO]/dt; k is the first-order rate constant containing the amount of catalyst or copper in the system; and [NO] and [NH_3] are the concentrations of NO and NH_3 at time t.

Upon integration, the rate eq 3 for the first-order heterogeneous reaction takes the form

$$-kt = \ln [NO] - \ln [NO]_0 \quad (4)$$

where $[NO]_0$ is the initial concentration of NO. At the low temperatures and reactant pressures used, no water condensed in the cooler portions of the reactor. Consequently, no corrections were made for the small amounts of ammonia that could have been dissolved in the water formed from the reaction.

The overall first-order rate constants for NO reduction were determined by plotting the log of nitric oxide pressures vs. time. The least-squares analysis of the results are given in Table I for the CuY samples studied. The rate constants as a function of temperature are plotted in Figure 1. Our data as illustrated in Figure 1 confirm the results obtained by Seiyama et al.[13] in that the NO reduction rate passes through a maximum slightly above 110 °C. The catalytic activity was completely reversible with respect to temperature over the range from 80 to 150 °C. The catalyst retained a deep blue color while reacting at temperatures up to 110 °C, but it turned white when the reaction temperature was raised above 110 °C. This suggested that the Cu(II) was being reduced above 110 °C and was not rapidly reoxidized. An activation energy was determined for the 6% CuY catalyst at temperatures from 93 to 106 °C where the reduction of Cu^{2+} was not significant. The Arrhenius plot yielded an activation energy for NO reduction of about 29 kcal/mol.

The reaction rate as a function of copper(II) concentration is plotted in Figure 2 for the reaction temperatures corresponding to the rate maximum at 110 °C of Figure 1 and for temperatures on either side of the maximum. For the three exchange levels of 1.9, 4.1, and 12.8 Cu^{2+} ions/unit cell the reaction rate increased linearly with an increase in copper concentrations.

The product selectivities of N_2/N_2O increased with temperature as shown in Table I for the three exchange levels. The ratio of N_2 to N_2O was independent of Cu^{2+} concentration and increased linearly with temperatures above 90 °C.

The Reaction between ^{14}NO and $^{15}NH_3$. In an effort to determine the pathway for the formation of products in the reduction of NO the reaction of ^{14}NO with isotopically labeled $^{15}NH_3$ was investigated. The reaction of 95% enriched $^{15}NH_3$ (50 Torr) with ^{14}NO (46.5 Torr) at 110 °C on a 14% CuY catalyst yielded products having masses of m/e = 28, 29, and 44 corresponding to $^{14}N_2$, $^{15}N^{14}N$, and $^{14}N_2O$, respectively. The reaction profile is depicted in Figure 3, where the removal of

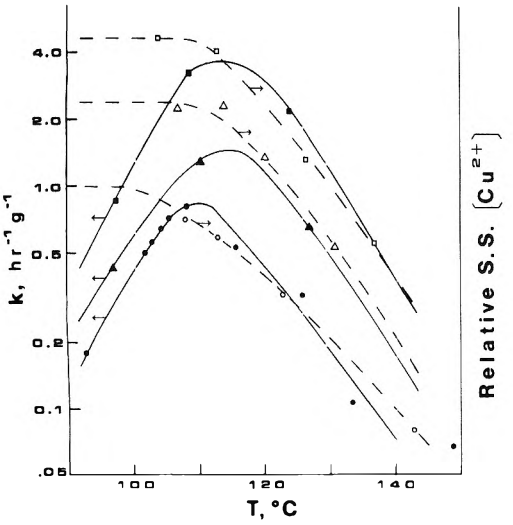

Figure 1. Rate constants for the reduction of NO by NH_3 over Cu(II)Y (closed symbols) and the relative steady state Cu^{2+} concentrations (open symbols) as a function of temperature: 6.5% (●,○); 14% (▲,△); 44% CuY (■,□).

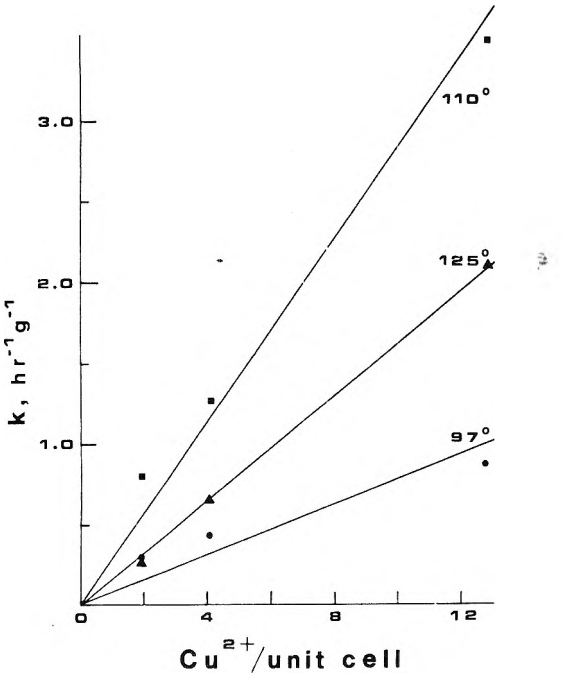

Figure 2. Rate constants as a function of Cu^{2+} ion concentration at three reaction temperatures.

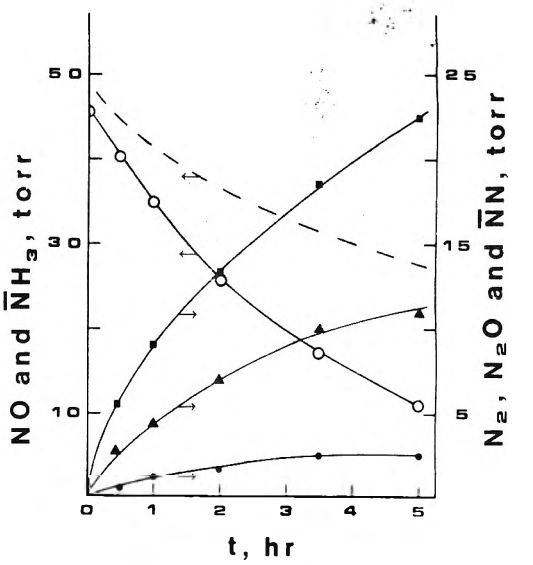

Figure 3. Products formed during the reduction of ^{14}NO (○) by $^{15}NH_3$ (– –) over 0.20 g of 14% CuY at 110 °C: $^{14}N_2$ (●), $^{14}N_2O$ (▲), $^{14}N^{15}N$ (■).

reactants is indicated on the left and the formation of products on the right. The ratio of nitrogen-containing products was $^{15}N^{14}N:^{14}N_2O:^{14}N_2 = 62:31:7$ as revealed by the product distribution of the reaction (Table II). The ratio of nitrogen to nitrous oxide of 2.2 agrees favorably with Table I and is independent of the extent of reaction. The formation of $^{14}N_2$ is the result of the reaction of $^{14}NH_3$ impurity with NO. This reaction would be expected to produce about 2.5 Torr of $^{14}N_2$ from the initial pressure of ammonia used. As shown in Figure 3 the formation of $^{14}N_2$ approaches a pressure of about 2.5 Torr. Each molecule of nitrogen is apparently formed by the reaction of one molecule of $^{15}NH_3$ with one molecule of ^{14}NO. Mixed nitrous oxide, $^{15}N^{14}NO$ ($m/e = 45$), was absent under these conditions, as were other possible products such as $^{15}N_2O$ and $^{15}N_2$. This indicates that the N_2O product came exclusively from the NO molecules.

The Reaction between NO and ND_3. The reaction rate of NO with deuterated ammonia, ND_3, was compared with the rate of the NO–NH_3 system to determine if the rate-limiting step of the reaction involved the breaking of a N–H bond. When ND_3 was substituted for NH_3, the reduction rate of NO over 14% CuY decreased at 112 °C but not at 130 °C as shown in Figure 4. The reaction rates and isotope effects in sequential pairs of experiments are compared in Table III. The average ratio of the overall rate constants at 112 °C is $k_{NH_3}/k_{ND_3} = 1.55$, whereas at 130 °C there is no essential difference in rate constants.

Side Effects of N_2O and NO_2. A possible side reaction could be the reduction of N_2O by NH_3:

$$2NH_3 + 3N_2O \rightarrow 4N_2 + 3H_2O \quad (5)$$

The reaction of NH_3 (120 Torr) and N_2O (175 Torr) at 152 °C over 14% CuY yielded no detectable decrease in the N_2O pressure after 12 h. This exceedingly slow reaction could thus be neglected under our reaction conditions.

The effect of NO_2 on the reaction of NO and NH_3 was determined by adding small amounts of NO_2 to the reaction mixture. The reduction rate of NO at 109 °C over a 14% CuY zeolite remained constant and unaffected by several additions of 2 Torr of NO_2 to the reaction mixture. This indicates that the reaction of NH_3 and NO was not poisoned by small amounts of NO_2.

Infrared Results. Infrared spectra recorded at room temperature in the frequency range of 1200–2000 cm^{-1} for a 44% Cu(II)Y are shown in Figure 5. The spectrum of the CuY zeolite outgassed to 120 °C is shown in curve a. Deuterated ammonia was utilized in the ir measurements since the deformation vibrations due to ND_3 and ND_4^+ are shifted to lower wavenumbers and do not obscure the region from 1400 to 1700 cm^{-1}. Nevertheless, upon addition of 50 Torr of ND_3 a peak at 1460 cm^{-1} was observed as indicated in curve b. This absorption band is attributed to the deformation band of NH_4^+ from NH_3 impurity in the ND_3. Curve c shows the spectrum 15 min after the addition of 50 Torr of NO to the CuY–ND_3 system. The absorption peak of gas-phase NO oc-

TABLE II: Product Distribution of ^{14}NO–$^{15}NH_3$ Reaction[a] over 14% CuY at 110 °C

%	%			
$\lvert\Delta^{14}NO\rvert$	$^{14}N^{15}N$	$^{14}N_2O$	$^{14}N_2$	$^{14}N^{15}N + {}^{14}N_2/{}^{14}N_2O$
13.5	63.6	30.7	5.7	2.26
24.9	61.9	29.9	8.2	2.34
44.7	60.3	32.0	7.7	2.12
63.4	59.5	32.2	8.3	2.11
76.3	62.6	30.2	7.2	2.31
Av	61.6	31.0	7.4	2.23

[a] Initial conditions 46 Torr of ^{14}NO, 50 Torr of $^{15}NH_3$, and 32 Torr of Ar.

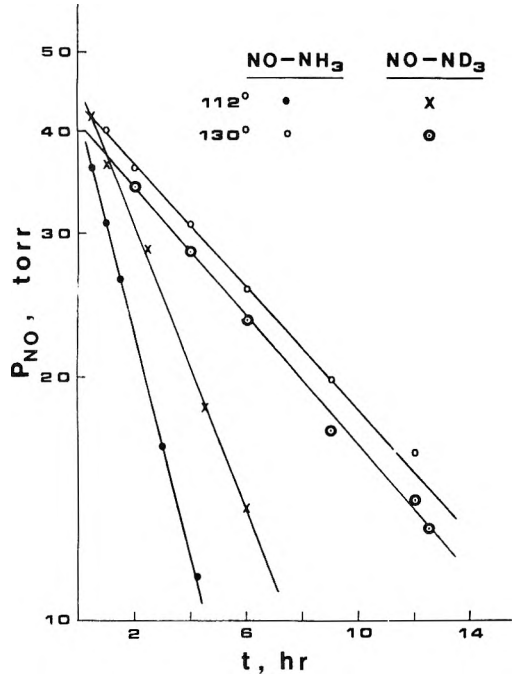

Figure 4. Decrease of NO as a function of time for NO–NH_3 and NO–ND_3 reactions at 112 and 130 °C.

curred at 1876 cm^{-1}, and the appearance of weak shoulders at 1330 and 1240 cm^{-1} were noted. Curve d depicts the room temperature spectrum 1.5 h after the NO addition. The shoulder at 1330 cm^{-1} has slightly increased and the weak absorption at 1240 cm^{-1} is more distinct. Experiments performed at elevated temperatures revealed a weak band at 1250 cm^{-1} upon reaction at 110 °C with the spectra recorded under reaction conditions. When NH_3 was substituted for ND_3 on CuY, a band at 1275 cm^{-1} charateristic of the square-planar $[Cu(NH_3)_4]^{2+}$ complex[17] was observed.

EPR Experiments. The EPR spectra of the Cu(II) complexes formed in 14% CuY upon addition of NH_3 and NO are shown in Figure 6. Spectrum a is that of the blue $[Cu(NH_3)_4]^{2+}$ complex formed at room temperature upon addition of 50 Torr of NH_3 to the CuY zeolite. The magnetic parameters at 27 °C for the square-planar $[Cu(NH_3)_4]^{2+}$ complex of Figure 6a are $g_\parallel = 2.216$, $g_\perp = 2.034$, and $A_\parallel = 160$ G. The addition of 50 Torr of NO for 10 min at 27 °C followed by a brief evacuation resulted in a light green sample and a spectrum depicted by Figure 6b. After standing for 19 h at 27 °C in the presence of 50 Torr of NH_3 and 50 Torr of NO, the green sample was briefly evacuated and the symmetric signal of

TABLE III: Summary of Reaction Rate and Isotope Effect in the Reduction of Nitric Oxide over 14% CuY

Run no.	T, °C	Ammonia reactant	k, $h^{-1}\,g^{-1}$	$k(NH_3)/k(ND_3)$	N_2/N_2O
1	112	NH_3	1.554	1.63	2.5
2	112	ND_3	0.954		2.3
3	112	ND_3	0.931	1.47	2.5
4	112	NH_3	1.364		2.6
5	130	ND_3	0.434	0.91	2.8
6	130	NH_3	0.396		2.9

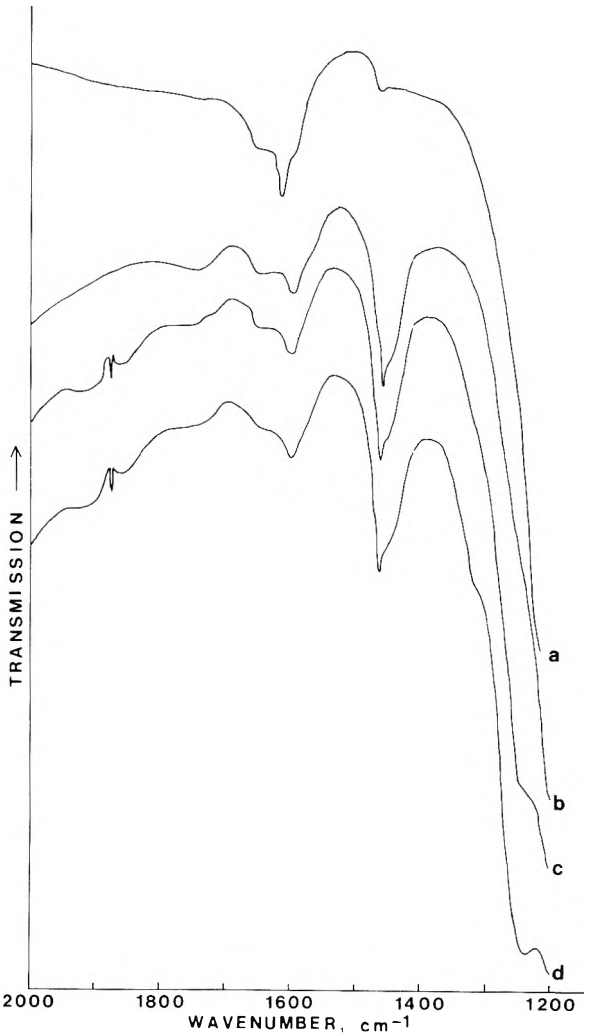

Figure 5. Infrared spectra in the region of 1200–2000 cm^{-1} for Cu(II)Y before and after addition of ND_3 and NO. Spectra were recorded at 27 °C: (a) after outgassing at 120 °C, (b) after addition of 50 Torr of ND_3, (c) 15 min after the addition of 50 Torr of NO to the system, (d) 1.5 h after addition of NO.

spectrum 6c was observed, having $g_{iso} = 2.120$. A symmetric signal with $g_{iso} = 2.114$ was also observed after NH_3 and NO were heated to 107 °C over the catalyst for 15 min and the gas phase was evacuated. When the sample was cooled without evacuation, the spectrum of the $[Cu(NH_3)_4]^{2+}$ complex was observed. No half-field signal characteristic of nonlinear copper pairs in CuNaY zeolites[19] was found in conjunction with the symmetric signal. The symmetric signal was also observed in the 6.5% CuY sample.

In the presence of only ammonia, the reduction of the Cu^{2+}

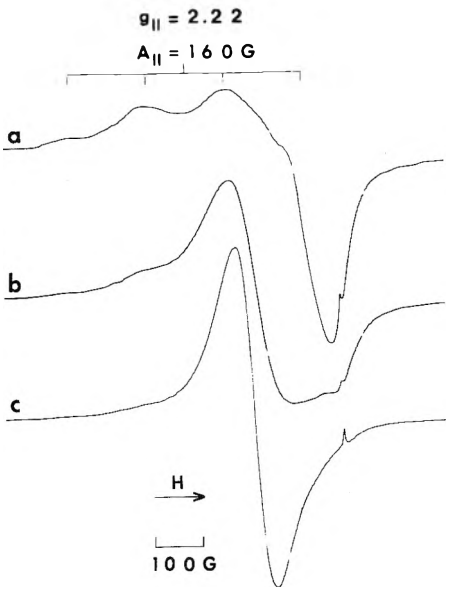

Figure 6. EPR spectra of Cu(II)–NH_3 and Cu(II)–NH_3–NO complexes recorded at 27 °C: (a) after addition of 50 Torr of NH_3 to 14% CuY at 27 °C; (b) subsequent addition of 50 Torr of NO for 10 min at 27 °C, followed by evacuation for 5 s; (c) after addition of 50 Torr of NH_3 and 50 Torr of NO for 19 h at 27 °C, followed by brief evacuation.

EPR signal did not proceed at an appreciable rate up to 150 °C (at 127 °C the EPR signal was reduced by approximately 5% over a 15-min period). In the presence of NO and NH_3, however, the reduction of Cu^{2+} to Cu^+ was enhanced considerably at temperatures as low as 110 °C. Since the line shape changed upon extensive reduction, the steady state Cu^{2+} concentrations were determined from double integration of the EPR spectra after heating the samples for a period of 15 min at temperatures ranging from 90 to 145 °C. The initial integrated areas before Cu^{2+} reduction indicated relative steady state copper concentrations of 4.6:2.4:1.0 for the three CuY samples whose Cu^{2+} ratio was 6.1:1.8:1.0. The relative steady state Cu^{2+} concentrations as a function of temperature are compared with the rate constants for NO reduction in Figure 1.

Discussion

The mechanism for the reduction of NO by NH_3 over Pt and CuO as proposed by Otto and Shelef[5,6] involves the associative adsorption of NO and dissociative adsorption of NH_3 to NH_2(ad) and H(ad). Reaction of the adsorbed species via a Langmuir–Hinshelwood mechanism leads to the formation of major products N_2, N_2O, and H_2O through the reactions:

$$^{14}NO + {}^{15}NH_2 \rightarrow {}^{14}N{}^{15}N + H_2O \quad (6)$$

$$2{}^{14}NO + 2H \rightarrow {}^{14}N_2O + H_2O \quad (7)$$

A similar mechanism has been postulated for the reaction over Cr_2O_3– and Fe_2O_3–Al_2O_3.[20] The NO reduction with CH_4 over Pt/Al_2O_3[21] has also been interpreted by a Langmuir–Hinshelwood model. Seiyama et al.[10] have similarly interpreted the NO–NH_3 reaction over CuY in terms of a Langmuir–Hinshelwood type of reaction mechanism.

We postulate that the reduction of NO with NH_3 over CuY zeolites must involve a change in the slow step of the mechanism as the reaction proceeds at increasing temperatures: (a) for temperatures below 110 °C the rate-determining step is the reaction of NO with coordinated NH_3; (b) at temperatures above the rate maximum the Cu^{2+} reduction to Cu^+ becomes significant and the reoxidation of the catalyst by NO is much slower than the reduction of the complex. Our observations of a KIE $\simeq$ 1.5 when substituting ND_3 for NH_3 is indicative of N–H bond breaking in the rate-limiting step. The EPR evidence for Cu^{2+} reduction and the formation of a white Cu^+ catalyst at temperatures above 110 °C supports the change in relative reaction rates at the higher temperatures. A plausible mechanism consistent with our experimental data is proposed:

$$[Cu(II)(NH_3)_3]^{2+} + NH_3 \rightleftarrows [Cu(II)(NH_3)_4]^{2+} \quad (8)$$

$$[Cu(II)(NH_3)_4]^{2+} + NO \xrightarrow[<110°C]{\text{slow}} [Cu(II)(NH_3)_3]^{2+} + N_2 + H_2O + H \quad (9)$$

$$H + NO \rightarrow HNO \quad (10)$$

$$2HNO \rightarrow N_2O + H_2O \quad (11)$$

$$[Cu(II)(NH_3)_3]^{2+} + HNO \rightarrow [Cu(I)(NH_3)_3]^{+} + NO + H^+ \quad (12)$$

$$[Cu(I)(NH_3)_3]^{+} + NO \xrightarrow[>110\ °C]{\text{slow}} [Cu(II)(NH_3)_3]^{2+} + NO^- \quad (13)$$

$$2H^+ + 2NO^- \rightarrow N_2O + H_2O \quad (14)$$

Reactions 8–11 are of major importance at the lower temperatures, approaching the rate maximum. The formation of the blue square-planar complex results upon addition of NH_3 to Cu(II). The reaction of NH_3 with weakly coordinated or gas phase NO by eq 9 leads to the formation of N_2 and H_2O as shown by the isotopic experiments:

$$(^{15}NH_3)_{complexed} + {}^{14}NO \rightarrow {}^{15}N{}^{14}N + H_2O + H \quad (15)$$

The possible reaction

$$^{15}NH_3 + {}^{14}NO \rightarrow {}^{15}N{}^{14}NO + \tfrac{3}{2}H_2 \quad (16)$$

did not occur since molecules with m/e = 45 were not detected in our experiments. The formation of N_2O may, in part, result from the bimolecular reaction of HNO on the surface.[22,23] This reaction apparently has a relatively low activation energy. The N_2O is derived strictly from the NO molecules since no isotope mixing was observed.

At the higher temperatures above the rate maximum, oxidation–reduction reactions 12–14 become significant. The HNO species produced by the reaction of NO with coordinated NH_3 is now capable of reducing Cu(II) to Cu(I); thus, through the formation of the HNO intermediate nitric oxide is responsible for the increased rate of Cu^{2+} reduction. The reoxidation of the reduced species above 110 °C by NO in eq 13 is obviously much slower under these conditions, and the white Cu(I) catalyst had to be cooled to temperatures below 110 °C before it reverted to the blue Cu(II) species in the presence of NO. Cooling the catalyst decreases the rate of reaction 12 relative to reaction 13. The NO^- formed in eq 13 by an electron transfer may rapidly react with the excess protons produced in the reduction step, yielding N_2O and H_2O. Since the NO^- was not detected in the infrared spectrum, its steady state concentration must be small. Reaction 14 is not a true mechanistic step, but it indicates the reaction pathway for the removal of H^+ and NO^-.

The increase in the ratio of N_2:N_2O at the higher temperatures may be understood in terms of the formation of N_2 from

HNO ($2HNO \rightarrow N_2 + 2OH$). The increasing ratio with increasing temperature is not due to the reduction of N_2O by NH_3 to N_2. We cannot completely rule out the possibility that a disproportionation reaction ($3NO \rightarrow N_2O + NO_2$) may contribute to the formation of N_2O, particularly during the early stages of the reaction.

In contrast to the CoY zeolites in which reactive $[Co(III)(NH_3)_nNO]^{2+}$ and $[Co(II)(NH_3)(NO)_2]^{2+}$ complexes are formed,[24] the ir spectra of the $[Cu(NH_3)_4]^{2+}$ complexes do not reveal the addition of a nitrosyl ligand. This is consistent with the observation of Enemark and Feltham[25] that no d^9 or d^{10} C_{4v} metal nitrosyl complexes have been observed. The presence of the weak bands at 1240 and 1330 cm^{-1} suggests that either nitrite or a bridging nitro ligand may be produced upon the addition of nitric oxide.[26]

The sequence of events leading to the formation of the species characterized by the isotropic EPR spectrum also indicates that the copper is strongly bonded to an oxide of nitrogen. The symmetric signal which was observed after the addition of NO and NH_3, followed by brief evacuation of the gas phase (the evacuation of NH_3 being the critical factor), may be interpreted in terms of a tetrahedral complex(I) in

(I) (II)

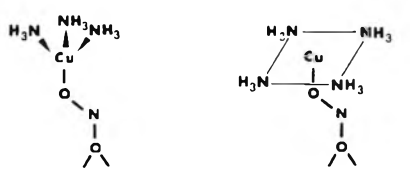

which the Cu^{2+} is bonded to three NH_3 ligands and a NO_2^- ion. The greenish color of the sample is consistent with the formation of a tetrahedral complex.[27] The NO_2^- ion may lift the complex away from the walls of the zeolite supercage, and thus give rise to motional averaging which would result in the symmetric signal. Although the origin of this unusual Cu^{2+} spectrum is not fully understood, it is clear that an oxide of nitrogen is necessary for the complex formation. One should emphasize, however, that the square-planar complex, perhaps bonded to the zeolite through a nitro ligand (II), is present under reacting conditions; i.e., in the presence of excess ammonia.

This bridging nitro ligand is not considered to be a critical factor in the reaction mechanism. Preliminary data on the catalytic activity of copper ammine complexes in aqueous solutions have revealed that the turnover numbers for the reduction of NO by NH_3 are only about a factor of 3 lower than those observed in this study. The observation that the reaction rates in solution approach those of the heterogeneous reaction indicates that the reactive intermediate is not unique to the CuY zeolite. It is unlikely that (II) would exist in solution, therefore, we conclude that the $[Cu(NH_3)_4]^{2+}$ complex is the essential feature of the active center, both in solution and in the zeolite.

The EPR evidence confirms that stable nitrosyl complexes are not formed with Cu^{2+} coordinated to ammonia. Such nitrosyl complexes would result in a decrease in the EPR signal since both the metal ion and the NO ligand are paramagnetic. This may be compared with the results of Naccache et al.,[12] who observed the formation of a nitrosyl complex in a dehydrated Cu(II)Y zeolite. In CoY zeolites where the nitrosyl ligand is more strongly bonded to the metal ion, the reduction reaction is zero order with respect to concentration of NO in the gas phase.[28]

The decrease in catalytic activity at temperatures greater than 110 °C correlates well with the reduction of Cu(II) ions in the ammine complex as shown in Figure 1. The presence of the square-planar $[Cu(NH_3)_4]^{2+}$ complex in excess ammonia has been previously confirmed by its ir spectrum at temperatures as high as 175 °C;[17] therefore, it is unlikely that migration of Cu^{2+} ions from the supercages could be responsible for the loss in activity, as suggested by Seiyama et al.[10]

When the reduction of NO with NH_3 over CuY is compared to the parallel reaction of NH_3 oxidation with O_2,[14] several distinctions in the kinetics and mechanisms become apparent. The rate dependence on reactant pressures are reversed: ammonia oxidation is characterized by a first-order dependence on ammonia and a zero-order dependence on oxygen; whereas, for nitric oxide reduction we found the reaction to be zero order in ammonia and first order in nitric oxide. The rate of NH_3 oxidation with O_2 was shown to coincide with the rate of Cu^{2+} reduction; hence, the slow step in this mechanism was the Cu^{2+} reduction (with the formation of NH_2 and H^+). In the present work the reaction was limited by the reaction of coordinated NH_3 with NO up to 110 °C, but became limited by the reoxidation of the catalyst at higher temperatures. The pathways for the two reactions over a CuY zeolite present at interesting example of the marked differences in mechanism which may be inherent in the same transition metal complex.

The specific rates of the NO–NH_3 reaction on CuY and CuO can be compared by converting the turnover numbers over CuO[6] to our reaction conditions. At 108 °C and 50 Torr of NO the turnover on CuO would be 0.0035 (molecule NO per Cu atom) min^{-1}, whereas on CuY it is 0.13 (molecule NO per Cu atom) min^{-1}. Thus, the specific reaction rate on CuY near the maximum activity is over 30 times faster than on CuO.

Conclusions

The $[Cu(NH_3)_4]^{2+}$ complex formed in a Y-type zeolite is an active catalyst for the reduction of NO by NH_3. Spectroscopic and kinetic evidence indicates that coordinated ammonia reacted with weakly coordinated or gas phase NO, yielding N_2 and a reactive intermediate. The latter intermediate produced N_2O and reduced the copper(II) ammine to a copper(I) complex. The reduced copper complex was not active in promoting the direct reaction between NO and NH_3; however, the Cu^+ was slowly oxidized to Cu^{2+} by NO. Formation of the inactive copper(I) complex leads to an unusual rate maximum at 110 °C. Since several of the elementary reaction steps may be followed in some detail, this system offers an excellent opportunity for studying catalysis at a molecular level.

Acknowledgment. The work was supported by The Robert A. Welch Foundation under Grant No. A-257.

References and Notes

(1) M. Markvart and V. Pour, *J. Catal.*, **7**, 279 (1967).
(2) H. C. Andersen, W. J. Green, and D. R. Steele, *Ind. Eng. Chem.*, **53**, 199 (1961).
(3) M. Shelef and J. T. Kummer, *Chem. Eng. Prog. Symp. Ser.*, **67**, 74 (1971).
(4) M. Shelef, *Catal. Rev.—Sci. Eng.*, **11**, 1 (1975).
(5) K. Otto, M. Shelef, and J. T. Kummer, *J. Phys. Chem.*, **74**, 2690 (1970).
(6) K. Otto and M. Shelef, *J. Phys. Chem.*, **76**, 37 (1972).
(7) K. Otto and M. Shelef, *Z. Phys. Chem. (Frankfurt am Main)*, **85**, 308 (1973).
(8) K. Otto, M. Shelef, and J. T. Kummer, *J. Phys. Chem.*, **75**, 875 (1971).
(9) H. S. Gandhi and M. Shelef, *J. Catal.*, **28**, 1 (1973).
(10) T. Seiyama, T. Arakawa, T. Matsuda, and N. Yamazoe, Preprint 9-1, Japan–U.S.A. Seminar on Catalytic NO_x Reactions, Susono, Japan, Nov, 1975.

(11) C. C. Chao and J. H. Lunsford, *J. Phys. Chem.*, **76**, 1546 (1972).
(12) C. Naccache, M. Che, and Y. Ben Taarit, *Chem. Phys. Lett.*, **13**, 109 (1972).
(13) T. Seiyama, T. Arakawa, T. Matsuda, N. Yamazoe, and Y. Takita, *Chem. Lett.*, 781 (1975).
(14) W. B. Williamson, D. R. Flentge, and J. H. Lunsford, *J. Catal.*, **37**, 258 (1975).
(15) J. Turkevich, Y. Ono, and J. Soria, *J. Catal.*, **25**, 44 (1972).
(16) E. F. Vansant and J. H. Lunsford, *J. Phys. Chem.*, **76**, 2860 (1972).
(17) D. R. Flentge, J. H. Lunsford, P. Jacobs, and J. B. Uytterhoeven, *J. Phys. Chem.*, **79**, 354 (1975).
(18) C. C. Chao and J. H. Lunsford, *J. Am. Chem. Soc.*, **93**, 71 (1971).
(19) C. C. Chao and J. H. Lunsford, *J. Chem. Phys.*, **57**, 2890 (1972).
(20) E. Echigoya, H. Niiyama, A. Ebitani, and K. Murata, Preprint 10-1, Japan–U.S.A. Seminar on Catalytic NO_x Reactions, Susono, Japan, Nov, 1975.
(21) Y. H. Hu and J. W. Hightower, Preprint 12-1, Japan–U.S.. Seminar on Catalytic NO_x Reactions, Susono, Japan, Nov, 1975.
(22) J. Zawadzki, *Discuss. Faraday Soc.*, **8**, 140 (1950).
(23) R. J. Kokes, *J. Phys. Chem.*, **70**, 296 (1966).
(24) K. A. Windhorst and J. H. Lunsford, *J. Am. Chem. Soc.*, **97**, 1407 (1975).
(25) J. H. Enemark and R. D. Feltham, *Coord. Chem. Rev.*, **13**, 339 (1974).
(26) K. Nakamoto, "Infrared Spectra of Inorganic and Coordination Compounds", Wiley, New York, N.Y., 1970, p 162.
(27) R. Schoonheydt and J. B. Uytterhoeven, to be published.
(28) K. A. Windhorst and J. H. Lunsford, to be published.

Substituent Effects on the Rate of Decay of *p*-Benzosemiquinone Anion Radicals

Alfred B. Sullivan

Monsanto Company, Organic Chemicals Division, Rubber Chemicals Research Laboratories, Akron, Ohio 44313

and G. Fredric Reynolds*

Department of Chemistry and Chemical Engineering, Michigan Technological University, Houghton, Michigan 49931

(Received November 17, 1975; Revised Manuscript Received July 19, 1976)

Publication costs assisted by the Monsanto Company

The rates of decay of *p*-benzosemiquinone radicals produced by reduction of the corresponding quinone at a platinum electrode have been studied by electron spin resonance. Nine monosubstituted quinones were studied with regard to the substituent effect on the decay rate in absolute methanol. The rates were found to be markedly accelerated by electron-withdrawing groups, and have been correlated by a Hammett plot of the logarithm of the decay rate vs. the σ_p^0 values for the substituents. The decay reactions are all second-order in radical concentration, and a reaction mechanism has been proposed that is consistent with the experimental observations.

Introduction

Since the *p*-benzosemiquinone radical was first observed by ESR spectroscopy,[1,2] a number of papers have appeared describing the details of the observed spectra as well as the mechanism of radical decay. Yamazaki and Piette[3-5] reported that semiquinone radicals formed by oxidation of hydroquinones decay by a disproportionation in basic solution

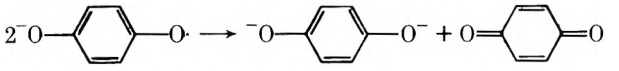

and by similar disproportionation of the monoprotonated semiquinones in acidic solution to yield quinones and hydroquinones. Bridge and Porter[6] proposed similar disproportionation reactions to account for the decay of the semiquinone radicals formed by the flash photolysis of duroquinone in ethanol and ethanol–water solutions. Another example is the dismutation of camphorquinone which was studied using electrochemical and ESR techniques.[7]

Despite the numerous mechanistic and kinetic studies, however, no systematic investigations of substituent effects have been made to date utilizing *p*-benzosemiquinone radicals. Indeed, Vyas and Wan[8] reported little, if any, substituent effects for the rapid decay of substituted semiquinone radicals formed by flash photolysis in dioxane solution, and suggested that their conditions led to diffusion-controlled decay reactions.

The work described here deals with conditions of relatively slow radical decay, utilizing electrochemically generated *p*-benzosemiquinone radicals in neutral methanol solutions, in which the substituent effect is readily apparent.

Experimental Section

ESR Spectrometer and Electrolysis Cell. The ESR instrument employed in this work was a Varian X-band, V-4502 spectrometer. It operates in the TE_{102} mode and employs a 9-in. magnet with 100 kHz/s field modulation. The semiquinone radicals were generated electrochemically using a Varian V-4556 electrolytic cell, equipped with a platinum screen cathode and a calomel reference electrode. The cell was slightly modified to permit a nitrogen purge at the base of the cell.

Reagents and Synthesis. Reagent grade absolute methanol was used throughout this work. The supporting electrolyte, tetraethylammonium perchlorate, was Eastman White Label.

p-Benzoquinone. A commercial sample was recrystallized from heptane and sublimed at 50 °C (5 mmHg) giving bright yellow crystals, mp 113.5–114 °C (lit. mp[9] 112.5–113.5 °C).

Chlorobenzoquinone. The oxidation of chloroquinol to the quinone was carried out with CrO_3 in acetic acid. Recrystallization from heptane and sublimation at 50–60 °C (2.5 mmHg) yielded a bright yellow product, mp 54–55 °C (lit. mp[9] 57–58 °C).

Bromobenzoquinone. Commercially available bromoquinol was oxidized with freshly prepared silver oxide.[9] (In all cases where silver oxide was used to oxidize quinols to quinones, it was freshly prepared as described in "Organic Reactions", Vol. IV, p 314). The product was twice sublimed at 50–60 °C (2.5 mmHg) resulting in yellow-orange crystals, mp 55.5–56 °C (lit. mp[9] 55–56 °C).

Cyanobenzoquinone. The intermediate cyanoquinol was prepared by the Elbs oxidation of o-cyanophenol.[10] The quinol was converted to quinone by oxidation with silver oxide in boiling benzene.[11] The crystalline product was purified by two sublimations at 50–60 °C (2.5 mmHg) giving yellow-brown crystals, mp 121–122 °C (lit. mp[11] 124–125 °C).

Methoxybenzoquinone. This compound was prepared by a two-step synthesis. Vanillin was oxidized to methoxyquinol with hydrogen peroxide.[12] The distilled quinol [143 °C (1 mmHg)] was oxidized to methoxybenzoquinone with aqueous sodium metaperiodate.[13] The crude product was purified by two sublimations at 60–70 °C (2.5 mmHg) resulting in bright yellow crystals, mp 145–146.5 °C (lit. mp[13] 142–146 °C).

Acetylbenzoquinone. 2,5-Dihydroxyacetophenone was oxidized to the corresponding benzoquinone in benzene with silver oxide.[14] The product was purified by two sublimations at 50–60 °C (2.5 mmHg) resulting in orange crystals, mp 63.5–65 °C (lit. mp[14] 65.5–66.5 °C).

Methoxycarbonylbenzoquinone. The methyl ester of gentisic acid was oxidized with silver oxide in benzene.[15] The conversion of the quinol to the quinone was followed by gas chromatography. The reaction was stopped when ~0.5% unreacted quinol remained. (Purification of all the quinones is difficult unless the amount of unreacted quinol is minimized. This is probably due to quinhydrone formation.) Purification was accomplished by two sublimations at 60–70 °C (2.5 mmHg) giving an orange crystal, mp 53–53.5 °C (lit. mp[15] 53.5–54 °C).

Methylbenzoquinone. A commercial sample was recrystallized twice from heptane yielding yellow crystals, mp 67–67.5 °C (lit. mp[9] 68–69 °C).

Phenylbenzoquinone. A commercial sample was recrystallized from heptane resulting in yellow-brown crystals, mp 114–114.5 °C (lit. mp[9] 112.5–113.5 °C).

Rate Measurements. The semiquinone radical anions were generated as follows: The quinone was dissolved in methanol (10 mM) containing 0.1 M tetraethylammonium perchlorate as supporting electrolyte. For the rate measurements, a 2.5-ml sample was introduced into the cell, and the solution then purged with nitrogen for 3–5 min. The purge valve at the base of the cell was then closed and the nitrogen diverted to the top of the cell for a continuous sweep during the experiment. An appropriate voltage was applied to the platinum cathode to reduce the quinone to the radical. In each case a negative voltage (vs. SCE) in the order of the first reduction potential (E_1) was applied. This turned out to be a very critical point, particularly with the less stable semiquinones. If larger voltages were applied, secondary radical species were formed which could be observed in the ESR spectrum.

The ESR spectrum was observed continuously by sweeping the field at selected time intervals until a maximum signal amplitude was reached. At this point the rate of formation of radicals was equal to the rate of their disappearance. To measure the decay rate, the sample was purged with nitrogen through the valve at the base of the cell to achieve mixing of the sample and eliminate diffusion effects. The mixing was continued for 1 min, then the perturbing voltage was removed and the spectrum scanned at 1-min intervals as the signal decayed. A nitrogen sweep was maintained over the sample throughout. All the measurements were made at temperatures between 22 and 25 °C.

The instrumental conditions for all runs were microwave power, 30 mW; sweep field, 30 G, sweep time, 1 min; and recorder, 100 mV full scale, 1 in./min chart speed. The 30-mW microwave power setting utilized gave approximately 10% less than maximum signal amplitude in order to avoid saturation effects.

Since the decay of the anion radical was found to be second order in radical, the units of the rate constant involved concentration. It was therefore necessary to measure the absolute radical concentration during each run. The intensity and line width of the output signal can be related to concentration by the equation $S = kA(\Delta H)h$,[16] where S is the number of spins, k is a line shape factor, A is a calibration factor, H is the peak-to-peak line width, and h is the amplitude of the derivative signal. To determine the calibration factor, a standard solution of the stable free radical galvinoxyl was prepared in the same solvent system. (Galvinoxyl was assumed to have the same line shape as the semiquinone radicals.) The spectrum of this solution was obtained in the electrolysis cell at the same instrumental settings used for the quinones. The signal intensity, line width, and known free radical concentration were used to obtain spin concentration calibration data as shown in Table I.

Results

The decay of all the *p*-benzosemiquinone radicals followed good second-order kinetics when followed to approximately 70% completion, provided reduction potentials of the order of E_1 were applied. These first reduction potentials were determined by polarography in methanol using a dropping mercury electrode and the values obtained closely paralleled the reduction potentials determined previously for these compounds in acetonitrile.[17] The rates of decay were obtained from the slope of the reciprocal of the radical concentration vs. time. Typical plots for these runs are shown in Figure 1. Although the absolute radical concentrations have an accuracy of only about ±25–50%, the relative accuracy between runs is much better, about ±5–10% as determined by duplicate experiments with benzoquinone and acetylbenzoquinone. This is to be expected since the error in the calibration factor should affect all the rate measurements by the same proportion. The concentration measurements were made under conditions where the fine structure was not observed; however, the high resolution spectra were recorded prior to decay and near the end of each kinetic run. In all cases no change in the hyperfine pattern was observed, indicating that the same radical species were being observed throughout.

The second-order decay rates obtained in methanol are given in Table II, along with Hammett substituent constants and the ESR hyperfine coupling constants with the ring protons. The hyperfine coupling constants were determined by first-order analysis using the reported value for the *p*-benzosemiquinone radical (2.37 G)[18] as a calibration standard.

The effect of substituents on the rate constant is marked, a 1000-fold increase being found in going from the electron-

TABLE I: Spin Concentration Calibration in Methanol/ 0.1 M TEAP

[G·], mM/l.[a]	Mod. ampl	*A*, cm^2 [b]	*A*/[G·], cm^2/mM
1.09×10^{-2}	500	1.23	1.13×10^2
1.09×10^{-2}	800	1.49	1.37×10^2
1.09×10^{-2}	1000	1.33	1.22×10^2
1.09×10^{-2}	1250	1.20	1.10×10^2
1.09×10^{-2}	1600	1.37	1.26×10^2

[a] The stable free radical, galvinoxyl, was used as a spin standard. Under the conditions used for ESR measurements, galvinoxyl gives a doublet. [b] The area *A* was calculated at each modulation amplitude from the product of signal intensity and the peak-to-peak line width (times 2).

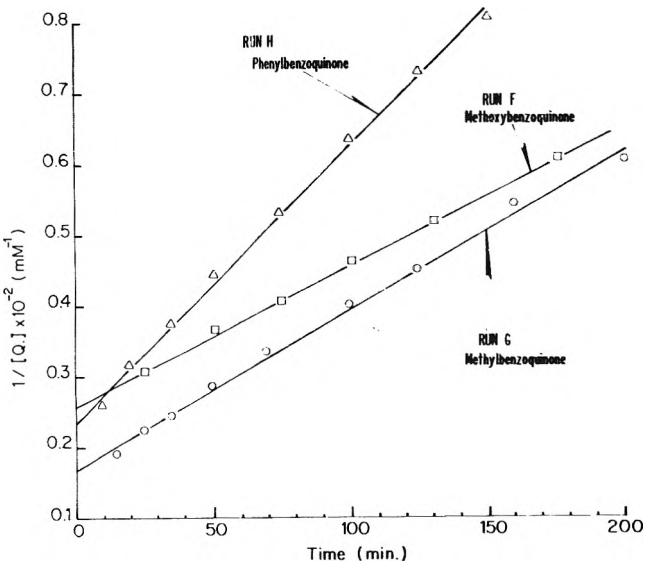

Figure 1. Typical second-order plots for the decay of semiquinone radicals in methanol.

donating substituent methoxy, to the electron-withdrawing substituent, cyano. The rates were found to correlate best with σ_p^0, the "normal" Hammett substituent coefficient,[19] with only the carbomethoxy substituent deviating substantially from the relation log $k_{obsd} = \rho\sigma_p^0$ + constant, as shown in Figure 2. The calculated reaction constant (ρ) is about 4, indicating a high sensitivity of the decay reaction to substituents compared to the ionization of benzoic acid ($\rho = 1$). The large ρ value is likely due to the reaction site involving an oxygen atom directly attached to the benzene ring, thus enhancing transmission of substituent effects.

Discussion

The Taft σ_p^0 values that have been used to correlate the rates of decay have been determined to represent mainly the inductive effects of a substituent,[19] and these values give quite precise correlations when resonance effects are absent. Since the Hammett plot obtained in this work (Figure 2) is satisfactory in correlating the rates of decay of the semiquinone radicals with the exception of the carbomethoxy substituent, it is tempting to postulate that a least part of the deviation may be due to resonance interaction of the type:

TABLE II: Observed Second-Order Rate Constants, Hyperfine Coupling Constants, and Substituent Coefficients for the Decay of Monosubstituted *p*-Benzosemiquinone Radicals in Methanol

Substituent	k_{obsd}, M^{-1} s^{-1}	A_{CH}, G[a]	σ_p^0 [b]
$-OCH_3$	3.3		−0.16
$-CH_3$	3.8	2.1	−0.15
$-C_6H_5$	6.7	2.2	-0.01
$-COOCH_3$	17	3.05, 1.85	0.46
−H	55	2.37	0.0
$-COCH_3$	430	3.0, 1.9	0.40
−Br	830	2.3	0.26
−Cl	1100	2.3	0.27
−CN	3300	3.0, 1.5	0.63

[a] The spin density for the substituents $-COOCH_3$, $-COCH_3$, and −CN is apparently more localized, and measurable coupling with only two of the ring protons is observed. The complexity of the $-OCH_3$ case did not lend itself to simple first-order analysis. [b] Values are from the tabulation of Taft.[19] The σ_p^0 for phenyl is not available and σ_p has been used instead.

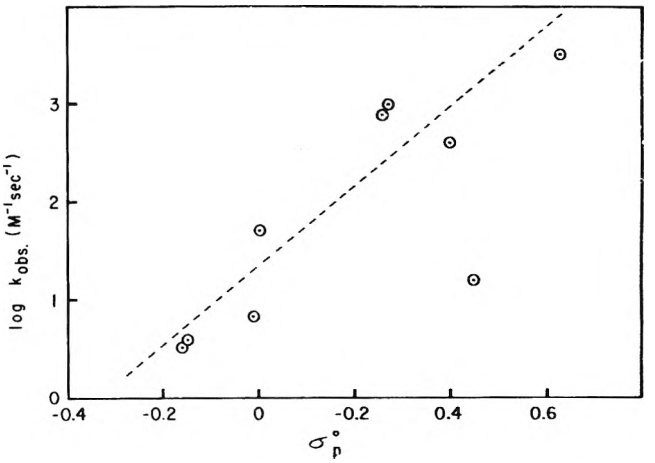

Figure 2. Plot of the logarithm of the observed rate constants for the decay of monosubstituted *p*-benzosemiquinone radicals vs. Hammett substituent coefficients.

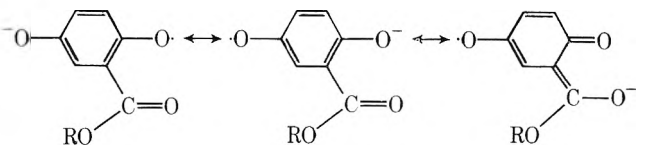

Bowers[20] found that in determining values of σ_p from ESR coupling constants of various para-substituted nitrobenzene radicals, the carboxy group was one of four substituents along with nitro, amino, and formyl in which the σ_p values appeared to be grossly in error, and all of these substituents were capable of resonance interaction with the phenyl ring. If we take the redetermined σ_p value for carboxy (carbomethoxy was not studied) from his work of 0.02 and use it to correlate our carbomethoxy substituent, it is interesting to note that good agreement with our Hammett plot is now obtained.

Hammond and co-workers[17] have also found that Hammett σ_p values can be used to correlate certain properties of *p*-benzoquinones. Thus, the first half-wave potentials of 12 monosubstituted quinones (including all those substituents employed by us in the present work) showed a linear Hammett

plot; a gross exception to the correlation was nitrobenzoquinone. In addition, Hammond[9] has studied the substituent effect on the charge transfer complexes of monosubstituted *p*-benzoquinones with hexamethylbenzene. He found that the position of maximum wavelength as well as the equilibrium constants for complex formation correlated well with the Hammett substituent constant, σ_p. The presence of substituents causes a shift in equilibrium for the formation of the complexes, the equilibrium constant being greater for the more electronegative substituents.

We propose that the effect of substituents on the rate constant for the decay of *p*-benzosemiquinone radicals can also be viewed as due to a shift in equilibrium. Allendoerfer and Papez[21] have recently shown that when durosemiquinone radicals are electrochemically generated in dimethoxyethane in the presence of supporting tetra-*n*-butylammonium perchlorate electrolyte, ion pairs are formed between the tetra-*n*-butylammonium cations and durosemiquinone radical anions, which are believed to be in equilibrium with the corresponding solvent-separated ions. In the case of our *p*-benzosemiquinone radicals, formed by reduction in the presence of excess tetraethylammonium perchlorate supporting electrolyte in methanol, a reasonable decay mechanism for the quinone radicals is

$$Et_4NQ\cdot \rightleftarrows Q\cdot^- + Et_4N^+ \quad (1)$$

$$2Q\cdot^- \rightarrow Q^{2-} + Q \quad (2)$$

Thus, the rate of disappearance of the radicals generated by reduction is related to their concentration as follows:

$$-\frac{d[Q\cdot^-]}{dt} = k_2[Q\cdot^-]^2 = \frac{k_2K^2[Et_4NQ\cdot]^2}{[Et_4N^+]^2}$$

and

$$-\frac{d[Et_4NQ\cdot]}{dt} = \frac{[Et_4N^+]}{K}\left(-\frac{d[Q\cdot^-]}{dt}\right) = \frac{k_2K}{[Et_4N^+]}[Et_4NQ\cdot]^2$$

where K is the equilibrium constant for step 1 and k_2 is the rate constant for step 2. Electron-withdrawing groups can be expected to increase the equilibrium constant K and thus increase the overall rate of decay of the *p*-benzosemiquinone radicals. Since the excess concentration of tetraethylammonium perchlorate was kept at 0.10 M for all kinetic runs, the observed rate constants in Table II are then given by $k_{obsd} = k_2K/[Et_4N^+] \simeq 10k_2K$.

A similar mechanism in the presence of acid

$$Et_4NQ\cdot + H^+ \rightleftarrows QH\cdot + Et_4N^+ \quad (1)$$

$$2QH\cdot \rightarrow Q + QH_2 \quad (2)$$

yields the rate equation

$$-d[Et_4NQ\cdot]/dt = (k_2K[H^+][Et_4NQ\cdot]^2)/[Et_4N^+]$$

This equation correctly predicts the rapid increase in the rate of radical decay found upon addition of acid.

An alternate decay mechanism that does not involve initial dissociation of ion pairs

$$Q\cdot^- + H^+ \rightleftarrows QH\cdot \quad (1)$$

$$2QH\cdot \rightarrow Q + QH_2 \quad (2)$$

yields the rate equation

$$-d[Q\cdot^-]/dt = k_2K[H^+][Q\cdot^-]^2$$

However, in this case the electron-withdrawing substituents should cause the equilibrium constant, K, for step 1 to become smaller, thus decreasing the decay rate. This is opposite to the overall effect found in this study.

The mechanism of reaction proposed above is consistent with the observation of (1) a second-order dependence on semiquinone radical concentration, (2) rate acceleration by electron-withdrawing groups, (3) faster reaction rates when acid added, (4) known tendency of semiquinone radicals to undergo disproportionation, and (5) no change in the ESR spectrum as the reaction proceeds. The good linearity of the second-order plots would appear to rule out any significant side reactions. With regard to the possibility of methanol being involved in the rate-determining steps, this cannot be determined from our data since in all cases the solvent methanol was present in large excess.

The effect of substituents in general on the hyperfine splitting constants and the stability of free radicals has been reviewed by Janzen.[22] In many cases, the hyperfine coupling constants were found to correlate well with the appropriate Hammett substituent constants. However, the limited number of hyperfine coupling constants obtained in this work show no obvious substituent effect, in contrast to the substituent effect on the rates of decay of the *p*-benzosemiquinone radicals. However, as pointed out by Janzen,[22] the substituent effect on spin distribution need not follow that for radical stability, since, in the latter case, it is the substituent effect on the initial and final states which must be taken into account.

References and Notes

(1) B. Venkataraman and G. K. Fraenkel, *J. Chem. Phys.*, **23**, 588 (1955).
(2) B. Venkataraman and G. K. Fraenkel, *J. Am. Chem. Soc.*, **77**, 2707 (1955).
(3) I. Yamazaki and L. H. Piette, *J. Am. Chem. Soc.*, **87**, 986 (1965).
(4) I. Yamazaki and L. H. Piette, *Biochem. Biophys. Acta*, **50**, 62 (1961).
(5) I. Yamazaki, H. S. Mason, and L. H. Piette, *J. Biol. Chem.*, **235**, 2444 (1960).
(6) N. K. Bridge and G. Porter, *Proc. R. Soc. London, Ser. A*, **244**, 259, 276 (1958).
(7) B. Kastening, *Collect. Czech. Chem. Commun.*, 30, 4033 (1965).
(8) H. M. Vyas and J. K. S. Wan, *Int. J. Chem. Kinet.*, 128 (1974).
(9) P. R. Hammond, *J. Chem. Soc.*, 471 (1964).
(10) E. Seebeck, *Helv. Chim. Acta*, **30**, 149 (1947).
(11) M. F. Ansell, B. W. Nash, and D. A. Wilson, *J. Chem. Soc.*, 3028 (1963).
(12) J. A. D. Jeffreys, *J. Chem. Soc.*, 2153 (1959); "Organic Syntheses", Vol. III, Wiley, New York, N.Y., p 759.
(13) E. Alder and R. Magnusson, *Acta Chem. Scand.*, **13**, 505 (1959).
(14) M. C. Kloetzel, R. P. Dayton, and B. Y. Abadir, *J. Org. Chem.*, **20**, 38 (1955).
(15) K. Brunner, *Monatsh. Chem.*, **34**, 913 (1913); J. Cason, "Organic Reactions", Vol. IV, Chapter 6, p 354.
(16) Varian Technical Information, V-4502 EPR Spectrometer System, Publ. No. 87-100-077, pp 5–10.
(17) K. M. C. Davis, P. R. Hammond, and M. E. Peover, *Trans. Faraday Soc.*, **61**, 1516 (1965).
(18) G. Vincow and G. K. Fraenkel, *J. Chem. Phys.*, **34**, 1333 (1961).
(19) R. W. Taft, Jr., *J. Am. Chem. Soc.*, **64**, 1805 (1960).
(20) K. W. Bowers in "Radical Ions", E. T. Kaiser and L. Kevan, Ed., Interscience, New York, N.Y., 1968, p 211.
(21) R. D. Allendoerfer and R. J. Papez, *J. Phys. Chem.*, **76**, 1012 (1972).
(22) E. G. Janzen, *Acc. Chem. Res.*, **2**, 279 (1969).

A Fractional Charge Model in the Molecular Orbital Theory and Its Application to Molecules in Solutions and Solids

J. Oakey Noell and Keiji Morokuma*

Department of Chemistry, University of Rochester, Rochester, New York 14627 *(Received July 12, 1976)*

Results of ab initio molecular orbital calculations employing the fractional charge representation of solvent molecules are presented. Extensive testing of the model for the hydration of Li^+ and F^- has been performed to assess the applicability of the method. The changes in the nature of the complex H_3N–HF associated with hydration are examined. The stability of the NH_4^+- - -F^- form of the complex is enhanced by hydration. The method is used to discuss the differences between gas and solution phase proton affinities of substituted ammonia. The method is also applied to the electronic structure of H_3N–BH_3 in the crystal state.

I. Introduction

The use of molecular orbital calculations as a probe of the electronic structure and properties of molecules in solution has only recently become the subject of much attention. The difficulties inherent in such a study are of two basic types. First, if one wants to perform a straight forward MO calculation for molecular aggregates as a supermolecule (see, e.g., Veillard et al.[1]), the number of orbitals which must be included is so large that it is generally not economically feasible to consider an extensive number of solvent conformations. At the same time the mobility of solvent molecules suggests that many such calculations would be required. The appeal of MO theory is, nonetheless, significant in that it is a tool for the study of the changes in the properties of the solute molecule upon solvation, a facet which is not present in classical descriptions of the energetics of solvation. Consequently much of the recent work in this area has been directed toward invoking simplifying assumptions such that the problems of interest become more tractable.

One model which has been used quite extensively is the development of pair, or higher order, empirical potentials.[2-5] The basic idea is to perform thorough ab initio calculations for moderately sized systems, e.g., include one or two solvent molecules. An analytic many body potential is then fit to the data. This potential may then be employed to include as many solvent molecules as are desired. This method has been particularly fruitful in its application to Monte-Carlo calculations, but it has a definite disadvantage in that the wave functions or electronic properties other than the total energy for the solute in the aggregate cannot be calculated.

A second technique which has been used is the electrostatic potential model.[6-8] This amounts to calculation of the interaction energy of solute and solvent employing the electron distribution of the monomers. This has proved to be a useful initial probe to supplement more complete ab initio calculations. This method is, however, not capable of considering changes in the wave function and electronic properties of the solute due to the presence of the solvent.

A third technique is to represent the solvent as a continuous medium, characterized by a dielectric constant, in whose cavity the solute (or the solute and a small number of solvent molecules) is embedded.[9-12] The principal application of this method has been to the hydrated electron. This method does allow a calculation of the wave function of the solute molecule in the solution. Another advantage of this method is that the statistical average over solvent conformations is inherent in the potential, but this is also a disadvantage because conformational variations of the solvent structure cannot be studied. Because of the numerical integration involved in the calculation of dielectric integrals, the method is rather expensive and is currently restricted to a spherical form for the cavity.

A fourth technique which has been useful is to consider the solvent molecules as point dipoles.[13] One may then perform an ab initio calculation on the solute in the presence of the dipolar fields. The electronic properties can be calculated by this method. This method, however, also requires a new type of integrals due to the potential of a dipole. A more serious disadvantage is that when the solvent molecule is large, or the solvent–solute distance is relatively small, the dipole representation of solvent molecules is a rather poor approximation.

Recently we proposed a model in which fractional point charges situated at atomic centers are used to represent solvent molecules.[14] The idea of using fractional charges as a representation of solvent molecules is, of course, not new. Such models were employed in early attempts to describe the structure of liquid water.[15] More recently, the potential used by Rahman and Stillinger in their molecular dynamics study was also based, in part, on such a picture.[16] The novel idea which we have presented is that such a representation of a solvent molecule may be incorporated into a calculation in which other molecules are being considered within the usual ab initio framework. In our earlier report we presented cursory results concerning the applicability of our model. In this paper we present more detailed data concerning the testing of the model, as well as present a few applications of the model to problems of chemical interest.

This paper will be structured in the following manner. The next section discusses the details of the method, special emphasis being given to its computational features. Sections III and IV will present detailed analysis of the testing which we have done on the hydration of Li^+ and F^-, respectively. Although much of this data was presented in our earlier communication,[14] it will be reiterated here for unity and clarity. Section V will be a discussion of the effect of a water solvent on the complex of ammonia and hydrofluoric acid. In section VI very cursory results will be presented concerning the solvent effect on the proton affinities of methylated ammonia. The results of a study on the effect of the crystal field on the monomeric charge transfer complex of ammonia and borane constitute section VII. Section VIII consists of a brief sum-

mary of what we feel are the virtues and limitations of our model.

II. Method of Calculation

The aim of the fractional charge model is to provide an economical, qualitatively correct means of inclusion of solvent molecules. It is reasonable therefore, that we choose a model for which inclusion of a solvent adds only minor complications to a gas phase calculation. The fractional charge model consists simply of situating fractional point charges at the location of solvent atomic centers. Neither electrons nor atomic basis functions are explicitly associated with such centers. The Hamiltonian for the solvent system is therefore identical in form with that for the solute itself. The only change is the addition of the nuclear attraction and repulsion integrals arising from the solvent sites. The evaluation of these integrals does not make a significant contribution to the total cost of a calculation. Of perhaps even greater importance is the fact that no new types of integrals are introduced, and hence implementation of the method requires only slight modifications in existing programs. Our experience has also shown that if the molecular orbitals of the solute are used as an initial guess for those of the solvated system, then convergence of the SCF is very rapid. This ease of evaluation should, in principle, facilitate calculations on a large number of solvent conformations. One final feature of the model which deserves emphasis is the flexibility inherent in its formalism. One need not replace all solvent molecules by fractional charges. If desired, a specified number of solvent molecules (e.g., a first shell) may be included explicitly in the usual ab initio framework. One could then consider this complex as the solute core to which additional solvent molecules may be added in the form of fractionally charged centers. Such a scheme is particularly desirable in those cases in which one suspects a high degree of charge transfer between the solute and the first solvation shell. We shall return to this point later in the text.

The assignment of the fractional charges for particular systems will be described in detail later, however a few comments are appropriate here. We have found that for solvents possessing a high degree of symmetry an excellent initial choice of the fractional charges are those which reproduce the dipole moment of molecule. If one wishes to replicate the results of other calculations with the fractional charge model, then one should employ fractional charges which yield the calculated dipole moment of a monomeric solvent molecule. For example, in many cases we were interested in comparing calculations in which all solvent molecules were replaced by fractional charges with those in which the first shell was included explicitly as part of the solute core. In these cases our reference fractional charges were those which gave the proper solvent dipole for the basis set which we used. In such computations the actual fractional charges which were used are characterized by a scale factor marking their deviation from these reference values. If, on the other hand, one wishes to compare calculated results with experimental data, then one should choose fractional charges which produce the experimental dipole of the solvent molecule. We shall discuss such a calculation for the hydration of the lithium cation in the next section.

At this point a few brief comments regarding the nature of the fractional charge model seem to be in order. It is clear that the principal type of solute–solvent interaction which is included by the model is electrostatic. This is probably the most important contribution for any polar solvent system, a fact for which results of a recent study provide good evidence.[17] We feel our model has an advantage over other electrostatic models both in its ease of implementation and its maintenance of proper bonding directionality, a feature which is lost in a dipolar approximation. Evidence for this latter property is given in the Appendix where limited geometry optimizations employing fractional charges are discussed. The fractional charge model also includes a portion of the polarization interaction, that being the polarization of the solute by the solvent. The reverse polarization, solvent by solute, is not accessible since the solvent does not have basis functions associated with it. In addition, this model is not capable of including either charge transfer or exchange interactions. These latter two are shorter range interactions, and are, therefore, not expected to make significant contributions at typical solute–solvent separations. It does place a limitation on the method, however, in that the absence of exchange repulsion will prevent meaningful solute–solvent geometry optimizations. If such optimizations are desired, some form of empirical repulsive potential must be added. In this vein, the recent molecular dynamics study of Gosling and Singer sets an interesting precedent.[18] Their potential utilized a combination of fractional charges and Lennard-Jones potentials in a dipolar approximation to a solvent molecule.

All calculations reported here were performed using the standard 4-31G basis set of Ditchfield et al.[19] (5-21G for Li[20]) employing a modified version of the GAUSSIAN70[21] programming system. For water with this basis set the point charges $q_H = 0.4657$ and $q_O = -0.9314$ reproduce the calculated dipole moment of 2.596 D at the experimental monomer geometry.[22] For several computations, the interaction energy is separated into component (electrostatic, exchange, polarization, charge transfer, and coupling) contributions using the methods of Morokuma[23] and Kitaura and Morokuma.[24]

The notation to be used throughout this paper is that all molecules which are included within the normal ab initio framework will be denoted by capital letters (e.g., H_2O) while those molecules represented by fractional charges will be characterized by small letters (e.g., h_2o).

III. Hydration of Li^+. A Test

In recent years the solvation of the lithium cation by polar solvents, in particular water, has been the subject of vigorous theoretical interest.[2,5,14,25,26] The unique appeal of this solvent system is the result of two properties. First it is small enough so that calculations at an ab initio level may be performed for hydrated systems of moderate complexity (e.g., explicit inclusion of a first hydration shell). In addition it is a system of inherent physical interest since the highly localized positive charge of the lithium cation results in strongly bound hydration complexes. Though there are widely conflicting experimental data concerning details of the hydration, it is generally conceded that there exists at least one shell for which exchange with the bulk medium is negligible.[27] Such a property implies that a static hydrated complex should be a reasonable model for the solution behavior of the ion. Such a simplification is necessary if molecular orbital investigations are to be feasible.

The calculations which have been reported to date may be roughly categorized into two classes. The intent has been either a delineation of the interaction potential between the lithium cation and one or possibly two water molecules,[25,26] or the development of "ab initio" pair potentials suitable for the consideration of larger molecular complexes.[2,5] Neither of these types of investigations is capable of yielding direct information concerning the effect of outer solvation spheres

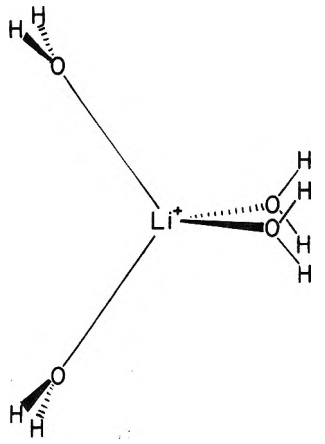

Figure 1. Assumed geometry of the first hydration shell of Li^+. R_{Li^+-O} = 2.0214 Å. Complex has C_{2v} symmetry.

on the solute system. It is in addressing this sort of question that the fractional charge model appears to be particularly well suited.

The intent of our calculations was not to perform a thorough investigation of all possible conformers of the ion–water clusters. Rather we were interested in assessing the applicability of the fractional charge model. In accord with this intent we chose to investigate only a single configuration of solvent molecules. The conformation of the inner shell consisting of four water molecules was restricted to the optimum configuration as determined by Kollman and Kuntz[5b] based upon pair potential studies. In this conformation the waters are dipole oriented with respect to the Li^+ with a Li^+–O distance of 2.0214 Å. Though the orientation of the water molecules with respect to one other is somewhat arbitrary, it was chosen such that the first shell was of C_{2v} symmetry. The geometry of this first solvation sphere is depicted in Figure 1. The second solvation shell was formed by hydrogen bonding water molecules to the first sphere molecules. This bonding was assumed to occur in essentially the same conformation as in the water dimer.[28] To avoid steric hindrance, however, the hydrogens of one water molecule in the "dimer" were placed cis to the hydrogens of the complexing partner. The water molecules in this complex, as well as in the rest of the studies reported here, were restricted to their equilibrium monomer geometry (r_{OH} = 0.956 Å, ∠HOH = 105.2°).[22]

As was discussed earlier, the fractional charge model which we are using is incapable of accounting for charge transfer or exchange interactions. In light of this inadequacy it was necessary that we obtain some sort of a feeling for the nature of the solvent–solute interaction. Toward this end an energy decomposition analysis, using the scheme of Morokuma et al.,[23] was performed for the interaction between a lithium cation and a prepared solvent host comprised of the four first shell water molecules. The results of this analysis are displayed in Table I. The salient conclusion which may be drawn from these data is that the electrostatic contribution to the interaction energy is the controlling term. The second largest contribution is the polarization interaction, which, incidentally, is the other type of interaction which the fractional charge model, in principle, is capable of handling. As one moves further away from the solute, i.e., when one considers outer-shell solvation, the interaction should be dominated to an even greater extent by these long-range interactions. Consequently, it is expected that this should be an ideal test

TABLE I: Energy Components (in kcal/mol) for the Process $Li^+ + (H_2O)_4 \rightarrow Li^+(H_2O)_4$

Total ΔE	−163.7
Electrostatic	−151.2
Exchange	8.0
Polarization	−19.3
Charge transfer + coupling	−1.2

system, insofar as suitability of the potential to the method is concerned.

The fractional charges of the first shell water solvents were chosen such that the interaction between the lithium ion and a host of four fractionally charged water molecules replicated the total interaction energy of the energy decomposition analysis discussed above. The fractional charges for outer-sphere water molecules, in a like manner, were chosen such that the electrostatic interaction was duplicated. Calculations were then performed for the solvation of the lithium cation by one, two, or three shells. The results of these calculations are shown in Table II. The critical information which may be gleaned from this study is that the interaction energy between the lithium ion and its solvent host is very nearly independent of whether the first shell water molecules are explicitly included in the calculation. We consider this to be strong evidence for the suitability of the fractional charge model as a means of representation for the outer solvation spheres. It is also important to note that the optimal fractional charges are very nearly those predicted by reproduction of the calculated dipole moment. This supports our earlier conjecture that this model will adequately reproduce electrostatic and polarization energies. A final note is in order concerning the energetics of solvation. As one expects, the stabilizing influence of each successive shell rapidly decreases. Although our results are certainly not definitive, they indicate that the stability of the cation is little effected by solvation beyond the second or third hydration sphere.

Perhaps a more demanding test of our model than reproducing interaction energies is the proper handling of qualitative changes in the wave function. As a probe for this purpose we have studied the orbital energy of the lithium 1s orbital. The results, as displayed in Table III, provide firm evidence that the wave function, in the region of the solute ion is well represented by the fractional charge model. The effect of the first solvation shell is replicated, to within 15%, by the fractional charge model. The influence of the outer hydration spheres is similarly well reproduced.

One final piece of evidence concerning the viability and applicability of the fractional charge model is worthy of mention. Using gas phase spectroscopic techniques, Kebarle[29] and co-workers are able to determine thermodynamic constants for gas phase "solvation" processes of the form:

$$M^+(H_2O)_{n-1} + H_2O \rightarrow M^+(H_2O)n$$

With this technique they have determined the ΔH for the process $Li^+ + 4H_2O \rightarrow Li^+(H_2O)_4$ to be 96.5 kcal/mol. Using fractional charges which reproduce the experimental dipole moment of 1.85 D,[30] our model yields an interaction energy of −98.9 kcal/mol. Though this result may be somewhat fortuitous, it is always encouraging when calculated results are in agreement with available experimental data.

A note of caution concerning the general applicability of the fractional charge model is appropriate at this point. The scale factors used in the calculations reported here were paramatrized to reproduce the interaction energy of the cation and

TABLE II: Total Complex and Point Charge Model Calculations for the Hydration of Li^+ [a]

System	Energy	Process	Energy change
$(H_2O)_4$	21.8		
$(h_2o)_4$	26.0		
$Li^+(H_2O)_4$	−141.8	$Li^+ + (H_2O)_4 \rightarrow Li^+(H_2O)_4$	−163.7
$Li^+(h_2o)_4$	−137.6	$Li^+ + (h_2o)_4 \rightarrow Li^+(h_2o)_4$	−163.7
$(H_2O)_4(h_2o)_8$	−11.1		
$(h_2o)_4(h_2o)_8$	−15.9		
$Li^+(H_2O)_4(h_2o)_8$	−234.1	$Li^+ + (H_2O)_4(h_2o)_8 \rightarrow Li^+(H_2O)_4(h_2o)_8$	−223.0
$Li^+(h_2o)_4(h_2o)_8$	−234.7	$Li^+ + (h_2o)_4(h_2o)_8 \rightarrow Li^+(h_2o)_4(h_2o)_8$	−219.3
$(H_2O)_4(h_2o)_8(h_2o)_{16}$	−78.0		
$(h_2o)_4(h_2o)_8(h_2o)_{16}$	−84.1		
$Li^+(H_2O)_4(h_2o)_8(h_2o)_{16}$	−310.0	$Li^+ + (H_2O)_4(h_2o)_8(h_2o)_{16} \rightarrow Li^+(H_2O)_4(h_2o)_8(h_2o)_{16}$	−232.0
$Li^+(h_2o)_4(h_2o)_8(h_2o)_{16}$	−316.7	$Li^+ + (h_2o)_4(h_2o)_8(h_2o)_{16} \rightarrow Li^+(h_2o)_4(h_2o)_8(h_2o)_{16}$	−232.6

[a] Energy in kcal/mol. The scale factors of h_2o point charges are 1.052 for the first solvation shell and 0.975 for the second and third shells. The zero point of energies is the sum of molecular energies. (H_2O: −75.907 648 6 hartree; Li^+: −7.233 209 1 hartree).

TABLE III: Orbital Energy of Li^+ 1s Shell

System	Orbital energy, hartree
Li^+	−2.791
$Li^+(H_2O)_4$	−2.487
$Li^+(h_2o)_4$	−2.530
$Li^+(H_2O)_4(h_2o)_8$	−2.393
$Li^+(h_2o)_4(h_2o)_8$	−2.442
$Li^+(H_2O)_4(h_2o)_8(h_2o)_{16}$	−2.379
$Li^+(h_2o)_4(h_2o)_8(h_2o)_{16}$	−2.431

a full solvation shell of four water molecules. Our experience indicates that this is not a suitable paramatrization for the interaction of the lithium ion and a single water molecule. The problem is that the fractional charge model does not retain the full many body nature of the interaction potential. Consequently the interaction between the ion and a single water molecule predicted by the fractional charge model, which has been paramatrized for interaction with a four molecule shell, will be too small. This inconsistency extends also to calculations involving a second shell. For example, the stabilization for the following two processes

$$Li^+ + (H_2O)(H_2O) \rightarrow Li^+(H_2O)(H_2O)$$

$$Li^+ + (H_2O)(h_2o) \rightarrow Li^+(H_2O)(h_2o)$$

are 56.0 and 53.1 kcal/mol, respectively. Nonetheless it is expected that the stabilization obtained by addition of an entire second shell should be well predicted by the fractional charge model.

IV. Hydration of F^-. A Test

In comparison with the localized charge of cations, such as Li^+, the electronic cloud of anionic solutes is quite diffuse. As a consequence, anionic solutes are generally more loosely solvated by polar solvents than cations.[27] One expects, therefore, that the hydration of the fluorine anion should provide a more stringent test for the applicability of the fractional charge model than did the lithium cation.

As we were more interested in testing our model than in generating an interaction potential surface we limited ourselves once again to the study of a single conformation of water molecules. The first shell was chosen to be a bond oriented tetrahedral complex of four water molecules, the exterior hydrogens oriented such that the entire complex was of S_4 symmetry (see Figure 2). This is the most stable symmetric complex involving just four water molecules as determined by Clementi employing an ab initio pair potential.[4] The second hydration sphere was generated by hydrogen bonding a water molecule, in its dimer conformation, to the oxygen atoms of the first solvation shell.

As in the hydration of Li^+, our first interest here was to determine the nature of the interaction between the fluoride ion and the solvent medium. The results of an energy decomposition analysis for the interaction with the first hydration sphere are given in Table IV. As a result of a fortuitous cancellation of terms, the energetics of solvation appear to be interpretable as an electrostatic effect. This is appealing in light of the strengths of our model. A strong word of caution must be interjected at this point, however. Due to the large absolute magnitude of the other terms it is not apparent that the fractional charge model will yield even a qualitatively correct interpretation of the effects of a solvent medium on the wave function or properties of the solute. This is a question to which we shall have to return later.

The nature of the calculations performed here are completely analogous to those for Li^+, the primary results of which are listed in Table V. It should be noted that the optimum scale factor for replication of the total interaction has a more pronounced deviation from unity than it did in the hydration of Li^+. The origin of this deviation cannot be precisely identified, though one factor is surely the effects of intermolecular charge rearrangement, an effect which may not be incorporated into the fractional charge model. Evidence for such a conjecture is that the "electrostatic" or outer-shell scale factor is quite near unity (1.068). The salient supporting evidence these data offer for the viability of the fractional charge model is once again the independence of the second shell calculation to the representation employed for inner-sphere molecules.

As in the study of Li^+, we used the eigenvalues of the "fluorine" orbitals as a probe for detection of changes in the solute wave function. Table VI lists the eigenvalues for the F^- "molecular" orbitals. It is clear that the changes induced by the solvent are qualitatively accounted for by the fractional charge model. The agreement here is not as impressive, however, as it was for Li^+, the fractional charge model yielding from 60 to 80% of the total change in the eigenvalues. The pronounced stabilization of the highest occupied MO's is predicted by the fractional charge calculation. It should be noted, however, that these orbitals did become strongly mixed

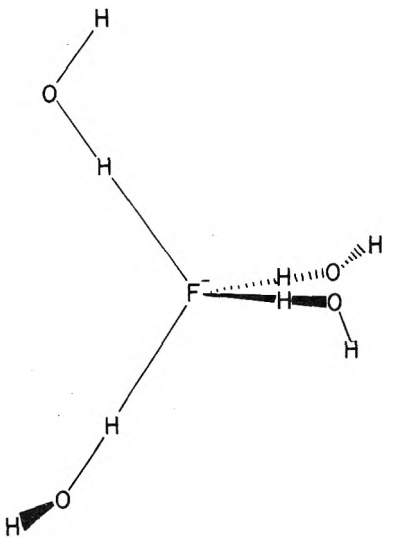

Figure 2. Assumed geometry of the first hydration shell of F^-. R_{F^-H} = 1.667 Å. Complex has S_4 symmetry.

TABLE IV: Energy Components (in kcal/mol) for the Process $F^- + (H_2O)_4 \rightarrow F^-(H_2O)_4$

Total	−120.0
Electrostatic	−111.7
Exchange	50.6
Polarization	−16.4
Charge transfer + coupling	−42.5

with the MO's of the first shell water cage. This effect was, of course, not perceivable in the fractional charge calculation. From this evidence one is forced to the conclusion that this model will yield only a qualitatively reliable wave function in those cases where there are strong charge-transfer or exchange contributions to the interaction between the solute system and the solvent molecules one wishes to simulate as fractional charges. If one is interested in more detailed characteristics of the wave function, it is suggested that first shell water molecules be explicitly included within the ab initio framework.

V. Hydration of NH_3HF

The hydration of the hydrogen adduct formed between an ammonia and a hydrofluoric acid molecule is a problem of considerable theoretical interest. The gas phase complex may be viewed as a covalent hydrogen bonded complex, NH_3–HF, a view supported by ab initio calculations.[31] The complex of NH_3 and HCl presents a contrasting analogue. The bonding there, even in the gas phase, has considerable ionic character NH_4^+–Cl^- as found in the early ab initio computation by Clementi.[32] The question to which we address ourselves here is the effect of hydration on the more covalent complex of H_3N–HF. In particular we wish to determine the degree of hydration necessary to induce a significant alteration in the intermolecular bond lengths.

There have been several treatments of this problem in recent years. In our earlier account[14] we presented some preliminary results using the fractional charge model. We reported cursory results concerning the potential surface obtained by allowing motion of the intermolecular hydrogen with a fixed NF distance. Two principal results were obtained from this study. First the addition of water molecules does stabilize the ionic form of the adduct. Secondly, it was apparent that addition of solvent molecules results in a contraction of the equilibrium N–F separation. This latter result infers the necessity of two-dimensional potential energy search allowing for changes in the N–F distance. Recently Kollman and Kuntz[5b] have studied this problem employing an empirical many body potential derived from extensive ab initio calculations. They generated surfaces for motion of the intermolecular hydrogen atom at a fixed N–F separation of 2.65 Å. They inferred that the addition of four or more water molecules results in the ionic proton transferred state (NH_4^+- - -F^-) being the preferred conformation of a double minimum potential. However, their results are not conclusive since they did not allow for the effects due to an alteration in the equilibrium N–F separation.

In accord with the discussion above we have performed a full two-dimensional search of the potential surface, varying both the N–F separation and the position of the intermolecular hydrogen atom. As an economizing simplification neither the intramolecular bond lengths nor the bond angles of the ammonia molecule were altered from their experimental values.[22] The first hydration shell was assumed to consist of six water molecules, three of which were bound to the fluoride ion, the remaining three being bound to the ammonia protons. The waters bound to the fluorine moiety were fixed in the same conformation as they were in the free anion with an F–H separation of 2.144 Å, while the solvent molecules complexed to the ammonia protons were in their equilibrium dimer conformation as it was determined by Diercksen et al.[33] The conformational details of the complex are shown in Figure 3. A second solvation shell was formed, once again, by hydrogen bonding water molecules to the first hydration sphere.

The fractional charges for these calculations were assigned in a manner analogous to that which was used for Li^+ and F^-. The first shell scale factors were chosen such that the total interaction energy between a single water molecule and the H_3N–HF complex in its gas phase equilibrium conformation was duplicated by the fractional charge model. The second shell factors were here assumed to be 1.0 based upon our experience with Li^+ and F^- that such a scale factor will very nearly replicate the electrostatic contribution to the total interaction. Energy decomposition results for the interaction of a water molecule with the fluorine and the ammonia end of the molecule are presented in Table VII. The fractional charges used in the calculation are also listed in the table. As a test of the viability of this means of assigning fractional charges, we performed a single calculation for (H_2O) $H_3NHF(H_2O)$ comparing the stabilization of the complex with that found for $(h_2o)H_3NHF(h_2o)$. The stabilization is −16.96 and −16.63 kcal/mol for the respective complexes. This result suggests that the effects of the two "types" of solvent molecules are nearly independent and hence our choice of fractional charges should be adequate for qualitative discussions. One final comment concerning the choice of the fractional charges seems to be in order. Our experience indicates that the choice of fractional charges based upon complexes of a single water molecule will probably slightly exaggerate the influence of the solvent, since cooperativity effects are not well duplicated by our model. If this effect is significant, then the calculations performed will be unduly favoring the NH_4^+- - -F^- structures.

The results of our potential energy surface scan for zero (gas phase), one, and two solvation shells are given in Table VIII. Lagrangian interpolation formulae were used to generate equienergy surfaces from these data points. These surfaces are depicted in Figures 4–6. In these figures the zero of energy

TABLE V: Total Complex and Point Charge Model Calculations for the Hydration of F^- [a]

System	Energy	Process	Energy change
$(H_2O)_4$	5.1		
$(h_2o)_4$	9.3		
$F^-(H_2O)_4$	−114.9	$F^- + (H_2O)_4 \rightarrow F^-(H_2O)_4$	−120.0
$F^-(h_2o)_4$	−110.8	$F^- + (h_2o)_4 \rightarrow F^-(h_2o)_4$	−120.1
$(H_2O)_4(h_2o)_4$	−24.5		
$(h_2o)_4(h_2o)_4$	−20.1		
$F^-(H_2O)_4(h_2o)_4$	−160.6	$F^- + (H_2O)_4(h_2o)_4 \rightarrow F^-(H_2O)_4(h_2o)_4$	−136.1
$F^-(h_2o)_4(h_2o)_4$	−154.2	$F^- + (h_2o)_4(h_2o)_4 \rightarrow F^-(h_2o)_4(h_2o)_4$	−133.7

[a] Energy in kcal/mol. The scale factors of the h_2o point charges are 1.154 for the first solvation shell and 1.068 for the second shell. The zero point of energy is the sum of the molecular energies (H_2O: = −75.907 648 6 hartree, F^-: −99.247 836 hartree).

TABLE VI: Orbital Energies (in hartree) for F^-

System	1s	2s	2p
F^-	−25.631	−0.956	−0.068
$F^-(H_2O)_4$	−25.938	−1.258	−0.317
$F^-(h_2o)_4$	−25.822	−1.147	−0.260
$F^-(H_2O)_4(h_2o)_4$	−25.963	−1.282	−0.350
$F^-(h_2o)_4(h_2o)_4$	−25.844	−1.169	−0.282

TABLE VII: Energy Components for the Process NH_3–HF + $H_2O \rightarrow NH_3HF(H_2O)$

	H_2O bound to F	H_2O bound to H of NH_3
Total	−8.73	−7.52
Electrostatic	−6.26	−7.14
Exchange	+1.41	+1.39
Polarization	−0.54	−0.51
Charge transfer + coupling	−3.35	−1.26
First shell scale factor	1.458	1.091
Second shell scale factor	1.000	1.000

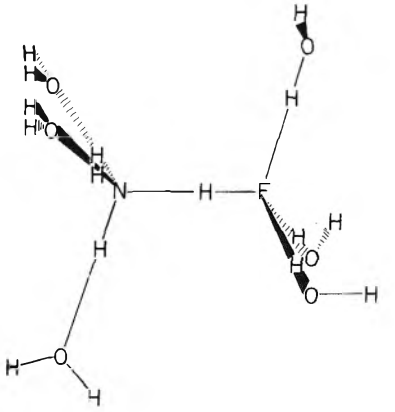

Figure 3. Assumed geometry of the NH_3–HF complex and its first hydration shell. R_{F^-H} = 2.144 Å, R_{N-O} = 3.36 Å.

is defined to be the minimum energy for the given solvation state. In the gas phase one has a steeply walled potential well whose minimum has an H–F distance of ~0.94 Å and an N–H distance of ~1.62 Å. The critical feature of this surface is that the H–F bond length is not far displaced from its equilibrium position in the isolated HF molecule (0.922 Å).[34] This evidence suggests that complexation of HF with NH_3 does little to disturb the nature of the H–F bond, a result which is in agreement with the conclusions reached by earlier workers.[31] As a reference for later discussion, note that the point r_{NH} = 1.1 Å, r_{HF} = 1.4 Å, a conformation representative of proton transferred type of structure ($NH_4^+ \cdots F^-$) has an energy which is approximately 27 kcal/mol above the minimum.

TABLE VIII: The Energy of H_3N–HF as Functions of H–F and N–H Distances and Number of Solvation Shells of Fractional Charges

		Energy, hartree		
R_{HF}	R_{NH}	0 shells	1 shell	2 shells
0.9	1.7	−156.0140		
0.9	1.6	−156.0122	−156.0767	−156.0900
1.0	1.6	−156.0149	−156.0838	−156.0983
1.0	1.5	−156.0134	−156.0846	−156.0993
1.0	1.4	−156.0097	−156.0832	−156.0982
1.0	1.3		−156.0785	−156.0937
1.1	1.5	−156.0053	−156.0814	
1.1	1.4	−156.0046	−156.0835	−156.0999
1.1	1.3	−156.0014	−156.0833	−156.1000
1.1	1.2		−156.0789	−156.0959
1.2	1.4	−155.9931	−156.0773	−156.0950
1.2	1.3	−155.9933	−156.0808	−156.0990
1.2	1.2	−155.9903	−156.0812	−156.0996
1.2	1.1		−156.0756	−156.0943
1.3	1.3	−155.9819	−156.0748	
1.3	1.2	−155.9827	−156.0789	−156.0988
1.3	1.1	−155.9783	−156.0779	−156.0980
1.4	1.2		−156.0743	−156.0982
1.4	1.1	−155.9722	−156.0767	−156.0912
1.4	1.0		−156.0695	
1.5	1.1		−156.0735	−156.0963
1.5	1.0		−156.0693	

The addition of the first hydration sphere has a significant effect on the general characteristics of the potential energy surface. The first notable feature is that the minimum of the potential surface has shifted to a longer H–F distance (~1.04 Å) and a shorter N–H distance (~1.46 Å). This shifting in the equilibrium position is certainly indicative of marked stabilization of the $NH_4^+ \cdots F^-$ form of the complex. In addition to a shift in the equilibrium position, one has a leveling of the potential surface. Our reference proton transferred structure now has an energy which is approximately 5 kcal/mol above the minimum. This is in sharp contrast to the 27 kcal/mol spread we found in the gas phase. It should be noted that with the addition of this first solvation shell we found no evidence for the existence of a double minimum.

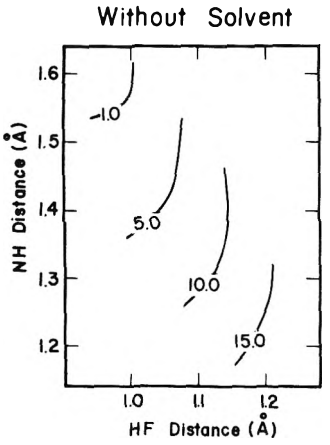

Figure 4. Energy of NH_3HF as function of HF and NH separations. Equienergy curves are given in kcal/mol above the minimum of surface.

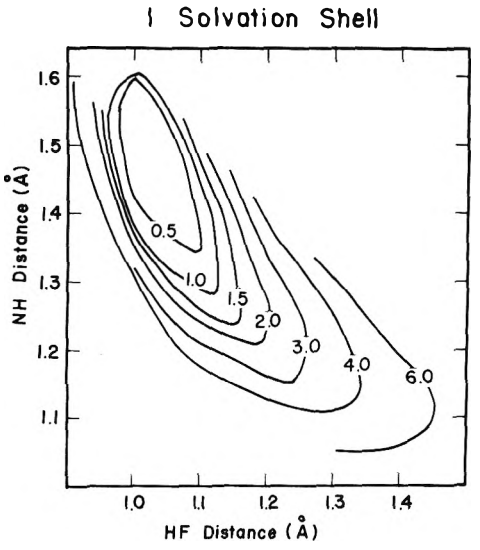

Figure 5. Energy of NH_3HF with one hydration shell as function of HF and NH separations. Equienergy curves are given in kcal/mol above the minimum.

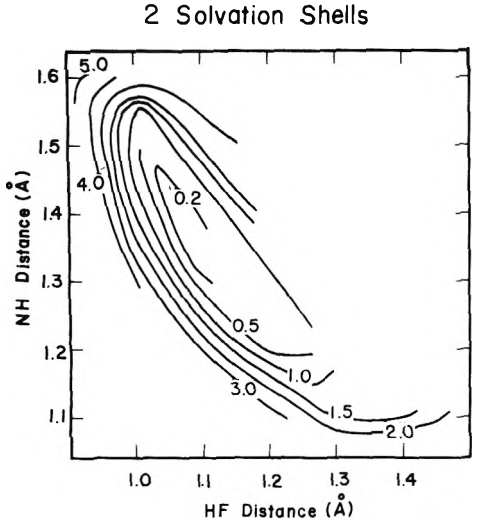

Figure 6. Energy of NH_3HF with two hydration shells, as function of HF and NH separations. Equienergy curves are given in kcal/mol above the minimum.

The naivite of intuition suggests that such a structure should exist for the hydrated complex so we added a second shell in hopes of finding it. The results as depicted in Figure 6 are somewhat ambiguous. A second minimum corresponding to a proton transfer state is not evident. On the other hand, the surface has been flattened to such an extent that it was difficult to interpolate between data points, rendering it impossible to characterize fine details concerning the surface. The reference configuration (r_{HF} = 1.43 Å, r_{NH} = 1.1 Å) of the complex is now only 1.09 kcal/mol above the minimum. In addition the minimum has, once again, shifted toward a more ionic, proton transferred, configuration (r_{HF} ~1.1 Å, r_{NH} ~1.35 Å).

Though we have not found even a local minimum which one would like to interpret as a proton transferred structure, we feel this work provides striking evidence for the stabilization of the proton transferred form of the complex upon hydration. We do admit of some inexactitude in our surfaces. It is certainly true that a change in basis set, an alteration in the conformation of the solvent molecules, or a modification in the mode of their incorporation will change the details of the surfaces, perhaps even yielding a double minimum for the solvated complex. However we feel the qualitative nature of the surfaces are correct, and not artifacts of our calculation.

One conclusion which we feel deserves special emphasis is the importance of allowing relaxation in the N–F bond length. It is clear that as one hydrates the complex the N–F distance is shortened. This is, of course, in agreement with one's intuitive feeling that hydration of the ion should stabilize the proton transferred state. This conclusion implies that judgments based on studies employing fixed N–F distances must be interpreted with care.[5b]

VI. Solution Phase Proton Affinities of Substituted Ammonia

The proton affinity of nitrogen bases in both gas and solution phases has been of considerable experimental interest.[35,36] As one expects there exist large differences between the gas phase and solution results. A particularly notable series in this regard is that obtained by successive methylation of ammonia. In the gas phase the proton affinity increases continuously as one goes from ammonia to trimethylamine, a result which is concordant with molecular orbital studies.[37,38] This ordering has recently been interpreted as being the result of an increase in the polarization stabilization upon successive methylation.[38]

In aqueous solution ΔH for the proton affinities are significantly altered resulting in the following somewhat anomolous series shown in order of decreasing proton affinity:

$$Me_3N > (Me_2)NH > NH_3 > MeNH_2$$

The intent of the calculations which we performed was in determining if a simple scheme employing the fractional charge model might qualitatively account for this observed behavior. The first assumption which we made was that the solute geometry does not relax in solution. This enabled us to use the same geometries employed in the earlier gas phase calculation.[38] In addition we assumed that the fractional charges for the water molecule were those dictated by the dipole moment, in accord with our experience that "optimum" fractional charges deviate only slightly from these. The only remaining variable was the assignment of the solvent number and conformation.

An intuitive first guess would say that the enhanced stability of the ammonium ion relative to the other cations in

TABLE IX: Calculated Proton Affinities (in kcal/mol) of Methylated Ammonia in Gas Phase and Solution Phase

	Gas phase	Solution phase[a]
NH_3	−221.9	−282.1
NH_2CH_3	−230.4	−273.6
$NH(CH_3)_2$	−236.1	−264.5
$N(CH_3)_3$	−239.7	−255.0

[a] Fractional charge model as described in text.

solution is due to the presence of a greater number of "binding sites" for the solvent molecules. Based on this premise we performed a series of calculations for the process:

$$R_{3-n}N[H(h_2o)]_n + H^+(h_2o) \rightarrow R_{3-n}N^+[Hh_2o]_{n+1}$$

The intermolecular hydrogen bond length was taken as 2.295 Å, the optimal distance for a dimer of ammonia and water.[33] The solution proton affinities obtained in this manner are displayed along with the gas phase results in Table IX. For convenience of comparison to experimental results we have also listed these data in the form of ΔH's for reactions of the type:

$$NH_4^+(h_2o)_4 + NH_n(CH_3)_{3-n}(h_2o)_n \rightarrow NH_3(h_2o)_3 + NH_{n+1}(CH_3)_{3-n}$$

These results, as well as the experimental data,[35] are listed in Table X. It is apparent that we have succeeded in enhancing the relative proton affinity of the less highly substituted amines. Unfortunately we completely reversed the ordering of the proton affinities, the less highly substituted amines being stabilized to far too great an extent.

There are two rather obvious oversimplifications which we have made which must be corrected if more quantitative results are desired. The first of these is the neglect of hydration at the nitrogen site of the free bases. One expects that this could act as a proton acceptor in a hydrogen bonding solute–solvent interaction. Secondly, we must account for alteration in the solvent–solute separation upon formation of multiple bonds, an effect which can be rather pronounced. For example Pullman et al., using the standard STO-3G basis, found that the intermolecular hydrogen bond changed from 2.3 Å for the ammonium ion bound to a single water molecule to 2.6 Å when it was complexed to four water molecules.[39] The implication is that we must alter the intermolecular hydrogen bond distances such that they are concordant with the number of solvent molecules present.

To obtain a feel for the importance of each of these problems we performed a few trial calculations. In an effort to test the significance of nitrogen hydration, we reevaluated the proton affinities of NH_3 and H_2NCH_3 including such a solvent coordination. The intermolecular N–H bond length was taken to be 2.194 Å.[31] The effect of including this hydration site is not highly significant. The proton affinity of ammonia was lowered by 5.8 kcal/mol to −276.3 kcal/mol. Unfortunately the proton affinity of methylamine was lowered by an almost identical amount (5.4 kcal/mol). It is apparent that one will obtain only small quantitative alterations in the proton affinities due to hydration at the nitrogen site.

As a test of the significance of the intermolecular separation we reevaluated the proton affinities of ammonia and methylamine, this time setting the intermolecular OH bond length to 2.60 Å. The proton affinity of ammonia was lowered by about 10 kcal/mol to −272.5 kcal/mol. The proton affinity of methylamine, on the other hand, was increased slightly (2 kcal/mol) to −276.6 kcal/mol. This is in quite satisfactory agreement with the experimental data in the sense that methylamine is now predicted to have a greater proton affinity than ammonia. Though we did not repeat calculations for dimethylamine or trimethylamine, it seems clear that their proton affinities will be changed little by lengthening the intermolecular O–H distance. Though it is tempting to say that we have now reproduced the qualitative trends which are observed experimentally, a word of caution must be voiced. The free bases are actually less stable with the intermolecular hydrogen bond length of 2.60 Å than they are with a bond length of 2.295 Å.

We do not claim at this point to have completely determined the nature of the solvent effect on these proton affinities. Nonetheless, we feel confident that the calculations we have performed do provide evidence for the suitability of a molecular orbital investigation of this type of problem. It is apparent that more complete geometry optimizations are required to obtain reliable results. At the present time this is beyond the scope of our method (due to a lack of close range repulsion) and our computing facilities.

VII. NH_3–BH_3 in the Crystal and on the Crystal Surface

Thus far all of the problems we have considered have been in the solution phase. As such, they have all been subject to the same dilemma, that is how does one go about adopting a conformation for the solvent system. Here we test the applicability of the fractional charge model to a molecular crystal where this ambiguity of structure is not a problem. The particular molecular complex which we examined is the electron donor–acceptor complex of ammonia and borane. The crystal structure of this 1:1 complex, independently determined by two research groups,[40,41] has a tetragonal body centered unit cell with the geometric parameters a = 5.234 Å, c = 5.027 Å.

The gas phase complex was recently subjected to an energy decomposition analysis[42] with the finding that the electrostatic interaction is the largest component to the total stabilization. Our intent here was to determine whether the nature of the interaction in either a crystal or on the crystal surface varies significantly from that in the gas phase. As a model for the crystal we considered a single molecular complex in the center of a unit cell as the "solute", and its ten nearest neighbors (roughly analogous to a first solvation shell) as the "solvent" system. The heavy atoms of this model crystal are depicted in Figure 7. The geometry of the monomer complex with respect to intramolecular parameters was identical with that used in the earlier gas phase study.[42] The ammonia is assumed to complex with its experimental geometry[22] (N–H = 1.0124 Å, ∠HNH = 106.67°), while the borane is assumed to be pyramidal (B–H = 1.19 Å, ∠HBH = 112.45°).[42] For the surface calculations we considered three possible rotomers obtained by passing a plane through the unit cell such that it was both parallel to the c axis, and perpendicular to one of the a axes. These are shown schematically as Newman projections in Figure 8. The fractional charges for the "solvent" complexes were taken to be the excess atomic charge as determined from a Mulliken population analysis (q_N = 0.9451, q_H = +0.3875, q_B = +0.2520, $q_{H'}$ = −0.1565). It is possible to use the Mulliken populations of the solute atoms to determine the fractional charges for the surrounding molecules. One may iterate in such a fashion until the "solute" Mulliken populations are

TABLE X: Energetics of Proton Transfer—Stabilization in Solution

	Expt[a]		Calcd
	ΔH	ΔG	ΔH
$NH_4^+ + NH_3 \rightarrow NH_3 + NH_4^+$	0	0	0
$NH_4^+ + N(CH_3)H_2 \rightarrow NH_3 + N(CH_3)H_3^+$	+0.69	+1.87	+8.5
$NH_4^+ + N(CH_3)_2H \rightarrow NH_3 + N(CH_3)_2H_2^+$	−0.52	+2.11	+17.6
$NH_4^+ + N(CH_3)_3 \rightarrow NH_3 + N(CH_3)_3H^+$	−3.57	+0.77	+27.1

[a] Reference 35.

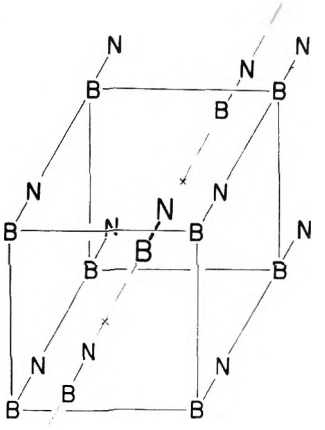

Figure 7. Geometry of the "solute" (dark letters) and its 10 nearest neighbors in a crystal of BH_3NH_3. Only heavy atoms are denoted in figure.

concordant with the "solvent" fractional charges In this case, such a process did not have a significant effect. The monomers for the energy decomposition analysis were an ammonia and a borane molecule, each separately under the influence of the crystal field. The results of the analysis are presented in Table XI and the last column of Table XII.[44] For purposes of comparison, the corresponding gas phase results are also shown. Since we were particularly interested in charge transfer effects in this complex, the decomposition scheme of Kitaura and Morokuma[24] which separates the pure charge transfer component from the mixing terms was employed. As is evident from the table, the interaction of an individual ammonia molecule with its conjugate borane molecule is not far different in the crystal state than it is in the gas phase. It was suspected that such a highly polar species (the calculated dipole moment of a complex in the crystal is 6.28 D) might induce a significant degree of charge transfer from the donor (ammonia) to the acceptor (borane). In support of the energy decomposition data, based on Mulliken populations, we find a transfer of 0.243 electrons from ammonia to borane in the crystal, as compared with 0.217 electrons in the gas phase. Apparently the large intercomplex distances are sufficient to prevent large polarizations of the monomeric wave functions. In this regard it is interesting to note that the H_3NBH_3 complex is about 12 kcal/mol lower in energy in the crystal than it is in the gas phase. Of this, two thirds results from stabilization of the monomers, and does not reflect an increase in the interaction between the ammonia and the borane. The evidence presented here would seem to imply that the principal source of interaction between the field and an individual complex is electrostatic in nature.

TABLE XI: Energy Components (in kcal/mol) for NH_3BH_3

System	Gas phase	Crystal
Total	−42.0	−46.2
Electrostatic	−129.2	−131.1
Exchange	+140.2	+139.9
Polarization	−33.3	−32.8
Charge transfer	−45.6	−46.2
Coupling	+25.8	+23.9

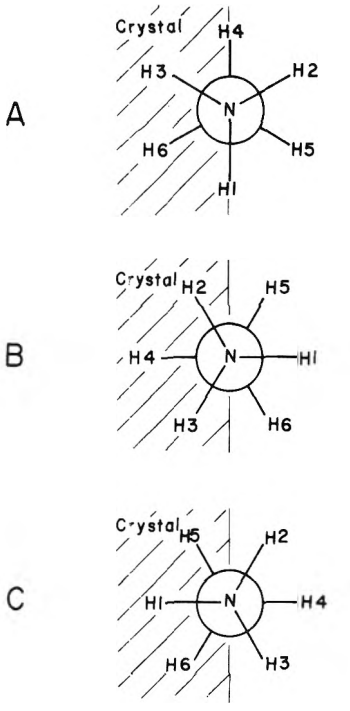

Figure 8. Newman projections representing the three surface conformers which were considered. In all cases the plane of the surface includes the principal axis of the solute, and is perpendicular to one of the remaining crystalographic axis.

The surface calculations were a further attempt to characterize the strength and nature of the crystal field. It was of particular interest to determine the asymmetry introduced into the wave function, as measured by Mulliken populations and the induced dipole. These data, along with the stabilization of the complex with respect to its gas phase energy, are listed in Table XII. The most notable result is that although we stripped away nearly half of the crystal field, the stabilization of the complex with respect to its gas phase energy is not appreciably altered. This implies that stabilization of the complex due to the field is principally the result of those neighbors whose dipole is directionally coincident with its

TABLE XII: NH_3BH_3 on the Surface of Crystal

Model	*A*	*B*	*C*	Full crystal
Energy, hartree	−82.511 56	−82.511 49	−82.511 50	−82.511 54
Stabilization, kcal/mol[a]	−12.60	−12.56	−12.57	−12.59
Induced dipole,[b] D	−0.145	−0.099	+0.355	
Mulliken population				
N	7.954 8	7.959 2	7.950 7	7.961 6
H_1	0.606 6	0.614 4	0.598 9	0.609 7
H_2	0.609 6	0.591 2	0.603 6	0.591 8
H_3	0.585 6	0.591 2	0.603 6	0.591 8
B	4.720 0	4.755 7	4.684 8	4.691 0
H_4	1.155 5	1.166 2	1.145 0	1.147 4
H_5	1.149 8	1.161 1	1.206 6	1.203 4
H_6	1.218 2	1.161 1	1.206 6	1.203 4

[a] Energy of surface molecule minus energy of gas phase molecule. [b] Dipole is positive if hydrogens directed away from crystal are more positive than those directed to the interior.

own. There is a slight asymmetry introduced in the surface molecule. In each of the three models, the bonds which point away from the crystal are less polar than analogous bonds pointing toward the interior of the crystal. This is not a large effect, however, the induced dipoles are all less than 0.4 D.

A final test was performed to determine whether the stabilization of a complex is primarily the result of those neighbors sharing the same principal axis. A calculation, not including these two molecules, was carried out. In support of our conjecture the complex was found to be stabilized by only 2.6 kcal/mol with respect to the gas phase energy. The charge transfer from the ammonia to the borane was 0.221 electrons, a value which is nearly identical with the gas phase result.

We feel that the following conclusions may be drawn from this study. First, the crystal field does not have a significant effect on the nature of the interaction between the monomers of an individual complexed pair. Energy decomposition analyses have shown that all components of this interaction are nearly identical in the crystal and gas phases. The complex, as a whole, is stabilized somewhat by the crystal, the principal contribution resulting from molecules lying along its C_{3v} axis. There is only a weak asymmetry induced in complexes situated at the surface, the asymmetry resulting in an increase in the polarity of those bonds which point toward the interior of the crystal.

VIII. Conclusions

We feel the calculations presented here give firm evidence for the applicability and utility of the fractional charge model in discussing a variety of solvation problems. If one can formulate a reasonable model for the conformation of the solute molecules, then it is possible to perform calculations at very nearly the same cost as if one considered an isolated solute molecule. In addition the calculations are quantum chemical in nature in that one obtains a wave function for the solute system. This allows one to evaluate changes in molecular properties of the solute which are induced by the solvent. The method is also flexible in that one need not represent all of the solvent molecules by fractional charges. This is useful in cases in which large charge transfer or polarization interactions are expected.

The principal shortcoming of the method in its present form is that it lacks the proper short-range repulsive behavior. This is due to the fact that orbitals are not explicitly associated with the fractionally charged solvent molecules. Consequently the method does not include the short-range exchange repulsion. This deficiency prevents the meaningful optimization of solvent conformations. To correct this, some sort of an empirical repulsive potential must be added to the model.

Acknowledgment. The authors are grateful to Drs. P. A. Kollman, M. D. Newton, H. Umeyama, and A. Komornicki for helpful discussions. The research was in part supported by the Center for Naval Analyses at the University of Rochester and the National Science Foundation. One of us (J.O.N.) acknowledges the Sherman Clarke Graduate Fellowship at the Chemistry Department of the University of Rochester.

Appendix

As a test of the utility of the fractional charge model for the prediction of equilibrium geometries, several calculations have been performed. First we optimized the conformation of the water dimer, each water being represented by three fractional charges. The intermolecular O–O distance was fixed at 2.98 Å, and the monomer water molecules were kept at their experimental geometry. Regardless of whether the fractional charges were chosen to reproduce the experimental monomer dipole of 1.85 D ($q_O = -0.664$, $q_H = 0.332$) or the 4-31G dipole of 2.56 D ($q_O = -0.9314$, $q_H = 0.4657$) one obtains a dimer conformation which is in excellent agreement with both ab initio and experimental results. The structure is predicted to be a "linear" (the intermolecular HOH angle is less than 5°), antiperiplanar (trans) complex, with the bisector, T, of the HOH angle of the proton acceptor being in the same plane as the proton donor molecule. The bisector T is found to form an angle of approximately 20° with the axis defined by the two oxygen atoms. This was the only minimum on the surface, local minima corresponding to bifurcated and cyclic dimers not being present. The principal point of this calculation is that a linear structure is found to be the most stable form of the complex. If a dipolar approximation is employed for the water molecules, then a bifurcated structure will be the most stable form of the dimer.

The second test calculation which we performed was a restricted geometry optimization of the lithium cation and its first solvation shell. The lithium ion was represented by a unit positive charge while the fractional charges employed for the water molecules were those which replicate the calculated monomer dipole moment. All Li^+–O distances were fixed at 2.024 Å. With this restriction, the model predicts a tetrahedral (±5°), dipole oriented (±2°) complex, in excellent agreement with the results of an ab initio pair potential study.[4a] The model does not predict the orientation of the hydrogens to be such that the total complex is of C_{2v} symmetry as we assumed

it to be in the calculations reported in the text. The specific orientation of the hydrogens is not highly significant, however, since the potential energy surface is not acutely sensitive to the rotation of a water molecule about its symmetry axis.

These two calculations provide strong evidence for what we feel is a major advantage of the fractional charge representation of solvent molecules. Many of the orientational aspects of solute–solvent interactions are correctly maintained with this model, a virtue which is lost if one attempts to further simplify the representation of the solvent by approximating it as a dipolar field.

References and Notes

(1) H. Veillard, J. Demuynck, and A. Veillard, *Chem. Phys. Lett.*, **33**, 221 (1975).
(2) H. Histenmacher, H. Popkie, and E. Clementi, *J. Chem. Phys.*, **61**, 799 (1974).
(3) R. O. Watts, E. Clementi, and J. Fromm, *J. Chem. Phys.*, **61**, 2550 (1974).
(4) J. Fromm, E. Clementi, and R. O. Watts, *J. Chem. Phys.*, **62**, 1388 (1975).
(5) (a) P. Kollman and I. Kuntz, *J. Am. Chem. Soc.*, **96**, 4766 (1974); (b) *J. Am. Chem. Soc.*, **98**, 6820 (1976).
(6) R. Bonnacorsi, C. Petrongolo, E. Scrocco, and J. Tomasi, *Theor. Chim. Acta*, **20**, 331 (1971).
(7) A. Pullman, G. Giuliano, and J. Tomasi, *Theor. Chim. Acta*, **33**, 87 (1974).
(8) R. Bonnacorsi, E. Scrocco, J. Tomasi, and A. Pullman, *Theor. Chim. Acta*, **36**, 339 (1975).
(9) M. D. Newton, *J. Phys. Chem.*, **79**, 2795 (1975).
(10) M. D. Newton, *J. Chem. Phys.*, **58**, 5833 (1973).
(11) J. Hylton, R. E. Christofferson, and G. G. Hall, *Chem. Phys. Lett.*, **26**, 501 (1974).
(12) S. Ray, *Chem. Phys. Lett.*, **11**, 573 (1971).
(13) S. Yamabe, S. Kato, H. Fujimoto, and K. Fukui, *Theor. Chim. Acta*, **30**, 327 (1973).
(14) J. O. Noell and K. Morokuma, *Chem. Phys. Lett.*, **36**, 465 (1975).
(15) A. Ben-Naim, "Water and Aqueous Solutions, Introduction to a Molecular Theory", Plenum Press, New York, N.Y., 1974.
(16) F. Stillinger and A. Rahman, *J. Chem. Phys.*, **55**, 3336 (1971).
(17) K. G. Spears and K. S. Hyung, *J. Phys. Chem.*, **80**, 673 (1976).
(18) E. M. Gosling and K. Singer, *Chem. Phys. Lett.*, **39**, 361 (1976).
(19) R. Ditchfield, M. D. Newton, W. J. Hehre, and J. A. Pople, *J. Chem. Phys.*, **54**, 724 (1971).
(20) J. P. Dill and J. A. Pople, *J. Chem. Phys.*, **62**, 2921 (1975).
(21) W. J. Hehre, W. A. Lathan, R. Ditchfield, M. D. Newton, and J. A. Pople, GAUSSIAN 70, Program No. 236, Quantum Chemistry Program Exchange, Indiana University, Bloomington, Ind., 1973.
(22) G. Hezberg, "Electronic Spectra of Polyatomic Molecules", Van Nostrand, Princeton, N.J., 1966.
(23) (a) K. Morokuma, *J. Chem. Phys.*, **55**, 1236 (1971); (b) K. Morokuma, S. Iwata, and W. A. Lathan in "The World of Quantum Chemistry", R. Daudel and B. Pullman, Ed., Reidel, Dordrecht, 1974, p 277.
(24) K. Kitaura and K. Morokuma, *Int. J. Quantum Chem.*, **10**, 325 (1976).
(25) P. Kollman and I. Kuntz, *J. Am. Chem. Soc.*, **94**, 9236 (1972).
(26) (a) W. P. Kraemer and G. H. F. Diercksen, *Theor. Chim. Acta*, **23**, 387 (1971); (b) G. H. F. Diercksen, W. P. Kraemer, and B. O. Roos, *ibid.*, **36**, 249 (1975).
(27) E. S. Amis and J. F. Hinton, "Solvent Effects on Chemical Phenomena", Academic Press, New York, N.Y., 1973.
(28) T. R. Dyke and J. S. Muenter, *J. Chem. Phys.*, **60**, 2929 (1974).
(29) I. Dzidic and P. Kebarle, *J. Phys. Chem.*, **74**, 1466 (1970).
(30) T. R. Dyke and J. S. Muenter, *J. Chem. Phys.*, **59**, 3125 (1973).
(31) P. A. Koilman and L. C. Allen, *J. Am. Chem. Soc.*, **93**, 4991 (1971).
(32) E. Clementi, *J. Chem. Phys.*, **46**, 3851 (1967).
(33) G. H. F. Diercksen, W. P. Kraemer, and W. von Niesen, *Theor. Chim. Acta*, **28**, 67 (1972).
(34) H. Umeyama, K. Kitaura, and K. Morokuma, *Chem. Phys. Lett.*, **36**, 11 (1975).
(35) R. P. Bell, "The Proton in Chemistry", Cornell University Press, Ithaca, N.Y., 1973.
(36) E. Caldin and V. Gold, "Proton Transfer Reactions", Chapman and Hall, London, 1975.
(37) W. J. Hehre and J. A. Pople, *Tetrahedron Lett.*, **34**, 2959 (1970).
(38) H. Umeyama and K. Morokuma, *J. Am. Chem. Soc.*, **98**, 4400 (1976).
(39) A. Pullman and A. M. Armbruster, *Int. J. Quantum Chem.*, Symp. No. 8, 189 (1974).
(40) E. Lippert and W. Lipscomb, *J. Am. Chem. Soc.*, **78**, 503 (1956).
(41) S. Shore and R. Parry, *J. Am. Chem. Soc.*, **77**, 6084 (1955).
(42) H. Umeyama and K. Morokuma, *J. Am. Chem. Soc.*, **98**, 7208 (1976).
(43) E. Sutton, "Tables of Interatomic Distances and Configurations In Molecules and Ions", The Chemical Society, London, 1958.
(44) In order to be certain that a charge transferred minimum in the potential does not exist, we performed calculations starting from the ionic monomers, $(H_3N)^+$·$(BH_3)^-$, with the corresponding field based on the excess atomic charges as derived from a Mulliken population analysis ($q_N = -0.4199$, $q_H = +0.4733$, $q_B = -0.1440$, $q_{H'} = -0.2853$). An iterative procedure was then carried out until a self-consistency between the crystal field point charges and the excess atomic charges of the "solute" complex was achieved. This calculation converged to identically the same place as the analogous procedure starting from neutral covalent monomers, (H_3N)·(BH_3).

Molecular Orbital Calculations on the Optical Activity of Chiral Benzene Derivatives

Harry Dickerson and Frederick S. Richardson*

Department of Chemistry, University of Virginia, Charlottesville, Virginia 22901 *(Received June 4, 1976)*

Publication costs assisted by the Petroleum Research Fund

The chiroptical properties of a series of chiral benzene derivatives are examined on a theoretical model in which electronic rotatory strengths are calculated *directly* from molecular wave functions derived from semiempirical molecular orbital calculations. The CNDO/S SCF–MO model is used to calculate ground state wave functions and excited states are constructed in the virtual orbital–configuration interaction approximation. A series of (chirally) monosubstituted benzene derivatives are examined for the purpose of testing the generality and validity of "sector" rules proposed for the ^1L_b and ^1L_a transitions of the phenyl chromophore. The calculated results generally support the proposed sector rules, although some refinements and exceptions to these rules are suggested. A series of 1-substituted indan derivatives are also examined and it is found that the calculated results for these systems are in excellent agreement with available experimental data. The shortcomings and range of applicability of the methods employed in the study are briefly discussed.

I. Introduction

The electronic transitions associated with the phenyl chromophore of benzene derivatives exhibit optical activity when substituent groups on the benzene ring contain chiral centers or are dissymmetrically disposed about the benzene ring. The signs and relative magnitudes of the Cotton effects associated with these transitions are presumed to be determined by the conformational and configurational relationships which the substituent groups bear with respect to the benzene moiety. If this presumption is true then it should be possible to develop "sector" or "regional" rules which relate the signs and relative magnitudes of the Cotton effects associated with transitions of the phenyl chromophore to specific conformational features or spatial distributions of substituent groups or atoms. A number of such sector rules applicable to chiral benzene derivatives have been proposed and have been reported in the literature.[1] Although in most cases these rules have been based on purely empirical considerations, a few attempts have been made to provide a semiquantitative theoretical basis for their application to specific electronic transitions.[1]

Most optical activity studies (optical rotatory dispersion and circular dichroism) on chiral benzene derivatives have been conducted over the spectral region spanned by the $^1L_b(^1B_{2u})$ and $^1L_a(^1B_{1u})$ benzene transitions (270–210 nm). Recently, however, Allen and Schnepp have reported the circular dichroism (CD) spectra of 1-methylindan[2] down to 170 nm and of (*S*)-(+)-*sec*-butylbenzene[3] down to 180 nm. Additionally, Salvadori and co-workers have measured the CD of (*S*)-(+)-2-phenyl-3,3-dimethylbutane in the 300–185-nm spectral region. Allen and Schnepp[2] interpreted their results on 1-methylindan in terms of an independent systems model[5,6] which included both coupled-oscillator (dynamic coupling) contributions and one-electron (static coupling) contributions. Calculations based on the one-electron model of molecular optical activity had been carried out earlier for 1-methylindan by Caldwell and Kauzmann[7] and by Caldwell and Eyring.[8]

In the present study we examine the chiroptical properties of a series of chiral benzene derivatives by calculating electronic rotatory strengths directly from molecular wave functions derived from semiempirical molecular orbital calculations. Ground state wave functions for the chiral systems are calculated using the CNDO/S semiempirical molecular orbital model[9] and excited states are constructed in the virtual orbital–configuration interaction (CI) approximation. It has been well documented that the CNDO/S–CI molecular orbital model is reliable for calculating the transition energies and oscillator strengths associated with the intravalence-shell electronic transitions in benzene and simple benzene derivatives. This, of course, does not assure that the model is equally reliable or well-suited for calculating chiroptical properties. However, previous calculations of molecular chiroptical properties based on CNDO/2–CI,[10] INDO–CI,[11] and CNDO/S–CI[12] molecular orbital models demonstrate that *direct* calculations of electronic rotatory strengths from wave functions computed with these models provide useful alternative representations to the independent systems approaches. Chiral benzene derivatives are particularly difficult to treat by independent systems methods since the dimensions of the chromophoric group (the phenyl moiety) are generally larger than, or as large as, the distances between extrachromophoric perturber groups and the centroid of the chromophore. When the latter conditions exist, it may be preferable to use a *direct* calculational approach. The reliability and accuracy of independent systems calculations are limited by one's ability to model the electronic states of the interacting subsystems and to represent the interaction mechanisms operating between subsystems. On the other hand, the reliability and accuracy of *direct* calculational models are limited by the approximations one must use in calculating total molecular wave functions (especially those of excited states). It is not clear that either the direct calculational models or the independent systems perturbation models are inherently more reliable or accurate in general. Taken together they provide alternative representations whose results may be usefully compared.

The structures examined in this study were chosen from among benzene derivatives whose CD spectra have been determined experimentally and model systems which permit testing of variously proposed "sector" or "regional" rules.

II. Structures

A. *Ethylbenzene* (*I*). Two chiral ethylbenzene conformers were examined (I and I').

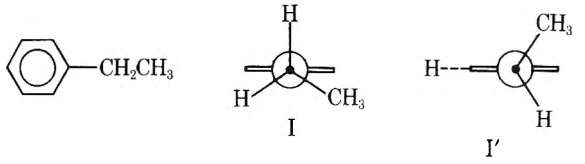

I I'

B. *n-Propylbenzene* (*II*). Nine chiral conformers of *n*-

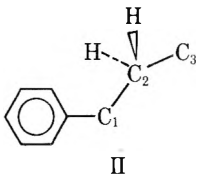

II

propylbenzene were studied. These conformers were generated by rotation about the C_1–C_2 bond (measured by angle θ).

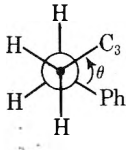

$\theta = 0°$ when the benzene ring and atoms C_1, C_2, and C_3 lie in a common plane. The *n*-propylbenzene conformers are designated by II(θ). In this study θ was varied between 15 and 150°.

C. *α-Phenylethyl Alcohol* (*III*). Twelve conformational

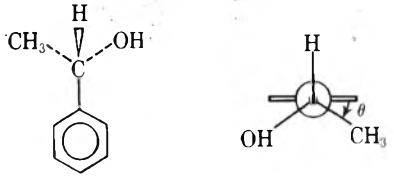

III

isomers of α-phenylethyl alcohol were examined. The absolute configuration at the asymmetric carbon atom in each of these isomers is *S* (in the Cahn–Ingold–Prelog notation). Six of the conformers were generated by rotation about the Ph–C_α bond (measured by the angle θ) with the O–H bond directed *toward* the phenyl group. The other six conformers were generated by rotation about the Ph–C_α bond with the O–H bond directed *away* from the phenyl group.The conformers in which the O–H bond is directed away from Ph are designated by III(θ) and the conformers in which the O–H bond is directed toward Ph are designated by III'(θ). Isomers in which θ = 0, 30, 60, 90, 120, and 150° were studied in this work.

D. *1-Phenyl-2-propanol* (*IV*). Twentyfour conformational

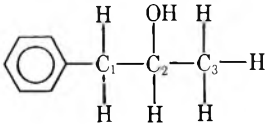

IV

isomers of IV were examined. The absolute configuration at the asymmetric carbon atom in each of these structures is *S* (in the Cahn–Ingold–Prelog notation). These conformational isomers are identified by a pair of dihedral angles (θ_1, θ_2) and by whether the O–H bond is directed toward or away from the phenyl group. If the O–H bond is directed away from the phenyl group we designate the isomer by IV(θ_1, θ_2). If the O–H bond is directed toward the phenyl group, then the isomer is designated by IV'(θ_1, θ_2). The angle θ_1 is defined in the following Newman projection (looking down the C_1–Ph bond axis):

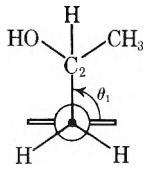

The angle θ_2 involves rotation about the C_1–C_2 bond and is defined in the following Newman projection (looking down the C_2–C_1 bond axis):

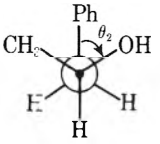

In the present study the following sets of (θ_1, θ_2) were chosen (expressed in degrees): (0, 60); (0, 180); (0, 300); (45, 60); (45, 180); (45, 300); (90, 0); (90, 60); (90, 120); (90, 180); (90, 240); (90, 300). In 12 structures, IV(θ_1, θ_2), the O–H bond was directed away from the phenyl group and in the remaining 12 structures, IV'(θ_1, θ_2), the O–H bond was directed toward the phenyl group.

E. *(S)-1-Methylindan* (*V*). Three conformational isomers

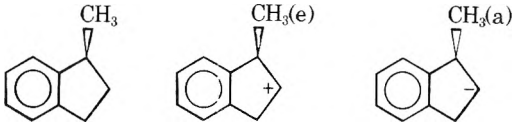

V V(e) V(a)

of (*S*)-1-methylindan were examined. In V the cyclopentene ring is planar. In V(e) and V(a) the cyclopentene ring is nonplanar with the C(2) atom displaced either above (as in V(e)) or below (as in V(a)) the plane of the phenyl group. In V(e) the methyl substituent is in an equatorial position, whereas in V(a) the methyl substituent is in an axial position.

F. *(S)-1-Aminoindan* (*VI*). Three C–NH_2 rotameric iso-

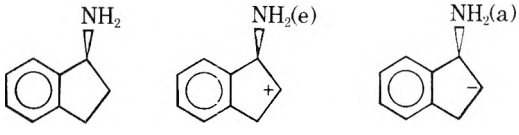

VI VI(e) VI(a)

mers of each of the VI, VI(e), and VI(a) structures were examined. These isomers were generated by making the amino group "lone-pair" orbital staggered with respect to the C(1)–Ph bond (α), the C(1)–C(2) bond (β), and the C(1)–H bond (γ).

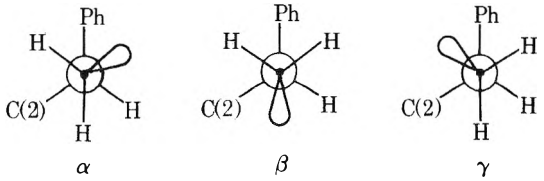

α β γ

G. *(S)-1-Hydroxyindan* (*VII*). Three C–OH rotameric

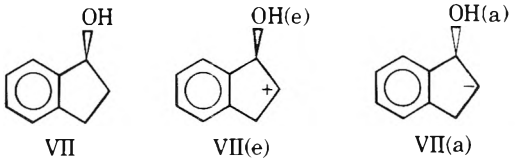

VII VII(e) VII(a)

isomers of each of the VII, VII(e), and VII(a) structures were examined. These rotameric isomers are depicted as follows:

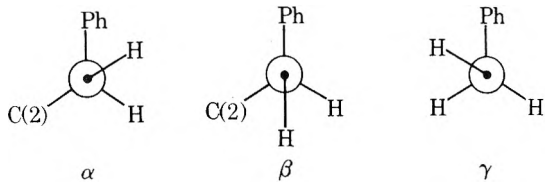

III. Methods of Calculation

Rotatory strengths, dipole strengths, oscillator strengths, and dissymmetry factors were calculated for the eight lowest energy singlet–singlet electronic transitions of each structure. These properties were calculated *directly* from total molecular electronic wave functions obtained by semiempirical molecular orbital methods. The semiempirical CNDO/S SCF–MO model was used to calculate ground state electronic structures.[9] Excited states were constructed in the virtual orbital–configuration interaction (CI) approximation with 35 singly excited configurations included in each CI calculation. Electronic dipole transition integrals were calculated in the dipole velocity formalism, and all one-, two-, and three-center terms were included in calculating both the electric dipole and the magnetic dipole transition moments.

Rotatory strengths are expressed in terms of "reduced rotatory strengths" where, for the electronic transition i → j

$$[R_{ij}] = \text{reduced rotatory strength}$$
$$= (100/\beta\mathcal{D})\ \mathrm{Im}\langle\psi_i|\hat{\mu}|\psi_j\rangle \cdot \langle\psi_j|\hat{m}|\psi_i\rangle \quad (1)$$

In eq 1, β is the Bohr magneton, $\mathcal{D}$ is the Debye unit, $\hat{\mu}$ is the electric dipole operator, and $\hat{m}$ is the magnetic dipole operator. Dipole strengths

$$D_{ij} = |\langle\psi_i|\hat{\mu}|\psi_j\rangle|^2 \quad (2)$$

are expressed in Debye^2 ($\mathcal{D}^2$) units, and dissymmetry factors are defined by

$$g_{ij} = 4R_{ij}/D_{ij} \quad (3)$$

where

$$R_{ij} = \mathrm{Im}\langle\psi_i|\hat{\mu}|\psi_j\rangle \cdot \langle\psi_j|\hat{m}|\psi_i\rangle \quad (4)$$

IV. Results and Discussion

A. *Acyclic Compounds.* 1. *^1L_b Transition.* The lowest energy singlet–singlet transition calculated for each of the structures examined in this study derives from the electric dipole forbidden, magnetic dipole forbidden $^1L_b(^1A_{1g} \rightarrow {}^1B_{2u})$ $\pi \rightarrow \pi^*$ transition of benzene. In the low-symmetry structures examined here this transition becomes weakly allowed in both electric dipole and magnetic dipole radiation with the calculated oscillator strengths falling in the range 0.0100–0.0080. The transition wavelengths calculated for this transition fall within the range 260–275 nm.

According to Snatzke, Kajtar, and Snatzke (ref 1, Figure 11) the appropriate sector rule for the ^1L_b transition of (chirally) monosubstituted benzene derivatives is given as shown in A. According to this rule the space about the phenyl

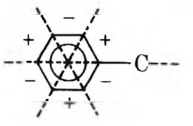

A (signs are for upper sectors)

Chart I

	[R]	|g|
I	−0.42	0.0031
I′	0.41	0.0023

Chart II

	[R]	|g|
II(45)	0.92	0.0009
II(90)	2.46	0.0028
II(135)	0.49	0.0022

Chart III

θ	0°	30°	60°	90°	120°	150°
$-CH_3$	⊗	−	−	⊗	+	+
−OH	+	+	⊗	−	−	⊗

chromophore is partitioned into 12 sectors whose boundaries are defined by three nodal planes which are perpendicular to the plane of the phenyl group and by a nodal plane which includes the entire phenyl group. Our calculations on the chiral ethylbenzene conformers (I and I′) are in agreement with the predictions of this simple sector rule. The computed rotatory strengths (reduced) and dissymmetry factors for the ^1L_b transition of I and I′ are given in Chart I.

Our calculations on the chiral *n*-propylbenzene derivatives, II(θ), are also in agreement with the sector rule depicted in A for the ^1L_b transition. For $0° < \theta < 180°$ the rotatory strength of this transition is predicted to be >0. Results calculated for representative II(θ) structures are given in Chart II. In II(90) the terminal methyl group is located near the center of a positive sector, whereas in II(45) and II(135) this group resides in the same positive sector but lies near a nodal plane.

Due to the presence of an asymmetric carbon atom in α-phenylethyl alcohol (III), all the conformational isomers of III are chiral. The locations of the $-CH_3$ and −OH groups in the sectors shown in A are given in Chart III (for selected values of the angle θ), where ⊗ denotes position on a nodal plane. The ^1L_b rotatory strengths and dissymmetry factors calculated for these structures are given in Chart IV. (These numbers correspond to values calculated for III′(θ) isomers in which the O–H bond is directed *toward* the phenyl group. The signs of the computed rotatory strengths do not change with rotation about the C–OH bond, although the magnitudes are slightly altered.) These results suggest that the sector rule shown in A can be applied to α-phenylethyl alcohol (III) if the location of the −OH group is given precedence over the location of the $-CH_3$ group. That is, the location of the −OH group determines the sign of the rotatory strength except when this group is positioned on a nodal plane, in which case the location of the $-CH_3$ group determines the sign (according to the sector rule).

An analysis of 1-phenyl-2-propanol (IV) conformational isomers is somewhat more difficult than those of the previous structures considered. When $\theta_1 = 0$ or 90°, chirality is generated entirely by the asymmetric substitution of C(2). However, when $\theta_1 = 45°$, an additional source of chirality is introduced. First we consider the sector locations of the $-CH_3$ and −OH groups for various values of θ_2 when θ_1 is fixed at either 0 or 90° (Chart V).

Chart IV

θ	0°	30°	60°	90°	120°	150°
$[R]$	0.07	0.03	−0.10	−0.14	−0.02	0.18
$\|g\|$	0.0010	0.0003	0.0006	0.0010	0.0005	0.0022

Chart V

	$\theta_1 = 0$			$\theta_1 = 90°$					
θ_2	60°	180°	300°	0°	60°	120°	180°	240°	300°
$-CH_3$	+	−	⊗	−	−	⊗	+	+	⊗
-OH	−	⊗	+	⊗	+	+	⊗	−	−

Chart VI

	$\theta_1 = 0$			$\theta_1 = 90°$					
θ_2	60°	180°	300°	0°	60°	120°	180°	240°	300°
$[R]$	−0.33	−0.54	0.98	0.78	0.44	−5.98	0.32	1.16	−4.16
$\|g\|$	0.0019	0.0022	0.0029	0.0018	0.0028	0.0034	0.0029	0.0019	0.0042

Chart VII

	IV′(45, 60)	IV′(45, 180)	IV′(45, 300)
$[R]$	1.92	0.24	3.59
$\|g\|$	0.0013	0.0008	0.0016

The ^1L_b rotatory strengths and dissymmetry factors calculated for these conformers of IV′(θ_1, θ_2), with the O–H bond directed *toward* the phenyl group, are given in Chart VI. For the $\theta_1 = 0$ structures (in which C(2) lies in the plane of the phenyl chromophore) we note again that sector rule behavior (according to diagram A) is obeyed so long as the position of the –OH group is given precedence over the position of the $-CH_3$ group. This also applies to the $\theta_1 = 90°$ structures when $\theta_2 = 60$, 180, or 300°. *Opposite* sign-sector correlations are obtained for the $\theta_1 = 90°$ structures when $\theta_2 = 0$, 120, or 240°. For $\theta_2 = 0$, 120, and 240° and $\theta_1 = 90°$, the C(1)–Ph bond eclipses one of the C(2)–substituent (–H, $-CH_3$, or –OH) bonds. In these cases, one of the C(2) substituents is always pointing directly back toward the π electron system of the phenyl group. For $\theta_2 = 60$, 180, and 300° and $\theta_1 = 90°$, one of the C(2)–substituent bonds is always trans to the C(1)–Ph bond. The reversal of sector rule behavior in going from $\theta_1 = 90$ ($\theta_2 = 60$, 180, and 300°) to $\theta_1 = 90°$ ($\theta_2 = 0$, 120, and 240°) suggests that the vertical nodal surfaces cannot be simply represented (as planes) near the periphery of the phenyl chromophore.

In the 1-phenyl-2-propanol (IV) structures in which $\theta_1 = 45°$ and $\theta_2 = 60$, 180, or 300°, the entire $-CH(CH_3)OH$ group lies in a positive sector of diagram A. The ^1L_b rotatory strengths calculated for these structures are all positive as shown in Chart VII.

2. *^1L_a Transition.* The second lowest energy singlet–singlet transition calculated for each of the structures examined in this study derives from the electric dipole forbidden, magnetic dipole forbidden $^1L_a(^1A_{1g} \rightarrow {}^1B_{1u}; \pi \rightarrow \pi^*)$ transition of benzene. As was the case for the ^1L_b transition this transition also acquires some (weak) electric dipole and magnetic dipole character in the low-symmetry compounds examined here. The calculated oscillator strengths for this transition fall within the range 0.040–0.0005, and the calculated transition wavelengths fall in the range 210–230 nm.

TABLE I: Rotatory Strengths and Dissymmetry Factors Calculated for the ^1L_a Transition of Selected Structures

Structure	$[R]$	$\|g\|$	Sector location[a]
I	0.07	0.0001	$-(CH_3)$
I′	−0.66	0.0004	$+(CH_3)$
II(45)	−10.16	0.0088	$-(CH_3)$
II(90)	−8.19	0.0068	$\otimes(CH_3)$
II(135)	3.57	0.0067	$+(CH_3)$
III′(0)	1.16	0.0015	$+$(OH); $\otimes(CH_3)$
III′(30)	2.23	0.0017	$+$(OH); $-(CH_3)$
III′(60)	−1.33	0.0007	$\otimes$(OH); $-(CH_3)$
III′(90)	−1.95	0.0011	$-$(OH); $\otimes(CH_3)$
III′(120)	−1.94	0.0017	$-$(OH); $+(CH_3)$
III′(150)	0.20	0.0002	$\otimes$(OH); $+(CH_3)$
IV′(90, 0)	−0.46	0.0011	$\otimes$(OH); $-(CH_3)$
IV′(90, 120)	1.34	0.0014	$+$(OH); $\otimes(CH_3)$
IV′(90, 240)	−0.22	0.0009	$-$(OH); $+(CH_3)$
IV′(90, 60)	0.96	0.0012	$+$(OH); $-(CH_3)$
IV′(90, 180)	0.48	0.0019	$\otimes$(OH); $+(CH_3)$
IV′(90, 300)	−1.96	0.0062	$-$(OH); $\otimes(CH_3)$

[a] ⊗ denotes position on nodal plane.

Snatzke, Kajtar, and Snatzke (ref 1, Figure 12) proposed a sector rule for the ^1L_a transition of (chirally) monosubstituted benzene derivatives which is of the form shown in B. The

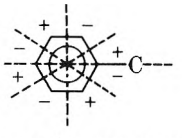

B (signs are for upper sectors)

space about the phenyl chromophore is again partitioned into 12 sectors whose boundaries are defined by three vertical nodal planes and a single horizontal nodal plane (defined by the plane of the phenyl group). In Table I the calculated results for a series of selected (representative) structures are displayed along with sector locations of substituent groups. Rotation about the C–OH bonds in structures III and IV did not alter the signs of the ^1L_a rotatory strengths, although this operation did change the magnitudes to a small extent.

TABLE II: Calculated Properties of Higher Energy Transitions (Singlet–Singlet) in Selected Acylic Chiral Benzene Derivatives

Structure	Transition	λ, nm	f^a	$[R]$	$\|g\|$	Excited state[b]
I	3	186.5	0.0212	2.57	0.0063	$\sigma\pi^*$
	4	185.9	0.0221	5.35	0.0116	$\sigma\pi^*$
	5	184.6	1.0280	−1.61	0.0001	$\pi\pi^*$
	6	183.0	0.8611	−4.69	0.0003	$\pi\pi^*$
	7	182.7	0.2487	0.09	0.0001	$\sigma\pi^*$
	8	181.4	0.0029	0.52	0.0041	$\sigma\pi^*$
I′	3	186.8	0.2627	2.88	0.0006	$\sigma\pi^*$
	4	186.3	0.0873	−4.69	0.0025	$\sigma\pi^*$
	5	183.9	0.8033	−10.67	0.0008	$\pi\pi^*$
	6	182.8	0.9673	4.37	0.0002	$\pi\pi^*$
	7	182.0	0.0500	3.48	0.0029	$\sigma\pi^*$
	8	179.9	0.0092	−0.70	0.0031	$\sigma\pi^*$
III′(0)	3	189.4	0.0378	−11.59	0.0152	$\sigma\pi^*$
	4	186.4	0.0496	2.00	0.0019	$\sigma\pi^*$
	5	184.9	0.3293	29.86	0.0051	$\sigma\pi^*$
	6	184.0	0.0930	−3.58	0.0017	$\sigma\pi^*$
	7	182.6	0.6958	−10.72	0.0009	$\pi\pi^*$
	8	181.6	1.0207	1.92	0.0001	$\pi\pi^*$
III′(30)	3	188.6	0.0822	−10.93	0.0068	$\sigma\pi^*$
	4	186.3	0.0906	1.78	0.0009	$\sigma\pi^*$
	5	184.6	0.8552	16.90	0.0011	$\pi\pi^*$
	6	183.6	0.5557	−5.58	0.0005	$\pi\pi^*$
	7	182.1	0.4458	9.10	0.0010	$\sigma\pi^*$
	8	181.3	0.1487	−7.81	0.0029	$\sigma\pi^*$
III′(60)	3	188.0	0.1545	3.53	0.0012	$\sigma\pi^*$
	4	186.1	0.1362	2.36	0.0008	$\sigma\pi^*$
	5	184.2	0.9114	1.71	0.0001	$\pi\pi^*$
	6	183.1	0.9483	−4.48	0.0002	$\pi\pi^*$
	7	181.8	0.0099	0.43	0.0011	$\sigma\pi^*$
	8	179.6	0.0032	−0.34	0.0037	$\sigma\pi^*$
III′(90)	3	188.5	0.2096	16.01	0.0040	$\sigma\pi^*$
	4	186.3	0.2336	0.55	0.0001	$\sigma\pi^*$
	5	184.1	0.7886	−10.73	0.0008	$\pi\pi^*$
	6	183.0	0.7733	5.96	0.0004	$\pi\pi^*$
	7	181.1	0.1199	−5.60	0.0021	$\sigma\pi^*$
	8	179.9	0.0536	3.54	0.0037	$\sigma\pi^*$
III′(120)	3	190.5	0.0433	7.92	0.0100	$\sigma\pi^*$
	4	187.6	0.0219	0.93	0.0019	$\sigma\pi^*$
	5	183.8	0.9174	−17.52	0.0011	$\pi\pi^*$
	6	182.9	0.6843	9.10	0.0006	$\pi\pi^*$
	7	181.8	0.4758	−8.75	0.0009	$\sigma\pi^*$
	8	180.5	0.0670	4.63	0.0039	$\sigma\pi^*$
III′(150)	3	190.4	0.0052	−5.28	0.0509	$\sigma\pi^*$
	4	187.2	0.0109	0.52	0.0019	$\sigma\pi^*$
	5	184.1	0.0663	9.06	0.0066	$\sigma\pi^*$
	6	183.2	0.8605	−9.55	0.0006	$\pi\pi^*$
	7	182.7	0.2297	2.59	0.0006	$\sigma\pi^*$
	8	181.7	1.0625	1.34	0.0001	$\pi\pi^*$

[a] Oscillator strength. [b] Principal singly excited configuration contributing to the excited state.

Correlations between the signs of the rotatory strengths calculated for the ^1L_a transition in structures III and IV and the signs predicted by the sector rule illustrated in B are excellent if we again assume that the position of the –OH group takes precedence over the position of the $-CH_3$ group. We note, however, that the sign correlations (between calculated values and values predicted according to the proposed sector rule) break down for structures I and I′ and are only partially existent for the II(θ) structures.

3. *Higher Energy Transitions.* The optical properties calculated for the third through eighth singlet–singlet transitions are listed in Table II for selected conformational isomers of ethylbenzene (I) and α-phenylethyl alcohol (III). In each case two of these transitions may be identified as $\pi \rightarrow \pi^*$ excitations of $^1A_{1g} \rightarrow {}^1E_{1u}$ benzene parentage, and the remaining transitions originate with $\sigma \rightarrow \pi^*$ excitations localized in the phenyl chromophore. The $\pi \rightarrow \pi^*$ transitions are characterized by high oscillator strengths and small dissymmetry factors. For each of the structures listed in Table II the two $\pi \rightarrow \pi^*$ transitions split out of the $^1A_{1g} \rightarrow {}^1E_{1u}$ benzene transition exhibit oppositely signed rotatory strengths. This result was also found for nearly all of the structures not shown in Table II.

The close spacing predicted to occur between the transitions falling in the 180–200-nm region suggests that the circular dichroism observed in this region for chiral benzene derivatives will be exceedingly difficult to interpret in terms of specific electronic excitations. Vibronic interactions of the

TABLE III: Optical Properties Calculated for (*S*)-1-Methylindan

Structure	Transition	λ, nm	f^a	[*R*]	|*g*|	Excited state
V	1	268.1	0.0118	0.22	0.0006	^1L_b
	2	215.0	0.0594	0.31	0.0004	^1L_a
	3	197.6	0.0196	−3.40	0.0009	$\sigma\pi^*$
	4	196.2	0.0164	4.10	0.0112	$\sigma\pi^*$
	5	188.1	1.0166	10.16	0.0007	$\pi\pi^*$
	6	187.2	0.9897	13.92	0.0016	$\pi\pi^*$
	7	181.3	0.0219	3.80	0.0068	$\sigma\pi^*$
	8	180.5	0.0098	−0.49	0.0059	$\sigma\pi^*$
V(e)	1	268.0	0.0112	−0.16	0.0004	^1L_b
	2	215.4	0.0567	−0.23	0.0002	^1L_a
	3	198.0	0.0158	−5.14	0.0236	$\sigma\pi^*$
	4	195.1	0.0120	1.68	0.0038	$\sigma\pi^*$
	5	188.4	0.9578	15.95	0.0049	$\pi\pi^*$
	6	187.3	1.1411	−2.32	0.0002	$\pi\pi^*$
	7	181.4	0.0316	3.14	0.0041	$\sigma\pi^*$
	8	180.2	0.0244	−4.16	0.0092	$\sigma\pi^*$
V(a)	1	268.3	0.0123	0.44	0.0010	^1L_b
	2	215.8	0.0605	0.58	0.0006	^1L_a
	3	196.7	0.0206	−4.49	0.0131	$\sigma\pi^*$
	4	194.5	0.0255	4.30	0.0111	$\sigma\pi^*$
	5	187.5	1.1232	9.40	0.0007	$\pi\pi^*$
	6	186.7	0.9941	16.69	0.0017	$\pi\pi^*$
	7	181.4	0.0418	3.14	0.0036	$\sigma\pi^*$
	8	180.5	0.0300	−7.94	0.0166	$\sigma\pi^*$

[a] Oscillator strength.

pseudo Jahn–Teller type are expected to occur between the excited states involved in these transitions and this will further complicate any detailed analysis of the chiroptical spectra. Detailed consideration of our calculated results for these higher energy transitions is not justified given the approximations of the theoretical model employed. Most serious in this latter regard are: (a) consideration only of "valence shell" orbitals in the CNDO/S–MO basis set; (b) inclusion only of singly excited configurations in the CI calculations; (c) inadequate treatment of σ–π interactions; and (d) neglect of vibronic interactions.

B. *Substituted Indan Derivatives.* 1. *(S)-1-Methylindan (V).* The optical properties calculated for the three isomeric forms of (*S*)-1-methylindan are given in Table III. The axial isomer, V(a), is calculated to be about 0.01 eV more stable than the equatorial isomer, V(e). If we assume an equilibrium mixture of the three isomeric species, V, V(a), and V(e), the signs of the ^1L_b and ^1L_a Cotton effects are predicted to be positive. This is in agreement with the experimental (circular dichroism) results of Allen and Schnepp.[2] Juxtaposed between the ^1L_b and ^1L_a transitions and the two $\pi \rightarrow \pi^*$ transitions of $^1A_{1g} \rightarrow {}^1E_{1u}$ benzene parentage, we calculate two transitions which originate with $\sigma \rightarrow \pi^*$ excitations localized on the phenyl chromophore. In each of the three isomers these transitions are calculated to occur in the 198–194-nm region. Allen and Schnepp[2] also found CD features in this spectral region which were of alternating signs, in apparent agreement with the calculated results given in Table III.

The fifth and sixth transitions calculated for the (*S*)-1-methylindan isomers are assigned to $\pi \rightarrow \pi^*$ excitations of $^1A_{1g} \rightarrow {}^1E_{1u}$ benzene parentage. The oscillator strengths calculated for these transitions are high and the transition wavelengths fall in the 189–186-nm region. The *net* rotatory strength associated with these transitions is calculated to be >0 for each of the three isomers. Only in isomer V(e) do the calculated rotatory strengths of the two individual transitions have opposite signs. Allen and Schnepp[2] observed positive CD throughout the 190–180-nm region and assigned this part of the spectra to components of the $^1A_{1g} \rightarrow {}^1E_{1u}$ transition. Below 180 nm, Allen and Schnepp observed the onset of a negative CD band system which they presumed to arise from electric dipole forbidden and magnetic dipole allowed transitions of the $\sigma \rightarrow \pi^*$ or $\pi \rightarrow \sigma^*$ type. These latter experimental observations are again in excellent agreement with the calculated results shown in Table III.

The rotatory strengths (experimentally determined) reported by Allen and Schnepp[2] for the ^1L_b, ^1L_a, and $^1E_{1u}$ transitions of (*S*)-1-methylindan are listed as follows (expressed in units of Bohr magneton-Debye): (a) ^1L_b, 1.6×10^{-41}; (b) ^1L_a, 9.5×10^{-41}; and, (c) $^1E_{1u}$ (total), 5.7×10^{-40}. These values are quite close to the theoretically calculated values given in Table III.

2. *(S)-1-Aminoindan (VI).* The optical properties calculated for the ^1L_b and ^1L_a transitions in nine isomeric forms of (*S*)-1-aminoindan (VI) are listed in Table IV. According to our CNDO/S calculations the relative stabilities of the nine isomers are given by: VI(a)β > VI(a)γ > VIβ > VI(e)β > VI(e)α > VIγ > VI(a)α > VIα > VI(e)γ. The energy difference between the most stable, VI(a)β, and the least stable, VI(e)γ, is ~0.25 eV. Our calculations predict, then, that the ^1L_b transition of (*S*)-1-aminoindan should exhibit a relatively weak negative Cotton effect, whereas the ^1L_a transition should exhibit a somewhat stronger positive Cotton effect. These results are in agreement with experimental ORD data reported by Brewster and Buta.[13]

3. *(S)-1-Hydroxyindan (VII).* The optical properties calculated for the ^1L_b and ^1L_a transitions in the nine isomeric forms of VII are qualitatively similar to those calculated for the (*S*)-1-aminoindan structures. That is, a weak negative Cotton effect is predicted for the ^1L_b transition and a somewhat stronger positive Cotton effect is predicted for the ^1L_a transition. These results also appear to be in agreement with the ORD data reported by Brewster and Buta.[13]

C. *Sector Rules for the Phenyl Chromophore.* Up to this

TABLE IV: Optical Properties Calculated for the ^1L_b and ^1L_a Transitions in (*S*)-1-Aminoindan

Structure	Transition	λ, nm	f^a	$\lvert R\rvert$	$\lvert g\rvert$
VIα	^1L_b	266.0	0.0019	−0.21	0.0007
	^1L_a	214.2	0.0066	0.97	0.0013
VIβ	^1L_b	267.6	0.0022	−0.17	0.0005
	^1L_a	213.8	0.0120	2.92	0.0018
VIγ	^1L_b	266.4	0.0017	−0.06	0.0002
	^1L_a	213.6	0.0060	1.36	0.0019
VI(e)α	^1L_b	266.8	0.0025	−0.18	0.0005
	^1L_a	213.9	0.0063	1.39	0.0018
VI(e)β	^1L_b	267.4	0.0019	0.05	0.002
	^1L_a	214.9	0.0125	1.96	0.0013
VI(e)γ	^1L_b	266.5	0.0017	−0.08	0.0003
	^1L_a	213.6	0.0070	1.18	0.0014
VI(a)α	^1L_b	266.1	0.0017	−0.19	0.0007
	^1L_a	213.2	0.0068	0.96	0.0012
VI(a)β	^1L_b	267.2	0.0020	−0.15	0.0005
	^1L_a	214.7	0.0117	3.56	0.0025
VI(a)γ	^1L_b	266.3	0.0017	−0.03	0.0001
	^1L_a	213.3	0.0057	1.30	0.0019

[a] Oscillator strength.

point in the discussion we have considered only the sector rules proposed by Snatzke et al.[1] for the ^1L_b and ^1L_a transitions of chiral benzene derivatives. These rules were based in large part on an adaptation of Platt's treatment[14] of the dipole strength of aromatic compounds and on the use of Platt's "spectroscopic moments" to account for substituent perturbations on the transitions of the aromatic chromophore. An alternative set of sector rules is suggested by a simple "one-electron" treatment carried to first order in perturbation theory.[15] In the "one-electron" model of molecular optical activity, the molecule is partitioned into a (symmetric-achiral) chromophoric group and a set of extrachromophoric groups. Optical activity is generated in the chromophoric transitions via chiral interactions between the chromophoric and extrachromophoric groups. Schellman[15] has shown that the interaction potential responsible for the induced optical activity must have the symmetry properties of a pseudoscalar in the symmetry group of the unperturbed chromophore. Sector rules based on the simple, first-order "one-electron" model are determined by the nodal properties of the pseudoscalar interaction potential in the space about the chromophoric center of the molecule.

For chiral benzene derivatives, the "one-electron" model predicts a sector rule with 24 sectors[15] if the unperturbed phenyl chromophore is assumed to possess "effective" D_{6h} symmetry. However, if the chromophoric unit is extended to include the first atom of the substituent group (in a monosubstituted derivative), then the chromophore has C_{2v} symmetry and a quadrant (four-sector) rule is predicted. In the latter case, more complicated sector rules (such as octant, hexadecant, etc.) are not precluded, but a quadrant rule is the *simplest* rule allowable. In the "one-electron" model the symmetry properties of the chromophoric–extrachromophoric interaction potential required to induce optical activity are entirely determined by the "effective" symmetry of the unperturbed chromophore. However, the detailed features of the resulting sector rules (such as sign patterns and number of sectors) are determined in large part by the detailed nature of the chromophoric electronic states and the extrachromophoric perturbing groups.

Both the monosubstituted benzene derivatives and the indan derivatives examined in the present study can be looked upon as possessing chromophoric units with "effective" C_{2v} symmetry. In the monosubstituted benzene derivatives the C_2 rotation axis and one of the σ_v planes of the C_{2v} phenyl chromophore pass through two atoms of the ring, whereas in the indan derivatives the C_2 rotation axis and one of the σ_v planes of the C_{2v} *m*-xylene chromophore pass through (and bisect) two of the C–C bonds in the benzene ring. According to the "one-electron" model, the simplest sector rule applicable to these structures is a quadrant rule. Depending upon where we locate the center of the chromophoric group (which, in turn, determines the locations of the nodal surfaces prescribed by the sector rule), most of our calculated results for the ^1L_b and ^1L_a transitions can be correlated and interpreted in terms of a simple quadrant rule. As was true for Snatzke's 12-sector rules, such correlations again require that the sector locations of the –OH groups take precedence over the sector locations of the $-CH_3$ groups (in compounds possessing both –OH and $-CH_3$ substituents) and, furthermore, there are a number of structures in which antiquadrant rule behavior is indicated.

As was pointed out in the Introduction, the optical activity of chiral benzene derivatives is particularly difficult to treat by any independent systems model, including the "one-electron" model. This is so because the dimensions of the chromophoric group are generally large compared to the distances between extrachromophoric perturber groups and the centroid of the chromophore. In this case, expansion of the chromophore group–extrachromophoric group interaction potential about a single point within the chromophore is no longer valid and the pseudoscalar function appearing in Schellman's treatment[15] is no longer well-defined or easily translated into a sector rule representation.

Direct calculations of molecular optical activity such as those reported in the present study cannot be readily analyzed in terms of, or reduced to, sector rule representations *except* by *tour-de-force* procedures. The results obtained in this study only permit comment regarding their consistency (or lack of consistency) with proposed sector rules. Although our calculated results appear in large part to be compatible with the 12-sector rules proposed by Snatzke et al.[1] for the ^1L_b and ^1L_a transitions, there are enough exceptions to support the conclusion that these sector rules lack general applicability and should be used with considerable caution and circumspection. It is possible that a quadrant rule would be adequate for most optically active benzene derivatives, but again this representation would appear to lack general applicability. The influence of chiral substituent groups upon the nodal properties of the phenyl excited states cannot be adequately represented by the simple "one-electron" perturbation model.

D. *Calculated Parameters and Procedures.* No attempt was made to evaluate the sensitivity of the calculated results to the parameterization of the semiempirical molecular orbital model (CNDO/S) which was used. However, several sets of calculations were carried out on the indan derivatives and on the ethylbenzene structures in which the number of configurations (singly excited only) was varied from 10 to 35 in the CI calculations. In each case, no qualitative changes and only small quantitative changes appeared in the calculated chiroptical properties after a CI basis of 25 was included. At least 20 configurations were required to give qualitative stability to the calculated results for the indan derivatives. All results reported here were obtained from calculations in which a CI basis set of 35 was used.

V. Summary

Comparison of the results calculated in this study for the 1-substituted indan derivatives (V, VI, and VII) with those obtained by experiment[2,13] suggests that the CNDO/S–CI molecular orbital model provides a useful and reliable method for examining the chiroptical properties of chiral benzene derivatives. The approximations inherent to this model (especially with respect to representing excited states and σ–π interactions) require that the results be considered with some circumspection. However, *direct* calculations of rotatory strengths based on such a model provide a useful, and possibly preferred, alternative to the usual calculations based on an independent systems/perturbation model. In the study reported here, only rotatory strengths associated with "pure" electronic transitions (between Born–Oppenheimer electronic states) were considered. A detailed analysis of the chiroptical spectra of optically active benzene derivatives most certainly will require further consideration of the influence of vibronic interactions arising from both Herzberg–Teller type mechanisms and pseudo Jahn–Teller type mechanisms.[16-20] It is likely that the principal effects of such vibronic coupling mechanisms will involve rotatory strength distributions (and CD intensity distributions) among vibronic levels, but will not alter the signs of the *net* rotatory strengths associated with individual electronic transitions.[18,19] If this assumption is correct then spectra–structure relationships based on consideration of electronic rotatory strengths alone will remain valid.

Assuming the validity of spectra–structure relationships based on the signs of rotatory strengths for "pure" electronic transitions, the results of this study lend support to the "sector" or "regional" rules previously proposed[1] for the ^1L_b and ^1L_a transitions (see diagrams A and B) of (chirally) monosubstituted benzene derivatives. In applying these rules to compounds in which the substituent includes both $-CH_3$ and –OH groups, we have found that the sector location of the –OH group must take precedence over the sector location of the $-CH_3$ group in predicting the sign of the ^1L_b or ^1L_a Cotton effect. Additionally, our results suggest that the nodal surfaces associated with the ^1L_a sector rule may be more complicated than suggested by diagram B.

Acknowledgments. This work was supported by the National Science Foundation, the donors of the Petroleum Research Fund, administered by the American Chemical Society, and the Camille and Henry Dreyfus Foundation (through a Teacher–Scholar Award to F.R.). The study was conducted as part of an undergraduate senior research project by H. Dickerson.

References and Notes

(1) G. Snatzke, M. Kajtar, and F. Snatzke in "Fundamental Aspects and Recent Developments in Optical Rotatory Dispersion and Circular Dichroism", F. Ciardelli and P. Salvadori, Ed., Heyden and Son, London, 1973, Chapter 3.4 and references therein.
(2) S. D. Allen and O. Schnepp, *J. Chem. Phys.*, **59**, 4547 (1973).
(3) S. D. Allen and O. Schnepp, *Chem. Phys. Lett.*, **29**, 210 (1974).
(4) P. Salvadori, L. Lardicci, R. Menicagli, and C. Bertucci, *J. Am. Chem. Soc.*, **94**, 8598 (1972).
(5) I. Tinoco, *Adv. Chem. Phys.*, **4**, 113 (1962).
(6) E. G. Höhn and O. E. Weigang, Jr., *J. Chem. Phys.*, **48**, 1127 (1968).
(7) D. J. Caldwell and W. J. Kauzmann, unpublished results.
(8) D. J. Caldwell and H. Eyring, *Annu. Rev. Phys. Chem.*, **15**, 281 (1964).
(9) (a) J. Del Bene and H. H. Jaffe, *J. Chem. Phys.*, **48**, 1807 (1968); (b) R. L. Ellis, G. Kuehnlenz, and H. H. Jaffe, *Theor. Chim. Acta*, **26**, 131 (1972).
(10) See, for example, (a) F. S. Richardson, D. Shillady, and J. Bloor, *J. Phys. Chem.*, **75**, 2466 (1971); (b) J. Linderberg and J. Michl, *J. Am. Chem. Soc.*, **92**, 2619 (1970); (c) J. Webb, R. Strickland, and F. S. Richardson, *ibid.*, **95**, 4775 (1973).
(11) See, for example, (a) F. S. Richardson and D. Caliga, *Theor. Chim. Acta*, **36**, 49 (1974); (b) F. S. Richardson and W. Pitts, *Biopolymers*, **13**, 703 (1974); (c) J. Webb, R. Strickland, and F. S. Richardson, *Tetrahedron*, **29**, 2499 (1973); (d) F. S. Richardson and N. Cox, *J. Chem. Soc., Perkin Trans. 2*, 1240 (1975); (e) F. S. Richardson and W. Pitts, *ibid.*, 1276 (1975); (f) F. S. Richardson and R. W. Strickland, *Tetrahedron*, **31**, 2309 (1975).
(12) See, for example, C. Yeh and F. S. Richardson, *Theor. Chim. Acta*, **39**, 197 (1975).
(13) J. H. Brewster and J. G. Buta, *J. Am. Chem. Soc.*, **88**, 2233 (1966).
(14) J. Platt, *J. Chem. Phys.*, **17**, 484 (1949); **19**, 263 (1951).
(15) J. A. Schellman, *J. Chem. Phys.*, **44**, 55 (1966).
(16) S. E. Harnung, E. C. Ong, and O. E. Weigang, Jr., *J. Chem. Phys.*, **55**, 5711 (1971).
(17) D. Caldwell, *J. Chem. Phys.*, **51**, 984 (1969).
(18) C. Yeh and F. S. Richardson, *J. Chem. Soc., Faraday Trans. 2*, **72**, 331 (1976).
(19) D. Caliga and F. S. Richardson, *Mol. Phys.*, **28**, 1145 (1974).
(20) J. Horwitz, E. H. Strickland, and C. Billups, *J. Am. Chem. Soc.*, **91**, 184 (1969).

Protonation of the 1-(Phenylazo)-2-naphtholhydrazone Tautomer: A CNDO Study

Richard W. Bigelow

Xerox Webster Research Center, Webster, New York 14580 *(Received April 30, 1976)*

Publication costs assisted by Xerox Corporation

Spectroscopic manifestations of protonation in the 1-(phenylazo)-2-naphtholhydrazone tautomer are investigated using a full SCF–CNDO–CI procedure. $\pi \rightarrow \pi^*$ transition energies, oscillator strengths, binding energies, and heteroatomic charge densities for the free molecule and several protonated models are compared with experimental spectra and pK behavior, and indicate that protonation of the oxygen site, designated O(1), is most probable. The O(1) lone pair is the only site considered where the protonated model reproduced each of the experimental findings. The oxygen atom is predicted to possess a highly basic character in the ground state which is significantly increased in the first excited singlet state. Assignment of the O(1) site as the position of proton attachment is further substantiated by the results of isopotential energy mappings in the space surrounding the ground and first $\pi \rightarrow \pi^*$ excited state of the free hydrazone tautomer. The increase in charge at the oxygen site in the excited state is reflected in the electrostatic potential energy diagrams as a deeper potential well opposite this atom. A surprising result is obtained from these mappings in the attractive region of the nitrogen atom attached to the naphthyl moiety. This atom is predicted to gain charge in the excited state; however, the depth of the potential well opposite this atom becomes less than that calculated for the ground state. This apparent contradiction is shown to be the result of increased electrostatic repulsions due to loss of charge at the surrounding carbon centers. It is also found that HMO theory lead to ambiguous conclusions in earlier studies in the description of the protonation behavior of this molecule because of the large excess charge predicted to reside on the oxygen atom in the ground state. This compels the atom to loose charge in the excited state: a result in direct opposition to the CNDO predicted behavior and the relative pK and pK^* constants.

Introduction

Recently certain experimental trends observed in the basic properties of a series of 1-(para-substituted phenylazo)-2-naphthols were reported when these compounds were subjected to varying ratios of a sulfuric acid/water mixture.[1] With the aid of Hückel molecular orbital (HMO) calculations it was shown that the free molecule, present at low acid content, was the hydrazone tautomer, Figure 1, and that this tautomer was the species which is protonated at higher acid concentrations. However, determination of a specific site of proton attachment was not forthcoming from these comparisons. Properties that were obtained from the HMO ground state orbitals appeared to give a satisfactory agreement with experiment—most notably the heteroatomic charge density variations as a function of substituent. These charge densities, in the hydrazone tautomer, were calculated to be independent of substituent, as were the experimental pK constants. Properties predicted from the HMO virtual orbitals to reflect excited state behavior gave either ambiguous results, as in the case of substituent dependent trends in the $\pi \rightarrow \pi^*$ transition energy shifts, or results which appear in direct opposition to experiment, as in the case of the excited state heteroatomic charge densities.

A more sophisticated molecular orbital treatment of the phenylazo-2-naphthols which can identify the site of protonation and determine the limitations of the HMO method is in order. Therefore, the self-consistent-field (SCF) complete neglect of differential overlap (CNDO) molecular orbital technique with configuration interaction is used to obtain various ground and excited state characteristics of the parent hydrazone tautomer and its assumed protonated forms. As a further indication of the most probable site of protonation the CNDO σ and π atomic charge densities in the ground and lowest excited $\pi \rightarrow \pi^*$ states are used to generate isopotential energy maps in the space surrounding the hydrazone tautomer for the interaction of a positive point test charge with the static molecular charge distribution.[2,3] Various approximations based on this method have been successfully used to distinguish between multiple protonation sites and to provide information on pathways of electrophilic reagent approach.[4-9]

Figure 2 is provided to show the specific spectroscopic properties observed for the 1-(phenylazo)-2-naphtholhydrazone tautomer which an adequate molecular orbital theory should duplicate. Note that protonation of the hydrazone tautomer leads to both a bathochromic shift and a substantial increase in the intensity of the long wavelength transition relative to the free tautomer. Also, experiment has shown that relative to the ground state the site of protonation is more susceptible to electrophilic attack in the lowest energy $\pi \rightarrow \pi^*$ excited state, and this should be reflected in the molecular orbital calculations by a similar increase in charge density for this site. Bonding energies obtained by an all valence electron theory for the various possible protonated configurations should also provide a measure of the relative stabilities of each species, and hence, a further indication of the site of protonation.

The use of atomic charge densities to predict sites of molecular reactivity has been criticized by several investigators, even when such correlations do exist.[10,11] It is well known that certain atomic centers which are predicted to bear a highly negative charge are resistant to protonation. However, in his treatise on chemical reactivity, Dewar has clearly indicated that charge density criterion can be used to predict sites of electrophilic activity in the cases where the reaction leaves the conjugated system of the base unchanged.[12] Since the com-

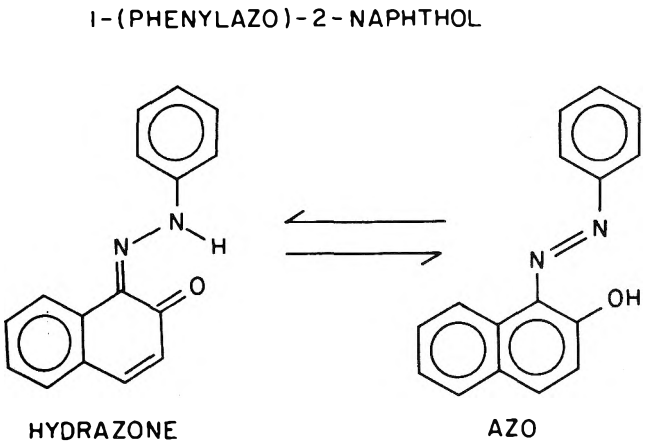

Figure 1. The structure of 1-(phenylazo)-2-naphthol showing hydrazone ⇌ azo tautomerism.

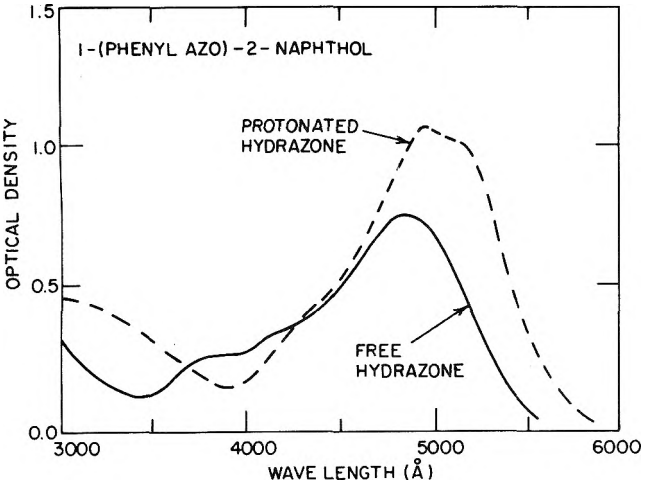

Figure 2. The absorption spectrum of the 1-(phenylazo)-2-naphthol free and protonated hydrazone species taken from ref 1. Both traces, taken at different acid/water ratios, were 2.27 × 10^{-5} M monitored in a 1.0-cm cell.

pound under consideration here is assumed to protonate at one of the heteroatomic electron lone pairs and, therefore, will involve no changes in conjugation within the molecule, charge density can be used as an unambiguous indicator of relative basicities.

Computational Procedures

Parameters for the HMO calculations were assigned in the usual way where heteroatomic Coulomb integrals, α_X, and resonance integrals between adjacent atoms, β_{XY}, are expressed in terms of the Coulomb and resonance integrals of benzene[13]

$$\alpha_X = \alpha + h_X\beta; \qquad \beta_{XY} = k_{XY}\beta$$

The values for h_X and k_{XY} used in this study were taken from Kuder's HMO calculations on hydroxyarylazo compounds.[14]

The CNDO treatment of the ground state follows the modified parameterization described by Clark[15] of the original CNDO method of Pople and Segal.[16] Excited state wave functions were generated from the CNDO ground state occupied and virtual orbitals by the configuration interaction technique described by Lowitz.[17] In the virtual orbital approximation to the excited state wave functions the atomic charge densities in the excited state are given by[18]

$$q(\mathrm{A})_i^* = q(\mathrm{A})^0 + \sum_{m=1}^{l}\sum_{r=1}^{n} C'_{im}{}^2 (C_{k'r}{}^2 - C_{jr}{}^2) \qquad (1)$$

where $q(\mathrm{A})^0$ is the ground state charge density, C'_{im} is the configuration interaction coefficient for the contribution to the ith state of the mth electronic configuration resulting from the excitation of an electron from orbital j to virtual orbital k', and C_{jr} and $C_{k'r}$ are the coefficients of the rth orbital on atom A in molecular orbitals j and k', respectively. In the absence of significant configuration interaction and when only π orbitals are involved in the transition eq 1 reduces to a form used to obtain excited state charge densities in the HMO approximation. In such a case the primary advantage derived from the CNDO approach is an improvement in both the ground state properties and the ability of the virtual orbitals to approximate the excited state wave function, rather than any major change in the method of treatment of the excited state.

The electrostatic potential in the space surrounding a molecule due to a static molecular charge distribution can be expressed in terms of nuclear and electronic components[2]

$$V(\vec{r}_p) = \sum_{\alpha}^{\mathrm{nucl}} \frac{z_\alpha}{|\vec{r}_\alpha - \vec{r}_p|} - \int \frac{\rho(\vec{r})}{|\vec{r} - \vec{r}_p|}\,d\tau \qquad (2)$$

where $\rho(\vec{r})$ is the electronic density function. The first term is directly obtained through a summation over all atomic centers and the electronic term is approximated according to Giessner-Prettre and Pullman's method II described in ref 2.[19] In this approximation it is assumed that the total charge on each atom is confined to a Slater S orbital describing the particular center and overlap between orbitals on different centers is neglected. The resulting two-center integrals over S orbitals are reduced to a summation of terms involving only $\vec{r}_p$ which can be rapidly evaluated.[20] The electrostatic potential energy at point $\vec{r}_p$ is then calculated from the relationship $W(\vec{r}_p) = qV(\vec{r}_p)$.

The molecular configuration used in the CNDO calculations was pieced together from known fragment geometries and was assumed to provide an adequate description of the hydrazone tautomer, Figure 3. The bond lengths and angles for the naphthalene moiety were taken from a crystallographic study of 1,1′-naphthylazo-2-naphthol[21] and lengths for the C–N (*trans*-azobenzene),[22] N–N (dimethylhydrazine),[23] C=O (benzoquinone),[24] and C=N (diphenyl triketone *sym*-*N*-benzoylphenylhydrazone)[25] bonds were taken from the compounds in parentheses which were assumed to exhibit representative values. The bond lengths and angles for the carbon–carbon bonds in the phenyl ring were taken from the crystal structure determination of acetanilide.[26] All carbon–hydrogen bonds in the phenyl moiety were assumed to be 1.080 Å in length and directed symmetrically away from the carbon atom. The angles joining these fragments were taken from the 1,1′-naphthylazo-2-naphthol structure.[21]

Results and Discussion

Results of the HMO and CNDO atomic electron density calculations for the ground and excited state of the 1-(phenylazo)-2-naphtholhydrazone tautomer are compared in Figure 4a (HMO values in parentheses). The values obtained for the heteroatoms using the HMO method are essentially the same as the results of the HMO treatment using auxiliary inductive parameters.[1] The oxygen atom is predicted to be the most basic heteroatom in both the ground and excited states; however, the loss of π charge in the excited state leads to the

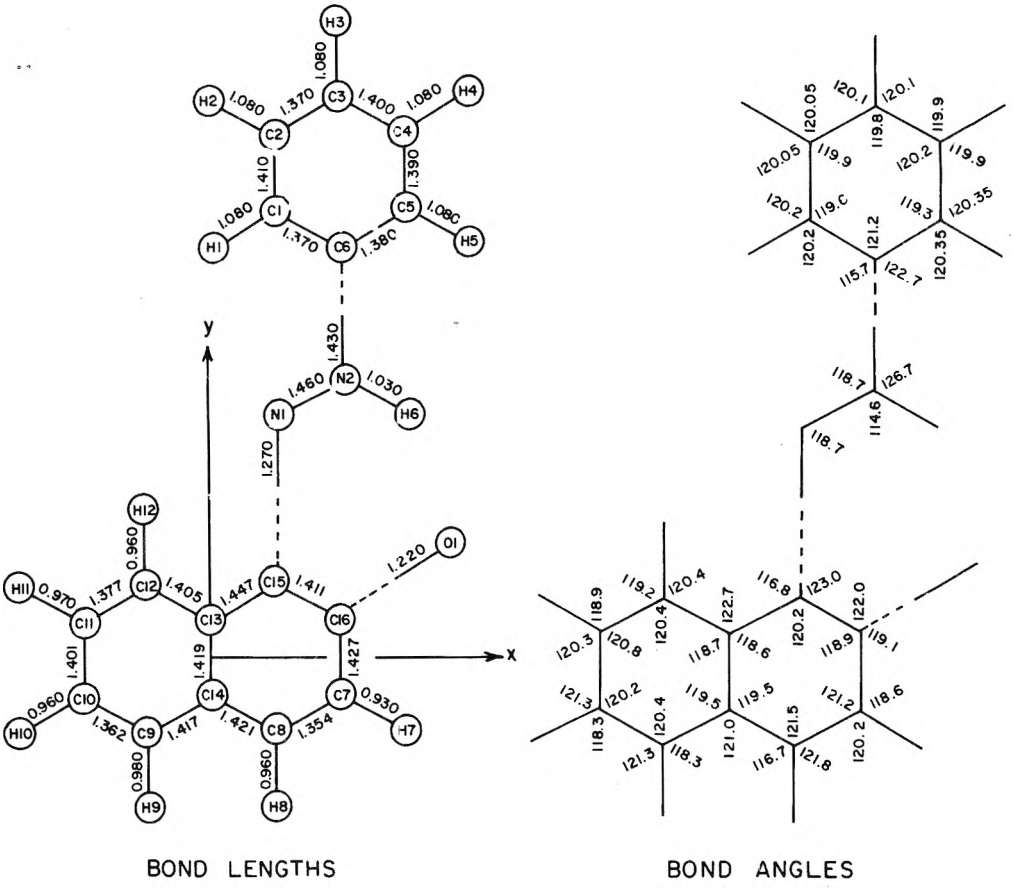

Figure 3. Bond lengths and bond angles for the 1-(phenylazo)-2-naphthol hydrazone tautomer used in the CNDO calculations.

conclusion that $pK > pK^*$ for this site. Both nitrogen atoms are predicted to be somewhat acidic in the ground state. Defining N(naph) as the nitrogen attached to the naphthyl moiety and N(phen) as the nitrogen atom next to the phenyl ring, it is shown that in the excited state the N(naph) site becomes strongly basic while the N(phen) nitrogen loses charge and becomes more acidic. Based solely on the HMO calculated π electron density correlations with the experimental pK and pK^* constants of ref 1 the N(naph) nitrogen appears to be the most likely site of protonation.

The lowest excited CNDO singlet state was obtained by configuration interaction between the highest six occupied and lowest six unoccupied molecular orbitals. The first allowed singlet–singlet transition (configuration interaction coefficient of −0.966 for the one-electron transition between the highest occupied and lowest unoccupied π molecular orbitals) was calculated to occur at 4.009 eV with an oscillator strength of 0.5025. This particular CNDO parameterization has been used mainly to calculate ground state properties and, therefore, this transition is predicted to be at much higher energy than the experimental value taken to represent this transition (~2.55 eV from Figure 2). Although the transition energies calculated in this study may not yield absolute comparisons with experimental values, they can be used to provide a better correlation of the spectral properties of specified protonated species than obtained by HMO methods. Comparisons of the HMO and CNDO π atomic charge densities for the ground and excited states show several differences which may prove significant in determining the site of protonation. The CNDO results for the ground state predict the N(naph) nitrogen to bear a slight negative charge and the oxygen atom, while still the most negatively charged site in the molecule, to be much less basic than predicted by the HMO method (1.245e vs. 1.616e). The CNDO results for the excited state predict a similar gain or loss of charge at the nitrogen sites as found in the HMO calculations; however, the oxygen atom now gains additional charge relative to the ground state. Figure 4b shows the CNDO total net charge (σ and π contributions) residing at each atomic site. Differences between ground and excited state values reflect only the change in π component as the σ core is predicted to be static in the excitation. Each heteroatom is shown to be a σ electron acceptor—N(naph), +0.102e; N(phen), +0.508e; Oxygen, +0.121e—which leads to a greater degree of basicity for each of these sites in the ground state than suggested from the π components alone. These results show that all three heteroatomic centers have a net basic character in the ground state, and that both the N(naph) nitrogen and the oxygen atom now appear to exhibit charge behavior which would explain the relative pK and pK^* constants obtained in ref 1. The oxygen atom is most basic in both the ground and excited states while the N(naph) nitrogen exhibits the greatest increase in basicity in going from the ground to the excited state.

Properties of the various protonated species were obtained by placing a hydrogen nucleus at the proposed site of protonation and performing a full SCF calculation on each new geometry. This was done assuming the heteroatoms containing the four electron lone pairs; the N(phen) nitrogen atom, the N(naph) nitrogen, and the two lone pairs, O(1) and O(2), on the oxygen atom, as the prime possibilities for protonation. The resulting properties of interest and the posi-

TABLE I: Total Energy, E(tot); Electronic Energy, E(elec); Energy of First Allowed Singlet–Singlet Transion, $E(\pi_1 \rightarrow \pi_1^*)$; Oscillator Strength of the First Allowed Transition, f; and Energies of the Highest Occupied, $E(\pi_1)$, and Lowest Unoccupied, $E(\pi_1^*)$, π Molecular Orbitals for the Parent Compound and Its Protonated Forms (energies are in electron volts)

	E(tot)	E(elec)	$E(\pi_1 \rightarrow \pi_1^*)$	f	$E(\pi_1)$	$E(\pi_1^*)$
Free molecule	−1211.815	−18 445.611	4.009	0.502	−8.167	−0.779
N(phen) protonated[a]	−1174.482	−18 854.272	4.224	0.313	−12.228	−5.033
N(naph) protonated[b]	−1178.544	−18 858.471	3.477	0.335	−12.824	−5.754
O(1) protonated[c]	−1186.765	−18 796.436	3.311	0.686	−12.577	−5.719
O(2) protonated[d]	−1167.283	−18 855.916	3.566	0.526	−12.597	−5.735

[a] Proton placed 1.0 Å directly above the N(phen) nitrogen atom. [b] N(naph)–H^+ bond directed symmetrically away from the C-15–N(naph)–N(phen) bonds. The bond length is 1.0 Å. [c] Oxygen–H^+ bond is directed outward 120° from the C-16–oxygen bond and toward the H-6 atom. The bond length is 0.971 Å. [d] Oxygen–H^+ bond is directed outward 120° from the C-16–oxygen bond and toward the H-7 atom. The bond length is 0.971 Å.

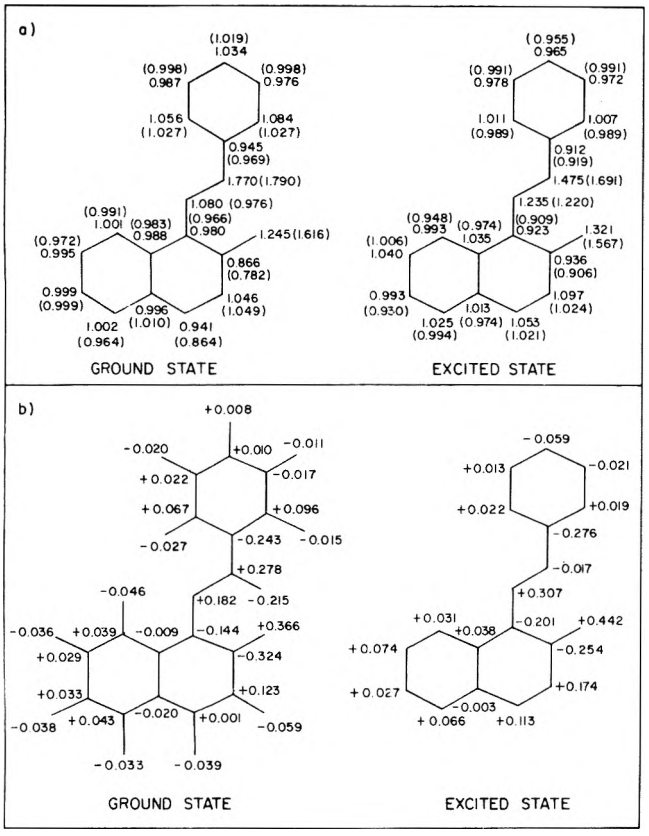

Figure 4. (a) HMO, in parentheses, and CNDO π charge densities for the ground and first excited singlet state of the 1-(phenylazo)-2-naphtholhydrazone tautomer. (b) The CNDO atomic charge deviation from neutrality including both σ and π contributions for the ground and first excited singlet state (+ denotes an excess of negative charge).

tioning of each additional proton are tabulated in Table I. It is shown that relative to the free molecule N(naph), O(1) and O(2) protonation leads to a bathochromic shift in energy of the first allowed singlet–singlet transition, but that only O(1) and O(2) protonation yields an increase in oscillator strength. The binding energy of a system is defined as the difference between the total energy of a molecule and the sum of the atomic energies of the component atoms.[20] In this study the individual atomic energies were not tabulated; however, the sum of these energies will be a constant for the various protonated species, and thus, the magnitude of the total energies can be taken as a measure of the relative binding energies. Protonation of the O(1) oxygen lone pair is shown to provide the greatest binding energy.

Protonation in each case leads to a lowering in energy of both the occupied and unoccupied molecular orbitals, Figure 5. With the exception of the N(phen) protonated species strict separation is maintained between the σ and π orbitals in both the ground and excited state. The N(phen) nitrogen protonation was treated as a three-dimensional system and resulted in some degree of mixing between the σ and π orbitals. It is also essential to establish the parentage of the molecular orbitals of the protonated species involved in the lowest $\pi \rightarrow \pi^*$ transition as it was inherent to the assumption of the Förster cycle in the calculation of the pK^* constants that the optical transitions observed in the free and protonated molecules possess the same character.[1] The calculations showed that the highest occpied and lowest virtual π orbitals were essentially identical in the free and O(1) protonated species, whereas the remaining π orbitals did not show such a direct correlation. The general lowering of the energy levels and π orbital mixing can be explained in terms of increased σ electron delocalization due to the orbital of the proton and electrostatic repulsions derived from the charge transferred to the incoming center.[27] This is evident from the degree of participation of the proton atomic orbital coefficient in each of the σ orbitals of the O(1) protonated molecule ($> \pm 0.100$ in 13 of the σ orbitals).

The CNDO description of the electron lone pairs in this study is in general agreement with the many previous all valence electron SCF calculations which have predicted the electron lone pairs to be partially delocalized throughout the molecule.[28–33] It is found that this delocalization increases with the size of the molecule and the number of different lone pairs and can also vary over wide ranges depending on the parameters used in the calculation. The two oxygen atom lone pairs are best represented by the σ_1 (−8.17 eV) and σ_{10} (−13.06 eV) molecular orbitals where there is 0.437e and 0.790e of charge, respectively, associated with this heteroatomic center. The lone pairs on the nitrogen atoms are approximated by the σ_7 (−11.85 eV) orbital where 0.560e is localized on the N(naph) center and by the π_1 (−8.70 eV) orbital where 0.668e is confined to the P_π orbital of the N(phen) nitrogen.

Figure 6 gives the isopotential energy curves in kilocalories per mole in the space surrounding the phenylazo-2-naphthol hydrazone tautomer, using the CNDO ground state $\sigma + \pi$ charge densities, for successive planes Z = 0.0, 1.0, 1.5, and 4.0 Å above the plane of the molecule. The maximum potential well in each case is calculated to be opposite or approximately above the oxygen atom. In the plane of the molecule there are two distinct proton attracting regions which are opposite the oxygen and N(naph) nitrogen atoms, corresponding roughly to the expected location of electron lone pairs on these atoms.

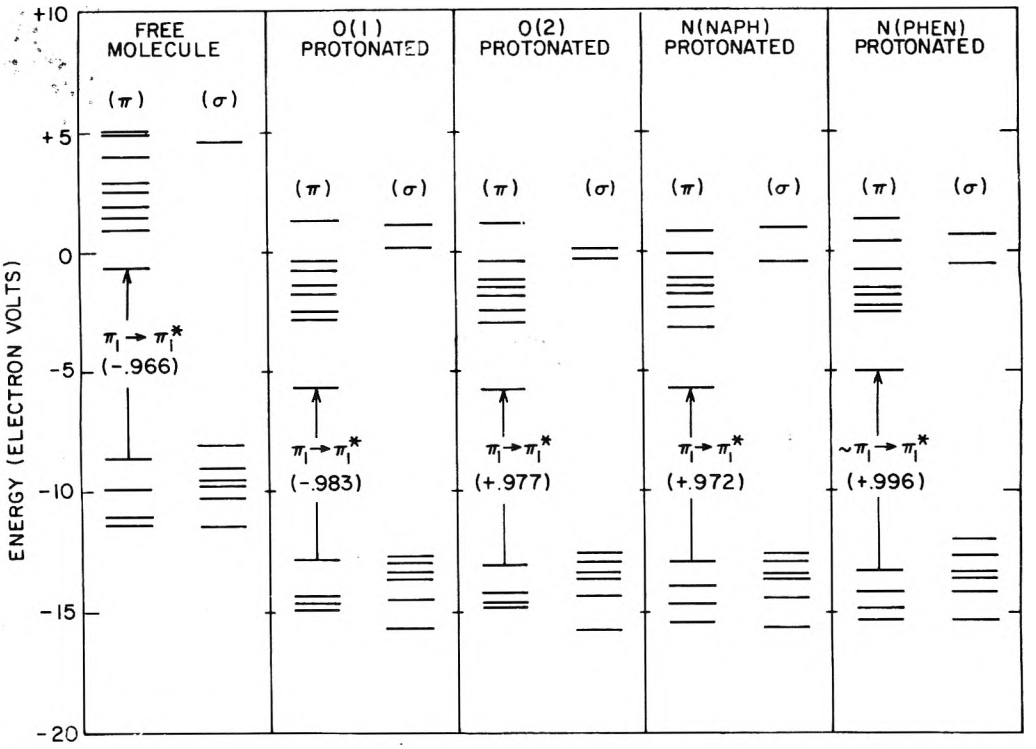

Figure 5. The energy levels of the ten highest occupied and ten lowest unoccupied molecular orbitals for the free molecule and the various protonated species. Each of the lowest energy transitions was calculated to be $\pi_1 \rightarrow \pi_1^*$. The configuration interaction coefficients for the contribution of the indicated one-electron transition to the total molecular wave function are given in parentheses.

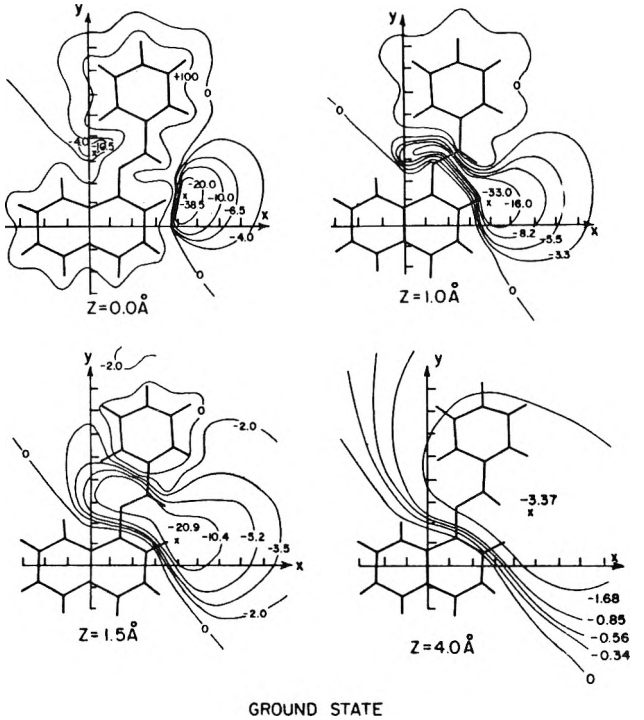

GROUND STATE

Figure 6. Isopotential energy curves in the space surrounding the 1-(phenylazo)-2-naphtholhydrazone tautomer in the ground state for the *X*–*Y* planes at the indicated distance above the plane of the molecule. Units are kilocalories per mole and a negative value indicates a proton attraction region. Lengths are measured in Ångstroms and the minimum of a potential energy well is indicated by *X*.

However, the attractive area opposite the N(naph) nitrogen is quite localized and is almost encompassed by regions of a repelling nature. Progressing above the plane of the molecule, the space over all the heteroatoms and the phenyl ring becomes entirely attractive while that surrounding the major portion of the naphthyl moiety remains slightly repulsive. The maximum attractive potential opposite the N(naph) nitrogen occurs somewhat above the $Z = 0.0$ Å plane. Although there is no discrete potential well above the N(phen) nitrogen, whose π conjugated lone pair extends in the Z direction, note that between $Z = 1.0$ and 1.5 Å this position does become overall attractive. The attractive region above this center is due primarily to the electron acceptor character of the N(phen) nitrogen σ orbitals as the π orbital of this atom is predicted to be substantially electron deficient. Figure 7 presents similar calculations for the $Z = 0.0$, 1.0, and 8.0 Å planes of the excited state. It is shown that close to the molecule ($Z = 0.0$ and 1.0 Å) the maximum attractive potential is still opposite the oxygen atom. Due to the increased charge density at this site the depth of the well has been substantially increased with respect to the ground state. An interesting result is obtained in the attractive region opposite the N(naph) nitrogen. This atom has gained charge in the excited state; however, the depth of this potential well is less than that calculated for the ground state! This apparent contradiction and the increased area of the attractive regions around the lower portion of the naphthyl moiety can be explained in terms of changes in the nearest neighbor contributions to the potential. Each of the π centers surrounding the region opposite the N(naph) nitrogen loses charge in the excited state and contributes either a more repulsive or less attractive element, and these changes more than counter the effects due to the increased charge on the nitrogen. The C-7, C-8, C-9, C-14, and C-16 carbons gain additional charge in the excited state and contribute to the large attractive potential energy pattern around the naphthyl group. Also, the amount of π charge lost by the N(phen) nitrogen in the excited state compensates for the excess σ charge on this atom and leads to a highly repulsive region above this center.

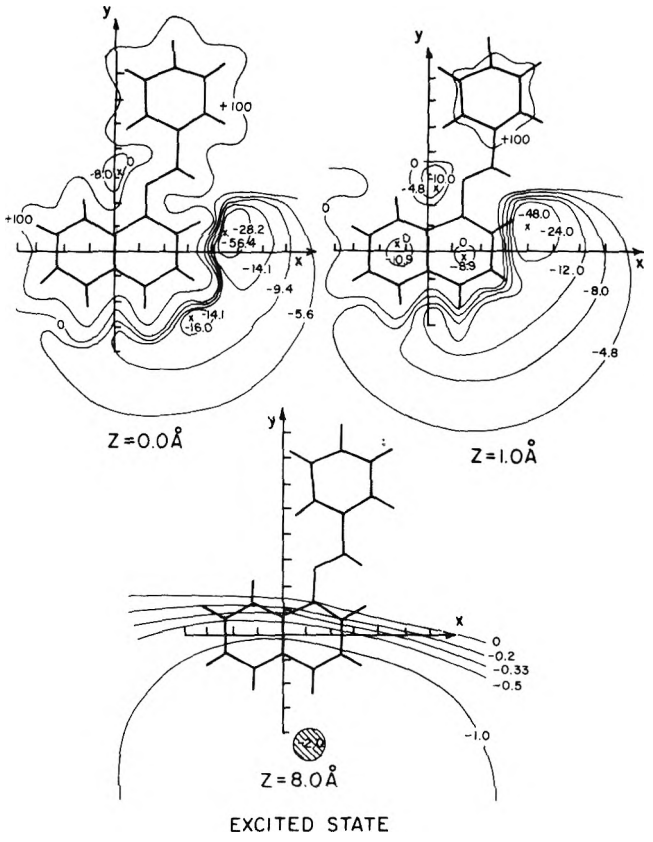

Figure 7. Isopotential energy curves for the first excited singlet state for the indicated *X*-*Y* planes.

The calculations not only provide an indication of the relative depths of the potential wells, but can be used to obtain estimates concerning avenues of electrophilic reagent approach to a reaction site and possible steric effects due to substituents. For the case at hand, it is shown for the ground and excited states, that once a proton has entered a region of attraction, the shapes of the isopotential energy curves provide a funnel effect directing the proton toward the oxygen site. The strong repulsive nature of the positively charged hydrogen atom and its ability to direct reagent approach is best demonstrated in the space opposite the N(naph) nitrogen atom.

It has been shown in the case of larger electrophilic reagents that when charge exchange effects are included in the potential energy calculations the overall reactivity pattern is not substantially different from the static approximation.[9] The use of CNDO wave functions and S orbital overlap only between the same centers in the calculation of the electrostatic potential has been discussed and the results compared to both ab-initio and other approximation techniques.[2] It was demonstrated that the method used in this study somewhat underestimated the depths of potential wells and failed to predict the exact directionality of the lone pair potential minimums obtained when P orbital overlap was included, but that the overall pattern, and particularly, the relative depths of potential wells were maintained.

Summary and Conclusions

Based on a comparison of experimental results with ground and excited state properties calculated by the CNDO method the O(1) electron lone pair is strongly indicated to be the site of protonation in the 1-(phenylazo)-2-naphtholhydrazone tautomer. The protonated O(1) and O(2) lone pairs were the only sites considered which correctly predicted both a bathochromic shift and a substantial increase in the intensity of the lowest singlet transition relative to the free tautomer. Charge density calculations predict the oxygen atom to be the most basic ground state site in the molecule. The basicity of this site is increased in the excited state in agreement with the relative values of the experimental pK and pK^* constants. This correlation is corroborated by the isopotential energy diagrams which predict a deeper potential well opposite the oxygen atom in the excited state. These mappings further suggest that the O(1) lone pair is the site of protonation as the position of the potential energy minimum corresponds to the expected configuration for this lone pair. Binding energy considerations also identified the O(1) lone pair to be the most energetically favorable protonated species.

The electrostatic potential energy diagrams also show that relative ground and excited state atomic charge densities, even when obtained by sophisticated methods, may sometimes be insufficient to indicate the preferred site of protonation. The basicity of any site in question is strongly dependent on the attractive or repulsive nature of the surrounding centers whose combined effect may neutralize or complement the contribution from the atom of interest.

Acknowledgments. I wish to thank J. B. Flannery, Jr., and F. D. Saeva for stimulating discussions concerning protonation of the phenylazo-2-naphthols and for suggesting the CNDO approach as a means of characterizing the spectroscopic properties of these compounds.

References and Notes

(1) R. W. Bigelow, *J. Phys. Chem.*, **79**, 2411 (1975).
(2) C. Giessner-Prettre and A. Pullman, *Theor. Chim. Acta*, **25**, 83 (1972).
(3) E. Scrocco and J. Tomasi, *Top. Curr. Chem.*, **42**, 95 (1973).
(4) R. Bonaccorsi, A. Pullman, E. Scrocco, and J. Tomasi, *Chem. Phys. Lett.*, **12**, 622 (1972).
(5) R. Bonaccorsi, A. Pullman, E. Scrocco, and J. Tomasi, *Theor. Chim. Acta*, **24**, 51 (1972).
(6) H. Weinstein, S. Maayani, S. Srebrenik, S. Cohen, and M. Sokolovsky, *Mol. Pharmacol.*, **9**, 820 (1973).
(7) J. Almlof, A. Henriksson-Enflo, J. Kowalewski, and M. Sundban, *Chem. Phys. Lett.*, **21**, 560 (1973).
(8) J. Bertraum, E. Silla, R. Carbo, and M. Martin, *Chem. Phys. Lett.*, **31**, 267 (1975).
(9) Y. Ellinger, R. Subra, G. Berthier, and J. Tomasi, *J. Phys. Chem.*, **79**, 2440 (1975).
(10) R. B. Herman, *Int. J. Quant. Chem.*, **11**, 165 (1968).
(11) D. Dolman and R. Stewart, *Can. J. Chem.*, **45**, 903 (1967).
(12) M. J. S. Dewar, "Advances in Chemical Physics", Vol. 8, Interscience New York, N.Y., 1965.
(13) A. Streitwieser, Jr., "Molecular Orbital Theory for Organic Chemists", Wiley, New York, N.Y., 1972.
(14) J. E. Kuder, *Tetrahedron*, **28**, 1973 (1972).
(15) D. T. Clark, *Tetrahedron*, **24**, 4689 (1968).
(16) J. A. Pople and G. A. Segal, *J. Chem. Phys.*, **44**, 3289 (1966).
(17) D. A. Lowitz, *J. Chem. Phys.*, **46**, 4698 (1967).
(18) J. Del Bene and H. H. Jaffe, *J. Chem. Phys.*, **49**, 1221 (1968).
(19) The computer program used in this study was written by C. Giessner-Prettre and obtained from the Quantum Chemistry Program Exchange. QCPE, Chemistry Department, Indiana University, Bloomington, Ind. QCPE #249.
(20) J. A. Pople and D. L. Beveridge, "Approximate Molecular Orbital Theory", McGraw-Hill, New York, N.Y., 1970.
(21) P. Cherin, private communication.
(22) C. J. Brown, *Acta Crystallogr.*, **21**, 485 (1966).
(23) W. Beamer, *J. Am. Chem. Soc.*, **70**, 2978 (1948).
(24) J. Trotter, *Acta Crystallogr.*, **13**, 86 (1960).
(25) D. B. Pendergrass, J. C. Paul, and D. Y. Curtin, *J. Am. Chem. Soc.*, **94**, 8730 (1972).
(26) O. Kennard, D. G. Watson, F. H. Allen, N. W. Issacs, W. D. S. Motherwell, R. Pettersen, and W. G. Town, Ed., "Molecular Structures and Dimensions", Vol. A1, "Interatomic Distances 1960-65 Organic and Organometallic Crystal Structures", A. Oosthock, 1972.

(27) A. Imamura and T. Hirano, *J. Am. Chem. Soc.*, **97**, 4192 (1975).
(28) W. Adam and A. Grimison, *Tetrahedron*, **21**, 3417 (1965).
(29) R. Hoffmann, *J. Chem. Phys.*, **40**, 2745 (1964).
(30) J. E. Bloor and D. L. Breen, *J. Am. Chem. Soc.*, **89**, 6835 (1967).
(31) E. Clementi, *J. Chem. Phys.*, **46**, 4731, 4737 (1967).
(32) J. Del Bene and H. H. Jaffe, *J. Chem. Phys.*, **48**, 1807 (1968).
(33) G. Hojer, S. Meza, and M. E. Ruiz, *Acta Chem. Scand.*, **27**, 1860 (1973).

Ultrasonic Relaxation of $Cu(ClO_4)_2$ and $Cu(NO_3)_2$ in Ethylene Glycol

M. Vincenzini, B. Sesta, M. Battistini,

Institute of Physical Chemistry, University of Rome, Rome, Italy

and S. Petrucci*

Polytechnic Institute of New York, Brooklyn, New York *(Received June 14, 1975; Revised Manuscript Received August 17, 1976)*

Ultrasonic absorption of solutions of $Cu(ClO_4)_2$ and $Cu(NO_3)_2$ in the concentration range 0.025–0.20 M, temperature range 15–45 °C, and frequency range 5–300 MHz has been measured. A single Debye relaxation process with a relaxation frequency of about 40 MHz at 25 °C, which within experimental error, is concentration independent, has been observed. To interpret the data, ultrasonic absorption results for $Ca(NO_3)_2$, $Ni(ClO_4)_2$, $Cu(en)_2(ClO_4)_2$, and $CuCl_2$ in ethylene glycol at 25 °C have been obtained and are also reported. Analysis of the temperature dependence of the ultrasonic relaxation time has been performed and the activation parameters are reported. Auxiliary conductance data for $Cu(ClO_4)_2$, $Cu(NO_3)_2$, and $CuCl_2$ in ethylene glycol reveal the former two electrolytes to be weakly associated whereas $CuCl_2$ shows considerable association. The relaxation process observed for $Cu(ClO_4)_2$ and $Cu(NO_3)_2$ is interpreted as due to cation desolvation (or vice versa) by the anion in accord with the Eigen I_d dissociative mechanism, this process being closely coupled with the diffusive approach of the two solvated ions in these viscous media.

Introduction

The Eigen I_d (dissociative interchange) mechanism of ionic association and complexation for octahedrally coordinated cations[1,2] is usually written as a multistep process. This starts from the diffusion-controlled approach between the two solvated ions and proceeds to a stepwise solvent elimination from the solvation shells of the anion and cation up to the "contact". Omitting charge symbols, one may write for monodentate ligands the following scheme

$$\underset{\text{I}}{MeS_x + LS_y} \underset{k_{21}}{\overset{k_{12}}{\rightleftharpoons}} \underset{\text{II}}{MeS_2L} \underset{k_{32}}{\overset{k_{23}}{\rightleftharpoons}} \underset{\text{III}}{MeSL} \underset{k_{43}}{\overset{k_{34}}{\rightleftharpoons}} MeL \qquad (1)$$

where MeS_2L represents MeS_{x-1}, S_2, LS_{y-1}, and MeSL represents MeS_{x-1}, S, LS_{y-1}. The rate-determining step of the forward process is the rate of cation desolvation, the ligand nature not influencing the energy profile of the process nor the rate constant (for ligands of equal charge).[1,2]

The above mechanism has been repeatedly proven to be operative in aqueous solution[1,2] although the anion desolvation step may have an energy barrier comparable to the diffusion process.[3] Equation 1 may then be simplified into the following

$$MeS_x + L \underset{k_{21}}{\overset{k_{12}}{\rightleftharpoons}} MeSL \underset{k_{32}}{\overset{k_{23}}{\rightleftharpoons}} MeL \qquad (2)$$

In nonaqueous solvents the consensus among the majority of authors[4] is that the I_d mechanism expressed by either of the two eq 1 and 2 is operative for monodentate ligands.

It is to be expected, however, that modifications of the Eigen process, writtten in general form (1), are in order once the reaction conditions are properly altered. For instance, in media of quite low permittivity such as THF the ionic association is so high that at concentrations 0.05–0.20 M free ions are almost nonexistent relative to other species. Then process (1) should be written as

$$\underset{\text{II}}{MeS_2L} \underset{k_{32}}{\overset{k_{23}}{\rightleftharpoons}} \underset{\text{III}}{MeSL} \underset{k_{43}}{\overset{k_{34}}{\rightleftharpoons}} MeL \qquad (3)$$

The above has been suggested to interpret ultrasonic results at radiofrequencies for $LiNO_3$,[5] Bu_4NNO_3,[5] $NaClO_4$,[6] and $AgClO_4$,[6] in THF.

An interesting situation may also be predicted in viscous solvents. According to the Eigen matrix analysis[1] applied to eq 2, two relaxation times should be observable, according to the relation

$$\tau_{I,II}^{-1} = \frac{1}{2}[S \pm \sqrt{S^2 - 4P}] \qquad (4)$$

where

$$S = k_{12}\theta + k_{21} + k_{23} + k_{32}$$

$$P = k_{12}\theta(k_{23} + k_{32}) + k_{21}k_{32}$$

$$\theta = f(\text{ionic concentrations})$$

The signs before the square root in eq 4 refer to the fast and slow relaxation times, respectively.

The Smoluchowski–Debye[7] and Eigen theories,[7] modified by the introduction of the Stokes–Einstein relation, predict both k_{12} and k_{21} to be inversely proportional to the viscosity

of the solution.[8] In media of high viscosity, in rather diluted solutions, it may occur that $k_{12}\theta, k_{21} \ll k_{23}, k_{32}$. Then $S \simeq k_{23} + k_{32}$ and $S^2 > 4P$. Therefore the fast relaxation time would be

$$\tau_I^{-1} \simeq S \simeq k_{23} + k_{32} \tag{5}$$

and the slow relaxation time would result equal to

$$\tau_{II}^{-1} = \frac{1}{2}\left[S - S\sqrt{1 - \frac{4P}{S^2}}\right] \simeq \frac{1}{2}\left[S - S\left(1 - \frac{1}{2}\frac{4P}{S^2}\right)\right]$$

$$\tau_{II}^{-1} = P/S$$

having used the series expansion $(1 - x)^n \simeq 1 - nx$. Then

$$\tau_{II}^{-1} \simeq \frac{k_{12}\theta(k_{23} + k_{32}) + k_{21}k_{32}}{k_{23} + k_{32}} = k_{12}\theta + k_{21}\frac{k_{32}}{k_{23} + k_{32}} \tag{6}$$

Therefore one of the two relaxation times should be concentration independent. Furthermore $\tau_I^{-1} > \tau_{II}^{-1}$ if the presumed condition $k_{23}, k_{32} \gg k_{12}\theta, k_{21}$ holds (since $(k_{32}/k_{23} + k_{32}) < 1$).

The above kinetic situation could have been predicted in the case of fast solvent exchanging cations such as Cu^{2+} and Ca^{2+} in a viscous solvent as ethylene glycol. Some information about the rate of exchange of ethylene glycol from the first coordination shell of Cu^{2+} is in existence in the literature.[9] The above considerations and the general lack of investigation of the mechanism of complexation of first raw transition metal cations in pure viscous solvents by monodentate ligands prompted us to perform the present work. To be precise, one should add that the complexation of Ni^{2+} had indeed been investigated kinetically in glycol by flow techniques.[10] However, the ligands used were all bidentate (or polydentate) ones. This might have introduced into the results complexities due to the additional chelation step (or steps).[11] Further, in the case of Ni^{2+}, there is not a Jahn–Teller effect but there is the additional existence of the crystal field stabilization in the activation enthalpy for solvent exchange. Therefore the rate of exchange of glycol around Ni^{2+} is much slower than the diffusional rate constants for outer-sphere ion pair formation. Indeed for Ni^{2+} the converse situation $k_{12}\theta, k_{21} \gg k_{23}, k_{32}$ would hold even in ethylene glycol, in the assumption of the validity of the I_d mechanism.

Experimental Section

Materials. Ethylene glycol (Fisher Scientific) was redistilled in vacuo collecting only the middle portion of the distillate. Its density was measured at 25 °C and is equal to $\rho = 1.1098_1 \pm 5$ g cm^{-3}. Literature[12] values are $\rho = 1.1099$, 1.10986, and 1.0987 g/cm^3.

$Cu(ClO_4)_2 \cdot 6H_2O$ (Smith, Cleveland, Ohio) and $Cu(NO_3)_2 \cdot 3H_2O$ (Fisher Scientific) were used to prepare the solutions in glycol at the approximate desired concentrations. These solutions were refluxed in vacuo (~1 mm) in an all glass refluxing apparatus[13] over molecular sieves (predried at 250 °C in a muffle and cooled in a dessicator over P_2O_5). The refluxing operation lasted at least 12 h and the color of the solution changed from blue to blue-green. To ensure that possible remaining traces of water did not affect the results, a solution was prepared by methathesis of anhydrous $CuCl_2$ and (predried) $AgNO_3$ (at 101 °C) in glycol. After acidimetry by Tham of the $HClO_4$ (obtained by cation exchange of sample solutions in cation exchanging resin columns) the solution was adjusted to the same concentration of one of the solutions prepared by the refluxing method. The ultrasonic absorptions of the two solutions were the same within experimental error. All the other solutions were also analyzed by cation exchange resin and titration by Tham and methyl red as indicator. The precision of these analyses was about 0.2%.

$CuCl_2$ (anhydrous) (K and K) was used without further purification after redrying at 101 °C up to constant weight.

$Cu(en)_2(ClO_4)_2$ was prepared by addition of stoichiometric (or slight excess) amounts of ethylenediamine to $Cu(ClO_4)_2 \cdot 6H_2O$ in aqueous solution followed by crystallization and drying at 101 °C. The material was anhydrous as shown by acidimetry of the $HClO_4$ solutions obtained by cation exchange of sample solutions.

$Ni(ClO_4)_2 \cdot 6H_2O$ (Smith, Cleveland, Ohio) was used to prepare the solutions in glycol. It was refluxed and analyzed as for the corresponding solutions of $Cu(ClO_4)_2$ in glycol.

Anhydrous $Ca(NO_3)_2$ (BDH) was redried in a muffle at 180 °C for several days until constant weight was achieved. Weighed samples of the salt were dissolved in distilled glycol and solutions prepared in volumetric flasks. The concentration of these solutions was checked by cation exchange and acidimetry as for the case of the Cu^{2+} solutions.

All the solutions used for the ultrasonic work were vacuum filtered through a fine fritted disk. The analyses were performed after the filtration procedure to avoid errors due to possible evaporation of the solutions. Contact with the atmosphere during filtration was minimized by using a stoppered funnel incorporating a fritted disk.

Stock solutions of $Cu(ClO_4)_2$ in glycol for the conductance work were prepared by metathesis, dissolving stoichiometric amounts of anhydrous $CuCl_2$ and $AgClO_4$ in distilled glycol. After filtration the solutions were analyzed for Cu^{2+} by EDTA solution using weight burettes and murexide as indicator at pH 10. The EDTA solutions in water were analyzed with aqueous $Cu(NO_3)_2$ solutions. These in turn were prepared from weighed Cu (99.99% pure, Erba Inc.) and HNO_3 (Merck). All the titrations were performed by weight.

Solutions for conductance work were prepared directly in the conductance cell starting from the pure solvent and adding the desired amount of the stock solution by weight burettes.

Anhydrous $Cu(NO_3)_2$ was prepared by allowing Cu metal to react with HNO_3 as indicated above in aqueous solution. After filtering and crystallization the product was dried in vacuo at room temperature. This anhydrous salt was employed to prepare a stock solution in glycol, the remaining procedure being identical with the one employed for the $Cu(ClO_4)_2$.

Instrumentation. The pulse ultrasonic apparatus (5–300 MHz) and interferometric cell were described elsewhere.[14] The conductance set up, thermostat, and cells were also described before.[15]

Density measurements were performed by using a 50-ml pycnometer whose volume was calibrated with distilled water. Ethylene glycol was let in contact with the atmosphere only for the time necessary to fill the pycnometer (less than 20 s). The pycnometer was capped during the temperature equilibration time in the thermostat. The temperature for the density measurements was maintained at the desired value within ±0.02 °C.

Results and Calculations

Solvent. Density data from the literature[12] at 0, 15, and 30 °C for ethylene glycol are reported equal to $\rho = 1.127\,63$, $1.117\,10$, and $1.106\,64$ g cm^{-3}, respectively. At 25 °C[12] the

TABLE I: Calculated f_R, μ_{max}, and B Parameters for $Cu(ClO_4)_2$, $Cu(NO_3)_2$, and $Ca(NO_3)_2$ in Ethylene Glycol at the Various Concentrations C and Temperatures Investigated

Electrolyte	t, °C	C, M	f_R, MHz	$\mu_{max} \times 10^5$	$B \times 10^{17}$, $cm^{-1}\ s^2$
$Cu(ClO_4)_2$	15	0.05	26	76	230.7
	25	0.200	44	427	184
	25	0.091	45	260	153
	25	0.049	38	83	160.5
	25	0.026	39	74	156
	35	0.05	49	69	118
	44.6	0.05	64	58	91
$Cu(NO_3)_2$	15	0.092	27	162	248
	25	0.191	43	402	180
	25	0.092	40	152	169
	25	0.047	40	151	148
	35	0.092	52	156.5	120
	45	0.092	68	159	93
$Ca(NO_3)_2$	25	0.093	64	310	162
		0.045	63	125	163.5
		0.023	62	64	159.5

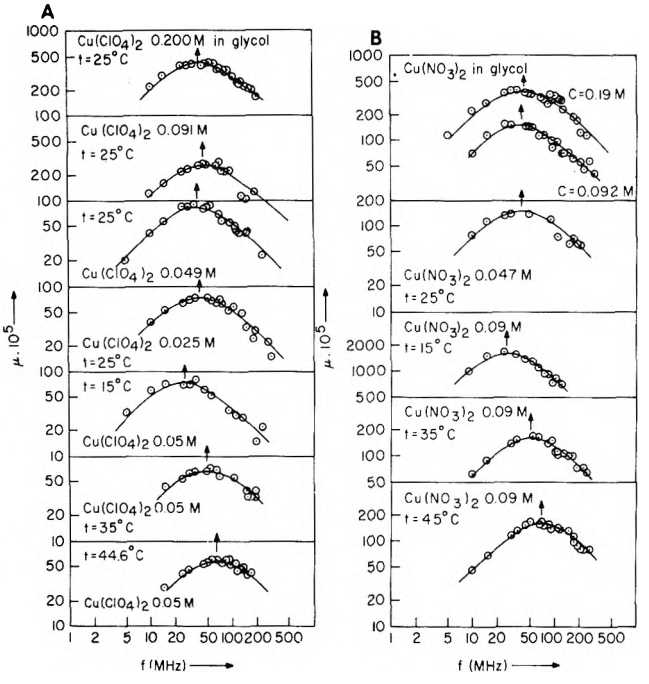

Figure 1. μ vs. f for $Cu(ClO_4)_2$ (A) and $Cu(NO_3)_2$ (B) in ethylene glycol.

average is $\rho = 1.1098_8$ g cm^{-3}. We have determined the density of glycol obtaining $\rho = 1.109\,81 \pm 5 \times 10^{-5}$, at 25 °C, $\rho = 1.102\,98 \pm 8 \times 10^{-5}$ at 35 °C and $\rho = 1.096\,15 \pm 1.0 \times 10^{-4}$ at 45 °C. These data can be expressed by a linear relation with temperature described by the equation

$$\rho = 1.1275_4 - 7.0052 \times 10^{-4}\, t$$

where t is expressed in degrees centigrade. This equation has been calculated by linear least squares. It agrees with the above experimental data within a standard deviation of $\Delta\rho = 1.6 \times 10^{-4}$ g cm^{-3}. Ultrasonic velocities have been determined in the frequency range 10–50 MHz for ethylene glycol at 15, 25, 35, 45, and 65 °C by the interferometric technique described elsewhere.[16] The results are u = 1680, 1657, 1630, 1607, and 1560 m s^{-1}, respectively. Linear least-squares analysis applied to the ultrasonic velocity vs. temperature data correlates these two quantities by the empirical expression $u = (1680 \pm 1) - (2.41 \pm 0.04)(t - 15)$ m s^{-1} where u is the ultrasonic velocity (in m s^{-1}) and t the temperature in degrees centigrade.

Ultrasonic absorption has been determined in the frequency range 15–330 MHz at 25 °C. No ultrasonic relaxation is observable and the average $\alpha/f^2 = (153.6 \pm 2.7) \times 10^{-17}$ cm^{-1} s^2 at 25 °C. α is the sound absorption coefficient (Np cm^{-1}) and f the frequency (in Hertz). To ensure that at the lowest temperature investigated for the electrolyte solutions, the solvent did not show a relaxation process, sound absorption measurements have been extended to the solvent at 15 °C. No relaxation process was observable and the average value was $\alpha/f^2 = (223 \pm 3) \times 10^{-17}$ cm^{-1} s^2 at 15 °C.

Electrolyte Solutions. Figure 1A and 1B reports the excess sound absorption coefficient per wavelength $\mu = \alpha_{exc}\lambda$ vs. the frequency for $Cu(ClO_4)_2$ and $Cu(NO_3)_2$ at the various temperatures and concentrations investigated. In the above $\alpha_{exc} = \alpha - Bf^2$ is the excess sound absorption coefficient, B is the value of (α/f^2) at frequencies $f \gg f_R$ where f_R is the relaxation frequency. λ is the wavelength of sound with $\lambda = u/f$ and u is the sound velocity of the solution approximated to the one of the solvent. The solid lines are the calculated functions valid for a Debye single relaxation process.[1]

$$\mu = \alpha_{exc}\lambda = 2\mu_{max}\frac{f/f_R}{1 + (f/f_R)^2} \tag{7}$$

where

$$\mu_{max} = \frac{Af_R u}{2}$$

and

$$\frac{\alpha}{f^2} = \frac{A}{1 + (f/f_R)^2} + B \tag{8}$$

The quantities A, μ_{max}, and f_R have been calculated by the iterative process described earlier.[6]

Table I reports the calculated parameters f_R, μ_{max}, and B for the two electrolytes $Cu(ClO_4)_2$ and $Cu(NO_3)_2$ in ethylene glycol at the various concentrations and temperatures investigated. Ultrasonic data expressed as (α/f^2) vs. f for $Ni(ClO_4)_2$ (0.098 M), $Cu(en)_2(ClO_4)_2$ (0.05 M), and $CuCl_2$ (0.05 M) at 25 °C do not show any relaxation effects with the exception of

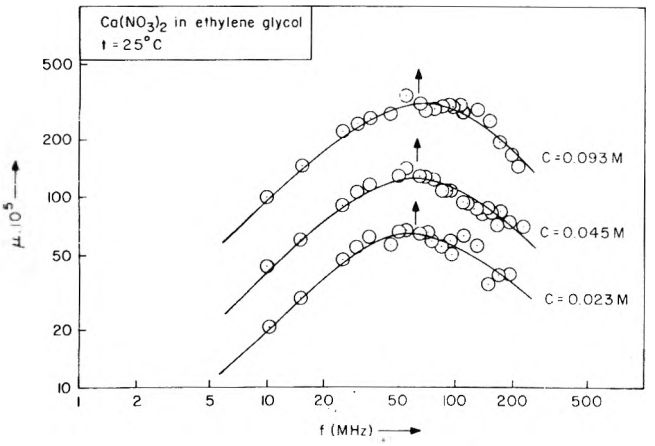

Figure 2. μ vs. f for $Ca(NO_3)_2$ in glycol at 25 °C.

the presence of possible tails of relaxation processes occurring at much lower frequency ranges for $Ni(ClO_4)_2$ and $Cu(en)_2(ClO_4)_2$. Further all these electrolytes show excess absorptions with respect to the solvent value of (α/f^2) at 25 °C.

Figure 2 shows the plots of μ vs. f for $Ca(NO_3)_2$ in ethylene glycol at 25 °C and at the concentrations investigated. A Debye single relaxation process (solid lines) appears to describe the data. The relaxation frequency f_R is different (~60 MHz) from the case of the Cu^{2+} salts in ethylene glycol, the latter process being centered around $f_R \sim 40$ MHz.

In Table I are reported the parameters f_R, μ_{max}, and B for $Ca(NO_3)_2$ in glycol at 25 °C and at the concentrations investigated. The calculation has been performed as in the case of the $Cu(ClO_4)_2$ and $Cu(NO_3)_2$ in glycol.

From Table I it may be seen that for $Cu(ClO_4)_2$, $Cu(NO_3)_2$, and $Ca(NO_3)_2$ the relaxation frequency is independent of concentration within experimental error. It may be assumed therefore that a first-order or pseudo-first-order process (characterized by two phenomenological rate constants k_f and k_R) is responsible for the observed process

$$A \underset{k_R}{\overset{k_f}{\rightleftharpoons}} B$$

with $\tau^{-1} = (2\pi f_R) = k_f + k_R$ and $K = k_f/k_R$. The temperature dependence of τ^{-1} permits the separation of the two rate constants as it has been shown elsewhere.[6] In fact

$$\frac{d \ln (\tau^{-1}/T)}{d(1/T)} = -\frac{\Delta H^{\ddagger}_R}{R} + \frac{d \ln (1+K)}{d(1+K)} \frac{dK}{d(1/T)}$$

$$= -\frac{\Delta H^{\ddagger}_R}{R} - \frac{K}{1+K} \frac{\Delta H^{\circ}}{R} \quad (9)$$

For both $Cu(ClO_4)_2$ and $Cu(NO_3)_2$ in ethylene glycol, the term $(K/1 + K)(\Delta H^{\circ}/R)$ is small with respect to $\Delta H^{\ddagger}_R/R$ (see below). Then eq 9 reduces to

$$\frac{d \ln (\tau^{-1}/T)}{d(1/T)} = -\frac{\Delta H^{\ddagger}_R}{R}$$

and a plot of $\ln (\tau^{-1}/T)$ vs. $(1/T)$ shall give $-\Delta H^{\ddagger}_R/R$ as the slope and $[\ln (k/h)] + (\Delta S^{\ddagger}_R/R)$ as the intercept.

Figure 3A reports the plot of $\ln (f_R/T)$ vs. $1/T$ for $Cu(ClO_4)_2$ and $Cu(NO_3)_2$ in ethylene glycol. The two solid lines have been calculated by linear least-squares analysis. For $Cu(ClO_4)_2$ the slope = -2.435×10^3 and the intercept = 19.876 from which one calculates $\Delta H^{\ddagger}_R = 4.84$ kcal mol^{-1} and $\Delta S^{\ddagger}_R = -4.07$ eu. These values at $T = 298.2$ K give in turn $\Delta G^{\ddagger}_R = 6.05$ kcal mol^{-1} and

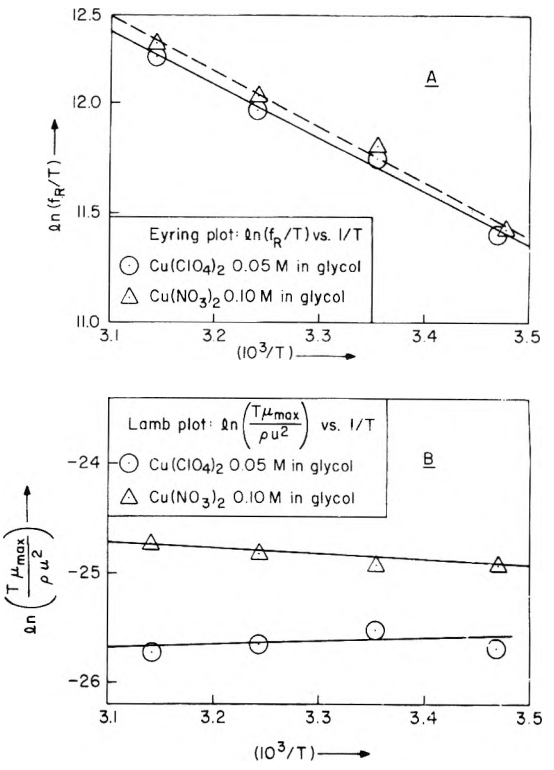

Figure 3. ln (f_R/T) vs. $1/T$ (A) and ln $(\mu_{max}T/\rho u^2)$ vs. $1/T$ (B) for $Cu(ClO_4)_2$ and $Cu(NO_3)_2$ in glycol.

$$k_R = \frac{kT}{h} \exp\left(-\frac{\Delta G^{\ddagger}_R}{RT}\right) = 2.3 \times 10^8 \text{ s}^{-1}$$

Similar analysis for $Cu(NO_3)_2$ gives a slope = -2.503×10^3 and an intercept = 20.158; $\Delta H^{\ddagger}_R = 4.97$ kcal mol^{-1}, $\Delta S^{\ddagger}_R = -3.5_1$ eu at $T = 298.2$ K, $\Delta G^{\ddagger}_R = 6.02$ kcal mol^{-1}, and $k_R = 2.4 \times 10^8$ s^{-1}. It is clear that the above parameters for the two electrolytes are numerically comparable as Figure 3A testifies (given the closeness of the two functions for the two sets of data).

In the above it was stated that the term $(K/1 + K)(\Delta H^{\circ}/R)$ was relatively small for the two electrolytes. This information derives from the calculated μ_{max} function, namely, from the excess sound absorption per wavelength at the relaxation frequency.

It has been shown[6] that for a first-order process one may write

$$\ln\left(\frac{\mu_{max}T}{\rho u^2}\right) = \ln\left(\frac{\pi(\Delta V_s)^2(B)}{2R}\right) - \ln(1+K) \quad (10)$$

$$\frac{d \ln (\mu_{max}T/\rho u^2)}{d(1/T)} = \frac{K}{1+K} \frac{\Delta H^{\circ}}{R} \quad (11)$$

assuming ΔV_s and (B) constant with T in a relatively small temperature interval.

Figure 3B reports the plot of $\ln (\mu_{max}T/\rho u^2)$ vs. $(1/T)$ for the two electrolytes. The two functions are separated because $Cu(ClO_4)_2$ has been investigated in its temperature dependence at $c = 0.05$ M, whereas for $Cu(NO_3)_2$ $c = 0.1$ M. (The difference in Figure 3B between the average position of the two functions reflects the different value of μ for the two electrolytes.) The slopes of the two functions are for $Cu(ClO_4)_2$ 258 ± 481 and for $Cu(NO_3)_2$ −510 ± 237. Because of the large relative standard error and of the smallness of the term $(K/1 + K)(\Delta H^{\circ}/R)$ with respect to the slope

$$-\left(\frac{\Delta H^{\ddagger}_R}{R} + \frac{K}{1+K} \frac{\Delta H^{\circ}}{R}\right)$$

calculated in the kinetic part of this work, one may safely neglect this quantity with respect to $\Delta H^{\pm}_R/R$, as done above. The conductance data for $Cu(ClO_4)_2$, $Cu(NO_3)_2$, and $CuCl_2$ in ethylene glycol at 25 °C have been interpreted by the Fuoss–Edelson theory[17] for associated unsymmetrical electrolytes. Accordingly, data of conductance in the diluted range should satisfy the linear correlation between Λ^* and χ

$$\Lambda^* = \Lambda_0 - \frac{K_A}{\Lambda_0}\chi \qquad (12)$$

where $\Lambda^* = \Lambda_0\gamma_1$

$$\gamma_1 = \frac{\Lambda}{\Lambda_0}F = \frac{\Lambda}{\Lambda_0}\left[1/1 + \frac{\lambda^0_{Cu}}{2\Lambda_0}\right]\left[\frac{1}{1 - \frac{S_{2:1}}{\Lambda_0}\Gamma^{1/2}} + \frac{\lambda^0_{Cu}}{2\Lambda}\right]$$

F is a factor that accounts for long range interionic effects, $S_{2:1}$ is the Onsager limiting coefficient, and $\Gamma = 3N\gamma_1$ is the ional concentration; N is the concentration of the electrolyte expressed in equivalent/liter. Also $\chi = \Lambda^*(\Lambda^* - 0.5\Lambda_0)Nf_{Cu^{2+}}$ and $f_{Cu^{2+}}$ is the single ion activity coefficient. $f_{Cu^{2+}}$ may be calculated through the limiting Debye–Hückel expression.[17] To perform the calculation of $S_{2:1}$, single ionic limiting conductances are necessary. From Spiro et al.[18] transference numbers in glycol are $\lambda_{Na^+} = 3.11$ and $\lambda^0_{Cl^-} = 5.073\ \Omega^{-1}\ cm^2\ equiv^{-1}$. Data for $NaClO_4$ in glycol[23] give $\Lambda_0 = 7.44\ \Omega^{-1}\ cm^2\ equiv^{-1}$ for this electrolyte. Then $\lambda_{ClO_4^-} = 4.33\ \Omega^{-1}\ cm^2\ equiv^{-1}$. After iteration $\Lambda^0(Cu(ClO_4)_2) = 6.84\ \Omega^{-1}\ cm^2\ equiv^{-1}$ and $\Lambda^0(CuCl_2) = 7.49\ \Omega^{-1}\ cm^2\ equiv^{-1}$ in ethylene glycol at 25 °C (see below). Therefore $\lambda^0_{Cu} = 2.51$ from $Cu(ClO_4)_2$ and $\lambda^0_{Cu} = 2.42\ \Omega^{-1}\ cm^2\ equiv^{-1}$ from $CuCl_2$ giving the average value $\lambda^0_{Cu} = 2.47\ \Omega^{-1}\ cm^2\ equiv^{-1}$.

Having determined λ^0_{Cu} and having taken λ^0_{anion} from the literature,[18] the Fuoss–Edelson method has been applied to the data for $Cu(ClO_4)_2$, $Cu(NO_3)_2$, and $CuCl_2$ in glycol. Figure 4A reports Λ^* vs. χ for $Cu(ClO_4)_2$. The solid straight line calculated by linear least-squares analysis yields from the intercept $\Lambda_0 = (6.83_5 \pm 0.00_4)\ \Omega^{-1}\ cm^2\ equiv^{-1}$, and from the slope $K_A = (34 \pm 2)\ M^{-1}$. Figure 4B reports Λ^* vs. χ for $Cu(NO_3)_2$ in glycol. The solid line gives intercept $\Lambda_0 = (7.28_2 \pm 0.007)\ \Omega^{-1}\ cm^2\ equiv^{-1}$ whereas from the slope $K_A = (86 \pm 4)\ M^{-1}$. Figure 4C reports Λ^* vs. χ for $CuCl_2$ in glycol. The solid straight line also calculated by linear least squares applied to the first four points yield from the intercept $\Lambda_0 = (7.49 \pm 0.03)\ \Omega^{-1}\ cm^2\ equiv^{-1}$ and from the slope $K_A = (1185 \pm 27)\ M^{-1}$.

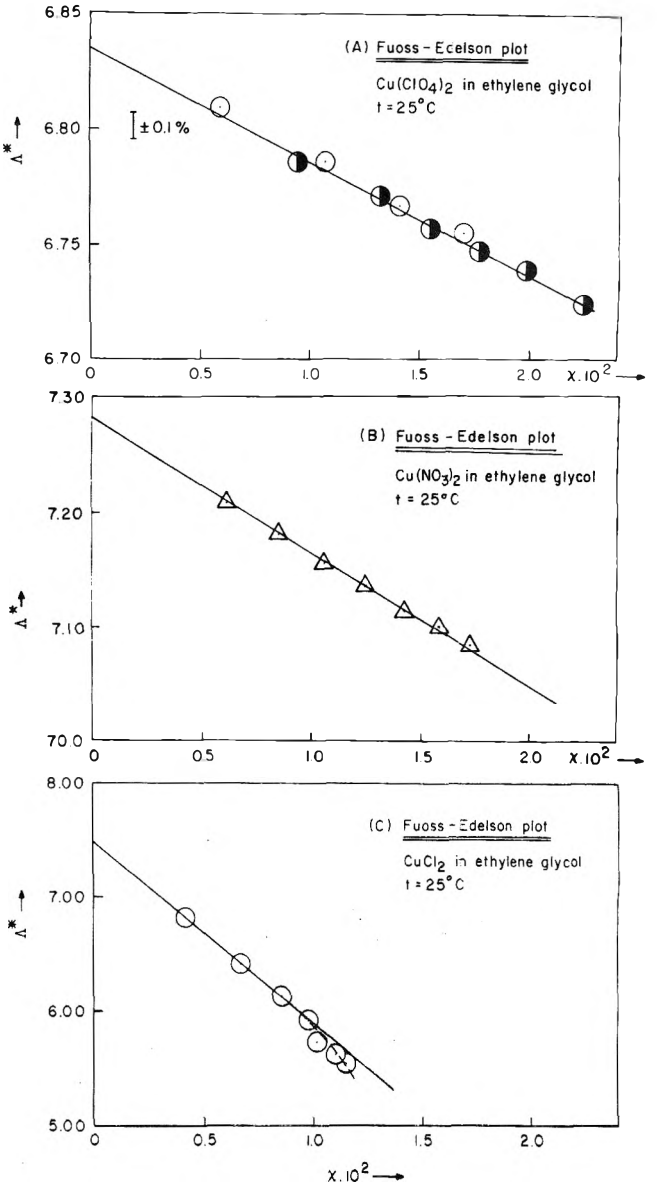

Figure 4. Fuoss–Edelson method: Λ^* vs. χ for (A) $Cu(ClO_4)_2$, (B) $Cu(NO_3)_2$, and (C) $CuCl_2$ in glycol, t = 25 °C.

Discussion

I. *Ultrasonic Relaxation.* It is of interest, at this point, to try to investigate the nature of the relaxation process studied above for $Cu(ClO_4)_2$ and $Cu(NO_3)_2$ in glycol.

The absence of a relaxation phenomenon in $Ni(ClO_4)_2$ and its presence in $Cu(ClO_4)_2$ excludes that the relaxation phenomenon is due only to the presence of ClO_4^- in glycol. Absence of the relaxation (in the experimental range of frequency) for $Cu(en)_2(ClO_4)_2$ makes the source of the relaxation process specific to the presence of Cu^{2+} and ClO_4^- in glycol solutions. On the other hand, $Cu(NO_3)_2$ shows an effect similar (in both f_R and μ_{max}) to $Cu(ClO_4)_2$ in glycol. The suspect that the relaxation process is due only to the presence of Cu^{2+} in glycol is ruled out by the absence of a relaxation process for $CuCl_2$ in glycol. Further the position of the relaxation frequency is specific to the cation, the two copper salts having $f_R \sim 40$ MHz whereas for $Ca(NO_3)_2$ $f_R \sim 60$ MHz.

The hypothesis is advanced that the relaxation phenomenon reflects the process of ionic association between Cu^{2+} and either ClO_4^- or NO_3^-. Ni^{2+} due to its slower rate of solvent exchange does not show a relaxation phenomenon in the megahertz frequency region. Ca^{2+} being a labile ion in terms of the residence of the solvent in the first coordination shell shows a relaxation process shifted to a different frequency with respect to Cu^{2+}. It is known that the rate constants of substitution of water from these two cations (axial position for Cu^{2+}) are within an order of magnitude.[19]

For $CuCl_2$ the comparatively large formation constant (see the conductance calculations) may make the degree of dissociation small enough at c = 0.05 M that a relaxation phenomenon may not be observable.

Also, the absence of a relaxation process for $Cu(en)_2(ClO_4)_2$ in the frequency range investigated could be explained (in addition of lack of association) either by assuming a square-planar structure for this ion, or by assuming that the rate of axial exchange of glycol is altered by the presence of the two equatorial "en" molecules. (One may recall that glycol chelates

Cu^{2+}.)[9] Although these rationalizations for the case of $CuCl_2$ and $Cu(en)_2(ClO_4)_2$, to explain the data, are speculative, the overall picture of the phenomena observed with the electrolytes investigated seems to concur with the hypotheses of ionic desolvation and association advanced above.

According to the above hypothesis and retaining the Eigen mechanism of association, one would expect eq 4 to apply. Identification of k_{12} and k_{21} with the diffusion controlled rate constants calculable through the Smoluchowski–Debye[7] and Eigen theories[7] (modified[8] by the introduction of the stokes–Einstein relations) gives

$$k_{12} = k_D = \frac{8NkT}{3000\eta}\frac{b}{1 - e^{-b}}$$

$$k_{21} = \frac{2kT}{\pi a^3 \eta}\frac{b}{e^b - 1}$$

$$b = \frac{|Z_+Z_-|e^2}{aDkT}$$

then $k_{12} = 2.2 \times 10^9$ M^{-1} and $k_{21} = 2.8 \times 10^7$ s^{-1} for a 2:1 electrolyte in ethylene glycol at 25 °C. In the above N is the Avogadro number, T the absolute temperature, b the Bjerrum parameter, and a the distance of approach of free ions. This parameter has been equated to the sum of the Stokes hydrodynamic radii. From the conductances of $Cu(ClO_4)_2$ and $CuCl_2$ in glycol it has been calculated $\lambda^0_{0.5Cu^{2+}} = 2.47$ Ω^{-1} cm^2 $equiv^{-1}$ and $\lambda^0_{ClO_4^-} = 4.33$ Ω^{-1} cm^2 $equiv^{-1}$. The Stokes relation $R^0_{\pm} = (0.820|Z_\pm|)/\lambda^0_{\pm}\eta$ gives $R^0_{Cu^{2+}} + R^0_{ClO_4^-} = (3.94 + 1.13)10^{-8} = 5.07 \times 10^{-8} \simeq 5 \times 10^{-8}$ cm $= a$. Other symbols have their usual meanings. The dielectric constant of glycol ($D = 40.75$) and its viscosity coefficient ($\eta = 0.1684$ P) have been taken from the literature.[8,20]

Also the expression for θ has been shown[21] to be equal to

$$\theta = \frac{\gamma_{2:1}^3}{\gamma_{1:1}^2}\left[(2\sigma + 1)C + (\sigma + 1)C\frac{\mathrm{d}\ln(\gamma_{2:1}^3/\gamma_{1:1}^2)}{\mathrm{d}\ln\sigma}\right]$$

where σ is the degree of dissociation of the electrolyte. $\gamma_{2:1}$ and $\gamma_{1:1}$ are the Debye–Hückel activity coefficients for a 2:1 and 1:1 electrolytes, respectively. They are meant to refer to electrostatic interactions between Cu^{2+} and ClO_4^- and between $CuClO_4^+$ and ClO_4^-. From the conductance data $K_A \simeq 34$ M^{-1}; forcing the Debye–Hückel expressions to hold approximatively at $C = 0.05$ M one calculates $\theta = 9.5 \times 10^{-3}$ M $\simeq 10^{-2}$ M. Then $k_{12}\theta = 2.2 \times 10^7$ s^{-1} and $k_{21} = 2.8 \times 10^7$ s^{-1}. It is obvious that a single diffusion controlled step cannot describe the experimental data. For this process Eigen shows[1] that

$$\tau^{-1} = k_{12}\theta + k_{21}$$

therefore the relaxation should be concentration dependent at 25 °C and at $C = 0.05$ M, $\tau^{-1} = 2\pi f_R = 5.0 \times 10^7$ or $f_R \simeq 8$ MHz whereas the experimental value is $f_R \simeq 40$ MHz and concentration independent within experimental error.

The alternative is to assume eq 4 to apply with the restraint that $k_{12}\theta$, $k_{21} \ll k_{23}$, k_{32} as shown in the Introduction of this paper.

If one tentatively identifies the experimental k_R with either k_{23} or k_{32}, say k_{23}, and sets $k_{23} > k_{32}$ it results from eq 4

$$S \simeq k_{12}\theta + k_{21} + k_{23} = (0.22 + 0.28 + 2.3)10^8 = 2.8 \times 10^8\ s^{-1}$$

$$P \simeq k_{12}\theta k_{23} = (0.22 \times 2.3)10^{16} = 0.5 \times 10^{16}$$

$$S_2 = 7.8 \times 10^{16} > 4P \simeq 2 \times 10^{16}$$

To ensure that the argument leading to eq 5, namely, neglect $4P$ with respect to S^2 is still permissible under the present circumstances, consider the series expansion $(1 - x)^n \simeq 1 - nx$. Then

$$\tau^{-1} = \frac{1}{2}[S + \sqrt{S^2 - 4P}] = \frac{1}{2}\left[S + S\left(1 - \frac{4P}{S^2}\right)^{1/2}\right] \simeq \frac{1}{2}\left[S + S\left(1 - \frac{2P}{S^2}\right)\right] = \frac{1}{2}\left[S + S - \frac{2P}{S}\right]$$

$$\tau^{-1} = S - \frac{P}{S} = 2.8 \times 10^8 - \frac{0.5 \times 10^{16}}{2.8 \times 10^8} = 2.8 \times 10^8 - 0.18 \times 10^8$$

implying an error of about 6% in retaining the simpler eq 5, namely

$$\tau^{-1} = S \simeq k_{23} + k_{32} \simeq k_{23}$$

Notice, however, that the experimental $k_R = 2.4 \times 10^8$ s^{-1} could be identified with either k_{23} or k_{32} without any possibility of distinction from the ultrasonic data alone. That S should be identified with either k_{23} or k_{32} transpires from the value of k_R itself. If $S \simeq 2.8 \times 10^8$ and $\tau^{-1} = S$, $f_R = 45$ MHz, namely, around the value obtained above. S has been calculated as $S \simeq k_{12}\theta + k_{21} + k_R$ whether $k_R = k_{23}$ or $k_R = k_{32}$. Addition of another term after k_R would bring τ^{-1} way off from the experimental value. Also, by retaining only $\tau^{-1} = S \simeq k_R = 2.3 \times 10^8$, $f_R = 37$ MHz which is slightly below the average experimental value.

The above discussion would bring us to the conclusion that $k_{23} > k_{32}$ or $k_{23} < k_{32}$ depending on the identification of k_R with either one of the two rate constants.

The fact that the two activation parameters $\Delta H^{\ddagger}_R$ and $\Delta S^{\ddagger}_R$ are comparable for Cu^{2+} with two different ligands might suggest, at first sight, that indeed we are observing the behavior of k_{23} for a SNI or Id mechanism, k_{23} being ligand independent. However, one may take exception to this conclusion recalling that in both cases a Cu^{2+}–oxygen bond is broken in relation to the rate constant k_{32} and mechanism 2 for both NO_3^- and ClO_4^- ions. Hence one could expect similarity for k_{32} for the two ligands.

One may borrow, however, information from conductance data recalling that $Cu(ClO_4)_2$ and $Cu(NO_3)_2$ are weakly associated to $CuClO_4^+$ and $CuNO_3^+$ in glycol (with $K_A = 34$ M^{-1} and $K_A = 86$ M^{-1}, respectively).

The Fuoss–Jagodzinski formation constant[14c] equated to $K_{12}^{-1} = k_{12}/k_{21}$ gives

$$K_F = \frac{4\pi Na^3}{3000}e^{-1/2}e^b = 46.6$$

for a 2:1 electrolyte in glycol at 25 °C taking $a = 5 \times 10^{-8}$ cm ($a = R_+^0 + R_-^0$).

Then given the Eigen[1] association relation

$$K_\Sigma = K_{12}^{-1}(1 + K_{23}^{-1})$$

If one identifies K_Σ with K_A one finds out that K_Σ is of the same order of magnitude as the calculated K_F for $a = 5$ Å. This would bring us to conclude that $K_{23}^{-1} = k_{23}/k_{32} < 1$ or that $k_{23} \lesssim k_{32}$. On the basis of this calculation one would be inclined to identify k_R with k_{32} rather than with k_{23}.

II. *Electrical Conductance.* Objections could be raised for having used the Fuoss–Edelson[17] equation which is based on the limiting law of Onsager for the equivalent conductance. In particular the physical significance of a small association

constant could be questioned since inclusion of more terms in the conductance equation than the $S_{2:1}$ Onsager interionic term could swamp off K_A. Murphy and Cohen[22] have indeed developed equations for unassociated unsymmetrical electrolytes containing terms up to the first power in the concentration. Unfortunately, these authors did not develop the theory up to the $c^{3/2}$ coefficient, their equation remaining therefore incomplete. Terms in $c^{3/2}$ are of basic importance[15] when trying to calculate small association constants with accuracy.

Indication of the physical meaning of the determined $K_A = 34\ M^{-1}$ for $Cu(ClO_4)_2$ in glycol, at least as an order of magnitude, may be offered by comparison with the same quantities determined earlier in acetonitile[21] ($K_A = 80\ M^{-1}$) and in methanol[4b] ($K_A = 193\ M^{-1}$). These values were obtained by applying the Fuoss–Edelson theory to conductance data of $Cu(ClO_4)_2$ with respective solvents. A plot of log K_A vs. $1/D$ for the above data shows a linear correlation. The assumption that the dependence of K_A on the dielectric constant D is mainly due to K_{12}^{-1}, as the relation

$$K_A = K_{12}^{-1}(1 + K_{23}^{-1}) = \frac{4\pi Na^3}{3000} e^{-1/2} e^b (1 + K_{23}^{-1})$$

may suggest (since K_{23}^{-1} is of the order of unity in all cases) ($b = |Z_+Z_-|e^2/aDkT$), leads to the identification of the slope of the log K_A vs. $1/D$ plot with the quantity $0.4343\,|Z_+Z_-|e^2/akT$). Least-squares analysis gives a slope = 123.0 and an intercept = −1.506.

From the computed slope one can calculate $a_K = 3.95 \times 10^{-8}$ cm $\simeq 4 \times 10^{-8}$ cm in fair accord with $a_\lambda \simeq (R_-^0 + R_-^0) = 5 \times 10^{-8}$ cm from the Stokes hydrodynamic relation. The above correlation between the K_A's seems to give support to the reliability of the physical significance of the determined association constants, at least as orders of magnitude of the actual association constants.

Supplementary Material Available: A plot of the quantity α/f^2 vs. f for $Ni(ClO_4)_2$, $Cu(en)_2(ClO_4)_2$, and $CuCl_2$ in glycol, the experimental equivalent conductances and the corresponding concentrations for $Cu(ClO_4)_2$, $Cu(NO_3)_2$, and $CuCl_2$ in glycol, and a plot of the quantity log K_A vs. $1/D$ for $Cu(ClO_4)_2$ (3 pages). Ordering information is available on any current masthead page.

References and Notes

(1) M. Eigen and L. DeMaeyer in "Investigation of Rates and Mechanisms of Reaction", Vol. VIII, part II, A. Weissberger, Ed., Wiley-Interscience, New York, N.Y., 1963.
(2) C. H. Langford and H. B. Gray, "Ligand Substitution Processes", W. A. Benjamin, New York, N.Y., 1965; S. Petrucci in "Ionic Interaction", Vol. II, Chapter II, C. H. Langford, Ed., Chapter I, Academic Press, New York, N.Y., 1971.
(3) L. G. Jackopin and E. Yeager, *J. Phys. Chem.*, **74**, 3766 (1970).
(4) (a) F. Dickert and H. Hoffmann, *Ber. Bunsenges. Phys. Chem.*, **75**, 1320 (1971); (b) J. Williams, S. Petrucci, B. Sesta, M. Battistini, *Inorg. Chem.*, **13**, 1968 (1974); (c) J. Williams and S. Petrucci, *J. Phys. Chem.*, **77**, 130 (1973).
(5) H. Wang and P. Hemmes, *J. Am. Chem. Soc.*, **95**, 5119 (1973).
(6) H. Farber and S. Petrucci, *J. Phys. Chem.*, **80**, 327 (1976).
(7) M. Von Smoluchowski, *Phys. Z.*, **17**, 557 (1916); P. Debye, *Trans. Electrochem. Soc.*, **82**, 265 (1942); M. Eigen, *Z. Phys. Chem. (Frankfurt am Main)*, **1**, 176 (1954).
(8) S. Petrucci, *J. Phys. Chem.*, **71**, 1174 (1967).
(9) R. G. Pearson and R. D. Lanier, *J. Am. Chem. Soc.*, **86**, 765 (1964).
(10) H. P. Bennetto and E. F. Caldin, *J. Chem. Soc. A*, 2191, 2198 (1971).
(11) Reference 4b.
(12) A. Weissberger, Ed., "Techniques of Organic Chemistry", Vol. VII, "Organic Solvents", 2d ed, Wiley, New York, N.Y., 1955.
(13) P. Arthur, W. M. Haynes, and P. Varga, *Anal. Chem.*, **38**, 1630 (1966).
(14) S. Petrucci and M. Battistini, *J. Phys. Chem.*, **71**, 1181 (1967); ref 8; P. Jagodzinski and S. Petrucci, *J. Phys. Chem.*, **78**, 917 (1974).
(15) C. DeRossi, B. Sesta, M. Battistini, and S. Petrucci, *J. Am. Chem. Soc.*, **94**, 2961 (1972).
(16) G. S. Darbari, M. R. Richelson, and S. Petrucci, *J. Chem. Phys.*, **53**, 859 (1970).
(17) R. M. Fuoss and D. Edelson, *J. Am. Chem. Soc.*, **73**, 269 (1951).
(18) M. Carmo Santos and M. Sprio, *J. Phys. Chem.*, **76**, 712 (1972).
(19) M. Eigen in "Coordination Chemistry", IUPAC 7th International Conference of Coordination Chemistry, Butterworths, London, 1963, p 97.
(20) F. Accascina and S. Petrucci, *Ric. Sci.*, **30**, 808 (1960).
(21) A. Diamond, A. Fanelli, and S. Petrucci, *Inorg. Chem.*, **12**, 611 (1973).
(22) T. J. Murphy and E. G. D. Cohen, *J. Chem. Phys.*, **53**, 2173 (1970).
(23) Unpublished data from this laboratory.

COMMUNICATIONS TO THE EDITOR

Alleged Solubility Product Variability at Constant Pressure and Temperature

Sir: In a recent paper, Stearns and Berndt[1] ascribe apparent variations in solubility product with solution composition to the effects of nonstoichiometric composition of the solid phase which was calcium fluoride. At high temperatures, departures from stoichiometric composition occur for compounds of multivalent elements, but it seems most unlikely that any actual departure of a compound such as CaF_2 from stoichiometric composition at room temperature could cause effects of the magnitude noted. On the other hand, the treatment by Stearns and Berndt of the activity coefficients in solution could easily be in error by the variation noted.

Stearns and Berndt assumed that the activity coefficient for a given solute was a function purely of ionic strength and independent of the specific ions actually present. While that is an acceptable basis for rough estimates, it has been known, at least since the papers of Brønsted,[2] that activity coefficients actually depend on interactions among the particular ions present, and Guggenheim and Turegon[3] presented a method of representing these specific ion interactions. Kim and the writer[4] recently developed a refined set of equations appropriate for mixed electrolytes yielding excellent agreement with data for mixtures as complex as sea water as well as for several mixtures of three solutes and a large number of mixtures of two solutes.

The solutions used by Stearns and Berndt[1] involving acetate buffers, could, in principle, be treated by the equations of Pitzer and Kim,[4] but the calculations would be complex and not all of the parameters are readily available. The effects of specific ion interaction on the activity coefficient for CaF_2 can be illustrated, however, in simpler systems where the important parameters have been tabulated.[5] For example, consider solutions of constant ionic strength I with NaCl(m_1) and either $CaCl_2$(m_2) or NaF(m_3). If we neglect the solubility of CaF_2, $I = m_1 + 3m_2$ or $I = m_1 + m_3$. Equation 15 of Pitzer and Kim[4] then yields $\ln \gamma(CaF_2)$ in terms of the interaction parameters $\beta^{(1)}$ and $\beta^{(1)}$ for NaCl, $CaCl_2$, and NaF, all of which are known.[5] The parameter for Na^+–Ca^{2+} interaction[4] is known to be zero; those for F^-–Cl^- and for Ca^{2+}–F^- interactions are not known and will be neglected, but they could not change our general conclusion.

Table I gives the ratio of the product $\gamma_{Ca^{2+}}\gamma_{F^-}{}^2$ for a solution with $CaCl_2$ or NaF added to that for the solution of NaCl alone of the same ionic strength. This ratio would be unity for the treatment used by Stearns and Berndt. An ionic strength of 0.6 was chosen to correspond to their conditions. It is noted that the ratio calculated from the equations recognizing specific ion effects differs from unity by nearly a factor of 2 for 0.1 M excess Ca^{2+}. In the paper of Stearns and Berndt the maximum departure from constancy of their solubility product was also about a factor of 2 for a similar 0.1 M excess of Ca^{2+}. Hence it is clear that the entire effect of Stearns and Berndt is no larger than variations which might be expected in view of the approximations in their calculations of activity coefficients. Thus there is no need to assume any variation in solubility product of CaF_2 with solution composition at constant pressure and temperature.

TABLE I: Calculated Values of the Ratio of the Product $\gamma_{Ca^{2+}}\gamma_{F^-}{}^2$ for Solutions with Excess $CaCl_2$ or NaF to that for NaCl at Constant Ionic Strength of 0.6 M

$m(CaCl_2)$	Ratio	m(NaF)	Ratio
0.01	0.953	0.01	0.976
0.02	0.908	0.02	0.953
0.05	0.791	0.05	0.887
0.1	0.632	0.1	0.784

References and Notes

(1) R. I. Stearns and A. F. Berndt, *J. Phys. Chem.*, **80**, 1060 (1976).
(2) J. N. Brønsted, *Kgl. Dan. Vidensk. Selsk., Mat. Fys. Medd.*, **4**, (4) (1921); *J. Am. Chem. Soc.*, **44**, 877 (1922); **45**, 2898 (1923).
(3) E. A. Guggenheim and J. C. Turgeon, *Trans. Faraday Soc.*, **51**, 747 (1955).
(4) K. S. Pitzer and J. J. Kim, *J. Am. Chem. Soc.*, **96**, 5701 (1974).
(5) K. S. Pitzer and G. Mayorga, *J. Phys. Chem.*, **77**, 2300 (1973).

Department of Chemistry **Kenneth S. Pitzer**
University of California
Berkeley, California 94720

Received June 14, 1976

On the Variable Solubility Product of Calcium Fluoride

Publication costs assisted by the University of Missouri—Rolla

Sir: Recently, Stearns and Berndt presented a theoretical development and experimental evidence for the variability of the solubility product of calcium fluoride at constant temperature and pressure.[1] Basing their theoretical development on the statement (referred to "any standard text on physical chemistry"), "When two phases are in equilibrium then *the* chemical potentials of each and every chemical species are the same in both phases," they equate the chemical potentials of individual ions in the solid and aqueous phases, and proceed to a thermodynamic proof that the chemical potential of the solid must vary as the concentrations of the ions in solution are varied. The quoted statement above may at first glance appear to be a paraphrasing of a statement by Moore,[2] "For any component i in the system, the value of the chemical potential μ_i must be the same in every phase, when the system is in equilibrium at constant T and P." However, shortly preceding this statement, Moore specifically defines *components* as, ". . . those constituents the concentrations of which may be *independently varied* in the various phases." Clearly, the concentrations of cations and anions in a phase

cannot be independently varied without violation of the condition of electrical neutrality. In the strict definition of a partial molar property, the term chemical potential can only be applied to a constituent for which the number of moles may be independently varied. Thus the assignment of chemical potentials to individual ions in solution is a matter of convenience, not of thermodynamic rigor.

Stearns and Berndt take the position that nonstoichiometry in the crystal, due to point defects, allows independent variation of the concentrations of cation and anion. While this may be true on the microscopic level, it cannot be true on the macroscopic level to which thermochemical properties are normally assigned. Since it is possible for crystals to be formed in some manner which will produce enough defects to alter the average chemical potential of the components, much in the same manner that extremely small crystals can show appreciably different thermochemical properties in comparison to larger crystals, one cannot rule out the possibility that a solid may show different thermochemical properties under different conditions at a particular temperature and pressure. However, the thermodynamic treatment presented by Stearns and Berndt requires that the degree of nonstoichiometry of the crystal vary (depending on the concentration of ions in the solution) in the approach to equilibrium—something of a contradiction in terms. Even if this were thermodynamically acceptable, the variation of crystalline stoichiometry would create net electrical charges in the bulk phases, more than a simple electrical double layer. The chemical potentials of crystalline ions arbitrarily defined by Stearns and Berndt as functions of temperature, pressure, and composition would also be dependent on the electrical work required to vary the nonstoichiometry of the crystal. Thus the "theory" presented by Stearns and Berndt is not thermodynamically rigorous. The thermodynamic treatment of point defects and nonstoichiometry in crystals would appear to be most properly approached from the principles of small system thermodynamics.

The experimental evidence presented to support the premise of a variable solubility product is tenuous at best. The calculations ignore the presence of species such as nonionic sodium acetate in solution[3] and CaF^+,[4] and while the complex $Ca(CH_3COO)^+$ is considered, the equilibrium constant used[5] differs appreciably from a more recent value,[3] and the effect of ionic strength on this equilibrium constant is not considered. Incorporation of these more detailed effects into the calculations of the data presented by Stearns and Berndt can substantially change the calculated values of the solubility product. However, the data presented are probably flawed by the lack of measurements of the total amount of calcium present in solution at equilibrium. Fluoride is assumed to exist entirely as F^- and HF in solution, and the concentration of calcium in solution is calculated as half of the sum of concentrations of F^- (measured with the fluoride electrode) and HF (calculated from the ionization constant of HF and the pH of the solution), plus the concentration added as calcium nitrate. These assumptions ignore the possibility of associated forms of fluoride, such as CaF^+, and the possibility of calcium as an impurity in the reagents used. We have analyzed some reagent grade samples of sodium acetate trihydrate by atomic absorption spectroscopy, and found that they contained 0.01–0.03% calcium. In a buffer solution containing 0.59 M sodium acetate, this could give a calcium concentration of 6×10^{-4} M, comparable to the concentration of fluoride observed by Stearns and Berndt in a saturated solution of CaF_2 to which no calcium was added. We attempted to reproduce their experiments using a solution prepared from anhydrous sodium acetate which showed very small calcium impurities. A solution containing 0.590 M sodium acetate and 0.030 M acetic acid had a pH of 5.97 and contained less than 2×10^{-5} M calcium. Calcium fluoride (Fisher Certified Reagent) was added to this solution, which was shaken for 3 h at 20.00 °C. The fluoride concentration as measured with the Orion 94-09 electrode was 6.2×10^{-4} M, as compared to the value of 7.0×10^{-4} M reported by Stearns and Berndt. The solution was filtered through a membrane filter with a pore size of 0.45 μm, giving a clear filtrate with no visible turbidity. Repetitive filtrations of different samples through the membrane filter and through a fine sintered glass filter gave calcium concentrations (as determined by atomic absorption analysis) of $(2.7 \pm 0.1) \times 10^{-3}$ M, eight times the value calculated from the fluoride concentration with the assumptions of Stearns and Berndt. While our experiments are not definitive, they indicate that the experimental situation studied by those workers is considerably more complex than they have assumed.

It is ironic that the experimental evidence on which Stearns and Berndt base their proof of a variable chemical potential of calcium fluoride is entirely based on measurements with the specific fluoride ion electrode, the operation of which assumes an invariant chemical potential of the europium-doped lanthanum fluoride crystal.

References and Notes

(1) R. I. Stearns and A. F. Berndt, *J. Phys. Chem.*, **80**, 1060 (1976).
(2) W. J. Moore, "Physical Chemistry", 4th ed, Prentice-Hall, Englewood Cliffs, N.J., 1972, p 207.
(3) D. W. Archer and C. B. Monk, *J. Chem. Soc.*, 3117 (1964).
(4) R. E. Connick and M. S. Tsao, *J. Am. Chem. Soc.*, **76**, 5311 (1954).
(5) C. A. Coleman-Porter and C. B. Monk, *J. Chem. Soc.*, 4363 (1952).

Department of Chemistry
University of Missouri—Roila
Rolla, Missouri 65401
Gary L. Bertrand*
Thomas E. Burchfield

Received June 21, 1976

Solubility Product Variability at Constant Pressure and Temperature

Publication costs assisted by the National Institute of Dental Research

Sir: Recently, Stearns and Berndt[1] reported variation in the apparent solubility product of CaF_2 with the activity of the Ca^{2+} ion in solution. They attributed the variation to changes in the defect composition of the solid phase even though "These deviations from stoichiometry may be too small to measure by ordinary chemical analysis. . . .". Their values of the apparent solubility products varied from 3.4 to 6.5×10^{-12} (a range of about 0.4 kcal/mol in the chemical potential of CaF_2). They also concluded that "the observed variation is real and is not caused by an artifact in the Debye–Hückel theory". The ionic strengths of their solutions varied between 0.585 and 0.734. Since the initial solid was the same for all the equilibrations, it was implicitly assumed that equilibration of this solid with a given solution shifted its defect composition spontaneously to fulfill the thermodynamic requirements of the solution. Their conclusions, if valid, would have far-reaching ramifications.

To test the thermodynamic feasibility of their proposal, assume that CaF_2 exists as a continuous series of nearly stoichiometric solids in which the chemical potential of the component CaF_2 varies as a function of the defect content. Assume further that one of these solids with a solubility product of 3.4×10^{-12} (solid A) is placed into a solution in equilibrium with solid B (ion activity product = 6.5×10^{-12}). According to the thesis of Stearns and Berndt, the solution in equilibrium with solid B would tend to convert the defect structure of solid A into that of solid B with an increase in Gibbs free energy of 0.4 kcal/mol of solid A. Since this process would not be accompanied by a significant change in the composition of the solution or in the chemical potential of CaF_2 in solid B, the net result would be a spontaneous increase in the Gibbs energy of the system, a thermodynamic impossibility. Actually, CaF_2 from the solution should precipitate on solid A because this would be accompanied by a decrease in Gibbs energy; the consequent decrease in the solution concentration would lead to dissolution of solid B, with a further decrease in Gibbs energy, so that at final equilibrium only solid A would be present and the ion activity product in the solution would be 3.4×10^{-12}. Thus, in general, only the solid with defect composition corresponding to the lowest solubility product (i.e., lowest chemical potential of the component CaF_2) would be the true equilibrium solid within any series of defect solids *with nearly the same composition* but different Gibbs energies. It is shown next that this conclusion is compatible with the Gibbs–Duhem equation.

Of various possible equilibrium models for the defect structure of CaF_2, Stearns and Berndt used one in which Ca^{2+} and F^- can be defined as the components. This choice, since it does not take into account neutrality of charge, cannot lead to significant variations in stoichiometry, and it is contrary to their eq 1–4 which are applicable only when the liquid and solid phases are at the same potential. However, the Gibbs–Duhem equation applied to their model gives

$$m_{Ca^{2+}}\, d\mu_{Ca^{2+}} = -m_{F^-}\, d\mu_{F^-}$$

where $m_{Ca^{2+}}$ and m_{F^-} closely approximate the stoichiometric coefficients 1 and 2, respectively, and μ is a chemical potential. Thus, as long as the composition of the solid is nearly stoichiometric, a change in the chemical potential of Ca^{2+} would have a compensatory change in the chemical potential of F^-, and the chemical potential of CaF_2 in the solid would remain essentially constant. More suitable, electrically neutral models of the defect solid represented by other choices of components (e.g., Ca and F_2; CaF_2 and Ca or F_2; and $Ca(OH)_2$, HF, and H_2O) can be shown to yield the same result.

Stearns and Berndt chose to ignore the 100-fold difference in the solubility products they calculated from the data of Auméras[2] as compared with those derived from their own data. Instead, they noted an apparent similarity in that both sets of data seem to define similarly shaped curves, but with less than twofold variations in the apparent solubility products. It seems tenuous, however, to attribute significance to a small variation and at the same time to disregard a 100-fold difference. It is more reasonable to attribute the variation in their apparent solubility product to inadequate descriptions of the equilibria within the solution phase, to difficulties in calculating the activities of Ca^{2+} and F^- ions at such high ionic strengths, and to experimental error.

These considerations do not preclude either of the two possibilities: (i) that solids prepared under equilibrium conditions can vary in composition (although these variations tend to be small except at elevated temperatures), and (ii) that the Gibbs energies of stoichiometric solids prepared under irreversible conditions may exceed their equilibrium values. The proposal of Stearns and Berndt, however, relates to the Gibbs energy of a nearly stoichiometric solid under equilibrium conditions. This proposal, as shown here, is contrary to theory and is based on inadequate experimental evidence; it should not be accepted as a satisfactory basis for invalidating the useful and well-established solubility product concept when it is applied to a solid with sensibly constant composition.

References and Notes

(1) R. I. Stearns and A. F. Berndt, *J. Phys. Chem.*, **80**, 1060 (1976).
(2) M. Auméras, *J. Chim. Phys. Phys., Chim. Biol.*, **24**, 548 (1927).

American Dental Association
Health Foundation Research Unit
National Bureau of Standards
Washington, D.C. 20234
Walter E. Brown

Received August 2, 1976

Reply to Comments on Solubility Product Variation

Sir: Since the appearance of our recent article[1] a number of investigators have written commentaries on this work. Three letters are reproduced here and others have been sent directly to us. Some of the commentators are disturbed by the conclusion and find it difficult to accept. Our paper challenges a concept universally accepted for over a century and, therefore, this is to be expected.

In trying to show that our conclusion is invalid, some of these commentators focus the thrust of their criticism on the experimental results and the calculations by which they were derived. In so doing they miss the main point. Our paper is a theoretical paper and not an experimental one. Our theory is based on the logical and systematic application of the basic laws of thermodynamics. It is not the result of an experimental investigation.

We presented a theoretical, deductive proof that the classical solubility product is not constant at constant temperature and pressure but must vary with activities in the liquid phase. We do not believe that the validity of the deductive proof has been seriously questioned. Experimental data were included in the paper because a theoretical argument is more easily accepted if experimental data are available to support it. If these data were not there, then one could say, "Yes, theoretically the classical solubility product does vary but the variation is far too small to be measured experimentally and is therefore of no consequence". Without experimental data we could not answer this.

We agree that the Debye–Hückel limiting law has its shortcomings and perhaps we should have considered the formation of complex ions other than the $CaAc^+$. Many of the other criticisms of the experimental techniques and calculations have a degree of validity. In this connection it is interesting to note that Professor Richard W. Ramette of Carlton College has recalculated our results using the Davies equation for the approximation of activities and found that the maximum persists. His results support our theory and are satisfying in that his values of the solubility product calculated from our

data are closer to the accepted literature value. Moreover, he has obtained independent experimental data with CaF_2 that further support our theory.

In an attempt to overcome Pitzer's objections surrounding the validity of the Debye–Hückel limiting law we have conducted some experiments in which the total ionic strength was quite low (<0.01). The resulting data tend to support our original conclusions, but unfortunately in these experiments the range of calcium ion activities is too small and the error in the measured fluoride ion activities (~4%) is too large to present firm conclusions. However, it is important to note that Pitzer's correction would not account for the observed maximum but would only account for a monotonic trend.

The CaF_2 system was not the only one studied nor calculated from literature data. In all other cases examined a variation of the apparent solubility product was found, but this variation was either monotonically increasing or decreasing. Since this type of variation could be easily dismissed as a shortcoming of the Debye–Hückel limiting law or due to inaccuracies in the values of equilibrium constants used, we felt that their inclusion would not strengthen our arguments. The CaF_2 system was discussed for two reasons. The maximum cannot be accounted for by errors in the Debye–Hückel theory and literature data were available as well as our own experiments.

Bertrand and Burchfield question the possibility of calcium contamination of reagent grade sodium acetate. We have prepared a 0.01 M sodium acetate solution which was simultaneously 0.01 M in F^-. No evidence of any precipitate was observed. If the solubility product of CaF_2 is taken as approximately 3×10^{-11} then the $[Ca^{2+}]$ in this solution must be less than 3×10^{-7} M which makes the molar ratio of Ca^{2+}/Na^+ in the reagent $< 3 \times 10^{-5}$.

In his letter Brown uses an experimental argument in an attempt to refute our theory. He states (correctly) that the chemical potential of CaF_2 is a function of the defect content and then considers the effect of adding solid CaF_2 (A) to a solution in equilibrium with solid CaF_2 (B) where the defect contents of A and B are such that the solubility product of A is less than that of B. He claims that, according to our thesis, a spontaneous process will occur which is accompanied by an increase in Gibbs free energy. This cannot be and is not stated or implied in anything we have said. What does happen is that the composition of the solution will change, albeit slightly, as the net result of precipitation of CaF_2 onto solid A and dissolution of some of the solid B. The defect content of both sides will change and equilibrate at some common intermediate value. This process is accompanied by a net decrease in the Gibbs free energy. If the solids did not change in defect content then his conclusion that B would dissolve and A would precipitate would be valid. The key here is that the defect contents of the solid change.

We appreciate the interest of those scientists who have studied and commented upon our results. We are confident that their efforts will ultimately result in acceptable experimental evidence of the validity of our theoretical conclusions.

Reference and Notes

(1) R. I. Stearns and A. F. Berndt, *J. Phys. Chem.*, **80**, 1060 (1976).

Department of Chemistry
University of Missouri—St. Louis
St. Louis, Missouri 63121
Robert I. Stearns
Alan F. Berndt*

Received June 21, 1976

Isotope Separation Using the Effect of Resonant Microwaves on the Rate of Triplet State Photochemistry in Solids

Publication costs assisted by the U.S. Energy Research and Development Administration

Sir: The rate of solid state photochemistry of excited triplet molecules at low temperatures, when the spin–lattice relaxation between the zero-field (zf) spin levels is slow, can be altered by exposing the excited sample to microwave radiation in resonance with its zf transitions.[1] In general, the effect can result either from changing the steady state population of triplet molecules in the triplet state or from the difference in the reactivity of molecules in the different spin levels.

Triplet molecules with atoms having a nuclear spin, $I > \frac{1}{2}$, normally show hyperfine lines resulting from electron–nuclear spin transitions, a set for each isotope in the isotopic mixture. The irradiation with microwaves having a frequency corresponding to only one isotope can change the rate of photochemistry of its triplet molecules from that for the molecules containing the other isotopes in the sample. This leads to preferential photochemical destruction of molecules containing one isotope over the other(s). In this note, we propose this technique for separating N, Cl, Br, B (and maybe U) isotopes and derive an expression relating the isotope separation factor to characteristic pumping and decay rate constants of the reacting triplet molecules.

Similar to Leung and El-Sayed's derivation for biphotonic reaction,[1,2] one obtains the following expression for the ground state population as a function of time as the monophotonic photochemical reaction proceeds at 1.6 K:

$$S_0(t) = S_0(0) \exp - \left[\frac{\sum_i \frac{\gamma_i \alpha_i}{\beta_i} I}{1 + \sum_i \frac{\alpha_i}{\beta_i} I} \right] t \qquad (1)$$

$$= S_0(0) \exp - K_{(I)} t$$

where γ_i is the photochemical rate constant of zero-field level i, α_i is the pumping rate constant to that level, and β_i is its total decay rate. I is the intensity of the exciting light and the summation is over all the nuclear and electron spin levels. Assuming the absence of nuclear spin diffusion, the microwave saturation of levels 1 and 2 that have different electron and nuclear spin quantum numbers changes eq 1 to

$$S_0(t) = S_0(0) \times \exp - \frac{\left[(\gamma_1 + \gamma_2) \frac{(\alpha_1 + \alpha_2)}{\beta_1 + \beta_2} + \sum_{i'} \frac{\gamma_{i'} \alpha_{i'}}{\beta_{i'}} \right] It}{1 + \left[2 \frac{(\alpha_1 + \alpha_2)}{\beta_1 + \beta_2} + \sum_{i'} \frac{\alpha_{i'}}{\beta_{i'}} \right] I} \qquad (2)$$

$$= S_0(0) \exp - [K_{12(I)} t]$$

where the primes refers to summation not including the levels being saturated.

For a sample containing A and B isotopes, with B-containing molecules reacting according to eq 2 and those containing A according to eq 1, the time dependence of the ratio of B to A molecules in the ground state is given by

$$\left(\frac{N_B}{N_A} \right)_t = \left(\frac{N_B}{N_A} \right)_0 \exp - [K_{12(I)} - K_{(I)}] t \qquad (3)$$

which gives the isotope separation factor (σ) as a function of time the form:

$$\sigma(t) = \left(\frac{N_B}{N_A}\right)_t \Big/ \left(\frac{N_B}{N_A}\right)_0 = \exp -[K_{12(I)} - K_{(I)}]t \quad (4)$$

Equation 4 applies to biphotonic processes too, except that $K_{12(I)}$ and $K_{(I)}$ are given by the equations derived by Leung.[1,2]

Equations 1, 2, and 4 show that at high light intensities, $\sigma(t)$ would differ from unity only if the spin levels being saturated differ in their chemical reactivity (i.e., different γ). At low and intermediate intensities, large population differences between the spin levels together with large differences in the decay rates ($\beta_i \neq \beta_j$) would lead to isotope enrichment even if the photochemical reactivity of the different spin levels is the same. Our calculations further show that, for the same system, monophotonic processes give more efficient separation than biphotonic ones. The above equations also indicate that the effect of microwaves is more pronounced the less the number of nuclear spin levels per electron spin level or if nuclear spin diffusion is fast. Statistical analysis shows that the effect of microwaves is reduced for molecules that contain more than one isotopic atom per molecule (e.g., di or tri instead of mono derivatives).

Acknowledgment. The authors wish to thank Dr. Peter Esherick for valuable discussion of this problem. The financial support of the United States Energy Research and Development Administration is gratefully acknowledged.

References and Notes

(1) M. Leung and M. A. El-Sayed, *J. Am. Chem. Soc.*, **97**, 669 (1975).
(2) M. Leung, Thesis, Chemistry Department, UCLA, 1974.
(3) Contribution No. 3704.

Department of Chemistry[3] **Talal Akasheh**
University of California **M. A. El-Sayed***
Los Angeles, California 90024

Received August 24, 1976

Stratospheric Formation and Photolysis of Chlorine Nitrate[1]

Publication costs assisted by the U.S. Energy Research and Development Administration

Sir: Our current experiments and calculations indicate the possible existence in the mid-stratosphere of an additional chlorine-containing species, $ClONO_2$,[3] which is usually identified by the name chlorine nitrate. Seven of the most important chemical reactions of chlorine in the stratosphere are summarized by the equilibria

$$HCl \underset{CH_4,H_2,HO_2}{\overset{OH}{\rightleftharpoons}} Cl \underset{O,\ NO}{\overset{O_3}{\rightleftharpoons}} ClO \quad (1)$$

involving Cl, ClO, and HCl, and have been described in considerable detail earlier.[4] The most probable method for formation of $ClONO_2$ involves the reaction of ClO with NO_2, with stabilization by a third body, as in[5]

$$ClO + NO_2 + M \rightarrow ClONO_2 + M \quad (2)$$

One important method for decomposition of $ClONO_2$ in the stratosphere is through its photolysis by ultraviolet radiation, presumably by one of the following mechanisms:[6]

$$ClONO_2 + h\nu \rightarrow ClO + NO_2 \quad (3a)$$

$$\rightarrow Cl + NO_3 \quad (3b)$$

Chlorine nitrate does not react rapidly with most stable atmospheric species (N_2, O_2, CO_2, SO_2, CH_4, H_2, NO_2), but does react with NO, with oxygen atoms[7,8] as in[7]

$$O + ClONO_2 \rightarrow ClO + ONO_2 \quad (4)$$

and perhaps by other radical reactions as well. The stratospheric chlorine equilibria of (1) can thus be extended to include $ClONO_2$, as in

$$ClO \underset{h\nu,\ O}{\overset{NO_2}{\rightleftharpoons}} ClONO_2 \quad (5)$$

If the alternative pathway of (3b) is important then the pathways to equilibrium are diagrammatically slightly more complex, without any appreciable quantitative effect on the equilibria themselves.

We report here the photochemical absorption cross sections for reaction 3. Our calculations of the stratospheric chlorine equilibria indicate that, if photochemical decomposition by reaction 3 is the only important removal mechanism for it, then $ClONO_2$ should probably be detectable at altitudes from 20 to 30 km, although less abundant than HCl at all altitudes.[9] Furthermore, the dependence of the equilibria of (1) and (5) on the intensity of solar ultraviolet radiation leads to the possibility of appreciable diurnal variations in $ClONO_2$ concentration, with larger values in morning than evening.

$$Cl + O_3 \rightarrow ClO + O_2 \quad (6)$$

$$ClO + O \rightarrow Cl + O_2 \quad (7)$$

$$ClO + NO \rightarrow Cl + NO_2 \quad (8)$$

The concentrations of $ClONO_2$ should diminish rapidly with increasing altitude above 30 km with the lowered pressure for its stabilization by M in (2), and with the rapidly increasing photodissociation rates for (3). Most of the ClO_x-catalyzed removal of ozone by reactions 6 and 7 occurs above 30 km, with its peak near 40 km,[4] and the presence of $ClONO_2$ in the 20–30-km region would not have a major effect on estimates of the extent of reaction 7 above 35 km. The disappearance at night of O and NO with which ClO usually reacts in the daytime (reactions 7 and 8) may permit the conversion of most ClO to $ClONO_2$ overnight, only to be photolyzed again in the morning. The detailed interaction between the ClO and NO_x cycles is described in a separate paper.[9]

Chlorine nitrate is a moderately well-known laboratory chemical,[10-21] and both its ultraviolet[13] and infrared spectra[15,18,19] have been reported earlier. It is a gaseous compound with a vapor pressure of 13 Torr at 220 K, and about 850 Torr near room temperature;[12,20] when liquefied it is pale yellow. In the laboratory $ClONO_2$ has regularly been formed by reaction 2, and recent observations indicate that the rate of reaction of ClO with NO_2 has a third-body rate coefficient (with N_2) of 1.5×10^{-31} cm^6 molecule^{-2} s^{-1} at room temperature.[22] The reported stability and reactivity of chlorine nitrate has varied with the conditions of the experiments, and caution is advised in handling. However, purified $ClONO_2$ in our experiments is quite stable in the gas phase at room temperature (no observable change in infrared cells for 12 h), even in the presence of N_2, O_2, CH_4, H_2, or SO_2. No reaction was observed

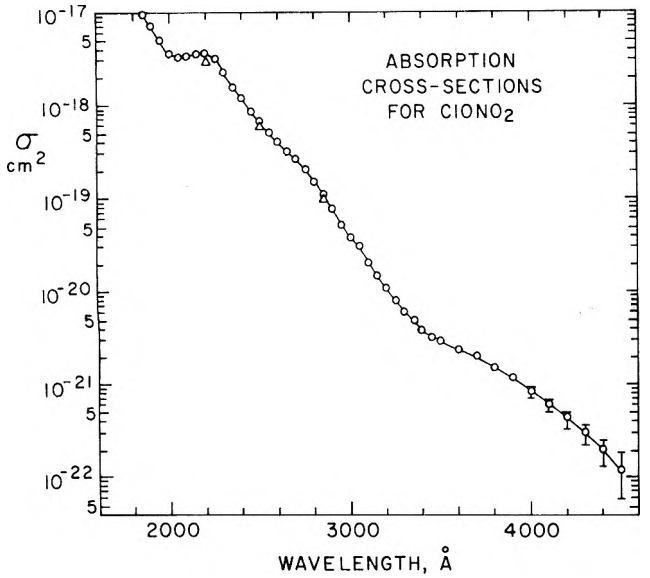

Figure 1. Ultraviolet spectrum of gaseous $ClONO_2$ between 1860 and 4600 Å: (O) this work; (Δ) data of ref 10, as read from published graph.

TABLE I: Photochemical Absorption Cross Sections, σ, for Chlorine Nitrate, $ClONO_2$

λ, Å	σ, 10^{-20} cm^2	λ, Å	σ, 10^{-20} cm^2
1860	995	3000	3.91
1900	690	3050	2.79
1950	502	3100	2.03
2000	372	3150	1.45
2050	344	3200	1.07
2100	348	3250	0.79
2150	375	3300	0.61
2200	376	3350	0.48
2250	307	3400	0.38
2300	231	3450	0.34
2350	159	3500	0.29
2400	118	3600	0.23
2450	85.4	3700	0.19
2500	65.7	3800	0.15
2550	50.9	3900	0.11
2600	40.7	4000	0.085
2650	32.8	4100	0.059
2700	26.1	4200	0.042
2750	20.2	4300	0.028
2800	14.5	4400	0.019
2850	10.5	4500	0.013
2900	7.34	4600	0.008
2950	5.12		

with NO_2 in 2 h, while NO reacted with an apparent bimolecular rate constant of about 10^{-21} cm^3 molecule^{-1} s^{-1}. For each of these molecules, the bimolecular reaction rates are sufficiently slow that at atmospheric concentrations none is important in the removal of $ClONO_2$.[23]

We have measured the ultraviolet spectrum of $ClONO_2$ with carefully purified samples, as shown in Figure 1 and Table I. Repeated purifications with several preparations (by two different routes) have confirmed that the weak absorption in the 3500–4600-Å region is attributable to $ClONO_2$, and not to impurities. Our measurements are in excellent agreement with the earlier measurements[12] in the region of strong absorption, as shown in Figure 1. We have combined these absorption cross sections with solar intensities[4] to calculate the

TABLE II: Altitude and Zenith Angle Variation of Direct Solar Photodissociation Coefficients, J, for Chlorine Nitrate, $ClONO_2$[a]

Altitude, km	Photodissociation coefficient, in units of 10^{-5} s^{-1}				
	Solar zenith angle:				
	0°	20°	40°	60°	80°
10	7.6	7.5	7.1	6.5	5.2
15	7.6	7.5	7.1	6.5	5.2
20	8.0	7.8	7.4	6.7	5.4
25	9.2	8.9	8.3	7.3	5.7
30	12	12	11	8.6	6.4
35	20	19	17	12	7.6
40	39	37	33	24	11
45	70	68	62	49	24
50	95	94	90	81	50

[a] Additional photodecomposition (~6 × 10^{-5} s^{-1} at all altitudes) arises from multiply scattered radiation between 3000 and 4600 Å.

direct photodissociation coefficients, J, for $ClONO_2$ shown in Table II. Molecules with appreciable absorption at wavelengths longer than 3000 Å also have important (and variable) dissociation from multiply scattered radiation as well. Estimates of the intensity of such scattered radiation indicate approximately a factor of 2 increase in J value for that part of the dissociation of $ClONO_2$ lying between 3000 and 4600 Å.[24,25] This is equivalent to the addition on the average of about 6 × 10^{-5} s^{-1} to the J value at all altitudes. The precise increment for scattered radiation varies with zenith angle and assumed albedo of the lower layers of the atmosphere. The rate of photodissociation of $ClONO_2$ is much faster than that of the known stratospheric species, $HONO_2$, which has very small absorption cross sections beyond 3000 Å.

The infrared spectrum of $ClONO_2$[19] shows several intense absorption peaks (e.g., 780.2 cm^{-1}) suitable for identification if its stratospheric concentrations are high enough.

References and Notes

(1) This research has been supported by ERDA Contract No. AT(04-3)-34, P.A. 126, and by NASA Contract No. NSG-7208.
(2) Alfred P. Sloan Foundation Fellow.
(3) Abstracts of the 12th International Symposium on Free Radicals, Laguna Beach, Calif., Jan 1976.
(4) F. S. Rowland and M. J. Molina, *Rev. Geophys. Space Phys.*, **13**, 1 (1975).
(5) The alternative bimolecular reactions leading to ClOO + NO, OClO + NO, or Cl + NO_3 are endothermic by 10.5, 13.7, and 13.7 kcal/mol, respectively.
(6) The quantum yield for photodecomposition of $ClONO_2$ has not yet been measured, but is assumed to be 1.0 because of the uv spectral characteristics, and the large excesses of available energy over that needed for decomposition.
(7) L. T. Molina, J. E. Spencer, and M. J. Molina, *Chem. Phys. Lett.*, in press. The observed secondary reactions in these experiments strongly indicate that the reaction products from (4) are ClO and NO_3 as shown.
(8) A. R. Ravishankara, G. Smith, G. Tesi, and D. D. Davis, 12th Informal Conference on Photochemistry, Gaithersburg, Md., June 1976.
(9) F. S. Rowland, J. E. Spencer, and M. J. Molina, *J. Phys. Chem.*, following paper in this issue.
(10) H. Martin and T. Jacobsen, *Angew. Chem.*, **67**, 524 (1955).
(11) H. Martin and R. Gareis, *Z. Elektrochem.*, **60**, 959 (1956).
(12) H. Martin, *Angew. Chem.*, **70**, 97 (1958).
(13) H. Martin, W. Meise, and E. Engelmann, *Z. Phys. Chem. (Frankfurt am Main)*, **24**, 285 (1960).
(14) M. Schmeisser, W. Fink, and K. Brändle, *Angew. Chem.*, **69**, 780 (1957).
(15) K. Brandle, M. Schmeisser, and W. Luttke, *Chem. Ber.*, **93**, 2300 (1960).
(16) M. Schmeisser and K. Brändle, *Angew. Chem.*, **73**, 388 (1961).
(17) L. F. R. Cafferata, J. E. Sicre, and H. J. Schumacher, *Z. Phys. Chem. (Frankfurt am Main)*, **29**, 188 (1961).

(18) A. J. Arvia, L. F. R. Cafferata, and H. J. Schumacher, *Chem. Ber.*, **96**, 1187 (1963).
(19) R. H. Miller, D. L. Bernitt, and I. C. Hisatsune, *Spectrochim. Acta, Part A*, **23**, 223 (1967).
(20) C. J. Schack, *Inorg. Chem.*, **6**, 1938 (1967).
(21) M. Schmeisser, *Inorg. Syn.*, **9**, 127 (1967).
(22) Unpublished experiments by W. B. DeMore et al., F. Kaufman et al., and J. Birks et al. The temperature dependence is approximately T^{-3}, leading to a rate constant for formation about a factor of 2 to 3 higher at stratospheric temperatures.
(23) Reference 16 also reports a rapid reaction of $ClONO_2$ with SO_2 and NO_2, but we have not observed such reactions at room temperature.
(24) D. Wuebbles and F. Luther, unpublished calculations.
(25) P. Crutzen, Joint IAOC/ICACGP Symposium on Atmospheric Ozone, Dresden, GDR, Aug 1976.

Department of Chemistry
University of California
Irvine, California 92717

F. S. Rowland*
John E. Spencer
Mario J. Molina[2]

Received June 3, 1976

Estimated Relative Abundance of Chlorine Nitrate among Stratospheric Chlorine Compounds

Publication costs assisted by the U.S. Energy Research and Development Administration

Sir: The stratospheric cross combination of the radicals ClO and NO_2 can lead to the formation of chlorine nitrate, $ClONO_2$, as in[1-3]

$$ClO + NO_2 + M \rightarrow ClONO_2 + M \quad (1)$$

The chief process for removal of chlorine nitrate from the stratosphere is solar photolysis, as in

$$ClONO_2 + h\nu \rightarrow ClO + NO_2 \quad (2a)$$

$$\rightarrow Cl + NO_3 \quad (2b)$$

which effectively reverses (1). Although photodissociation is theoretically possible with radiation in the infrared to about 11 000 Å, chlorine nitrate is transparent at wavelengths longer than about 4600 Å.[3] At altitudes above about 35 km the most important wavelengths for photolysis of chlorine nitrate are in the 2000–2200-Å range for which it has absorption cross sections of 300–400 $\times 10^{-20}$ cm^2. Radiation of such wavelengths, however, is strongly absorbed by both O_2 and O_3 (although not as strongly as radiation with $\lambda < 1900$ Å by O_2 or $\lambda > 2200$ Å by O_3). Below 30 km $ClONO_2$ photolysis occurs primarily with wavelengths longer than 3000 Å. A process of secondary importance for stratospheric removal of $ClONO_2$ is its attack by $O(^3P)$ atoms, as in[4,5]

$$O + ClONO_2 \rightarrow ClO + NO_3 \quad (3)$$

While very complete models of the stratosphere with tens of interacting species, a hundred or more chemical reactions, and diffusion of species in one or more dimensions are necessary for detailed understanding of stratospheric chemistry, the very complexity of the models forces approximations of varying crudeness to avoid computer calculations of prohibitive length. By contrast, reasonable estimates of the expected stratospheric ratio of $(ClONO_2)/(ClO)$ vs. altitude can be obtained simply from the measured concentrations of NO_2,[6] known rate constant for (1),[7] and calculated photodissociation coefficient, J, for reaction 2,[3] based on the measured laboratory absorption cross sections vs. wavelength. The $(ClONO_2)/(ClO)$ ratios can then be coupled with (ClO)/(HCl) ratios from more complex calculations for estimates of the stratospheric distribution of Cl among the chlorine species, ClO, HCl, $ClONO_2$, and Cl itself. The calculation is simple if the mechanism for photolysis is the reverse of the formation reaction, i.e., (2a). If part or all of the photolysis goes by (2b) the Cl atoms thus released react immediately (<5 s) with O_3 to form ClO and the result is essentially the same insofar as the $(ClONO_2/ClO/HCl)$ distribution is concerned. However, if mechanism 2b were accompanied by the photolysis of $NO_3 \rightarrow NO + O_2$ the net effect of $ClONO_2$ photolysis would involve removal of two O_3 molecules (one by Cl, one by NO) in returning to $ClO + NO_2$. No mechanistic information is available at present which distinguishes between (2a) and (2b).

The calculation which follows is based on direct straight-line absorption of solar ultraviolet and visible radiation. This approximation is generally quite reasonable for ultraviolet wavelengths which do not penetrate to the earth's surface (i.e., $\lambda < 3000$ Å). However, for the wavelengths which *do* penetrate below the stratosphere, multiple scattering from tropospheric air, cloud layers, and/or the earth's surface will increase the total photolytic flux. Luther and Wuebbles have estimated that the effective rate for photodecomposition of $ClONO_2$, J_{eff}, is from 1.5 to 2 times larger in the 20–35-km range than that calculated from the straight-line absorption method.[8] Accordingly, the calculations which follow must be considered as illustrative, but result in an *over*estimate of the amount of $ClONO_2$ by a factor of 1.5–2.0 in the important 20–35-km altitudes. The precise value is dependent upon the earth's albedo and will certainly vary with solar zenith angle.[8]

The chief significance of the following calculation is that it demonstrates, even without the inclusion of multiple scattering, that chlorine nitrate is expected to be considerably *less* abundant than HCl at all stratospheric altitudes under essentially all circumstances. These quantities of chlorine nitrate are very much less than those indicated by calculations described elsewhere.[9,10]

Since the wavelengths beyond 3100 Å penetrate completely to the earth's surface, the $ClONO_2$ photodissociation coefficient, J, rises very rapidly immediately after sunrise to 6 or 7×10^{-5} s^{-1}, and then gradually increases as the sun approaches the zenith, as illustrated in Figure 1. At 25-km altitude, the 2000–2200-Å range contributes very little absorption even for directly overhead sun because this radiation is nearly completely absorbed at higher altitudes. However, as also shown in Figure 1, the J value at 30 km and overhead sun is already about 10^{-4} s^{-1}. Still larger J values are found at altitudes of 35 km or higher, reaching 1×10^{-3} at about 50 km.[3] The formation rate by reaction 1 is now well-established with a three-body rate coefficient (with N_2) of 1.5×10^{-31} cm^3 $molecule^{-1}$ s^{-1} at 298 K and $3–5 \times 10^{-31}$ at stratospheric temperatures.[7] The calculated distribution of Cl among ClO, HCl, and $ClONO_2$ at 25 km is illustrated in Figure 2 for an assumed NO_2 concentration of 2×10^9 molecules cm^{-3} and the rate constant of (1) for stratospheric temperatures. The (ClO)/(HCl) ratio is typical (= 0.12) of those calculated for 25 km in some of the detailed calculations. The (ClO)/(HCl) ratio used at each altitude can be read from the ClO and HCl concentration shown in Figure 3.

The ClO concentration is assumed to go to zero after sunset each night by reaction with NO_2,[11] and the sunrise $ClONO_2$ concentration is equal to the sunset $ClONO_2 + ClO$ concentrations. Although a J value of 6×10^{-5} s^{-1} corresponds to an average time for photolysis of $ClONO_2$ of about 4.5 h, the ClO concentration rapidly approaches an equilibrium concentration for reactions 1 and 2 because the equilibrium

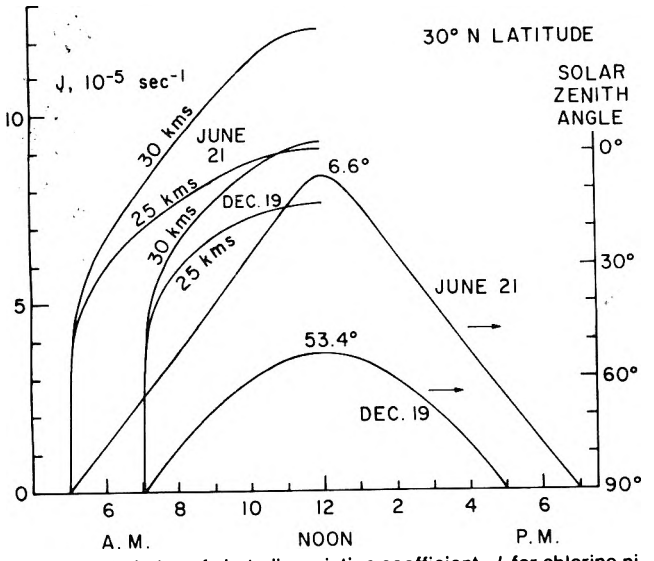

Figure 1. Variation of photodissociation coefficient, J, for chlorine nitrate vs. time of day, 30°N, June 21 and Dec 19.

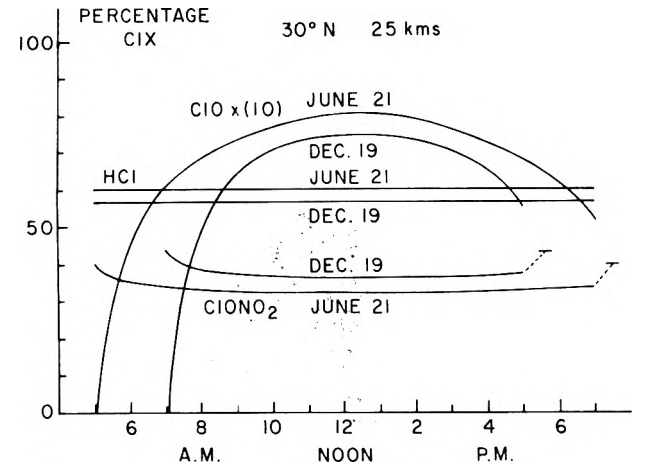

Figure 2. Calculated percentage distribution of Cl among ClO, $ClONO_2$, and HCl vs. time of day, 30°N, 25-km altitude, June 21 and Dec 19.

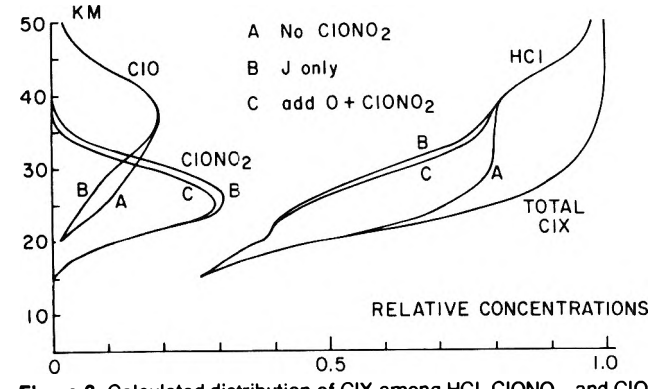

Figure 3. Calculated distribution of ClX among HCl, $ClONO_2$, and ClO vs. altitude: (A) without $ClONO_2$ present; (B) $ClONO_2$ present, removed only by solar photolysis; (C) $ClONO_2$ present, removed both by solar photolysis and by O atom attack with a rate constant of 4×10^{-13} cm^3 $molecule^{-1}$ s^{-1}. (Example for B, at 30-km altitude: ClO, 0.12; $ClONO_2$, 0.22; HCl, 0.62; total ClX = 0.12 + 0.22 + 0.62 = 0.96.)

$(ClONO_2)/(ClO)$ ratio is roughly 5 and therefore only 15% of the $ClONO_2$ must be photolyzed (less than 1 h) to approach equilibrium for $ClONO_2$ and ClO. During the rest of the day, the ClO concentration closely tracks the changing J value. A better approximation could be obtained by allowing NO_2 to increase during the day as it actually does, but the change is not very large and the use of an average value provides a reasonable estimate of the total $ClONO_2$ formation during the day. The inclusion of multiple scattering approximately doubles the J values in the 20–30-km region on the average, and therefore reduces the average time for photolysis even more.

TABLE I: Daylight Average Percentage Concentrations of ClX (Solar Photolysis only for $ClONO_2$)

	30 km		25 km	
	June 21	Dec 19	June 21	Dec 19
ClO	11.2	10.7	6.9	6.6
$ClONO_2$	26	30	33	36
HCl	63	59	60	57
$(ClONO_2/HCl)_{diurnal}$	0.41	0.51	0.56	0.64
$(ClONO_2/HCl)_{equil}$	0.36	0.44	0.51	0.58

Comparison of the calculated ratios of the chlorine species for mid-summer and mid-winter at 30°N indicates only a very small seasonal effect for chlorine nitrate from solar intensity effects alone. The calculations also indicate relatively small variations in $(ClONO_2)/(HCl)$ ratios with season or with time of day. On the other hand, ClO exhibits a strong diurnal variation, going to zero at night and changing rapidly immediately after sunrise. The comparison of days with peak zenith angles of 6.6 and 54.3° indicates, too, that not too much variation in $ClONO_2$ ratios should be expected with latitude. Since zenith angles of 75–80° also have large J values, even high latitudes are little different.

These calculations have all been performed with a standard atmosphere, and do not make allowance for seasonal variations in total O_3. However, in the stratospheric range of 23–32 km for which $(ClONO_2)/(HCl)$ reaches its peak ratio (~0.6), most of the absorption occurs beyond 3000 Å, and is therefore not very dependent on the actual O_3 content of the stratosphere. The observed latitude dependence of $HONO_2$, with higher stratospheric concentrations at high latitudes, especially in the winter atmosphere,[12] contrasts sharply with the $ClONO_2$ predictions. However, $HONO_2$ absorption beyond 3000 Å is very much less, and the importance of 1900–2200-Å radiation for photodecomposition of $HONO_2$ is correspondingly increased. The penetration of *this* uv radiation *is* affected by O_3, and the higher O_3 concentrations and lower zenith angles characteristic of the higher latitudes of the winter hemisphere greatly reduce the J values there for $HONO_2$ photodecomposition.

A comparison is given in Table I of the daytime average of $(ClONO_2)/(HCl)$ integrated over Figure 2 vs. the "equilibrium" value expected taking J at its value midway between sunrise (or sunset) and noon. The small excess of $ClONO_2$ over the "equilibrium" value represents chiefly the early morning period during which $ClONO_2$ is first being photolyzed, and the ClO concentration is low.

The distribution of chlorine among ClO, $ClONO_2$, and HCl throughout the stratosphere calculated by these methods is shown in Figure 3. Curve A represents the calculated ClO/HCl distribution without any $ClONO_2$ present; curve B shows the distribution with solar photolysis alone; curve C shows the affect of including reaction 3 with a rate constant of 4×10^{-13} cm^3 $molecule^{-1}$ s^{-1}.[13] In this overall distribution, the amount of $ClONO_2$ between 20 and 30 km is considerably less than the amount of HCl, in agreement with the observation by Hanst

that the abundance of $ClONO_2$ in the stratosphere is much less than that of HCl.[14] Those stratospheric model calculations which have predicted much larger $ClONO_2$/HCl ratios (and as a corollary, sharply diminished estimates of overall O_3 depletion by ClO_x) have generally used one or more of the following: (1) 24-h "average" sun, thereby allowing formation of $ClONO_2$ for 24 h in the calculation, although the actual night time formation is limited to the conversion of the ClO already existing at sunset; (2) photodissociation coefficients truncated at 4000 Å or even 3500 Å; (3) higher average NO_2 concentrations than the values listed in the C.I.A.P. report; and/or have (4) neglected multiply scattered radiation, as we have done.

Acknowledgment. This research was supported by ERDA Contract AT(04-3)-34, P.A. 126.

References and Notes

(1) F. S. Rowland and M. J. Molina, *Rev. Geophys. Space Phys.*, **13**, 1 (1975).
(2) F. S. Rowland, M. J. Molina, and J. E. Spencer, 12th International Free Radical Symposium, Laguna Beach, Calif., Jan 1976.
(3) F. S. Rowland, J. E. Spencer, and M. J. Molina, *J. Phys. Chem.*, preceding paper in this issue.
(4) L. T. Molina, J. E. Spencer, and M. J. Molina, *Chem. Phys. Lett.*, in press. The products from (3) have not been conclusively identified but are strongly suggested by the secondary reactions observed in these experiments.
(5) A. R. Ravishankara, G. Smith, G. Tesi, and D. D. Davis, 12th Informal Conference on Photochemistry, Gaithersburg, Md., June 1976.
(6) T. Hard in "The Natural Stratosphere of 1974", CIAP Monograph 1, DOT-TST-75-51, Department of Transportation, Sept 1975, pp 3–163.
(7) Unpublished experiments by W. B. deMore et al., P. Kaufman et al., and J. Birks et al. The temperature dependence is approximately T^{-3}, leading to a rate constant for formation about a factor of 2 higher at stratospheric temperatures than at 298 K.
(8) F. M. Luther and D. J. Wuebbles, preprint June, 1976.
(9) A. E. J. Eggleton, R. A. Cox, and R. G. Derwent, AERE-R-8383; see also by the same authors, *New Sci.*, 402 (May 20, 1976).
(10) J. P. Jesson, quoted in *Aerosol Age* (May 1976); and American Chemical Society section meeting, Newport Beach, Calif., April 1976. See also A. Gribbin, *National Observer* (May 8, 1976).
(11) Dr. S. Liu has pointed out that above about 40 km the rate constant for reaction 1 is slow enough that most ClO cannot combine with NO_2 during the nighttime hours.
(12) See pp 3–77 of ref 6.
(13) The actual rate constant for reaction 3 as measured in ref 4 is given by the expression $k = (3.4 \pm 0.6) \times 10^{-12} \exp[(-840 \pm 60)/T]$. At stratospheric temperatures the rate is about 1×10^{-13} cm^3 molecule^{-1}, correspondingly more closely to B than to C in Figure 3.
(14) P. Hanst, preprint May 1976.

Department of Chemistry
University of California
Irvine, California 92717

F. S. Rowland*
John E. Spencer
Mario J. Molina

Received June 28, 1976

ADDITIONS AND CORRECTIONS

1976, Volume 80

J. N. Spencer,* Judy R. Sweigart, Michael E. Brown, Ronald L. Bensing, Thomas L. Hassinger, William Kelly, Donna L. Housel, and G. William Reisinger: Solvation Effects on the Thermodynamics of Hydrogen Bonded Systems. II

Page 811. The thermodynamic data for the guaiacol–pyridine complex presented in this paper in Table II are incorrect due to a calculational error caused by transposition of digits in the molecular mass of guaiacol. The corrected data are given below. The data of Table III should be correspondingly corrected. The conclusions given in the paper are unchanged. We regret the error and offer our apology.

Solvent	$K_{20°C}$	$-\Delta H$, kcal mol^{-1}	$-\Delta S$, cal deg^{-1} mol^{-1}
Cyclohexane	2.71	3.13 ± 0.07	8.7
CS_2	2.67	3.74 ± 0.13	10.8
CCl_4	1.44	3.07 ± 0.38	9.7
Benzene	1.72	4.11 ± 0.15	12.9
1,2-Dichloroethane	2.10	3.12 ± 0.41	9.2
Chloroform	1.90	2.53 ± 0.30	7.3

—J. N. Spencer.

Corrected
V. Ph. 3. March 1977

Tatsuo Tashiro and Masayoshi Oiwa: The Two-Step Equilibrium Reaction of 2-Substituted 4,6-Diamino-*s*-triazine with Formaldehyde.

Page 1460. The footnote for Table VI should read as follows:

[a] [iPT] = 0.050 M.

—Tatsuo Tashiro.

Corrected
V. Ph
7 March 1977

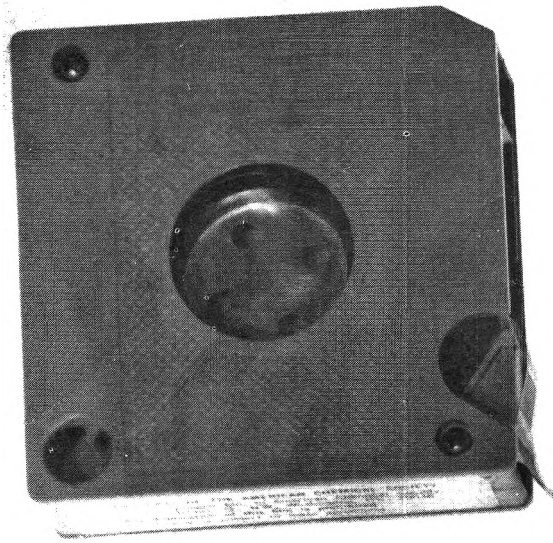

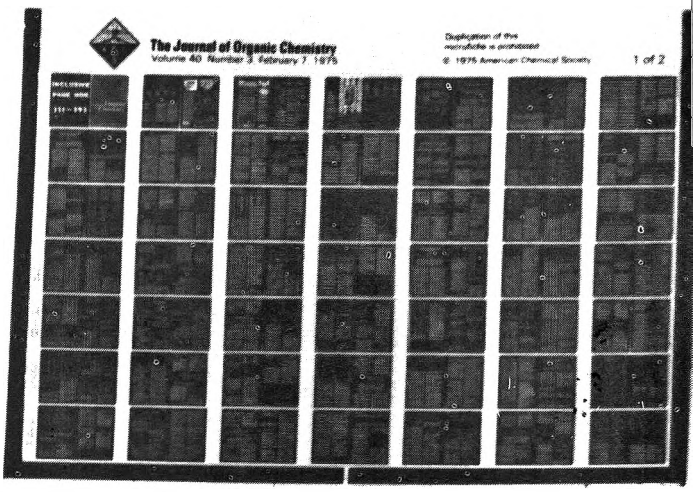

MICROFORMS

American Chemical Society publications in microform

MICROFILM OR MICROFICHE?

With the ACS microform program you can receive either, or both

Microfilm

All periodical publications back to volume one

Copying privileges included with current subscriptions

All non-print supplementary materials provided free on microfiche

Archival quality silver halide film supplied as you request; positive or negative; 16 or 35mm; cartridge, reel, or cassette.

Microfiche

Current issues of primary journals, beginning with January 1975

Individual issues or full volumes available

Supplementary materials also available on microfiche

Fiche supplied are archival quality silver halide, negative, 105 x 148mm (4" x 6"); 24x, with eye legible headers, start and end targets, and page numbers

For information about our microfilm/microfiche write:

Microform Program
Special Issues Sales
American Chemical Society
1155 16th Street, N.W.
Washington, D.C. 20036
(202) 872-4363